



UNIVERSITÉ DE STRASBOURG

EDSC
École Doctorale des
Sciences Chimiques

ÉCOLE DOCTORALE DES SCIENCES CHIMIQUES

Laboratoire de Chimie des Matériaux Moléculaires – UMR 7042



THÈSE présentée par :

Nihed BECHARGUIA

soutenue le : 18 décembre 2023

en co-tutelle avec l'université de Carthage

pour obtenir le grade de : **Docteur de l'université de Strasbourg**

Discipline/ Spécialité : Chimie

Préparation de rotaxanes incorporant une sous-unité pillar[5]arène

THÈSE dirigée par :

M. NIERENGARTEN Jean-François

Mme. ABIDI Rym

Dr, Université de Strasbourg

Pr, Université de Carthage

RAPPORTEURS :

M. GINGRAS Marc

M. MAJDOUB Hatem

Pr, Université d'Aix-Marseille

Pr, Université de Monastir

MEMBRES DU JURY :

M. FALLER Peter

Mme. BARHOUMI-SLIMI Thouraya

Pr, Université de Strasbourg

Pr, Université de Carthage

MEMBRE INVITÉ :

Mme. NIERENGARTEN Iwona

Dr, Université de Strasbourg

Remerciements

La description de tout travail réalisé débute par des remerciements. Cependant, il paraît difficile de remercier en quelques lignes et comme je le voudrais toutes les personnes qui ont contribué, de près ou de loin, à la réalisation de cette thèse, car une thèse n'est pas l'histoire d'une seule personne.

Cette thèse a été réalisée dans le cadre d'une collaboration entre le Laboratoire de Chimie des Matériaux Moléculaires (UMR 7042) de l'Université de Strasbourg en France, et le Laboratoire d'Application de la Chimie aux Ressources et Substances Naturelles et à l'Environnement (LACReSNE) de l'Université de Carthage en Tunisie.

Mes premiers remerciements vont à Dr. Jean-François Nierengarten de m'avoir accueillie au sein de son laboratoire. Au cours de ma thèse, il m'a soutenue sans relâche, m'a encouragée, a supporté mes questions souvent évidentes, mais toujours avec bienveillance et pour cela il a ma reconnaissance inconditionnelle. J'ai sincèrement apprécié de travailler à ses côtés avec l'autonomie qu'il m'a accordée. Grâce à lui, j'ai eu la chance d'élargir mes horizons en rencontrant des personnes à l'échelle internationale. Ces rencontres m'ont permis de m'enrichir à la fois sur le plan scientifique et technique, que sur le plan humain. En plus de cela, ses qualités scientifiques exceptionnelles m'ont permis de réaliser mon travail et de faire mes premiers pas dans la recherche dans un environnement très agréable. Grâce à cette expérience, j'ai appris à apprécier l'importance des détails en recherche scientifique et j'aspire à atteindre un jour son niveau de compréhension des détails.

Je tiens à exprimer mes sincères remerciements au Pr. Rym Abidi pour avoir dirigé ma thèse avec une rigueur scientifique exemplaire et pour les discussions enrichissantes que nous avons eues tout au long de cette expérience. Sa confiance constante en moi, du début à la fin du travail, m'a permis de mener à bien cette recherche. Je suis reconnaissante de l'appui et du soutien scientifique et humain qu'elle m'a accordé, ce qui a été essentiel pour surmonter les difficultés que j'ai rencontrées. Je suis fière de faire partie de ses étudiants et de bénéficier de son expertise et de son mentorat tout au long de ma carrière.

Je tiens à exprimer mes sincères remerciements à Dr. Iwona Nierengarten pour son soutien indéfectible tout au long de ma thèse. Sa présence, son attention de tout instant sur mes travaux, ses conseils avisés et son écoute bienveillante ont été des éléments prépondérants pour la

réussite de cette thèse. J'ai pris un grand plaisir à travailler avec elle et je suis fière d'avoir pu bénéficier de son accompagnement et de son expertise. Sa contribution a été essentielle pour la réussite de cette thèse et je lui suis reconnaissante de son soutien constant, de son engagement et de son amitié.

Je tiens à exprimer mes sincères remerciements aux membres du jury: le Pr. Marc Gingras, le Pr. Hatem Majdoub, le Pr. Thouraya Barhoumi-Slimi et le Pr. Peter Fallor pour avoir accepté de juger mes travaux de thèse. Je suis reconnaissante pour le temps et l'attention qu'ils ont consacré à l'examen de mon travail. Leur expertise et leur contribution ont été essentielles pour l'évaluation de mon travail.

Je remercie l'équipe de Chimie des Matériaux Moléculaires, y compris le Pr. Michel Holler, le Dr. Uwe Hahn, Dr. Marine Remy et les doctorants Boram Park et Julien Ra, pour leur soutien et leur expertise qui m'ont aidé à progresser dans ma thèse. Leur présence positive a contribué à une ambiance de travail agréable et leur soutien moral m'a aidé à persévérer dans les moments difficiles. Je leur suis éternellement reconnaissante car cette thèse n'aurait pas été possible sans eux. Je remercie les stagiaires avec qui j'ai eu la chance de travailler. L'ambiance de travail a été excellente et nous avons pu ainsi allier bons moments et séances de travail: Till Nitschke, Jorge Marco Guimbao, Miguel Uceda, Eya Larnaout, Célia Jager et Loïc Eby.

Je désire en outre remercier tous les membres de l'équipe LACReSNE: Mohamed Habib Noamane, Takwa Khanchouch, Marwa Boutar et Jnd Haifa.

Je suis profondément reconnaissante à l'Université de Carthage pour le financement qui a rendu possible mon séjour en France et ma thèse. Ce soutien financier a été essentiel pour poursuivre mes études et m'immerger dans un environnement scientifique stimulant. Je remercie l'Université de Carthage pour sa confiance et son engagement à soutenir la recherche scientifique, grâce à ce financement j'ai acquis de nouvelles compétences et connaissances, et je suis fière d'avoir bénéficié de cette opportunité.

Un grand merci aux services analytiques du campus de Cronenbourg. Je remercie le Dr. Emeric Wasielewski pour toutes les mesures de RMN, Matthieu Chessé pour les mesures de spectrophotométrie et Dr. Jean-Marc Strub pour les mesures de spectrométrie de masse. Merci également aux services scientifiques situés sur le campus de l'Esplanade, notamment le Dr. Lydia Karmazin, Corinne Bailly et Nathalie Gruber pour la résolution des structures par

diffraction des rayons X, et Martine Heinrich pour les analyses élémentaires. Merci également à Dr. Béatrice Delavaux-Nicot (LCC-CNRS, Toulouse) pour les mesures d'électrochimie.

Réaliser ce travail dans le contexte de la cotutelle n'aurait pas été possible sans ma famille qui a toujours encouragé et soutenu toutes mes idées et mes projets, aussi loin qu'ils peuvent être parfois. Je souhaite remercier ma mère Samira, mes sœurs Hiba et Houaida, ainsi que mon frère Ahmed pour l'intérêt qu'ils ont toujours porté à ce que je réalise. C'est grâce à leur amour et à leurs encouragements que je suis ici aujourd'hui. Même s'ils vivent loin de moi, je sens leur présence autour de moi. Ils m'ont donné du courage, de la force et de la joie. Merci d'avoir toujours été là et de m'avoir tant aidé.

Pour finir, je souhaite exprimer ma gratitude la plus sincère à toutes les personnes qui ont contribué à la réussite de cette thèse. Leur soutien et leur engagement ont été inestimables, et je suis fière de pouvoir les considérer comme des amis et des collègues de confiance.

Nihed Becharguia

Résumé en Français

I. Introduction

Une branche intéressante de la chimie traite des molécules présentant une structure entrelacée, telles que les caténanes ou les rotaxanes. Ces espèces moléculaires exotiques sont constituées de sous-unités moléculaires mécaniquement imbriquées, maintenues ensemble par des liens mécaniques (Figure 1). Un [2]caténane est constitué de deux macrocycles entrelacés formant deux maillons d'une chaîne (le nom vient du latin *catena* et le chiffre entre crochets indique le nombre de constituants). Un [2]rotaxane est quant à lui composé d'un macrocycle (une roue, en latin *rota*) dans lequel un axe a été inséré. Ce dernier comporte des groupements volumineux ou bouchons qui empêchent le défilage du macrocycle, les deux sous-unités sont ainsi liées l'une à l'autre par un lien mécanique.

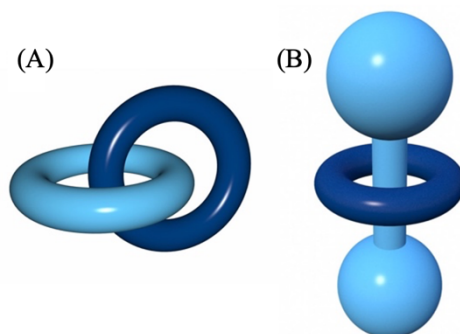


Figure 1. Représentation schématique d'un [2]caténane (A) et d'un [2]rotaxane (B).

La structure unique des caténanes et des rotaxanes les rend tout aussi intéressants pour les chimistes. Grâce aux liens mécaniques entre les sous-unités moléculaires, ces composés ont des propriétés fascinantes, notamment parce que ces composés présentent des mouvements de grande amplitude qui peuvent être déclenchés par différents stimuli externes tels que la lumière,

les changements de température ou de pH, l'échange d'ions ou d'autres signaux chimiques. Ainsi, le contrôle de ces mouvements au sein de ces systèmes moléculaires dynamiques est à l'origine du domaine des machines moléculaires. Ces dernières ont des applications variées, telles que le transfert d'électrons ou d'énergie, le développement de dispositifs de stockage d'informations, ou encore la délivrance de médicaments ciblant spécifiquement les cellules malades.

Dans ce domaine, notre équipe mène des travaux de recherche centrés sur des rotaxanes incorporant des sous-unités de type pillar[5]arène. Ce macrocycle est composé de cinq sous-unités hydroquinones reliées entre elles par des ponts méthyléniques. Son incorporation au sein de rotaxanes est difficile du fait de la faible affinité de ce macrocycle pour le précurseur de l'axe. Par ailleurs, l'auto-assemblage des différentes sous-unités en un complexe d'inclusion est souvent incompatible avec les conditions de réaction utilisées pour réaliser les transformations chimiques nécessaires à l'introduction des bouchons pour former le rotaxane. Notre équipe a montré que des réactions entre un chlorure d'acide et une amine ou un alcool permettaient d'obtenir des rotaxanes incorporant une sous-unité pillar[5]arène. Cependant, les rendements n'étaient pas toujours satisfaisants et variaient beaucoup en fonction de la nature du nucléophile utilisé. Pour contourner ce problème, notre équipe a réussi à préparer très efficacement des briques de construction comportant deux groupements activés sur les extrémités de l'axe du rotaxane. Ils ont ensuite montré qu'il était possible de les remplacer par réaction avec divers nucléophiles pour générer des rotaxanes portant les fonctions chimiques souhaitées (Figure 2).

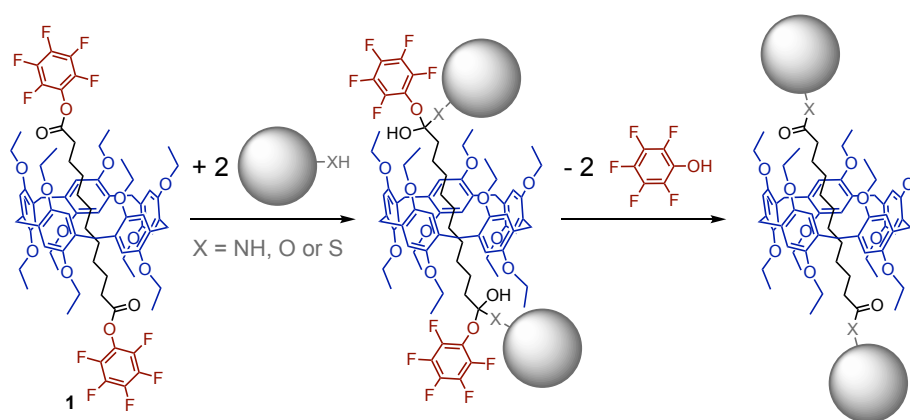


Figure 2. Echange des bouchons du rotaxane 1 par une réaction d'addition-élimination.

Comme ces réactions se font par un mécanisme d'addition-élimination, les groupements présents de part et d'autre de l'axe moléculaire restent toujours volumineux et empêchent la libération du macrocycle. La structure du rotaxane est donc préservée durant ces transformations chimiques. De nombreux rotaxanes impossibles à préparer avec les méthodes classiques deviennent maintenant facilement accessibles. Dans ce contexte, les objectifs de la présente thèse étaient d'étudier la réactivité du rotaxane à bouchons échangeables **1** et d'évaluer son potentiel pour la construction de machines moléculaires.

II. Fonctionnalisation du rotaxane à bouchons échangeables

Lors des réactions du rotaxane **1** avec les amines **3a-g**, nous avons observé que la première addition-élimination est très rapide, mais que la seconde est plus lente. Cette observation suggère que l'encombrement stérique résultant de la présence du pillar[5]arène à proximité du bouchon pentafluorophényl dans le produit intermédiaire mono-acylé peut limiter l'accessibilité du nucléophile amine pour le deuxième échange de bouchon. Afin d'évaluer l'effet de la sous-unité pillar[5]arène sur la réactivité de l'ester pentafluorophényl dans le rotaxane **1**, nous avons alors traité le rotaxane **1** et le l'axe modèle **2** avec un équivalent de divers amines **3a-g** dans THF à 0°C (Figure 3).

Dans tous les cas, la proportion relative du produit de départ, des produits mono- et bis-acylés a été déterminé à partir des spectres RMN du proton enregistrés pour les bruts réactionnels. Les résultats sont résumés dans le tableau 1. Le traitement de **2** avec un équivalent des amines **3a-g** a toujours donné un mélange de **2**, **4a-g** et **5a-g** dans le rapport statistique attendu (1 :2 :1). Il est intéressant de noter que ce n'est plus le cas lorsqu'on part du rotaxane **1**. En effet, la formation du produit mono-acylé a toujours été largement favorisée, révélant ainsi que la seconde acylation de **6a-g** menant à **7a-g** est beaucoup plus lente que la première acylation du produit de départ **1**. Cette sélectivité cinétique est attribuée à des effets stériques résultant de la présence de la sous-unité pillar[5]arène qui doit probablement être attiré par le bouchon pentafluorophényl électro-déficient dans **6a-g**, limitant ainsi son accessibilité. Il convient également de noter que la température joue un rôle important dans la formation préférentielle des mono-amides **6a-g**. En effet, la sélectivité a été significativement diminuée lorsque la réaction a été effectuée à température ambiante plutôt qu'à 0°C. Cette observation confirme également l'origine cinétique de la formation sélective des mono-amides à partir du bloc de construction symétrique **1**.

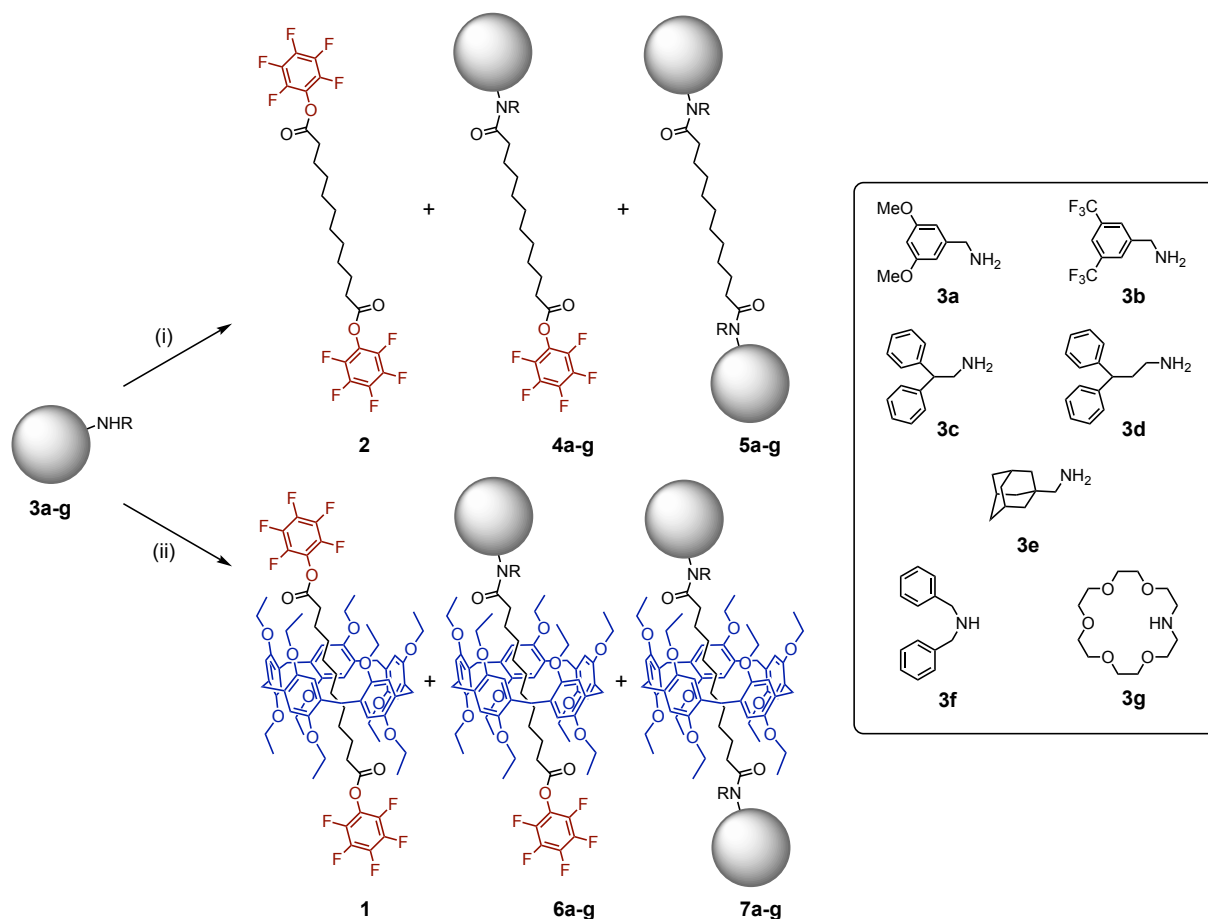


Figure 3. Traitement des blocs de construction **1** et **2** avec les amines **3a-g** (1 équiv.). La proportion du produit de départ, des produits mono-acylés et bis-acylés a été déterminée sur la base de l'analyse des spectres ^1H RMN enregistrés pour les bruts (voir tableau 1). Réactifs et conditions : (i) **2** (1 équiv.), THF, 0°C ; (ii) **1** (1 équiv.), THF, 0°C .

Tableau 1. Proportion relative du produit de départ, des produits mono- et bis-acylés résultant de l'intégration des spectres ^1H RMN enregistrés pour les bruts obtenus par la réaction de **1** et **2** (1 équiv.) avec les amines **3a-g** (voir schéma 1).

Amine	Relative proportion of 2 / 4 / 5	Relative proportion of 1 / 6 / 7
3a	24 / 52 / 24	3 / 94 / 3
3b	25 / 50 / 25	7 / 87 / 6
3c	23 / 51.3 / 25.7	3 / 94 / 3
3d	28 / 48 / 24	10 / 81 / 9
3e	25 / 50 / 25	13 / 74 / 13
3f	25 / 50 / 25	19 / 76 / 5
3g	25 / 50 / 25	5 / 90 / 5

Le pillar[5]arène joue ainsi le rôle d'un groupe protecteur permettant une sélectivité cinétique pour la mono-fonctionnalisation du synthon **1**. À la suite de cette observation, une étude d'optimisation a été réalisée dans le but d'obtenir des rendements quasi-quantitatifs de [2]rotaxane mono-substitués, en augmentant le nombre d'équivalents de rotaxane **1** à 2 équivalents, ce qui a permis d'obtenir les produits **6a-e** avec un rendement de 91-98%. Ces dérivés [2]rotaxanes mono-fonctionnalisés servent de point de départ intéressant pour aborder la synthèse dans les chapitres suivants de cette thèse. Par conséquent, la bis-fonctionnalisation successive du rotaxane de départ est facile à réaliser pour générer des rotaxanes dissymétriques avec deux bouchons différents avec d'excellents rendements. En outre, nous avons également montré que le pillar[5]arène peut agir comme un groupe protecteur permettant la synthèse d'axes dissymétriques particulièrement difficiles à préparer dans des conditions statistiques (Figure 4).

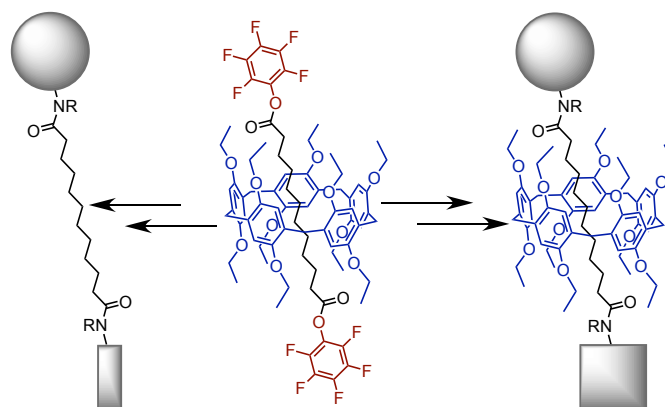


Figure 4. L'introduction d'un second bouchon est alors possible pour générer des rotaxanes ou des axes dissymétriques avec des excellents rendements.

Enfin, des études détaillées de RMN des [2]rotaxanes non symétriques ont également été réalisées afin de comprendre pleinement l'influence des interactions polaires faibles sur leurs préférences conformationnelles.

III. Préparation de [2] et [3]rotaxanes

Dans la deuxième partie de ce travail de thèse, nous avons utilisé le dérivé [2]rotaxane mono-fonctionnalisé **6b** pour préparer des [2]rotaxanes et des [3]rotaxanes symétriques avec des axes allongés. Pour cela, nous avons étudié la réactivité du rotaxane **6b** avec les diamines **8a-e** en solution mais aussi en conditions sans solvant (Figure 5).

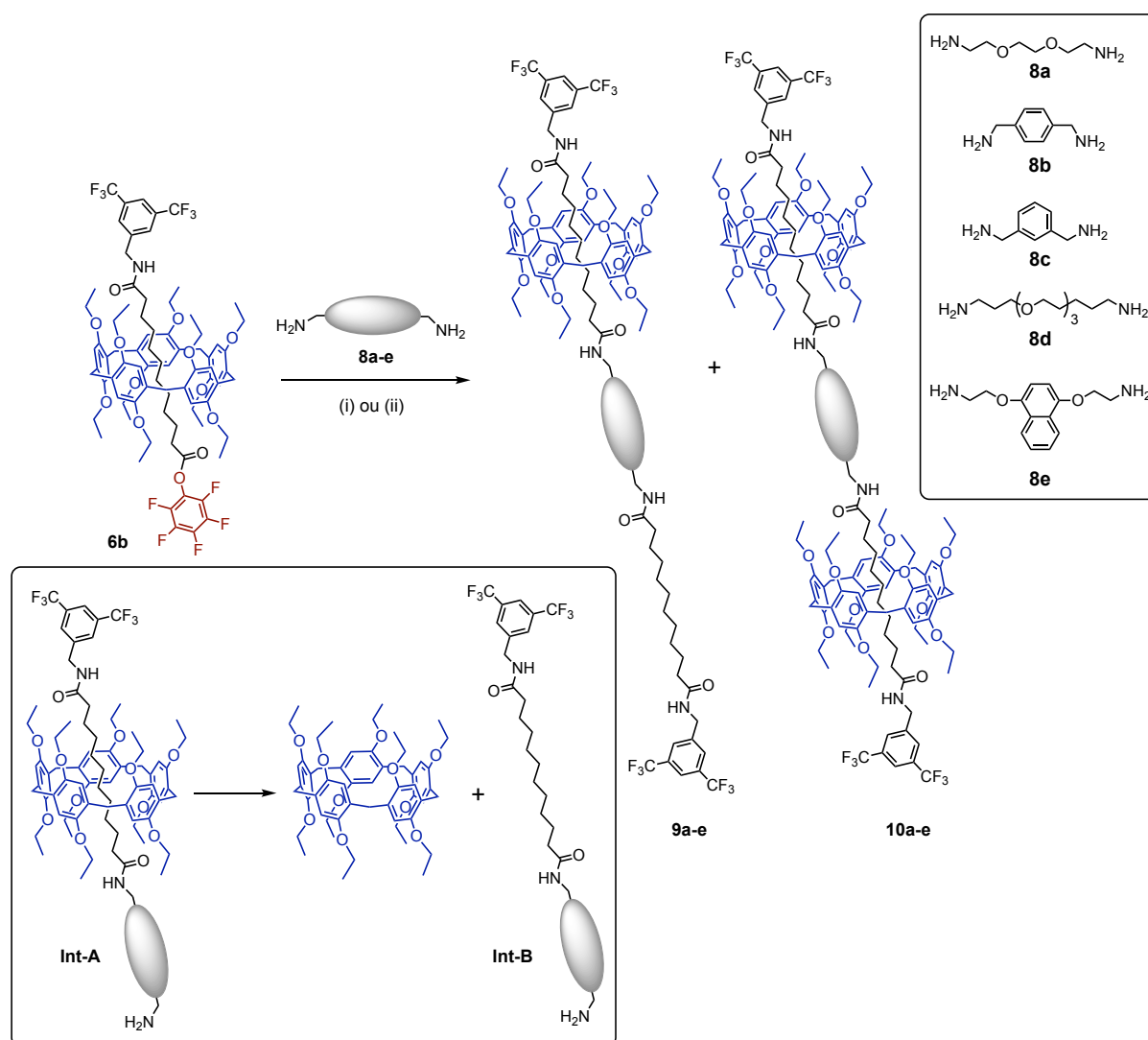


Figure 5. Préparation de [2] et [3]rotaxanes par réaction de **6b** avec des diamines. (i) THF (**9a**: 93% à partir de **8a**; **9b**: 94% à partir de **8b**; **9c**: 89% à partir de **8c**; **9d**: 95% à partir de **8d**; **10e**: 99% à partir de **8e**). (ii) Sans solvant; Ball-Mill [**9a**: 72% et **10a**: 24% (à partir de **8a**); **9b**: 50% et **10b**: 47% (à partir de **8b**); **9c**: 29% et **10c**: 68% (à partir de **8c**)].

Une première acylation entre une diamine et **6b** produit un pseudo-rotaxane intermédiaire **Int-A** avec une fonction amine terminale. Le résultat de la réaction dépend alors de la capacité du pillar[5]arène à s'échapper de son axe. Lorsque le réactif diamine est suffisamment volumineux

pour empêcher la dissociation de l'intermédiaire monoacylé comme dans le cas de **8e**, la réaction avec un deuxième équivalent de rotaxane **6b** produit un [3]rotaxane. En revanche, lorsque le réactif diamine est plus petit (**8a-d**), l'intermédiaire **Int-A** se dissocie pour donner **Int-B** et du pillar[5]arène, et la réaction de l'intermédiaire **Int-B** non complexé avec un second équivalent de **6a** produit un [2]rotaxane. Dans ce cas, le [3]rotaxane peut être obtenu si les conditions de réaction sont appropriées pour stabiliser l'intermédiaire pseudo-rotaxane (**Int-A**). En solution, la dissociation de l'intermédiaire **Int-A** est favorisée. En revanche, en effectuant l'échange de bouchons dans des conditions mécano-chimiques sans solvant, la dissociation du complexe d'inclusion de l'intermédiaire **Int-A** est largement limitée, ce qui permet la formation de [3]rotaxanes.

Les rotaxanes **9a-d**, **10a-c** et **10e** ont été caractérisés par spectroscopie RMN confirmant leurs structures proposées. Un exemple est représenté sur la Figure 6. le spectre ^1H RMN de **9b** enregistré dans CDCl_3 à température ambiante a révélé que les deux bouchons 3,5-bis(trifluorométhyl)benzyle de **9b** apparaissent comme équivalents, ce qui suggère des mouvements dynamiques de glissement rapides du pillar[5]arène le long de la chaîne moléculaire du rotaxane. Dans ces conditions, le déplacement dynamique doit être proche de l'échelle de temps de mesure RMN, car les signaux provenant des deux chaînes décyl sont larges. Cela nous a incité à effectuer des mesures RMN en fonction de la température. A basse température, les mouvements dynamiques de glissement sont plus lents que le temps de mesure RMN et les deux moitiés de l'axe de **9b** sont apparues comme non équivalentes dans le spectre ^1H RMN enregistré à 218 K dans le CDCl_3 (Figure 6). Compte tenu de l'effet de blindage important du pillar[5]arène sur les résonances des groupes situés dans sa cavité, il apparaît clairement que le macrocycle est situé sur une station décyl de l'axe, la seconde restant inoccupée.

Dans l'ensemble, des études de RMN à température variable ont révélé que le pillar[5]arène est situé de préférence sur l'une des deux stations décyl des [2]rotaxanes **9a-d**. En revanche, le conformère dans lequel la sous-unité macrocyclique de **9a-d** est située sur l'espaceur centrale de l'axe n'est pas significativement peuplé. De fait, cette station centrale peut être considérée comme l'état de transition pour l'échange dynamique permettant au macrocycle de faire la navette entre les deux différentes stations décyl.

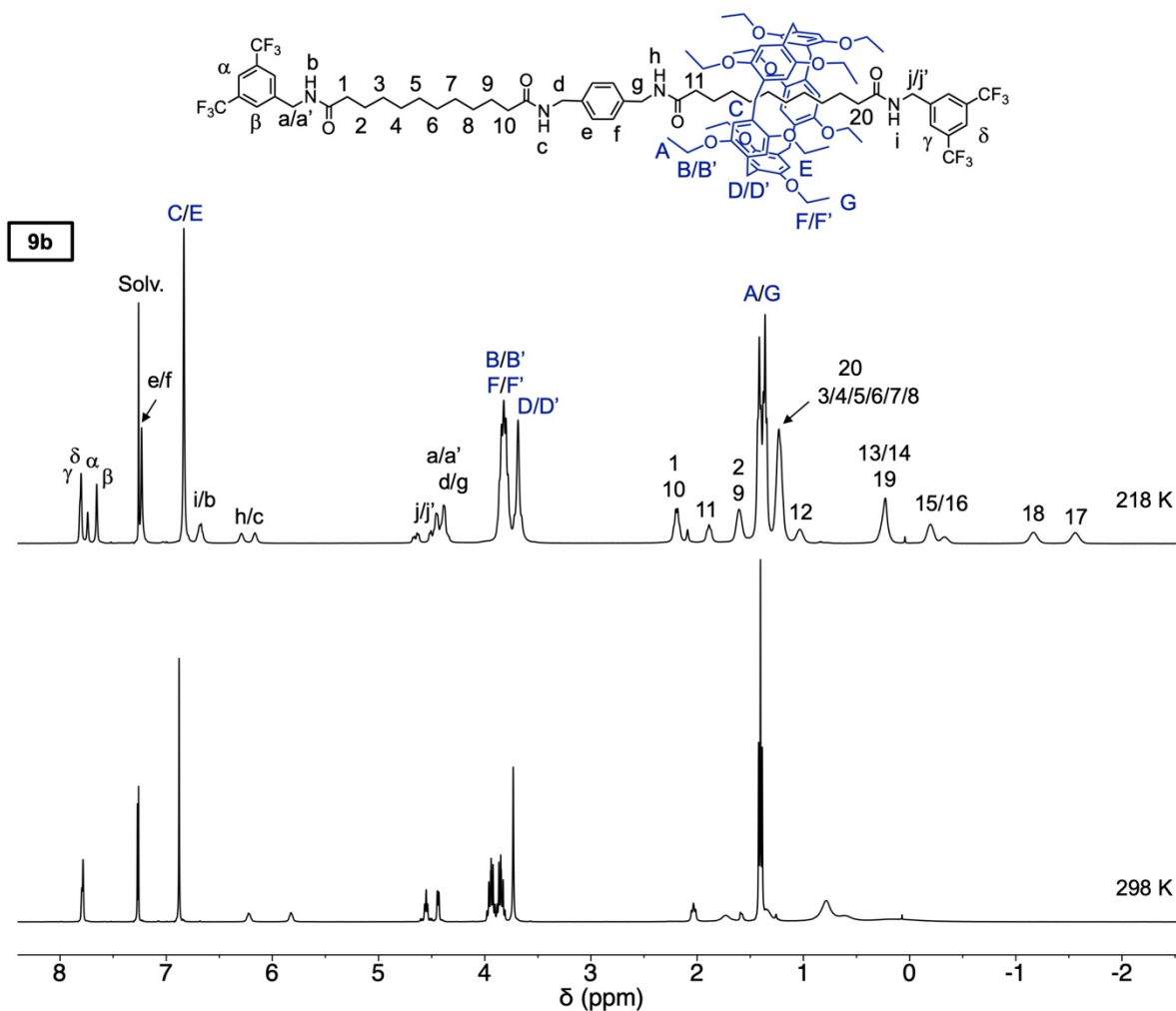


Figure 6. Spectres ^1H RMN (400 MHz) du [2]rotaxane **9b** enregistrés dans CDCl_3 à différentes températures.

IV. Élaboration de machines moléculaires

Enfin, nous avons mis à profit les connaissances acquises dans les sections précédentes pour concevoir de nouvelles machines moléculaires contenant des pillar[5]arènes dans lesquelles les changements de conformation peuvent être contrôlés par un stimulus externe (acide/base).

Afin de concevoir nos navettes moléculaires, nous avons combiné sur l'axe moléculaire une station alkyle (station 1) avec une sous-unité triazole protonable (station 2) et un connecteur de type tétraéthylène glycol entre ces deux stations. Ces [2]rotaxanes sont présentés dans la Figure 7.

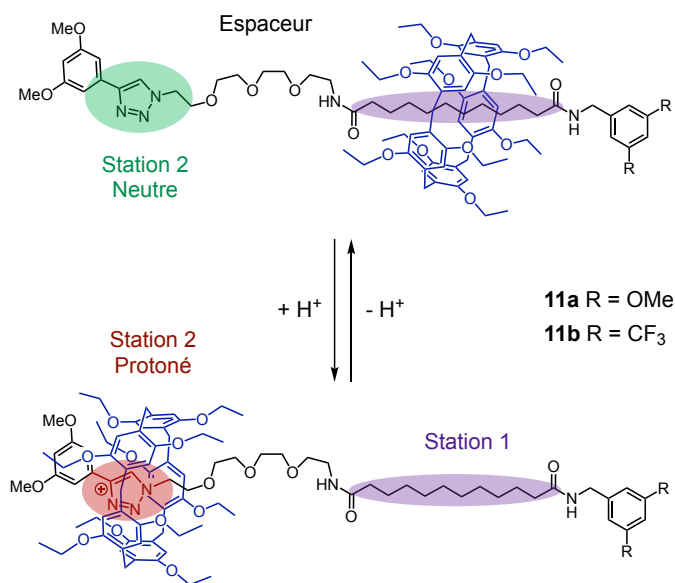


Figure 7. [2]Rotaxanes **11a-b** au sein desquels la position du pillar[5]arène sur son axe peut être contrôlée par protonation/déprotonation du triazole terminal.

À l'état neutre, le pillar[5]arène est localisé préférentiellement sur la station décyle de l'axe au sein des rotaxanes **11a-b**. Des interactions CH- π entre les groupements méthylènes et la cavité du macrocycle favorisent ce positionnement. Après l'ajout d'un acide permettant la protonation du cycle triazole, le pillar[5]arène se déplace vers la station triazolium. Le pillar[5]arène forme un complexe de transfert de charge avec le groupement aromatique cationique protoné. L'énergie d'interaction de pillar[5]arène avec la station cationique est de fait plus élevée que dans la forme neutre. Par conséquent, la station triazolium est aussi peuplée. Ce processus est parfaitement réversible, l'addition d'une base permettant de déprotoner le triazolium conduit au glissement du pillar[5]arène vers sa position initiale. Les équilibres conformationnels des navettes moléculaires **11a-b** dans leur état neutre et protoné ont été entièrement élucidés par des études RMN à température variable. Un résumé de tous les résultats expérimentaux est présenté à la Figure 8. Enfin, des études spectroscopiques détaillées appuyées par des calculs DFT nous ont permis de comprendre pleinement la conformation de ces systèmes dans leurs états neutres et protonés.

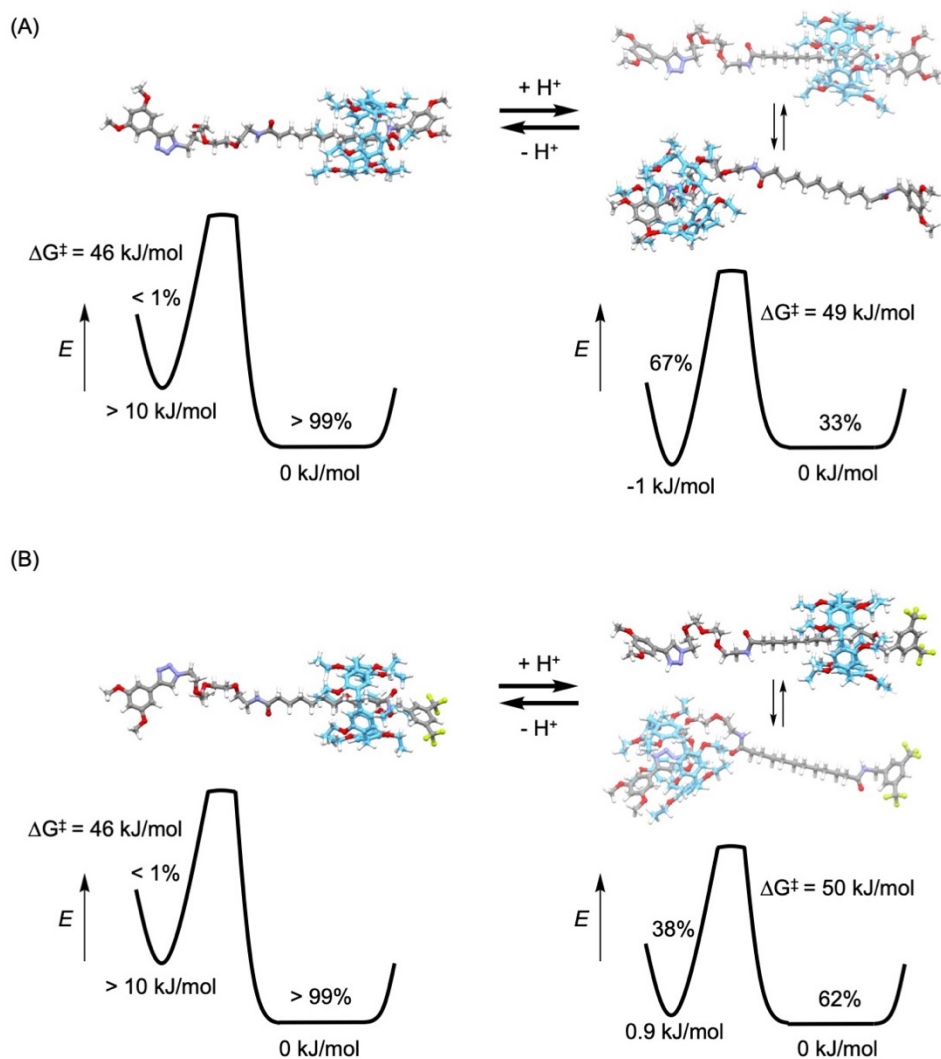


Figure 8. Représentation des énergies potentielles de **11a** (A) et **11b** (B) à l'état neutre et à l'état protoné déduites à partir des études ^1H RMN à température variable; les niveaux d'énergie et la proportion des conformères sont donnés à 223 K ; les valeurs de l'énergie libre d'activation (ΔG^\ddagger) pour l'échange dynamique sont celles obtenues à la température de coalescence (223 K à l'état neutre et 243 K à l'état protoné).

V. Conclusion générale

Ce travail de thèse a permis de montrer tout le potentiel de la stratégie de synthèse développée dans notre groupe pour la synthèse de rotaxanes par des réactions d'échange de bouchons. Nous avons ainsi montré qu'un [2]rotaxane possédant deux bouchons activés peuvent être mono-fonctionnalisés avec des rendements quasi-quantitatifs. Les dérivés de [2]rotaxanes mono-fonctionnalisés peuvent alors être utilisés pour conduire soit à des [2]rotaxanes, soit à des [3]rotaxanes, suivant la nature de la diamine utilisée. Ces méthodes de

synthèse ont alors été utilisées pour la préparation de machines moléculaires. Nous avons montré que la position du pillar[5]arène au sein des rotaxanes peut être contrôlée par un stimulus acide-base.

Table of contents

Chapter 1	1
<i>Introduction</i>	
I-1. History of mechanically interlocked molecules	2
I.2. General strategies for the synthesis of rotaxanes	5
I.2.1. Threading - Stoppering (capping) approach	5
I.2.2. Clipping approach	9
I.2.3 Slipping approach	11
I.2.4. Active metal template	13
I.2.5. Stopper exchange	15
I.3. Molecular machines	19
I.5. Research plan	26
I.6. References	27
Chapter 2	32
<i>Stepwise functionalization of pillar[5]arene-containing [2]rotaxane building blocks with pentafluorophenyl ester stoppers</i>	
II-1. Introduction	32
II-2. Results and discussion	34
<i>Preparation of the key building blocks</i>	34
<i>Mono-functionalization of building blocks 1 and 5</i>	35
<i>Preparation of dissymmetrical rotaxane 12</i>	43
<i>The pillar[5]arene as a protecting group</i>	45
<i>Conformational analysis</i>	47
II-3. Conclusion	63

II-4. References	63
------------------	----

Chapter 3	67
------------------	-----------

***Preparation of pillar[5]arene-containing [2] and [3]rotaxanes
by a stopper exchange strategy***

III-1. Introduction	67
---------------------	----

III-2. Results and discussion	68
-------------------------------	----

<i>Stopper exchange with diamine reagents in solution</i>	68
---	----

<i>Stopper exchange with diamine reagents under solvent-free ball-milling conditions</i>	70
--	----

<i>Characterization of the rotaxanes</i>	73
--	----

<i>DFT calculations</i>	83
-------------------------	----

<i>Characterization of the [3]rotaxanes</i>	88
---	----

III-3. Conclusion	91
-------------------	----

III-4. References	91
-------------------	----

Chapter 4	93
------------------	-----------

Pillar[5]arene-containing molecular shuttles

IV-1. Introduction	93
--------------------	----

IV-2. Results and discussion	94
------------------------------	----

<i>Synthesis</i>	94
------------------	----

<i>Characterization of the new compounds in the neutral state</i>	96
---	----

<i>Binding studies</i>	101
------------------------	-----

<i>Protonation of model compounds</i>	102
---------------------------------------	-----

<i>Protonation of molecular shuttles 24a-b</i>	106
---	-----

<i>DFT calculations</i>	115
-------------------------	-----

<i>Electrochemistry</i>	122
-------------------------	-----

IV-3. Conclusion	128
------------------	-----

IV-4. References	128
------------------	-----

Chapter 5	130
------------------	-----

Conclusion

Chapter 6	131
------------------	-----

Experimental section

VI-1. General	131
VI-2. Synthesis	131
VI-3. Binding studies	167
VI-4. Electrochemistry	179
VI-5. DFT calculations	179
VI-6. X-ray crystal structures	185

Introduction

Mechanically interlocked molecules (MIMs) are exotic molecular species.^{1,2} Typical examples are rotaxanes and catenanes (Figure 1). In general, these interlocked molecules are composed of molecular subunits linked together by mechanical bonds and their synthesis remains challenging as their preparation requires the pre-organization of molecular components in appropriate supramolecular ensembles.^{3,4} MIMs played a central role in the development of the field of molecular machines with the seminal work of Sauvage and Stoddart.^{5,6}

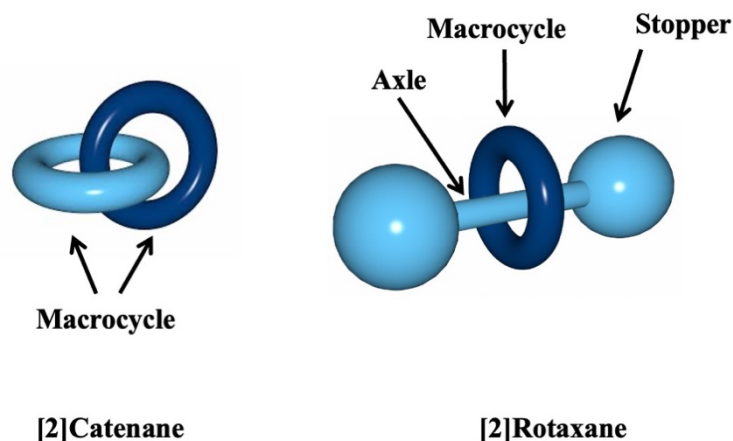


Figure 1. Schematic representations of a [2]catenane composed by two interlocked macrocycle (left) and a [2]rotaxane composed by a macrocycle and a molecular axle terminated by stoppers preventing the dissociation of the two components (right).

The names “catenanes” and “rotaxanes” are derived from Latin words: *catena* meaning "chain", *rota* and *axis* respectively meaning "wheel" and "axle". The number in square brackets at the beginning of the name indicates the total number of molecular components. A catenane is composed by at least two mechanically interlocked macrocycles. Owing to the mechanical link in the catenane structure, separation of the macrocycles is not possible without breaking a chemical bound to open one of the components. A rotaxane comprises a macrocycle (one or more) threaded by an axle like molecular entity, or ‘dumbbell’, with endgroups (stoppers) that are too bulky for the macrocycle to transgress.²

I-1. History of mechanically interlocked molecules

Historically, the first known mention to mechanical bonds was discussed prior to 1912 by Wilstätter during a symposium in Zürich but the idea did not appear in the chemical literature until 1953.⁷ In 1961, Frisch and Wasserman were the first to discuss the connection between MIMs and stereochemistry, a field also called *chemical topology*.⁸ As far as their synthesis is concerned, the first claim to a successful catenane synthesis was published in 1960, while the first rotaxane synthesis was reported in 1967.^{9,16} In both cases, the preparation of the MIM was based on a statistical method.²

Catenanes. The first [2]catenane was prepared by E. Wasserman in 1960.⁹ The synthesis was achieved by macrocyclization of a diester through sodium-mediated acyloin condensation in the presence of a deuterated cyclohydrocarbon (Figure 2). However, this statistical approach gave a very low yield (0.0001%, assessed by infrared spectroscopy) and no definitive structural proof was presented. This work was very recently revisited by D. Leigh and co-workers.¹⁰ They repeated the synthesis on a large scale. They were then able to isolate and prove the structure of the putative [2]catenane by using modern analytical tools.

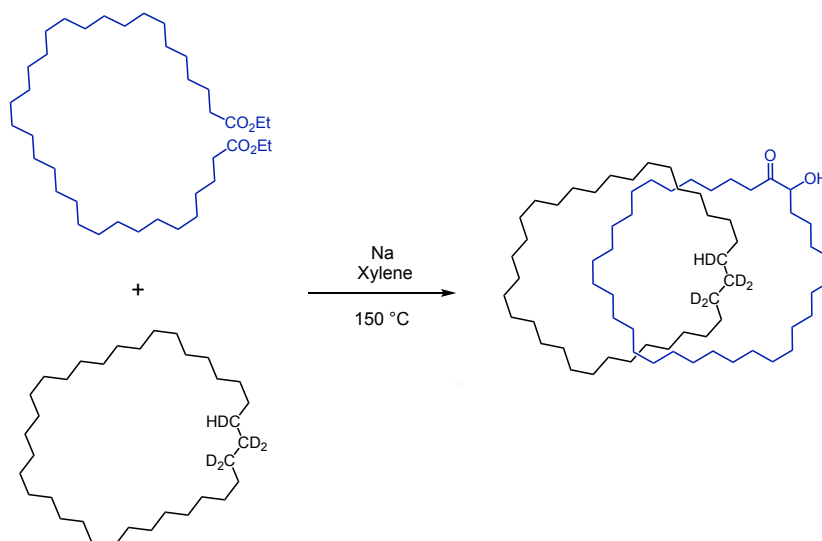


Figure 2. First synthesis of a [2]catenane developed by E. Wasserman in 1960.^{9,10}

Shortly after Wasserman's report, G. Schill and A. Lüttringhaus proposed an elegant directed approach based on the catenation of two macrocycles connected to each other by a covalent bond, leading to small amounts of catenanes.¹¹ An important advance in the synthesis of catenanes was made by C. O. Dietrich-Buchecker and J.-P. Sauvage in 1983 (Figure 3).¹² They proposed the use of a metal template, namely copper (I), to gather and pre-organize the chelating organic moieties in an

interlocking way prior to ring cyclisation and demetallation to give the metal-free catenane. This preorganization is referred to as "template effect" or "matrix effect" and afforded a [2]catenane in 42% yield.

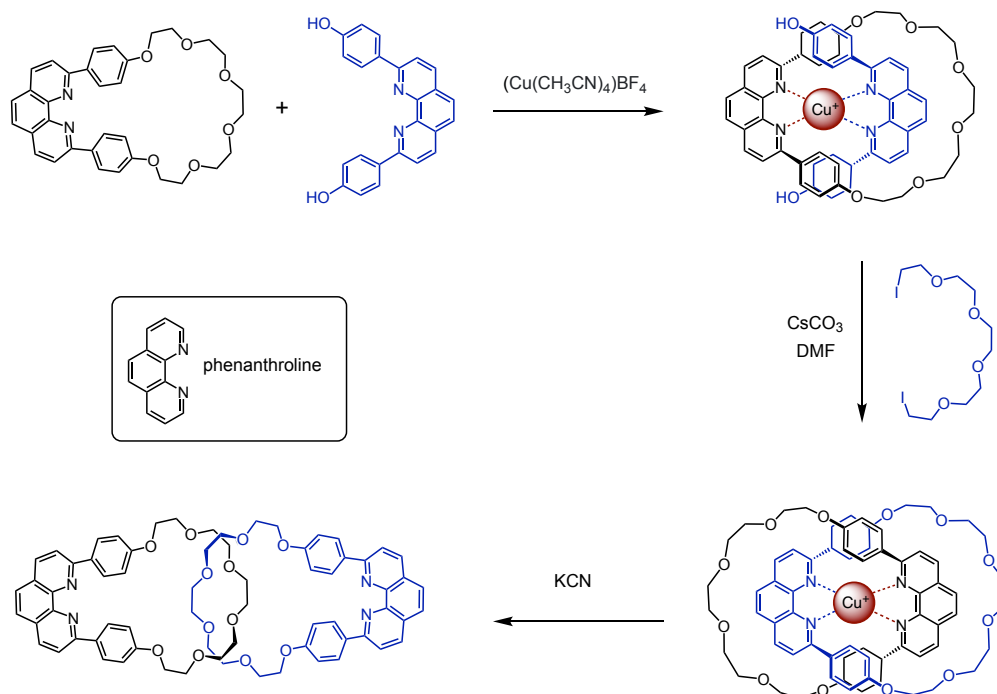


Figure 3. First synthesis of a [2]catenane developed by C.O. Dietrich-Buchecker and J.-P. Sauvage based on the template effect.¹²

Subsequently, other catenanes have been synthesized based on the template effect. We can mention here the work of J. F. Stoddart for which the building blocks are preorganized via electron donor-acceptor interactions,¹³ as well as the work of C. A. Hunter and F. Vögtle who independently described the syntheses of two very similar catenanes based on hydrogen bonding and π - π interactions.^{14,15}

Rotaxanes. The first synthesis of a [2]rotaxane was performed by I. T. Harrison and S. Harrison in 1967 using a statistical method.¹⁶ They proposed calling this type of compound a *hooplane*. They proceeded as follows: the macrocycle was grafted onto a resin in order to perform successive cycles of a statistical stoppering by reaction of 1,10-decanediol (the axle) with trityl chloride (the stopper) in the presence of the modified resin. After 70 cycles, the products were released from the resin by hydrolysis. The [2]rotaxane was then isolated in 6% yield by column chromatography (Figure 4).

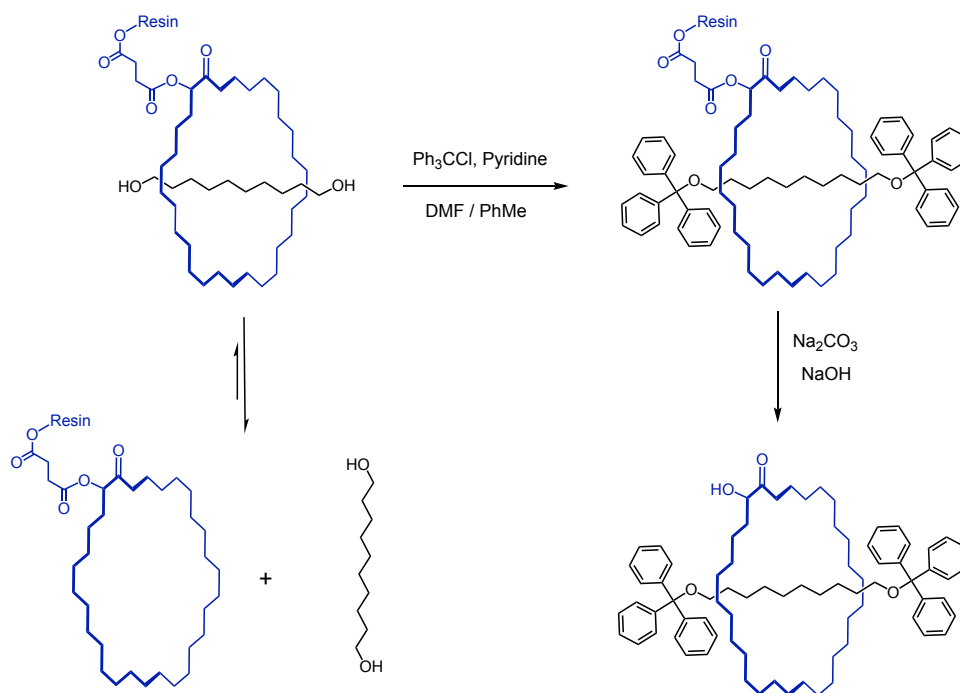


Figure 4. First synthesis of a [2]rotaxane using a statistical approach.¹⁶

The term rotaxane was later adopted as suggested by G. Schill who described the first directed synthesis of a rotaxane in 1969.¹⁷ This ingenious strategy, involved the use of covalent bonds as templates. He synthesized a bis-macrocycle with two functionalized chains hooked on either side of the bis-macrocycle plane. The introduction of bulky end groups and cleavage of the oriented covalent bonds afforded the free [2]rotaxane (Figure 5). Despite Schill's elegant approach, this strategy resulted in a multi-step synthetic route and low yields.

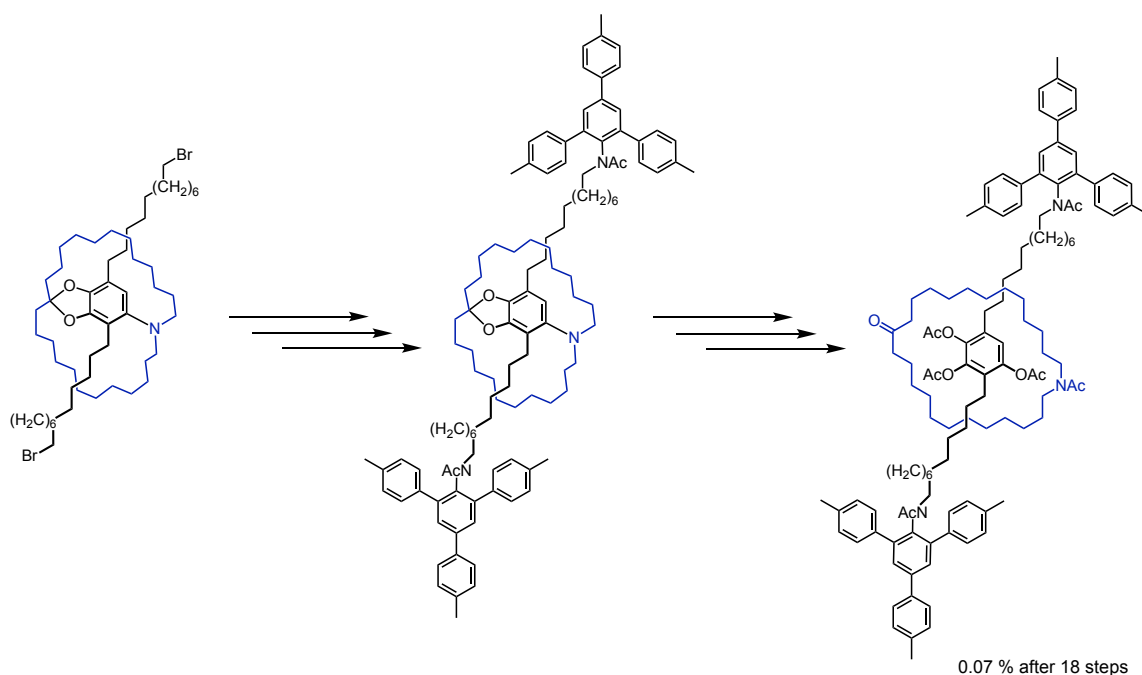


Figure 5. Strategy used by G. Schill for the first directed rotaxane synthesis.¹⁷

Mechanically interlocked molecules (MIMs) such as catenanes and rotaxanes have fascinated topological chemists for decades, and their challenging syntheses continue to inspire them. The development of new interlocked architectures, especially rotaxane structures, is part of the motivation for this PhD project. In particular, our research focuses on the preparation of rotaxanes incorporating a pillar[5]arene subunit. These macrocycles are *para*-cyclophane derivatives composed of five 1,4-disubstituted hydroquinone subunits linked by methylene bridges in their 2,5-positions. The pillararenes are symmetrical tubular-shaped compounds with two identical rims.¹⁸⁻²⁶ Following the first report in 2008, these receptors have been extensively used in the field of supramolecular chemistry leading to a rich set of assemblies for various applications.²

I.2. General strategies for the synthesis of rotaxanes

Since the discovery of the first rotaxane, several efficient synthetic approaches have been developed to assemble building blocks into rotaxane structures in a way that makes it impossible to unthread the macrocycle from the dumbbell components once the rotaxanes are formed.^{27,28} In the following sections, these synthetic approaches will be discussed and illustrated with some selected examples with a special focus on pillar[5]arene-containing systems as they are directly related to the experimental work of the present thesis.

I.2.1. Threading - Stoppering (capping) approach

Threading involves mixing linear and macrocyclic components to form a self-assembled pseudorotaxane.^{29,30} Stoppering involves attaching bulky groups to both ends of the axle of a pseudorotaxane in order to prevent the macrocycle from deslipping (Figure 6).



Figure 6. Graphical representation of a [2]rotaxane formed by the "capping" approach.

The first successful [2]rotaxane formed on the basis of this approach, was published by H. Ogino in 1981, who used metal-ligand complexation to stopper a 1,12-diaminododecane/ α -

cyclodextrin (α -CD) pseudorotaxane (Figure 7).³¹ In DMSO, the 1,12-diaminododecane is stabilized inside the (α -CD) through hydrophobic effects, producing the formation of a pseudorotaxane. Two amine/ Co^{III} complexes are subsequently formed based on the terminal amines and the cobalt (III) salt, thus allowing the cyclodextrin to be locked onto the axle and the [2]rotaxane was isolated in 19% yield.

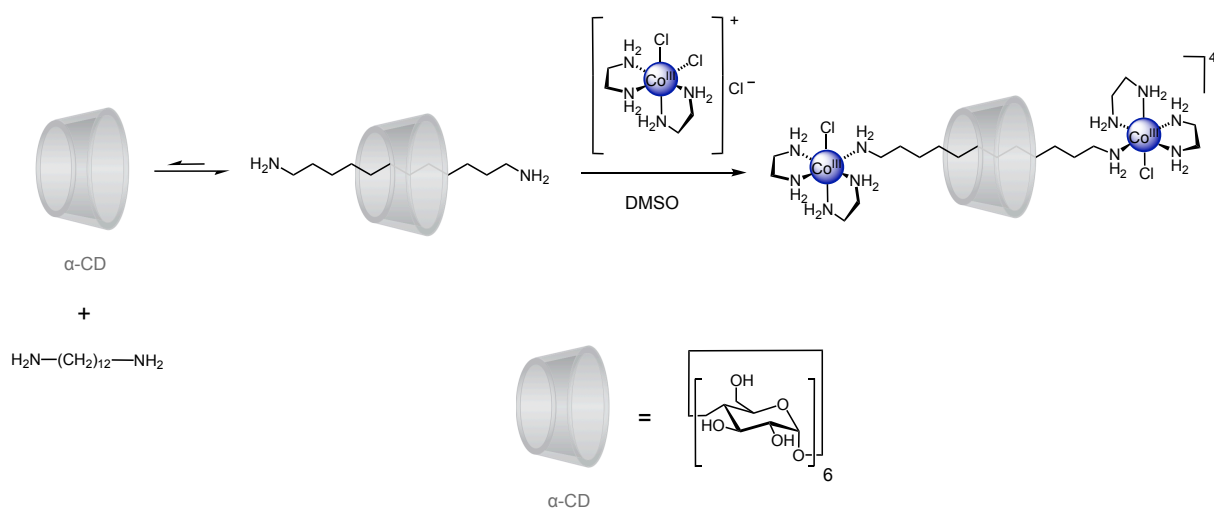


Figure 7. Ogino's [2]rotaxane synthesis by "capping" strategy.³¹

A key point for obtaining high yields in rotaxanes resides in the use of a *templated* synthesis that will drive the system towards the formation of the interlocked species and favor it over the independent components. This can be done either through coordination to a metal cation or through interactions between the macrocycle and the axle, or their precursors (e.g., hydrogen bonds, aromatic donor-acceptor interactions, or hydrophobic interactions).³²⁻³⁵ A few examples of rotaxanes prepared by the stoppering approach³⁶⁻³⁸ are depicted in Figure 8.

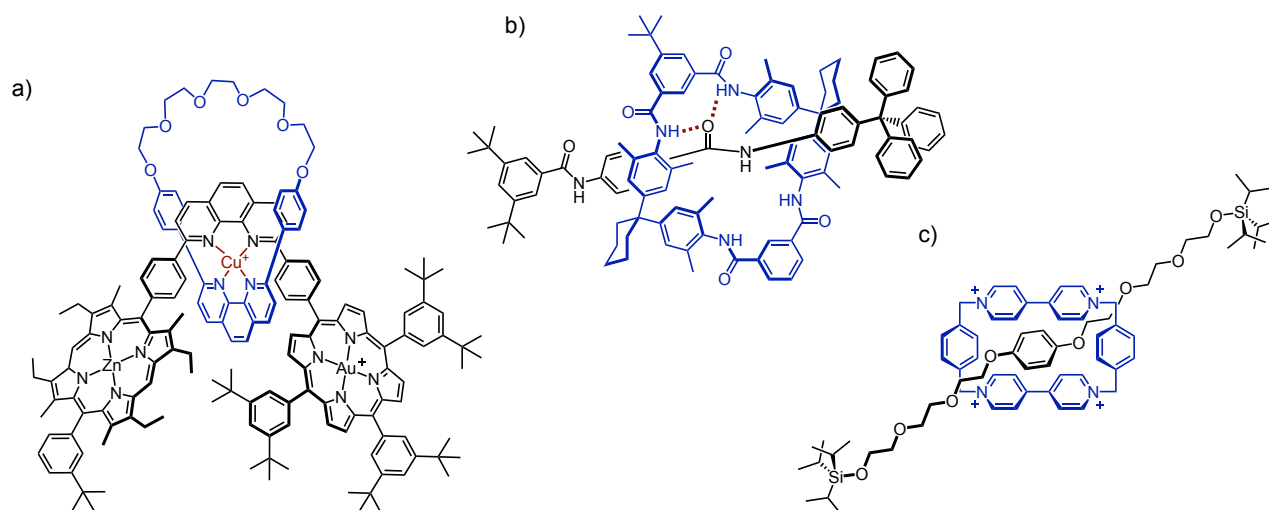


Figure 8. Examples of [2]rotaxanes assembled by the "capping" approach. The preorganization of the system was achieved by (a) a copper(I) template³⁶, (b) hydrogen bonding,³⁷ (c) π -donor/ π -acceptor interactions.³⁸

Copper(I) can be used as a templating agent as described for the synthesis of catenanes in the previous section. As copper(I) preferentially forms tetrahedral complexes, coordination with two bidentate chelates gives complexes whose ligands are orthogonal to each other and thus ideally preorganized for the formation of an interlocked species (Figure 8a), this process has been extensively explored by the group of J.-P. Sauvage.³⁶ Other assembling methods involving non-covalent interactions between the ring and dumbbell precursors have been widely exploited. For instance, F. Vögtle and co-workers³⁷ designed a macrocycle containing amides and an axle that interact through multiple hydrogen bonds (Figure 8b). Similarly, rotaxanes can be assembled based on aromatic donor-acceptor interactions between the axle and the macrocycle (Figure 8c), this method has been extensively exploited by the group of J. F. Stoddart.³⁸

This approach has been also used for the preparation of pillar[5]arene-containing rotaxanes.³⁹ The first example has been reported by J. F. Stoddart and is depicted in Figure 9.⁴⁰ The [2]rotaxane was synthesized from the host-guest complex formed between 1,4-dimethoxypillar[5]arene and 1,8-diaminooctane by reacting the primary amino groups of the guest with 3,5-di-tert-butylbenzaldehyde. Subsequent reduction of the diimine with NaBH₄ in THF afforded the [2]rotaxane in 7% yield.⁴⁰

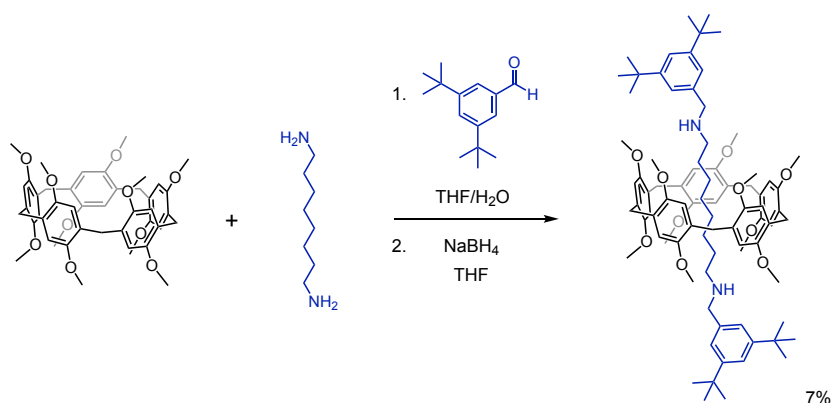


Figure 9. Preparation of the first pillar[5]arene-containing [2]rotaxane by "capping" strategy.⁴⁰

Following this first example, several other pillar[5]arene-based rotaxane constructed by the stoppering approach have been reported.⁴¹⁻⁴³ As part of this research, our group has investigated in details the preparation of [2]rotaxanes from the reaction of host-guest complexes obtained from a pillar[5]arene derivative and diacyl chloride with amine reagents (Figure 10).⁴⁴

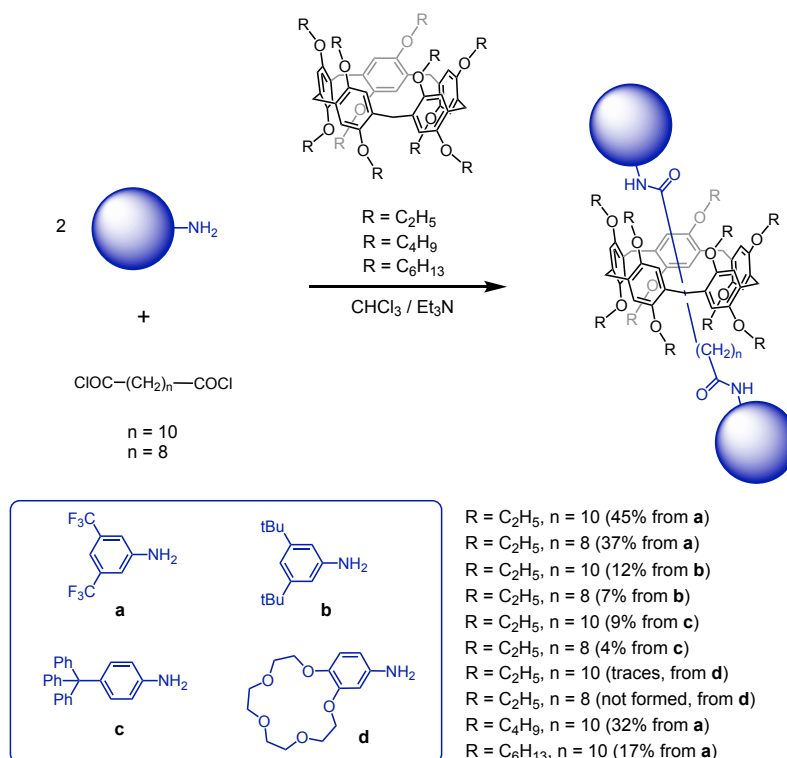


Figure 10. Typical examples of pillar[5]arene-based [2]rotaxanes obtained from the reaction of diacyl chloride reagents with various amine stoppers.⁴⁴

The yields in [2]rotaxanes has been found sensitive to the reaction conditions (solvent, stoichiometry and temperature). Moreover, the nature of the amine reagent plays also an important role in the outcome of the reactions as it modulates the affinity of the monoacylated intermediates for the

pillar[5]arene (Figure 11).⁴⁵ The reaction is efficient when electron-deficient stoppers are introduced as they give rise to attractive interactions with the electron-rich pillar[5]arene host thus contributing to increase the K'_a values. In contrast, rotaxanes with electron-rich stoppers cannot be obtained under these conditions due to unfavorable interactions between the mono-acylated intermediate and the macrocycle. This dependence on the nature of the stopper represents actually a major limitation for the synthesis of rotaxanes incorporating pillar[5]arene macrocycles by a stoppering approach.

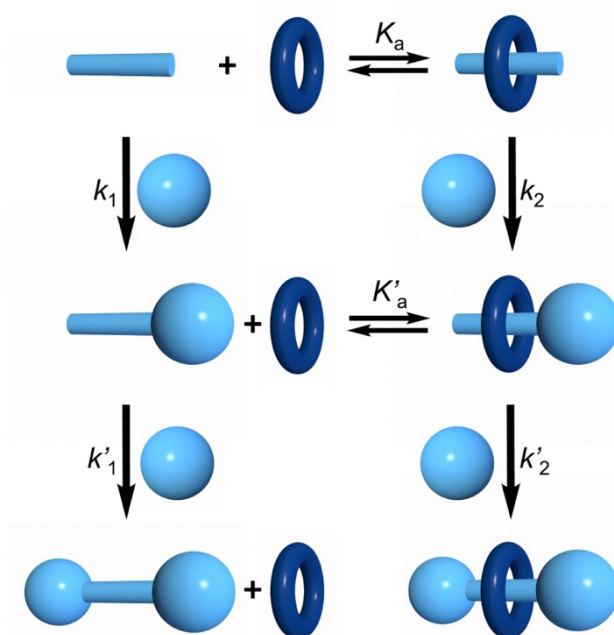


Figure 11. Schematic illustration of the formation of a [2]rotaxane based on a pillar[5]arene derivative. The yield of [2]rotaxane is related to the binding constant K'_a for the formation of the inclusion complex between the mono-acylated intermediate and the pillar[5]arene.⁴⁵

1.2.2. Clipping approach

The "clipping" approach⁴⁶ involves the macrocyclization of an open macrocycle component around a dumbbell-shaped component. First, complexation between the partially formed macrocycle and the dumbbell occurs through supramolecular interactions, followed by a macrocycle-closing reaction to form the rotaxane (Figure 12).

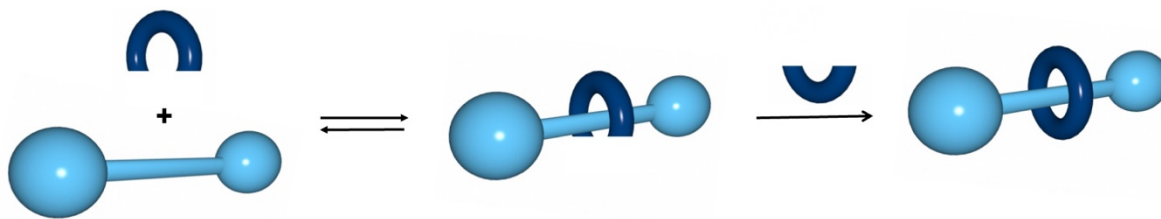


Figure 12. Schematic representation of a [2]rotaxane formed by the "clipping" approach.

In 2007, J. F. Stoddart and co-workers developed an efficient template-directed, thermodynamically controlled clipping approach for the preparation of [2]rotaxanes. The condensation of 2,6-pyridinedicarboxaldehyde and tetraethyleneglycol bis(2-aminophenyl)ether in presence of the dumbbell-shaped compound containing a dialkylammonium ion recognition site, forms selectively and near quantitatively a [24]crown-8 ring that becomes clipped onto the dumbbell. Such thermodynamically controlled, template-directed amplification is driven by a series of noncovalent bonding interactions that include $[N^+-H\cdots X]$ ($X = O$ or N) and $[N^+C-H\cdots O]$ hydrogen bonds and aromatic $\pi-\pi$ interactions between the dumbbell and the ring. The thermodynamic product, a [2]rotaxane, was converted into a stable [2]rotaxane by reduction of the two imine bonds (Figure 13).⁴⁷

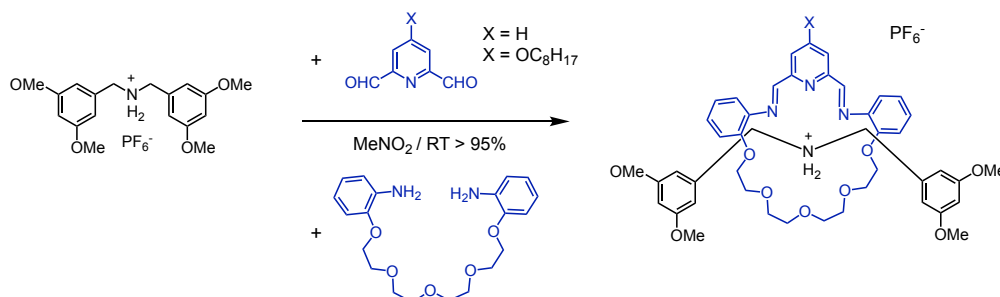


Figure 13. Stoddart's [2]rotaxane synthesis using the "clipping" strategy.⁴⁷

In this context, we can also mention the work of Y. Li and co-workers, who exploited a synthesis method for the construction of a macrocycle and an interlocked rotaxane via a thiol-yne reaction. The dumbbell-shaped thread containing a secondary dialkylammonium ion has been used as a template, interlocking the macrocyclic polyether moiety terminated with two thiol groups which would react with the alkyne terminus of propargyl paratoluate. The template-induced clipping reaction has been carried out under the irradiation of UV light. The reaction proceeds in good yield (75%) in an air atmosphere under ambient conditions in CH_2Cl_2 (Figure 14).⁴⁸

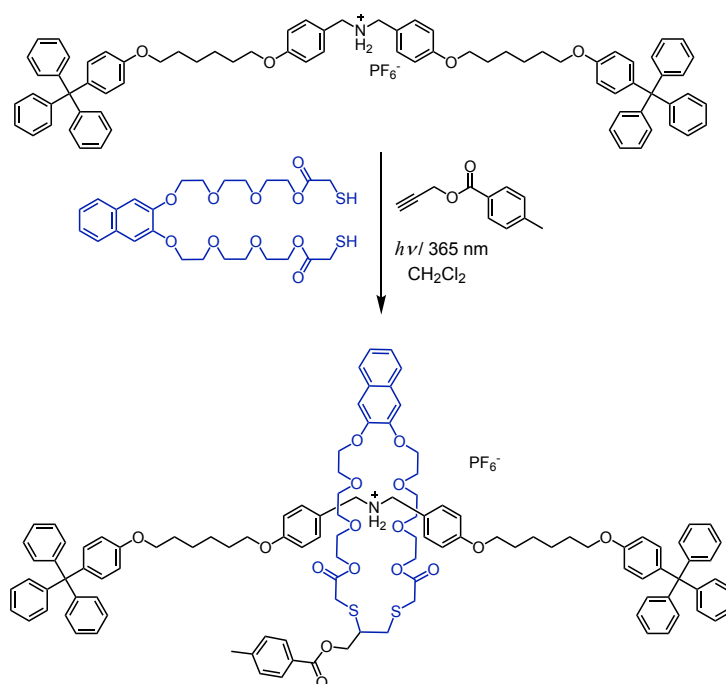


Figure 14. Rotaxane synthesis via the clipping approach.⁴⁸

This clipping approach is an effective tool for the construction of rotaxanes in interesting yields and remains important for scientists in this field,^{49,50} however it remains limited for a very few types of macrocyclization reactions.

1.2.3 Slipping approach

In this approach, the macrocycle and dumbbell components are synthesized separately. This method is based on a finely tuned size complementarity between the macrocycle and the stoppers, so that the macrocycle can bypass the stoppers only when sufficient energy is applied in the form of heat or pressure to provide a kinetically stable rotaxane under ambient conditions (Figure 15).⁵¹



Figure 15. Schematic representation of a [2]rotaxane formed by the "Slipping" approach.

One of the first examples of rotaxane synthesis using this approach has been reported by the group of J. F. Stoddart. The formation of the rotaxane is based on the size complementarity between

the macrocyclic polyether, bisparaphenylene-34-crown-10, containing two π -electron-rich recognition sites, and the stoppers consisting of suitably substituted tris(aryl)methyl groups linked to a dumbbell-shaped molecule containing a 4,4'-bipyridinium as the corresponding π -electron-deficient binding site. While no rotaxane is formed at room temperature, "threading" occurs at 55°C, and as the temperature decreases, the rotaxane becomes more stable (Figure 16).⁵²

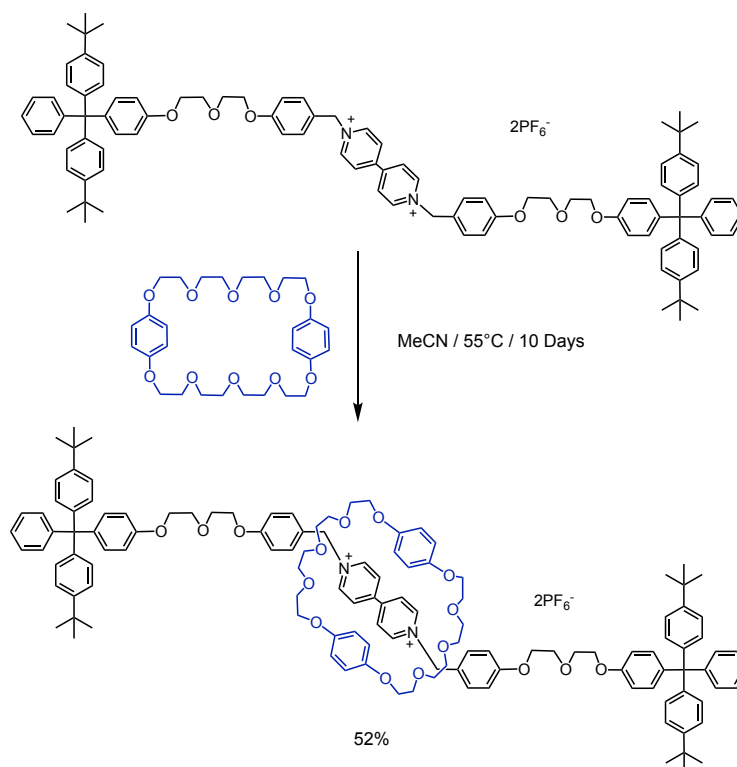


Figure 16. Stoddart's [2]rotaxane synthesis using the "slipping" strategy.⁵²

In 2016, the group of Ogoshi has successfully synthesized a pseudo[2]rotaxane system via a slippage approach, which is the first example of synthesis of pillar[5]arene-based pseudorotaxanes via this method. The formation of pseudo[2]rotaxane did not occur at 25 °C, and heating at 50 °C is necessary but the system did not reach thermodynamic equilibrium even after 600 hours. At 70°C, the equilibrium conversion to the pseudo[2]rotaxane was 51%. The conversion to pseudo[2]rotaxane decreased with increasing reaction temperature. The dumbbell contained reactive azido moieties at both ends; thus, a bulky stopper could be installed by the CuAAC reaction between the azido moieties in the dumbbell and the alkyne in the bulky stopper. Thermally stable [2]rotaxanes could be obtained by the slippage method followed by end-capping reactions via the CuAAC reaction in liquid pillar[5]arene. T. Ogoshi's group also demonstrated the solvent effect on the conversion to pseudo[2]rotaxane. The pseudo[2]rotaxane has not been observed by heating the dumbbell with liquid pillar[5]arene in CDCl₂CDCl₂ as solvent, whereas it was produced in the absence of CDCl₂CDCl₂.

Complete dissociation of pseudo[2]rotaxane was observed on heating in $\text{CDCl}_2\text{CDCl}_2$ at 100°C . (Figure 17).^{53,54}

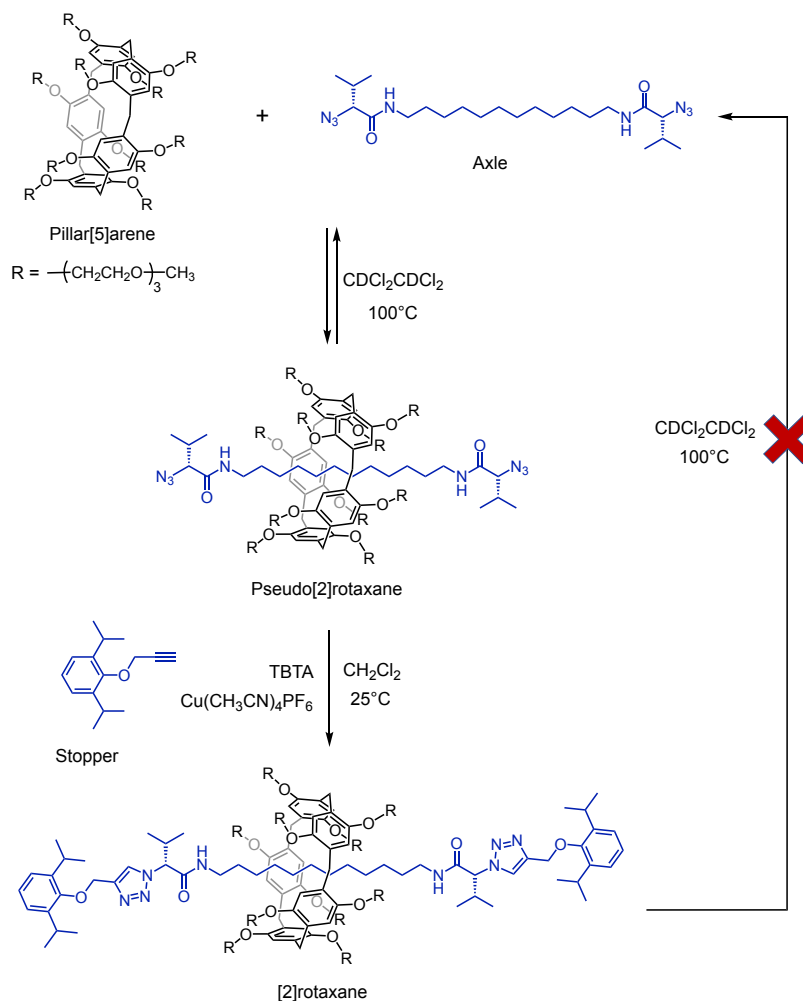


Figure 17. Ogoshi's [2]rotaxane synthesis using the "slipping" strategy.⁵³

This slipping method is unique among all other approaches because it does not involve the formation and breaking of chemical bonds. As suggested by its name, this method allows the macrocycle to slip along the axle, which requires precise control of the cavity and stopper sizes.⁵⁵ The thermal energy must be sufficient to allow the macrocycle to cross the energy barrier of the stopper steric hindrance. However, the stabilization provided after the reaction, i.e. when the macrocycle is around the axle, must be strong enough to prevent deslipping.⁵⁶ As a result, this method is not currently widely used to design interlocked molecules.

1.2.4. Active metal template

This approach is one of the most recent methods, it consists in using a metal, chelated in the center of a macrocycle in which the metal serves to pre-organize the different parts of the rotaxane.⁵⁷

At the same time, the metal plays an active role in the formation of the last covalent bond of the axle leading to the formation of a rotaxane (Figure 18).

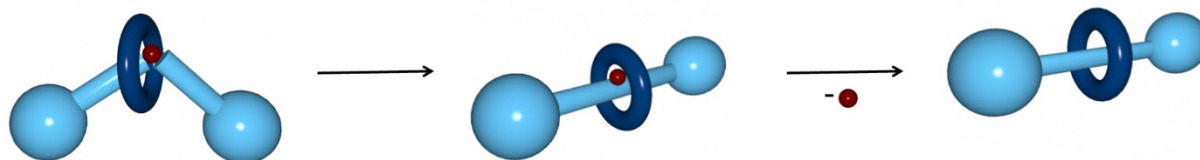


Figure 18. Schematic representation of a [2]rotaxane formed by an active metal template approach.

For example, Leigh's group synthesized [2]rotaxanes using a Pd(II)-catalyzed cross-coupling reaction. Chelation of Pd(II) within the macrocycle followed by transmetalation with a boronic acid- allows the positioning of the first unit on one side of the macrocycle. The π coordination between the alkene and the metal takes place on the opposite side of the molecule due to steric constraints. A migratory insertion followed by β -hydride elimination allows the formation of the conjugated alkene within the cavity and consequently the [2]rotaxane is formed in 73% yield. Since the Heck reaction liberates a Pd(0) species and only the metal cation Pd(II) is chelated by the macrocycle, the palladium oxidation with benzoquinone (BQ) in O_2 allows a truly catalytic turnover (Figure 19).⁵⁸

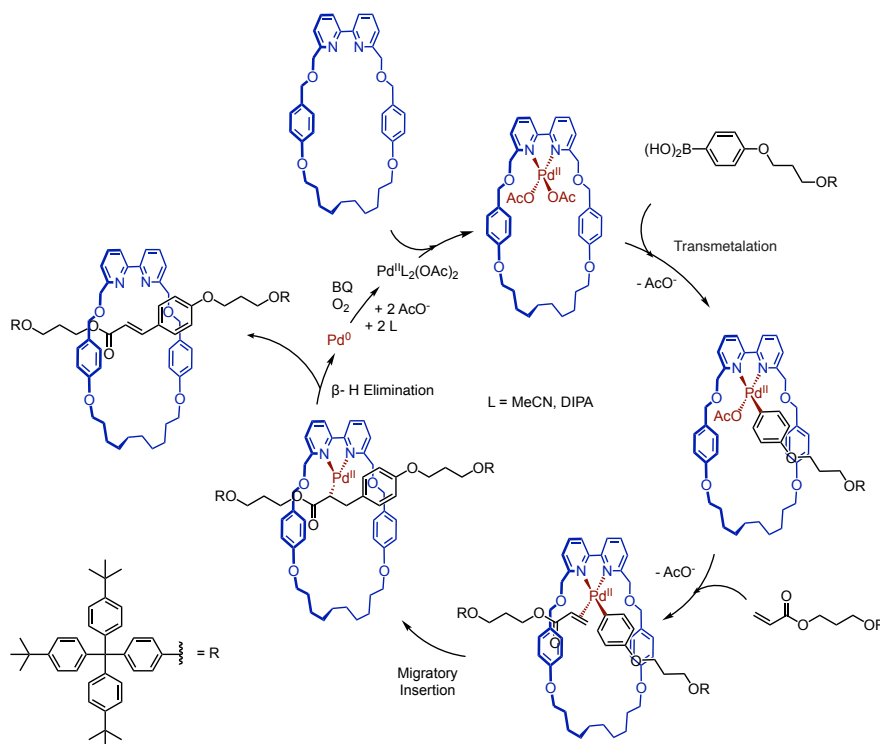


Figure 19. Proposed mechanism of Leigh's active palladium template synthesis of [2]rotaxanes.⁵⁸

The active model metal template approach was independently developed and reported by the groups of D. A. Leigh and S. Saito in 2006.^{59,60} In this approach, the metal template has a dual function: firstly, it assembles and pre-organizes the rotaxane precursors into an intertwined geometry; and secondly, it acts as a catalyst for the formation of the covalent bonds between the dumbbell precursors that will lock the system into the thread architecture. This approach is an interesting way to construct rotaxanes.⁶¹⁻⁶³ However, it remains limited to a few specific macrocyclic building blocks.

1.2.5. Stopper exchange

The last approach is based on the post-modification of a pre-constructed rotaxane structure by a stopper exchange reaction.^{64,70} The first step is to prepare an intermediate rotaxane equipped with activated stoppers, and then stopper exchange is performed to generate the desired rotaxane. Importantly, this second step does not rely on the formation of a host-guest intermediate. It therefore allows for the preparation of rotaxanes difficult or even impossible to prepare by a one-step synthetic approach based on the direct introduction of stoppers (Figure 20).

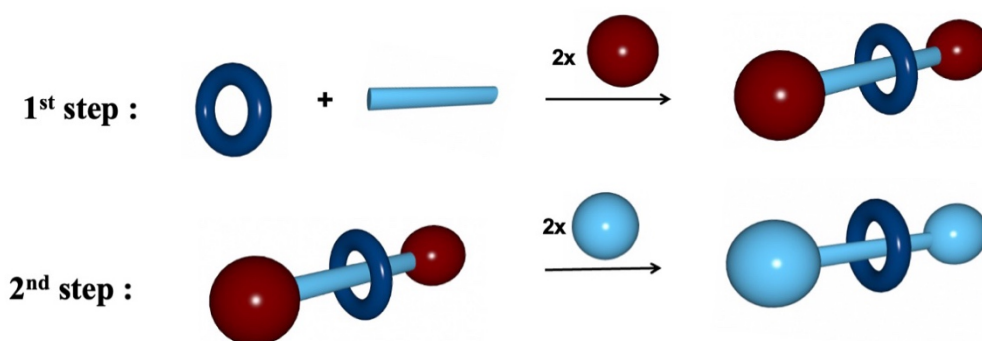


Figure 20. Schematic representation of a [2]rotaxane formed by a " Stoppers exchange " approach.

In order to prepare a rotaxane with an activated stopper, certain criteria must be met. First, it has to be prepared in good yield. Second, it must be stable enough to be stored and used later. Finally, the structure of the rotaxanes has to be preserved during the chemical transformation. The first example was developed in 2000 by the group of J. F. Stoddart.⁶⁴ They have prepared a [2]rotaxane bearing a phosphonium salt stopper in 80% yield by a stoppering approach. Subsequent stopper exchange has been then efficiently achieved by reaction of the phosphonium salt stopper with an aldehyde under Wittig conditions (Figure 21).

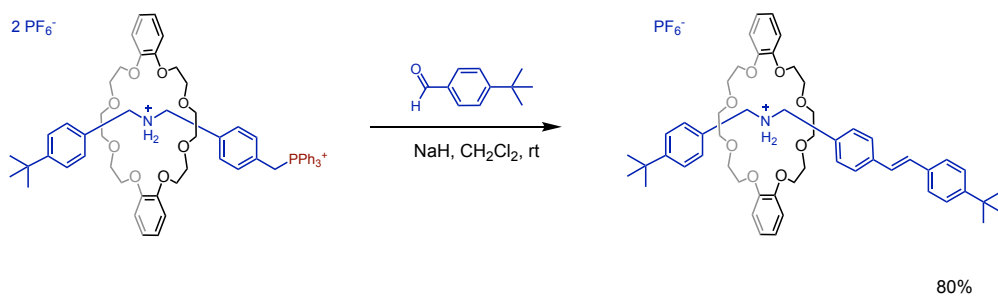


Figure 21. Stopper exchange by Wittig reaction.⁶⁴

In 2005, T. Takata prepared a [2]rotaxane building block with cinnamyl ester stoppers. Stopper exchange reactions with a bulky malonate ester have been carried out by a Tsuji-Trost allylation reaction.⁶⁵ The resulting [2]rotaxane have been however obtained in moderate yields (Figure 22).

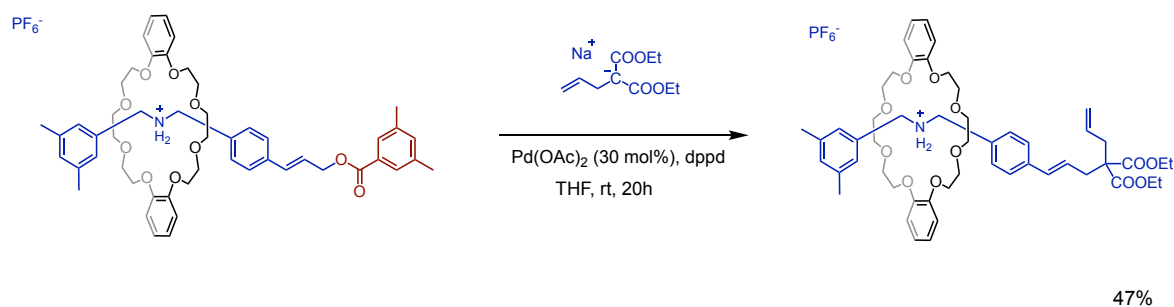


Figure 22. Stopper exchange by Tsuji-Trost reaction.⁶⁵

This synthetic strategy has been rarely used and only few examples have been reported in the literature⁶⁴⁻⁶⁸ until 2018 when the group of J.-F. Nierengarten became interested in this method and developed an efficient preparation of [2]rotaxane building blocks bearing activated esters (Figure 23).⁴⁵

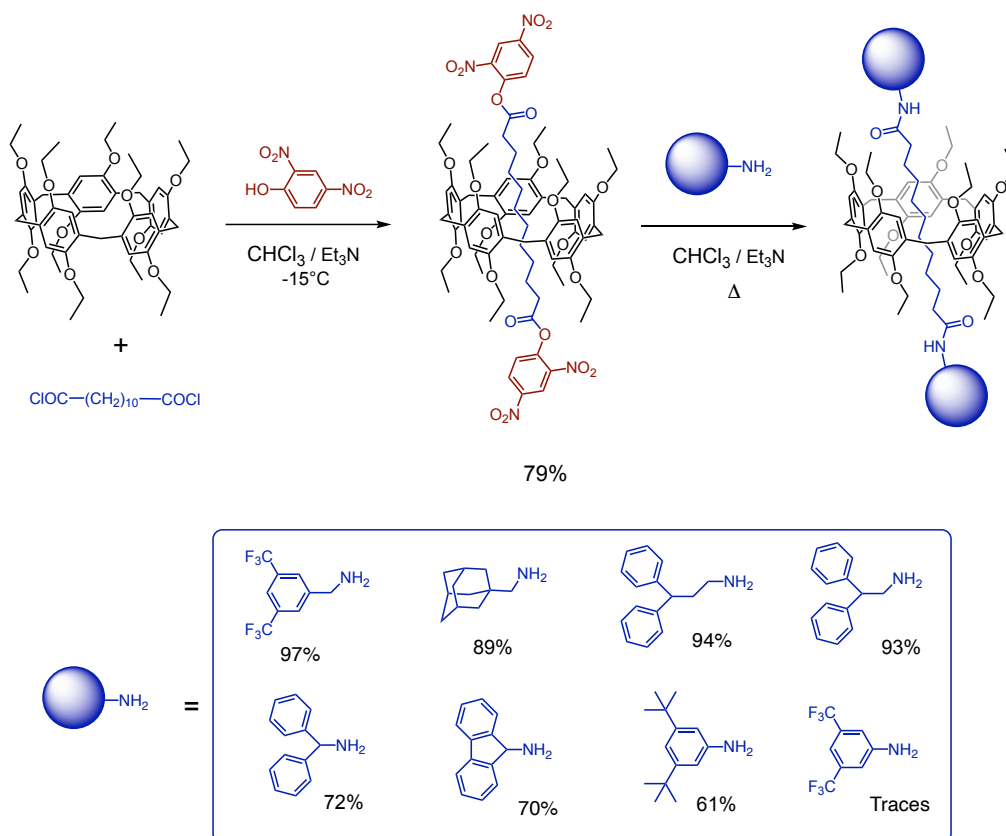


Figure 23. Preparation of [2]rotaxanes by stopper exchange reactions between a rotaxane building block with activated stoppers and primary amine reagents.⁴⁵

A [2]rotaxane building block bearing exchangeable stoppers has been prepared in multi-gram scale quantities with high yields from the reaction of 2,4-dinitrophenol with the inclusion complex resulting from the association of dodecanedioyl chloride with 1,4-diethoxypillar[5]arene. Stopper exchange reactions have been then carried out by reaction with different amine reagents. The addition-elimination mechanism prevented the unthreading of the axle. As a result, the [2]rotaxane structure is preserved during the chemical transformation.

J.-F. Nierengarten's group has continuously developed this method in order to obtain versatile building blocks allowing the preparation of pillar[5]arene-containing [2]rotaxanes with a large structural diversity.⁶⁹ For example, the introduction of arylsulphonates as exchangeable stoppers has allowed the stopper exchange by reaction with various nucleophiles (Figure 24). As the nucleophilic substitution occurs via a concerted mechanism ("S_N2"), the rotaxane structure is preserved during these chemical transformations, leading to [2]rotaxanes with ester, thioether or ether stoppers.

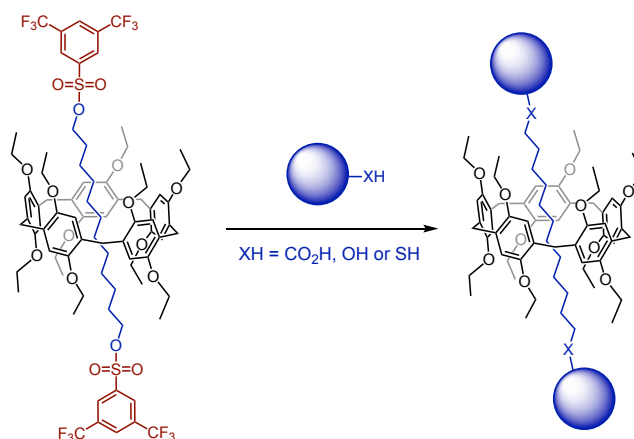


Figure 24. Preparation of [2]rotaxanes from building block arylsulfonate stoppers with various nucleophiles.⁶⁹

Although very efficient for the preparation of [2]rotaxanes, the main limitation of these building blocks bearing dinitrophenol and arylsulfonate stoppers, is related to their moderate stability, especially on silica gel, which often makes their purification difficult. In order to overcome this stability problem, J.-F. Nierengarten's group decided to explore a different strategy using new exchangeable stoppers (Figure 25).⁷⁰

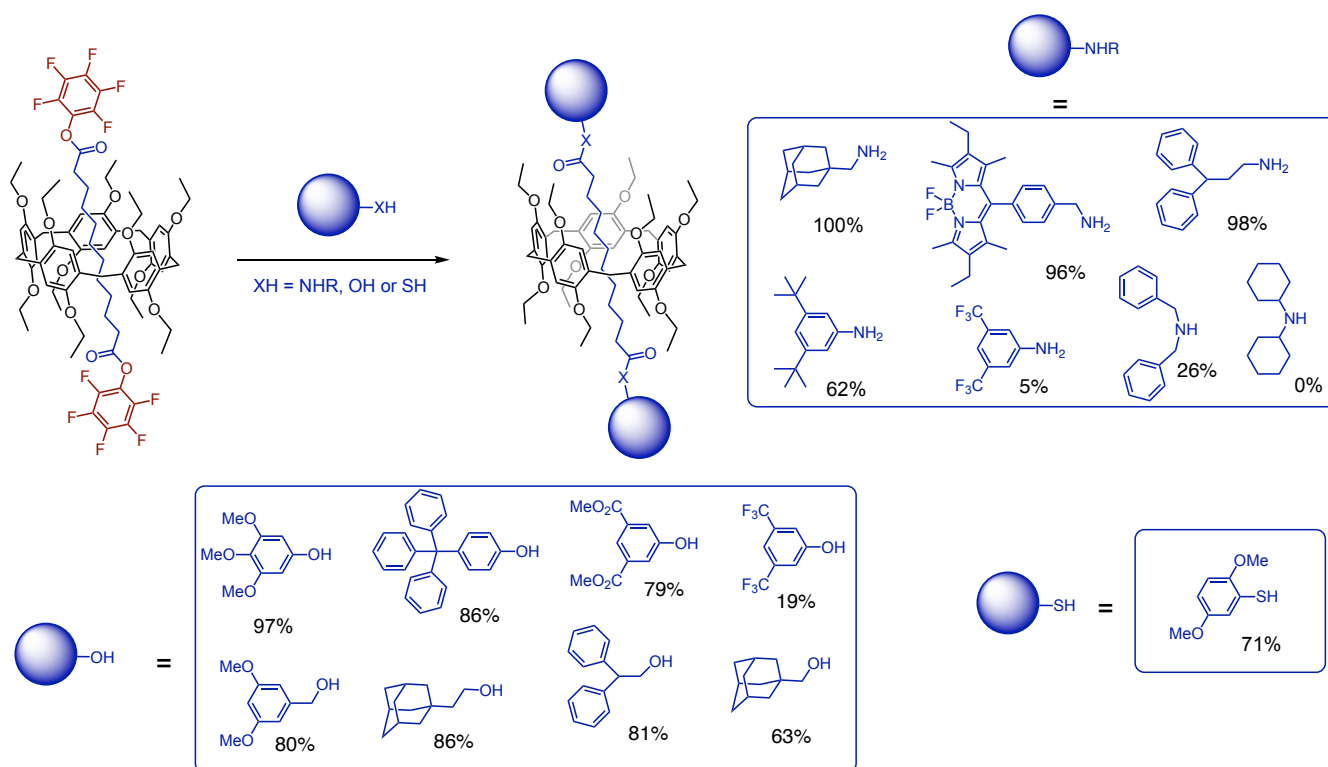


Figure 25. Preparation of [2]rotaxanes starting from a rotaxane building block with pentafluorophenol ester stoppers and various nucleophiles.⁷⁰

The [2]rotaxane building blocks with pentafluorophenol ester stoppers are easily prepared on a multi-gram scale and easily purified by column chromatography on silica gel. They are perfectly stable under standard laboratory conditions, allowing storage for several months before further transformation. Stopper exchange reactions of these building blocks have been carried out with various nucleophiles, giving access to a wide variety of [2]rotaxanes with amide, ester or thioester functions in high yields.

1.3. Molecular machines

A molecular machine is a molecular system able to perform mechanical movement of large amplitude.⁷¹⁻⁷⁵ In general, a molecular machine consists of at least two components that can be made to move relative to each other. This motion can be triggered by an external stimulus and controlled over a relatively large amplitude. Typically, the stimulus can be chemical (acid/base, redox, ion exchange) or physical (light, heat, solvent polarity). In addition, the motion of a molecular machine is characterized by its reversibility: the system has been able to return to its initial state and start the cycle again. There are two main families of molecular machines, which are molecular motors and molecular switches. The difference between a motor and a switch is whether the molecule returns to its initial state unidirectionally or not. A molecular switch can go from one state to another, but it does not perform unidirectional motion or work. On the other hand, a molecular motor can undergo unidirectional movements from one state to another to produce useful work.⁷⁶⁻⁷⁹ In 2016, J.-P. Sauvage, J. F. Stoddart and B. Feringa have been awarded the Nobel Prize in Chemistry for their seminal contributions in the development of this field.^{5,6,80}

Owing to their unique structure, rotaxanes offer specific degrees of conformational freedom, allowing them to adopt different "co-conformations". This means that the macrocycle and the dumbbell have different orientations to each other. The rotaxane can move from one co-conformation to another by two types of motion: pirouetting and shuttling. Pirouetting is the rotation of the macrocycle around the axle, and shuttling is the movement of the macrocycle along the axle. (Figure 26).

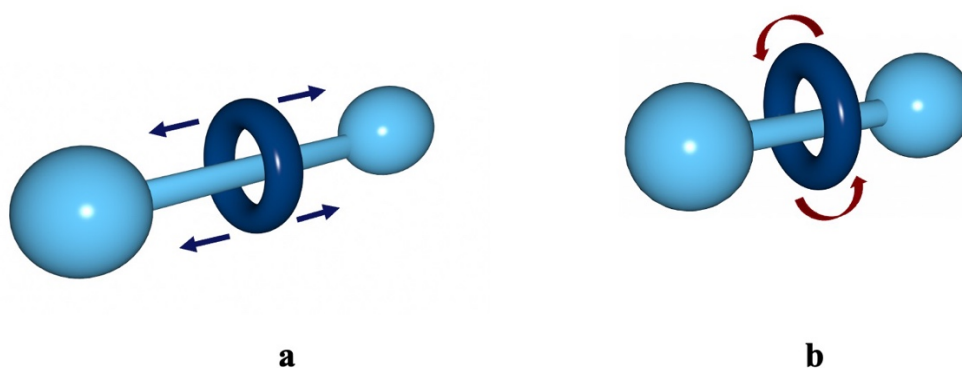


Figure 26. Schematic representation of shuttling (a) and pirouetting (b) motions in rotaxanes.

When the dumbbell of a rotaxane contains two different recognition sites ("stations"); the system can exist in two different co-conformations in equilibrium. In the initial state, the macrocycle is preferentially located on the first station. The macrocycle can be transferred from the first to the second station by gliding motions by applying an appropriate external stimulus capable of changing the affinity of one of the stations for the macrocycle. In this way, the macrocycle moves from the first to the second station. The macrocycle returns to the first station when the axle returns to its initial state, either by another stimulus or by a spontaneous process (Figure 27).

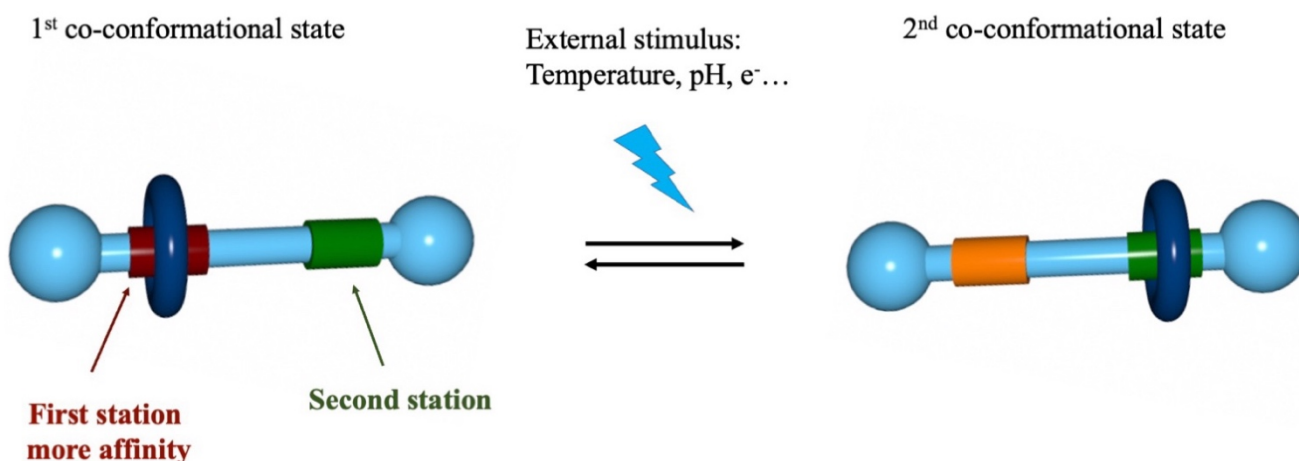


Figure 27. Schematic representation of the shuttle principle in a rotaxane.

A key concept in molecular switching is bistability. A molecule is defined as bistable when there are two co-conformations representing energy minima instead of one. In a mechanically interlocked bistable molecule, the overall energy minimum is called the ground state co-conformation (GSCC), and any higher energy minimum is called the metastable state co-conformation (MSCC).^{71,81} The relevant terms, such as the difference in free energies of translational isomers (ΔG°), and the

activation free energy for translation (ΔG^\ddagger), are defined on the potential energy surface of a bistable [2]rotaxane. Control of co-conformational switching typically relies on the application of an appropriate external stimulus - chemical or physical - that alters the magnitude of ΔG° by increasing or decreasing the stability of one or more translational isomers, often with a corresponding modulation of ΔG^\ddagger (Figure 28).^{2,82}

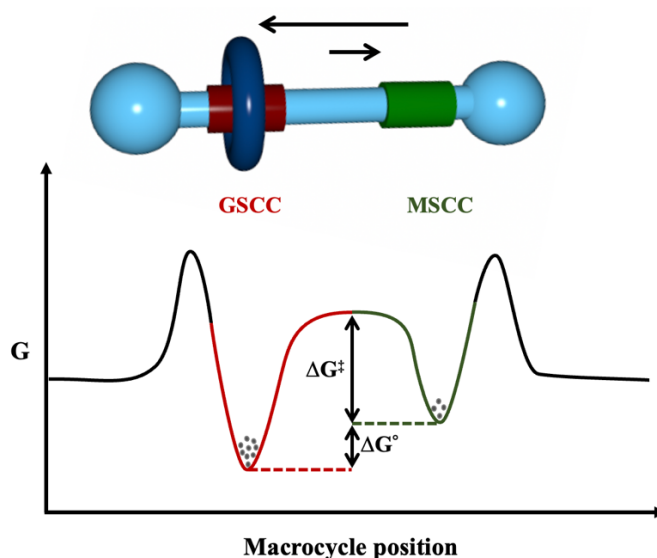


Figure 28. Potential energy surface diagram of a bistable [2]rotaxane, showing the difference in free energy (ΔG°) between translational isomers and the activation barrier (ΔG^\ddagger) for translational isomerization from a metastable state co-conformation (MSCC) to the ground state co-conformation (GSCC).²

In 1994, J. F. Stoddart and co-workers⁸³ reported the first synthesis of a bistable donor-acceptor molecular shuttle driven by redox stimuli. This bistable system consists of a macrocycle containing bipyridinium functions (positively charged) interlocked with a dumbbell containing a redox-active benzidine recognition site and a biphenol moiety. The macrocycle has strong interactions with the most electron-rich group. Initially, the macrocycle encircles the benzidine moiety, which represents the GSCC (84% of the molecular population), while the weaker-binding biphenol recognition site is occupied in the MSCC (16%). Introducing a positive charge to the benzidine moiety by electrochemical oxidation produces a pentacationic radical, in which a repulsive interaction between the benzidine radical cation and the macrocycle results in an almost quantitative switching of the macrocycle to the biphenol recognition site (Figure 29).⁸³

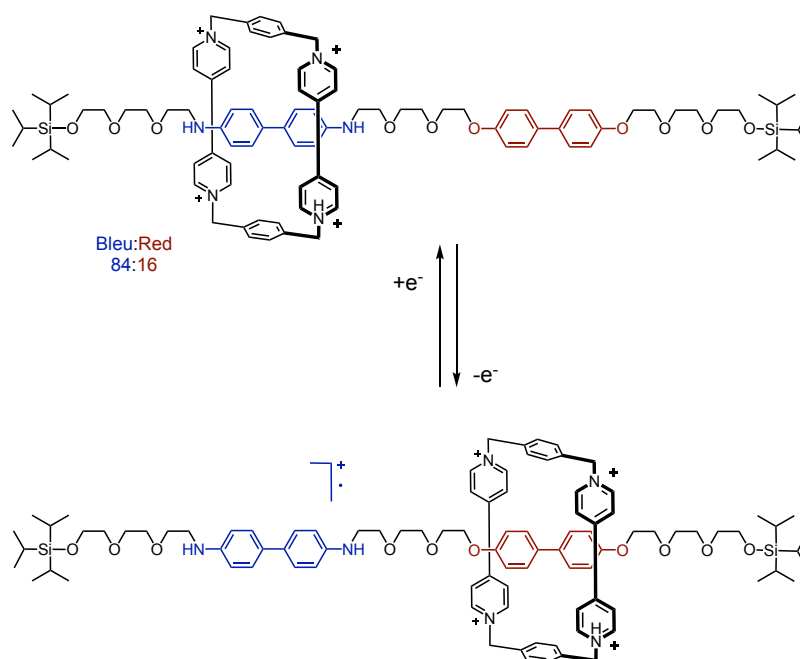


Figure 29. The first bistable donor-acceptor molecular shuttle driven by redox stimuli.⁸³

Control of co-conformational (translational) isomerism using acid-base chemistry as a stimulus typically involves the addition or removal of protons at one or more sites in a molecule, resulting in changes in local hydrogen bonding and/or electrostatic interactions, and ultimately leading to mechanical motion.⁸⁴ An example of this is the work of J. F. Stoddart, who also developed the first pH-controlled molecular shuttle based on a dialkylammonium/crown ether motif. The bistable [2]rotaxane contains a dialkylammonium $[R_2NH_2^+]$ and a bipyridinium recognition site on its dumbbell moiety. The macrocyclic crown ether is located exclusively around the ammonium recognition site as a result of a combination of $[^+N-H...O]$ and $[C-H...O]$ interactions between the $[CH_2NH_2^+]$ hydrogen atoms of the dumbbell and the oxygen atoms of the macrocycle. When an excess of $i\text{-Pr}_2\text{NEt}$ is added, the ammonium recognition site is deprotonated. As a result, the hydrogen bonds between the components are broken and the macrocycle shuttles to the bipyridinium recognition site. The original co-conformation can be easily regenerated by simply re-protonating the amine with TFA. (Figure 30).⁸⁵

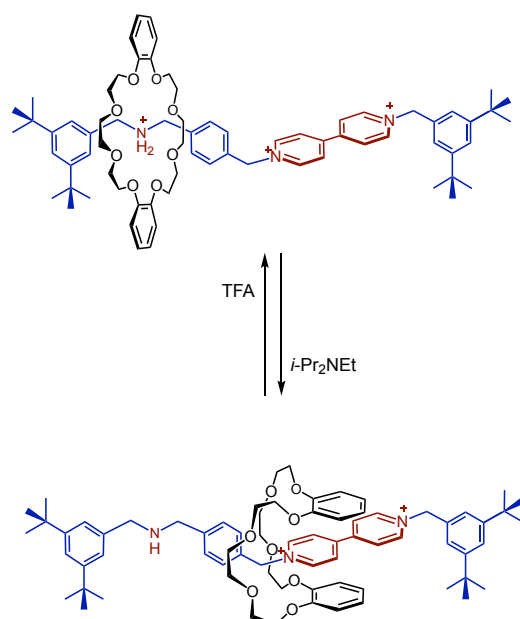


Figure 30. Typical example of an acid–base-controllable molecular shuttle.⁸⁵

Another basis for switching is the interaction between cations and one or more chelating sites in a MIM.⁸⁶ In fact, using appropriately designed systems, chemists have demonstrated this concept with a variety of cations, including transition metals.⁸⁷ J.-P. Sauvage was the pioneer of this switching process. In 1997, the group of J.-P. Sauvage developed the preparation of a molecular shuttle in which the translation of the macrocycle along the axle is electrochemically controlled, based on the different coordination behaviors of Cu(I) and Cu(II) (Figure 31).⁸⁸ Cu(I) preferentially forms tetrahedral complexes and is stabilized by hindered ligands, whereas Cu(II) can be penta-coordinated. In this [2]rotaxane shuttle, the axle contains two bidentate chelating sites, and movement is based only on a difference in steric hindrance between the binding sites. The Cu(I) complex resides on the hindered phenanthroline site, but oxidation to Cu(II) is followed by a rapid translational movement that results in complexation of the Cu(II) center to the less hindered terpyridine chelate. This process is reversible, and reduction of the metal center to Cu(I) returns the macrocycle to its original position.

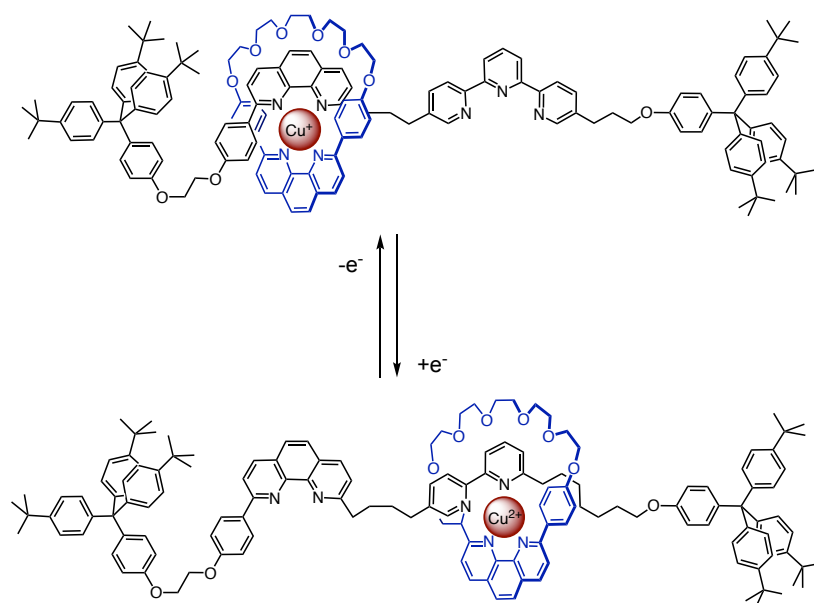


Figure 31. Molecular machine developed by the group of J.-P. Sauvage and based on the different coordination behaviors of Cu(I) and Cu(II).⁸⁸

Temperature can be used as a handle to control the co-conformations of mechanomolecules. The first pillar[6]arene-based rotaxane reported by T. Ogoshi exhibits thermally controlled alternating behavior (Figure 32).⁸⁹ The axle consists of two alkyl linker stations: a long alkyl linker between the pyridinium and triazole moieties (station I) and a short alkyl linker between the pyridinium and trityl moieties (station II). The electron-rich cavity of the pillar[6]arene is able to interact with the cationic pyridinium moiety of each of these stations. The length of the linker at station I is longer than that at station II, allowing the pillar[6]arene to move freely along the linker at station I. The free movement of the pillar[6]arene at station I is favorable from the point of view of entropy dominance. By lowering the temperature to -50°C , the pillar[6]arene is more populated at station II, the binding site of the pyridinium cation moiety was contained at station II, so the location at station II should be preferred from the point of view of enthalpy dominance. The larger cavity of the pillar[6]arene ($\sim 7.5 \text{ \AA}$) with respect to the pillar[5]arene (4.7 \AA) is important in enabling this thermally controlled switching, since a pillar[5]arene remains encircled around station I and does not shuttle on an identical dumbbell.

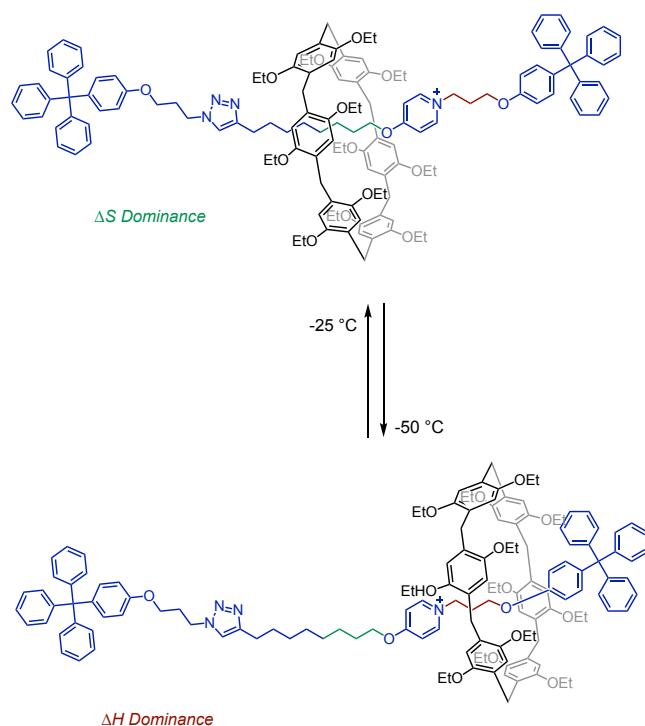


Figure 32. Pillar[6]arene-based [2]rotaxane thermally responsive shuttling behavior.⁸⁹

Since the local environment of a molecule in solution is largely defined by the surrounding solvent molecules, solvent polarity is one of the most universal handles to control the co-conformational isomerism of mechanomolecules.⁹⁰⁻⁹² F. Huang has described the solvent-induced switching between different co-conformations of a pillar[5]arene-based rotaxane (Figure 33).⁹³ In CDCl_3 , the pillar[5]arene macrocycle is located around the methylene units adjacent to an imidazolium recognition site, but in $\text{DMSO-}d_6$ the macrocycle is pushed to the other end of the dodecamethylene chain of the dumbbell, closer to the carbamate-linked stopper. A possible reason is the ability of $\text{DMSO-}d_6$ to disrupt the interactions between the pillar[5]arene and the imidazolium moiety. However strong solvophobic effects for the dodecamethylene chain may also play an important role.

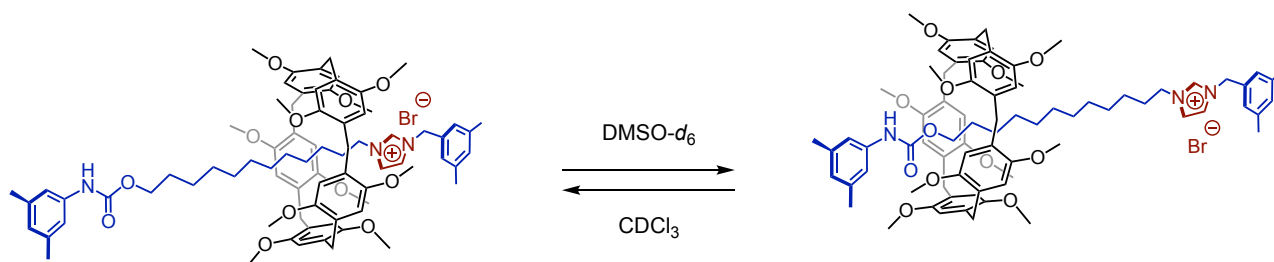


Figure 33. A pillar[5]arene/imidazolium [2]rotaxane: solvent-driven switches.⁹³

Light is a particularly useful stimulus for molecular machines because it can be introduced with excellent spatial and temporal precision over a highly wavelength-tunable energy range.⁹⁴⁻⁹⁷ Azobenzene derivatives are widely used as photo-responsive compounds, which undergo *cis-trans* (*E/Z*) isomerization around a central double bond in response to visible light or ultraviolet (UV) and can be exploited to construct light-driven molecular shuttles.⁹⁸⁻¹⁰³ Recently, T. Ogoshi and co-workers have designed a light-driven molecular shuttle containing a pillar[6]arene macrocyclic ring and an axle with two equal energy level stations connected by an azobenzene unit (Figure 34).¹⁰⁴ The *E* isomer of the azobenzene acted as an "open gate", allowing the pillar[6]arene ring to rapidly shuttle between the two stations. Irradiation of *E*-[2]rotaxane with UV light (365 nm) induced the *Z*-isomer of the azobenzene moiety, which is populated up to 90%. The *Z* isomer of the azobenzene acted as a "closed gate", inhibiting the shuttling of the pillar[6]arene ring.

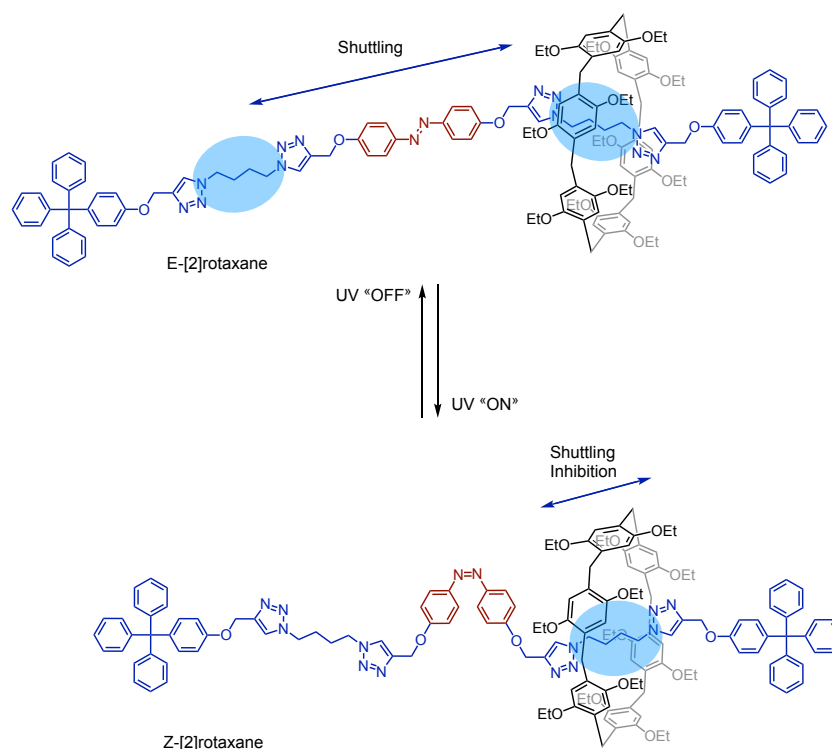


Figure 34. Light-controlled shuttling in a [2]rotaxane with a photo-switchable azobenzene gate.¹⁰⁴

I.5. Research plan

Rotaxanes are a particularly active field of research in chemistry. In this thesis, we will further evaluate the potential of the synthetic strategy developed in our group for the synthesis of rotaxanes

by the stopper exchange method. Specifically, the reactivity of rotaxanes with pentafluorophenyl ester stoppers will be further investigated to prepare [2]rotaxanes bearing two different stoppers as well as [3]rotaxanes. Finally, based on the developed synthetic methods, molecular shuttles will be prepared and investigated.

I.6. References

- 1) J.-P. Sauvage, C. Dietrich-Buchecker (Eds.), *Molecular Catenanes, Rotaxanes and Knots – A Journey Through the World of Molecular Topology*, J. Wiley and Sons, **2008**.
- 2) C. J. Bruns, J. F. Stoddart, *The Nature of the Mechanical Bond – From Molecules to Machines*, J. Wiley & Sons, **2016**.
- 3) G. Schill, *Catenanes, Rotaxanes and Knots*, Academic Press, New York, **1971**.
- 4) D. B. Amabilino, J. F. Stoddart, *Chem. Rev.* **1995**, *95*, 2725-2828.
- 5) J.-P. Sauvage, *Angew. Chem. Int. Ed.* **2017**, *56*, 11080-11093; *Angew. Chem.* **2017**, *129*, 11228-11242.
- 6) J. F. Stoddart, *Angew. Chem. Int. Ed.* **2017**, *56*, 11228-11242; *Angew. Chem.* **2017**, *129*, 11244-11277.
- 7) H. Frisch, I. Martin, H. Mark, *Monatsh. Chem.* **1953**, *84*, 250-256.
- 8) H. L. Frisch, E. Wasserman, *J. Am. Chem. Soc.* **1961**, *83*, 3789-3795.
- 9) E. Wasserman, *J. Am. Chem. Soc.* **1960**, *82*, 4433-4434.
- 10) A. S. Baluna, A. Galan, D. A. Leigh, G. D. Smith, J. T. J. Spence, D. J. Tetlow, I. J. Vitorica-Yrezabal, M. Zhang, *J. Am. Chem. Soc.* **2023**, *145*, 9825-9833.
- 11) G. Schill, A. Lüttringhaus, *Angew. Chem. Int. Ed. Engl.* **1964**, *3*, 546-547.
- 12) C. O. Dietrich-Buchecker, J.-P. Sauvage, J. P. Kintzinger, *Tetrahedron Lett.* **1983**, *24*, 5095-5098.
- 13) P. R. Ashton, T. T. Goodnow, A. E. Kaifer, M. V. Reddington, A. M. Z. Slawin, N. Spencer, J. F. Stoddart, C. Vicent, D. J. Williams, *Angew. Chem. Int. Ed.* **1989**, *28*, 1396-1399.
- 14) C. A. Hunter, *J. Am. Chem. Soc.* **1992**, *114*, 5303-5311.
- 15) F. Vögtle, S. Meier, R. Hoss, *Angew. Chem. Int. Ed.* **1992**, *31*, 1619-1622.
- 16) I. T. Harrison, S. Harrison, *J. Am. Chem. Soc.* **1967**, *89*, 5723-5724.
- 17) G. Schill, H. Zollenkopf, *Justus Liebigs Ann. Chem.* **1969**, *721*, 53-74.
- 18) T. Ogoshi, S. Kanai, S. Fujinami, T. Yamagishi, Y. Nakamoto, *J. Am. Chem. Soc.* **2008**, *130*, 5022-5023.
- 19) P. J. Cragg, K. Sharma, *Chem. Soc. Rev.* **2012**, *41*, 597-607.

- 20) M. Xue, Y. Yang, X. Chi, Z. Zhang, F. Huang, *Acc. Chem. Res.* **2012**, *45*, 1294-1308.
- 21) T. Ogoshi, *J. Incl. Phenom., Macrocycl. Chem.* **2012**, *72*, 247-262.
- 22) T. Ogoshi, T.-a. Yamagishi, *Eur. J. Org. Chem.* **2013**, 2961-2975.
- 23) H. Zhang, Y. Zhao, *Chem. Eur. J.* **2013**, *19*, 16862-16879.
- 24) D. Cao, H. Meier, *Asian J. Org. Chem.* **2014**, *3*, 244-262.
- 25) T. Ogoshi, T. Yamagishi, *Chem. Commun.* **2014**, *50*, 4776-4787.
- 26) N. L. Strutt, H. Zhang, S. T. Schneebeli, J. F. Stoddart, *Acc. Chem. Res.* **2014**, *47*, 2631-2642.
- 27) A. Saura-Sanmartin, C. A. Schalley, *Chem.* **2023**, *9*, 823-846.
- 28) N. Hoyas Pérez, J. E. M. Lewis, *Org. Biomol. Chem.* **2020**, *18*, 6757-6780.
- 29) M. Deska, J. Kozłowska, W. Sliwa, *Arkivoc* **2013**, 294-332.
- 30) A. Saura-Sanmartin, *Eur. J. Org. Chem.* **2023**, *26*, e202201512.
- 31) H. Ogino, *J. Am. Chem. Soc.* **1981**, *103*, 1303-1304.
- 32) A. H. G. David, P. García-Cerezo, A. G. Campaña, F. Santoyo-González, V. Blanco, *Chem. Eur. J.* **2019**, *25*, 6170-6179.
- 33) C. A. Hunter, C. M. R. Low, M. J. Packer, S. E. Spey, J. G. Vinter, M. O. Vysotsky, C. Zonta, *Angew. Chem. Int. Ed.* **2001**, *40*, 2678-2682.
- 34) H. Sasabe, N. Kihara, Y. Furusho, K. Mizuno, A. Ogawa, T. Takata, *Org. Lett.* **2004**, *6*, 3957-3960.
- 35) J. J. Gassensmith, L. Barr, J. M. Baumes, A. Paek, A. Nguyen, B. D. Smith, *Org. Lett.* **2008**, *10*, 3343-3346.
- 36) J. C. Chambron, V. Heitz, J.-P. Sauvage, *J. Chem. Soc., Chem. Commun.* **1992**, 1131-1133.
- 37) C. Seel, A. H. Parham, O. Safarowsky, G. M. Hübner, F. Vögtle, *J. Org. Chem.* **1999**, *64*, 7236-7242.
- 38) P. L. Anelli, P. R. Ashton, R. Ballardini, V. Balzani, M. Delgado, M. T. Gandolfi, T. T. Goodnow, A. E. Kaifer, D. Philp, M. Pietraszkiewicz, L. Prodi, M. V. Reddington, A. M. Z. Slawin, N. Spencer, J. F. Stoddart, C. Vicent, D. J. Williams, *J. Am. Chem. Soc.* **1992**, *114*, 193-218.
- 39) I. Nierengarten, R. Deschenaux, J.-F. Nierengarten, *Chimia* **2016**, *70*, 61-66.
- 40) N. L. Strutt, R. S. Forgan, J. M. Spruell, Y. Y. Botros, J. F. Stoddart, *J. Am. Chem. Soc.* **2011**, *133*, 5668-5671.
- 41) T. Ogoshi, D. Yamafuji, T. Aoki, K. Kitajima, T.-a. Yamagishi, Y. Hayashi, S. Kawauchi, *Chem. Eur. J.* **2012**, *18*, 7493-7500.
- 42) T. Ogoshi, R. Shiga, T.-a. Yamagishi, *J. Am. Chem. Soc.* **2012**, *134*, 20322-20325.
- 43) S. Dong, C. Han, B. Zheng, M. Zhang, F. Huang, *Tetrahedron Lett.* **2012**, *53*, 3668-3671.

- 44) R. Milev, A. Lopez-Pacheco, I. Nierengarten, T. M. N. Trinh, M. Holler, R. Deschenaux, J.-F. Nierengarten, *Eur. J. Org. Chem.* **2015**, 2015, 479-485.
- 45) I. Nierengarten, E. Meichsner, M. Holler, P. M. Pieper, R. Deschenaux, B. Delavaux-Nicot, J.-F. Nierengarten, *Chem. Eur. J.* **2018**, 24, 169-177.
- 46) X. Han, G. Liu, S. H. Liu, J. Yin, *Org. Biomol. Chem.* **2016**, 14, 10331-10351.
- 47) J. Wu, K. C.-F. Leung, J. F. Stoddart, *Proc. Natl. Acad. Sci. USA* **2007**, 104, 17266-17271.
- 48) W. Zhou, H. Zheng, Y. Li, H. Liu, Y. Li, *Org. Lett.* **2010**, 12, 4078-4081.
- 49) J. B. Wittenberg, M. G. Costales, P. Y. Zavalij, L. Isaacs, *Chem. Commun.* **2011**, 47, 9420-9422.
- 50) J. Wu, K. C. F. Leung, J. F. Stoddart, *Proc. Natl. Acad. Sci.* **2007**, 104, 17266-17271.
- 51) F. M. Raymo, J. F. Stoddart, *Pure Appl. Chem.* **1997**, 69, 1987-1997.
- 52) P. R. Ashton, M. Bělohradský, D. Philp, J. F. Stoddart, *J. Chem. Soc., Chem. Commun.* **1993**, 1274-1277.
- 53) T. Ogoshi, Y. Tamura, D. Yamafuji, T. Aoki, T. Yamagishi, *Chem. Commun.* **2016**, 52, 10297-10300.
- 54) T. Ogoshi, T. Kakuta, T. Yamagishi, "Cyclic Host Liquids for the Formation of Rotaxanes and Their Applications" In "Functional Organic Liquids -New-generation and Advanced Liquid Matter-", Ed. by T. Nakanishi, *Wiley-VCH*, **2019**, 53-74.
- 55) M. Asakawa, P. R. Ashton, R. Ballardini, V. Balzani, M. Bělohradský, M. T. Gandolfi, O. Kocian, L. Prodi, F. M. Raymo, J. F. Stoddart, M. Venturi, *J. Am. Chem. Soc.* **1997**, 119, 302-310.
- 56) D. B. Amabilino, J. F. Stoddart, *Chem. Rev.* **1995**, 95, 2725-2828.
- 57) M. Denis, S. M. Goldup, *Nat. Rev. Chem.* **2017**, 1, 61.
- 58) J. D. Crowley, K. D. Hänni, A.-L. Lee, D. A. Leigh, *J. Am. Chem. Soc.* **2007**, 129, 12092-12093.
- 59) V. Aucagne, K. D. Hänni, D. A. Leigh, P. J. Lusby, D. B. Walker, *J. Am. Chem. Soc.* **2006**, 128, 2186-2187.
- 60) J. E. Beves, B. A. Blight, C. J. Campbell, D. A. Leigh, R. T. McBurney, *Angew. Chem. Int. Ed.* **2011**, 50, 9260-9327.
- 61) V. Aucagne, K. D. Hanni, D. A. Leigh, P. J. Lusby, D. B. Walker, *J. Am. Chem. Soc.* **2006**, 128, 2186-2187.
- 62) H. M. Cheng, D. A. Leigh, F. Maffei, P. R. McGonigal, A. M. Z. Slawin, J. Wu, *J. Am. Chem. Soc.* **2011**, 133, 12298-12303.

- 63) A. F. P. Alcântara, L. A. Fontana, M. P. Almeida, V. H. Rigolin, M. A. Ribeiro, W. P. Barros, J. D. Megiatto, *Chem. Eur. J.* **2020**, *26*, 7808-7822.
- 64) S. J. Rowan, J. F. Stoddart, *J. Am. Chem. Soc.* **2000**, *122*, 164-165.
- 65) N. Kihara, S. Motoda, T. Yokozawa, T. Takata, *Org. Lett.* **2005**, *7*, 1199-1202.
- 66) D. W. Zehnder II, D. B. Smithrud, *Org. Lett.* **2001**, *3*, 2485-2487.
- 67) J. S. Hannam, S. M. Lacy, D. A. Leigh, C. G. Saiz, A. M. Z. Slawin, S. G. Stitchell, *Angew. Chem. Int. Ed.* **2004**, *43*, 3260-3264.
- 68) R. J. Bordoli, S. M. Goldup, *J. Am. Chem. Soc.* **2014**, *136*, 4817-4820.
- 69) I. Nierengarten, J.-F. Nierengarten, *ChemistryOpen* **2020**, *9*, 393-400.
- 70) M. Remy, I. Nierengarten, B. Park, M. Holler, U. Hahn, J.-F. Nierengarten, *Chem. Eur. J.* **2021**, *27*, 8492-8499.
- 71) M. A. Olson, Y. Y. Botros, J. F. Stoddart, *Pure Appl. Chem.* **2010**, *82*, 1569-1574.
- 72) V. Balzani, A. Credi, F. M. Raymo, J. F. Stoddart, *Angew. Chem., Int. Ed.* **2000**, *39*, 3348-3391.
- 73) W. R. Browne, B. L. Feringa, *Nat. Nanotechnol.* **2006**, *1*, 25-35.
- 74) E. R. Kay, D. A. Leigh, F. Zerbetto, *Angew. Chem. Int. Ed.* **2007**, *46*, 72-191.
- 75) E. A. Neal, S. M. Goldup, *Chem. Commun.* **2014**, *50*, 5128-5142.
- 76) K. Kinbara, T. Aida, *Chem. Rev.* **2005**, *105*, 1377-1400.
- 77) Y. Feng, M. Ovalle, J. S. W. Seale, C. K. Lee, D. J. Kim, R. D. Astumian, J. F. Stoddart, *J. Am. Chem. Soc.* **2021**, *143*, 5569-559.
- 78) D. Dattler, G. Fuks, J. Heiser, E. Moulin, A. Perrot, X. Yao, N. Giuseppone, *Chem. Rev.* **2020**, *120*, 310-433.
- 79) R. D. Astumian, S. Mukherjee, A. Warshel, *ChemPhysChem* **2016**, *17*, 1719-1741.
- 80) D. Leigh, *Angew. Chem. Int. Ed.* **2016**, *55*, 14506-14508.
- 81) G. Barin, R. S. Forgan, J. F. Stoddart, *Proc. R. Soc. A* **2012**, *468*, 2849-2880.
- 82) S. Erbas-Cakmak, D. A. Leigh, C. T. McTernan, A. L. Nussbaumer, *Chem. Rev.* **2015**, *115*, 10081-10206.
- 83) R. A. Bissell, E. Cordova, A. E. Kaifer, J. F. Stoddart, *Nature* **1994**, *369*, 133-137.
- 84) M. Baroncini, L. Casimiro, C. de Vet, J. Groppi, S. Silvi, A. Credi, *ChemistryOpen* **2018**, *7*, 169-179.
- 85) M.-V. Martinez-Diaz, N. Spencer, J. F. Stoddart, *Angew. Chem. Int. Ed. Engl.* **1997**, *36*, 1904-1907.
- 86) B. Champin, P. Mobian, J.-P. Sauvage, *Chem. Soc. Rev.* **2007**, *36*, 358-366.

- 87) J.-P. Collin, C. Dietrich-Buchecker, P. Gaviña, M. C. Jimenez-Molero, J.-P. Sauvage, *Acc. Chem. Res.* **2001**, *34*, 477-487.
- 88) J. -P. Collin, P. Gaviña, J.-P. Sauvage, *New. J. Chem.* **1997**, *21*, 525-528.
- 89) T. Ogoshi, D. Yamafuji, T. Aoki, T. -A. Yamagishi, *Chem. Commun.* **2012**, *48*, 6842-6844.
- 90) Z. Wu, S. Wang, Z. Zhang, Y. Zhang, Y. Yin, H. Shi, S. Jiao, *RSC Adv.* **2022**, *12*, 30495-30500.
- 91) K. Kato, S. Fa, S. Ohtani, T. Shi, A. M. Brouwer, T. Ogoshi, *Chem. Soc. Rev.* **2022**, *51*, 3648-3687.
- 92) S. Li, M. Liu, J. Zhang, B. Zheng, C. Zhang, X. Wen, N. Li, F. Huang, *Org. Biomol. Chem.* **2008**, *6*, 2103-2107.
- 93) S. Dong, J. Yuan, F. Huang, *Chem. Sci.* **2013**, *5*, 247-252.
- 94) J-X. Yang, Z. Li, X-H. Gu, T-G. Zhan, J. Cui, K-D. Zhang, *Tetrahedron* **2021**, *92*, 132284.
- 95) J-S. Geng, L. Mei, Y-Y. Liang, L-Y. Yuan, J-P. Yu, K-Q. Hu, L-H. Yuan, W. Feng, Z-F. Chai, W-Q. Shi. *Nat. Commun.* **2022**, *13*, 2030.
- 96) A. Saura-Sanmartin, *Beilstein J. Org. Chem.* **2023**, *19*, 873-880.
- 97) J. Berna, D. A. Leigh, M. Lubomska, S. M. Mendoza, E. M. Perez, P. Rudolf, G. Teobaldi, F. Zerbetto, *Nat. Mater.* **2005**, *4*, 704-710.
- 98) W. Abraham, K. Buck, M. Orda-Zgadzaj, S. Schmidt-Schäffer, U-W. Grummt, *Chem. Commun.* **2007**, 3094-3096.
- 99) W. Abraham, L. Grubert, U. W. Grummt, K. Buck, *Chem. Eur. J.* **2004**, *10*, 3562-3568.
- 100) V. Balzani, A. Credi, M. Venturi, *Chem. Soc. Rev.* **2009**, *38*, 1542-1550.
- 101) D. Bléger, S. Hecht, *Angew. Chem. Int. Ed.* **2015**, *54*, 11338-11349.
- 102) B. Yao, H. Sun, L. Yang, S. Wang, X. Liu, *Front. Chem.* **2022**, *9*, 832735.
- 103) P. Raiteri, G. Bussi, C. S. Cucinotta, A. Credi, J. F. Stoddart, M. Parrinello, *Angew. Chem. Int. Ed.* **2008**, *47*, 3536-3539.
- 104) T. Ogoshi, D. Kotera, S. Fa, S. Nishida, T. Kakuta, T.-a. Yamagishi, A.-M. Brouwer, *Chem. Commun.* **2020**, *56*, 10871-10874.

Stepwise functionalization of pillar[5]arene-containing [2]rotaxane building blocks with pentafluorophenyl ester stoppers

II-1. Introduction

The chemistry of mechanically interlocked molecules (MIMs) has been mainly focused on the development of new synthetic strategies for their preparation.^{1,2} As soon as efficient methodologies were developed, the pioneering work of Sauvage and Stoddart revealed that MIMs are perfectly suited compounds for the preparation of molecular machines.^{3,4} MIMs are indeed able to adopt very different conformations that can be interconverted in a controlled manner by applying appropriate chemical, electrical or optical stimuli.⁵ On the other hand, the intertwined structure of MIMs provides also a non-covalent shielding protective effect decreasing the reactivity of some of their subunits.⁶⁻⁹ This effect has been beautifully exploited by Anderson and co-workers to enhance the photostability of azo- and cyanine-dyes encapsulated in macrocyclic components of rotaxanes.⁷⁻⁸ Similarly, sensitive molecular wires such as cumulenes or oligoynes have been also stabilized by a surrounding macrocycle in rotaxane architectures.⁹ In contrast, the chemical reactivity of MIMs has been largely overlooked.^[6] Moreover, only a few examples of post-synthetic modifications in which the

mechanical bonds alter the chemical reactivity of one component in interlocked structures have been investigated so far.¹⁰ As part of this research, our group became recently interested in the preparation of versatile pillar[5]arene-containing rotaxane building blocks equipped with activated stoppers allowing the synthesis of a large variety of derivatives by stopper exchange reactions.¹¹⁻¹³ As these chemical transformations occurred by either an addition/elimination mechanism or a concerted nucleophilic substitution, no intermediate allows for the disassembly of the interlocked molecular ensemble and the rotaxane structure is fully preserved during the stopper exchange reactions. As a typical example, rotaxane building block **1** with pentafluorophenyl stoppers is shown in Figure 1.

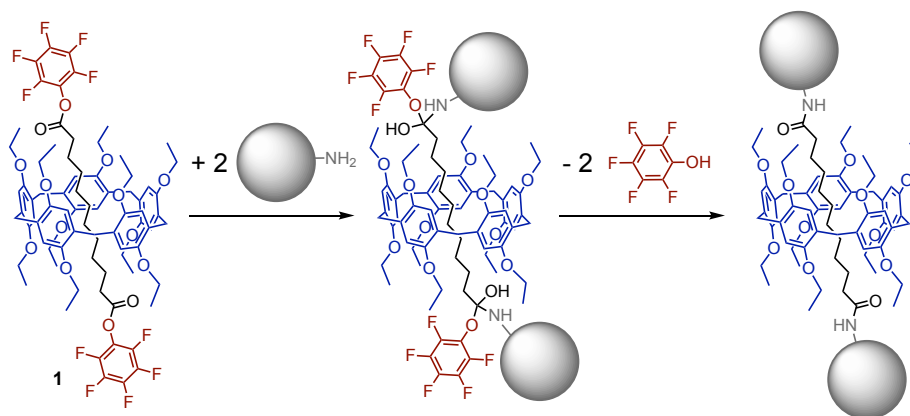


Figure 1. Pillar[5]arene-containing [2]rotaxane building block **1** with pentafluorophenol ester stoppers. Reaction of **1** with amines gave access to a wide range of rotaxanes with amide stoppers in excellent yields. The rotaxane structure is fully preserved during these chemical transformations as the addition-elimination mechanism prevents the unthreading of the axle moiety of the mechanically interlocked system.

Reaction of **1** with nucleophiles such as amines gave access to a wide range of rotaxanes with amide stoppers. Interestingly, it has been noticed that the first addition-elimination is always very fast and the second one significantly slower. This has been ascribed to steric hindrance resulting from the preferential position of the macrocycle close to the pentafluorophenyl stopper in the intermediate mono-acylated product owing to attractive interactions between this electron-deficient stopper and the electron-rich pillar[5]arene. In this chapter, we now report a detailed investigation of the stepwise bis-functionalization of building block **1** with different stoppers thus providing easy access to unsymmetrically functionalized rotaxanes (Figure 2).

Moreover, we have also shown that the pillar[5]arene moiety can act as a protecting group allowing the efficient synthesis of unsymmetrically substituted bis-amides particularly difficult to prepare from the axle. For this purpose, the second amine reagent will be small enough to allow the unthreading of the axle upon the second acylation reaction.

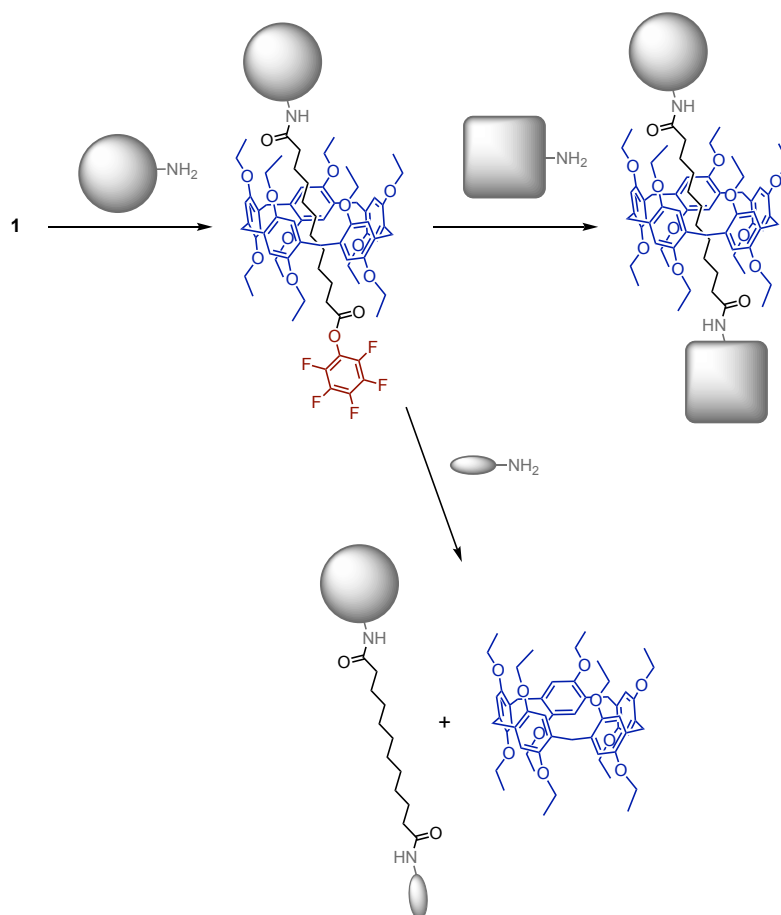
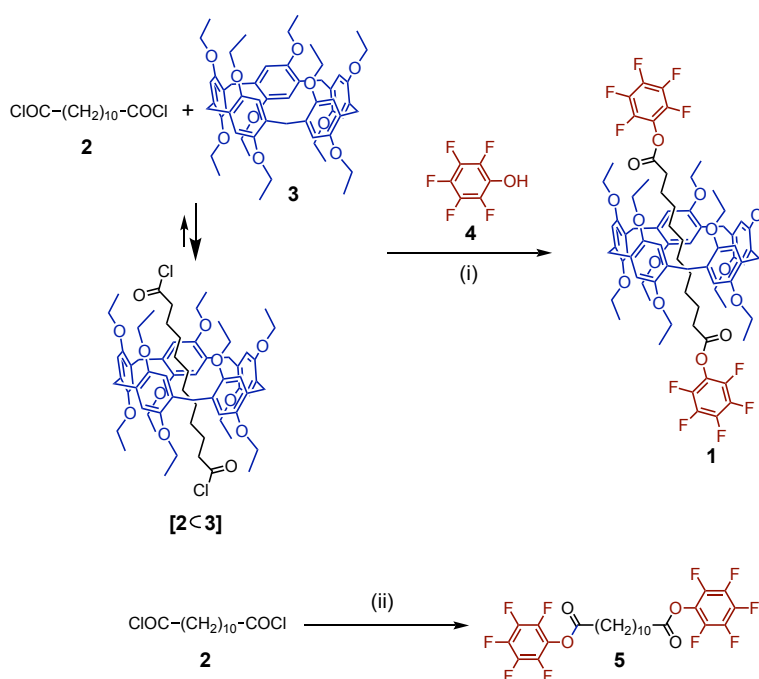


Figure 2. In this section, reaction conditions will be optimized to prepare mono-amide rotaxane building blocks efficiently. These new building blocks will then be used to produce dissymmetrical rotaxanes, and dissymmetrical axles.

II-2. Results and discussion

Preparation of the key building blocks. Building block **1** was prepared from diacyl chloride **2** and pillar[5]arene **3** as reported in the literature (Scheme 1).¹² Successful rotaxane preparation relies on the ability of axle **2** and macrocycle **3** to self-assemble into the appropriate host-guest supramolecular ensemble. The binding constant (K_a) for the 1:1 supramolecular ensemble resulting from the association of **2** and **3** is rather low ($\log K_a = 1.85$ in CDCl_3 at

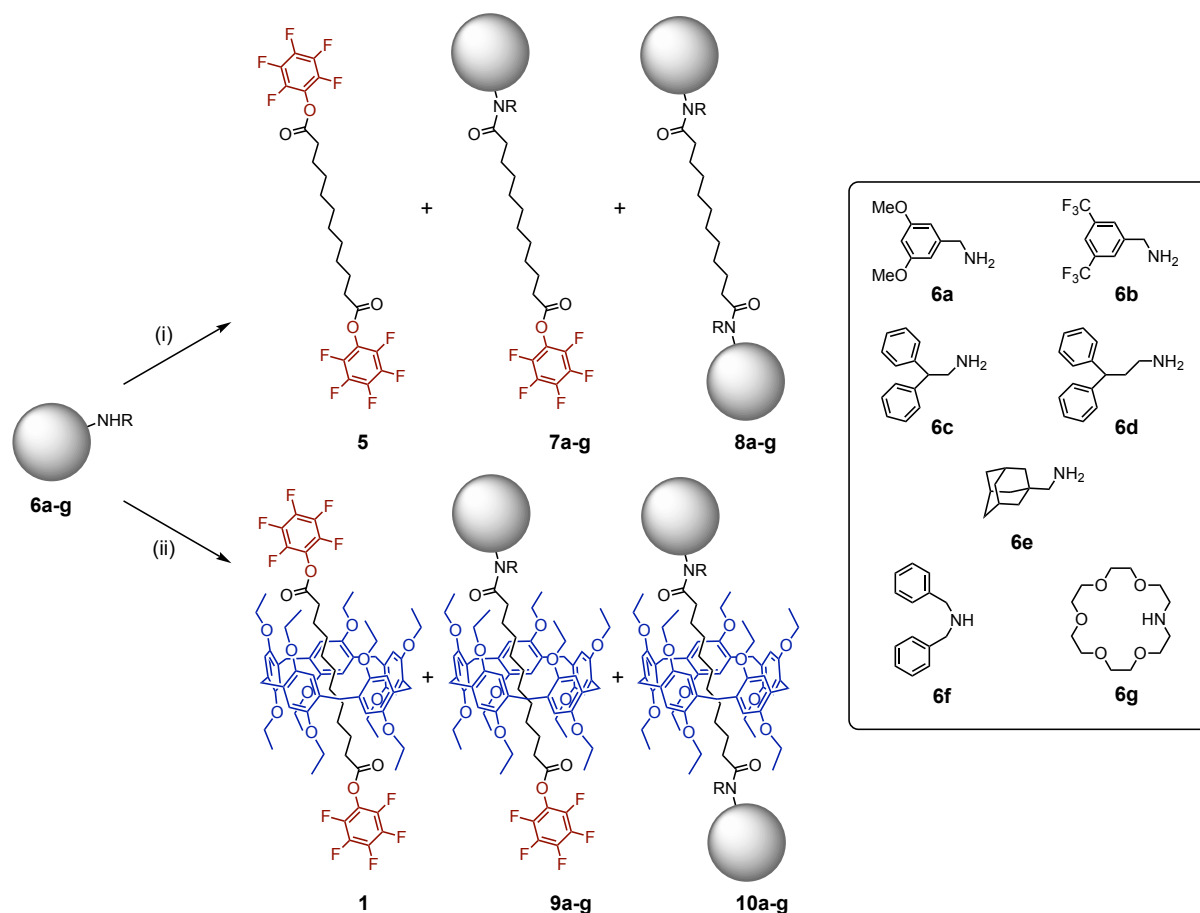
25°C).¹⁴ It is therefore essential to properly adjust the reaction conditions used for the introduction of the pentafluorophenyl stoppers in order to favor the assembly of **2** and **3**. For this reason, all reactions were performed at the lowest possible temperature (-15°C) and at the highest possible concentration. Moreover, pillar[5]arene **3** was also used in excess (3 equiv.). The reaction of diacyl chloride **2** with pentafluorophenol (**4**) in the presence of macrocycle **3** and Et₃N in CHCl₃ gave rotaxane **1**. Compound **1** and the excess of pillar[5]arene **3** were conveniently separated by column chromatography on silica gel. Rotaxane **1** was thus obtained pure in a nearly quantitative yield (98%). Model compound **5** was prepared in 87% yield by treatment of diacyl chloride **2** with pentafluorophenol (**4**).



Scheme 1. Preparation of building blocks **1** and **5**. *Reagents and conditions:* (i) Et₃N, CHCl₃, -15°C (98%); (ii) **4**, Et₃N, CHCl₃, 0°C (87%).

Mono-functionalization of building blocks 1 and 5. In order to evaluate the effect of the pillar[5]arene moiety on the reactivity of the pentafluorophenyl ester subunits in rotaxane **1**, both **1** and model compound **5** were treated with one equivalent of various primary amine reagents (**6a-e**). All reactions were performed in THF at 0°C (Scheme 2). After 3 hours, the resulting mixtures were filtered over a short plug of silica gel and the crude materials were directly analyzed by ¹H NMR spectroscopy to evaluate the outcome of the reactions. Secondary amine reagents **6f-g** were also used. In these particular cases, completion of the reactions with

axle **5** required 12 h at 0°C. At this temperature, no reaction was observed between **6f-g** and rotaxane **1** thus already highlighting a significant influence of the pillar[5]arene moiety on the reactivity of its pentafluorophenyl ester moieties. In the case of **1**, complete consumption of the secondary amine reagents was only observed after several days at room temperature. Again, the outcome of these reactions was directly analyzed by recording ¹H NMR spectra of the resulting crude materials.



Scheme 2. Treatment of building blocks **1** and **5** with amine reagents **6a-g** (1 equiv.). The proportion of starting material, mono-acylated and bis-acylated products was determined based on the analysis of the ¹H NMR spectra recorded for the crude products (see Table 1). *Reagents and conditions:* (i) **5** (1 equiv.), THF, 0°C; (ii) **1** (1 equiv.), THF, 0°C.

In all cases, the relative proportion of starting material, mono- and bis-acylated products was derived from the integration of the ¹H NMR spectra recorded for the crude materials. The results are summarized in Table 1. In the case of axle **5**, the two reactive pentafluorophenyl subunits are independent and perfectly equivalent. As expected, the treatment of **5** with one equivalent of amine nucleophiles **6a-g** always yielded unreacted **5**, **7a-g** and **8a-g** in a statistical

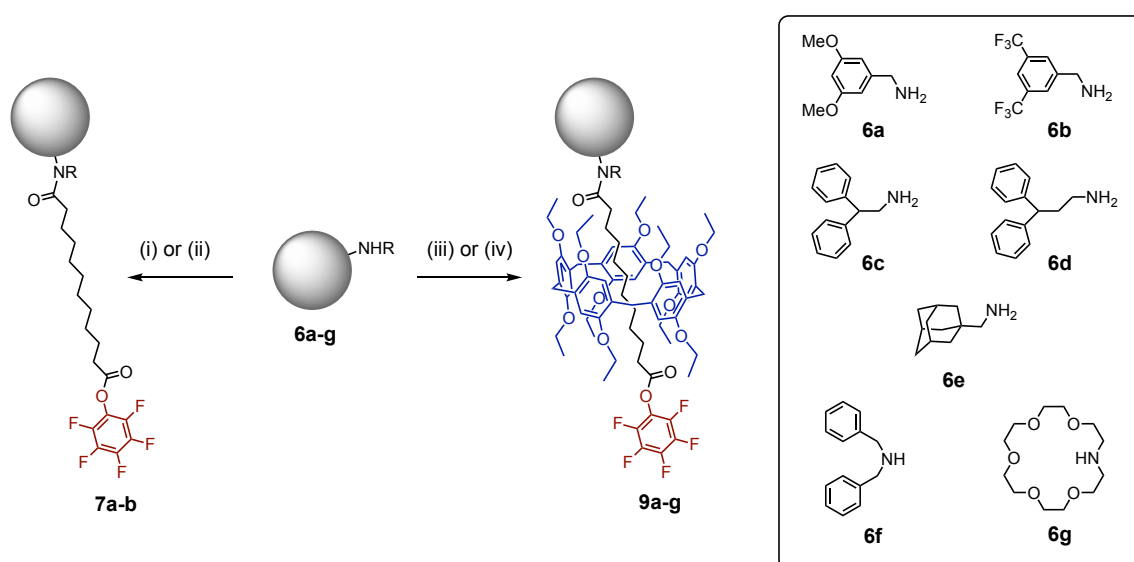
1:2:1 relative ratio. Interestingly, this is not the case anymore when starting from rotaxane **1**. Effectively, formation of the monoacylated product was always largely favored thus revealing that the second acylation of **9a-g** leading to **10a-g** is much slower when compared to the first acylation of starting material **1**. This kinetic selectivity is ascribed to steric effects resulting from the presence of the pillar[5]arene moiety that must be likely attracted by the electro-deficient pentafluorophenyl stopper in **9a-g** and thus limiting the accessibility of its reactive pentafluorophenyl ester group. This view was fully supported by the detailed analysis of the ^1H NMR spectra of **9a-g** (*vide infra*). It is also worth noting that the temperature plays an important role in the preferential formation of mono-amides **9a-g**. Effectively, the selectivity was significantly decreased when the reaction was performed at room temperature rather than at 0°C . This observation also fully supports the kinetic origin for the selective formation of mono-amides from symmetrical building block **5**.

Table 1. Relative proportion of starting material, mono- and bis-acylated products derived from the integration of the ^1H NMR spectra recorded for the crude materials resulting from the reaction of **1** and **5** with 1 equiv. of amine reagents **6a-g** (see Scheme 1).

Amine reagent	Relative proportion of 5 / 7 / 8	Relative proportion of 1 / 9 / 10
6a	24 / 52 / 24	3 / 94 / 3
6b	25 / 50 / 25	7 / 87 / 6
6c	23 / 51 / 26	3 / 94 / 3
6d	25 / 50 / 25	10 / 81 / 9
6e	25 / 50 / 25	13 / 74 / 13
6f	25 / 50 / 25	19 / 76 / 5
6g	25 / 50 / 25	5 / 90 / 5

The reaction conditions were then optimized for the preparative synthesis of mono-acylated products from **1** and amine reagents **6a** and **6b** (Scheme 3). Treatment of amines **6a-b** with a one equiv. of **1** in THF at 0°C provided mainly the desired mono-amide products but small amounts of diacylated byproducts were also formed under these conditions. Compounds **9a** and **9b** were then isolated in a pure form in 94 and 87% yields, respectively. By using an excess of **1** (2 equiv.), only residual traces of diacylated byproducts were observed and the mono-acylated products were almost exclusively obtained. The excess of starting rotaxane **1** and products **9a-b** were then easily separated by column chromatography on silica gel owing to a large difference in polarity. Compounds **9a** and **9b** were isolated in 98 and 97% yields, respectively. Importantly, treatment of **6a-b** (1 equiv.) with model compound **5** (2 equiv.) under

the same conditions provided the corresponding mono-amide products (**7a-b**) with significant amounts of di-acylated byproducts **8a-b**. Under these conditions, compounds **7a** and **7b** were isolated in 66 and 61% yields, respectively. By further increasing the excess of **5** (3 equiv.), the yields in **7a** and **7b** were improved to 88 and 75%, respectively. However, significant amount of bis-acylated were still obtained under these conditions.



Scheme 3. Preparation of mono-acylated products from building blocks **1** and **5**. *Reagents and conditions:* (i) **5** (2 equiv.), THF, 0°C (**7a**: 66%; **7b**: 61%); (ii) **5** (3 equiv.), THF, 0°C (**7a**: 88%; **7b**: 75%); (i) **1** (1 equiv.), THF, 0°C (**9a**: 94%; **9b**: 82%); (ii) **1** (2 equiv.) THF, 0°C for **6a-e** and rt for **6f-g** (**9a**: 98%; **9b**: 97%; **9c**: 91%; **9d**: 94%; **9e**: 98%; **9f**: 98%; **9g**: 91%).

The conditions optimized for the preparation of **9a-b** were then used for the synthesis of compounds **9c-g**. For primary amines **6c-e**, treatment with an excess of **1** (2 equiv.) in THF at 0°C provided mono-amide rotaxanes **9c-e** in excellent yields. With the secondary amine reagents **6f-g**, the reactions with **5** were carried out at room temperature. Compounds **9f** and **9g** were thus obtained in very good yields.

Mono-amide rotaxanes **9a-g** were fully characterized by NMR and IR spectroscopies and mass spectrometry. Crystals suitable for X-ray crystal structure analysis were obtained for both **9a** and **9b**. The structures are shown in Figure 3. Owing to their D_5 -symmetry imposed by their pillar[5]arene subunit, compounds **9a** and **9b** are chiral. Close inspection of the crystal lattice revealed that both **9a** and **9b** crystallized as racemates. As shown in Figure 3, π -stacked pairs of enantiomers with opposite chirality are effectively observed in both cases. Further

inspection of the supramolecular organization within the crystals of **9a** and **9b** revealed a very similar packing. Indeed, both compounds gave crystals belonging to the same monoclinic lattice for space group 14, namely $P2_1/c$ for **9a** and $P2_1/n$ for **9b**. These space groups refer actually to the same lattice but they differ in the choice of the axes used to define the unit cell. Both **9a** and **9b** adopt a similar conformation in the solid state. Moreover, similar intermolecular interactions are observed between neighboring molecules in the two crystal lattices.

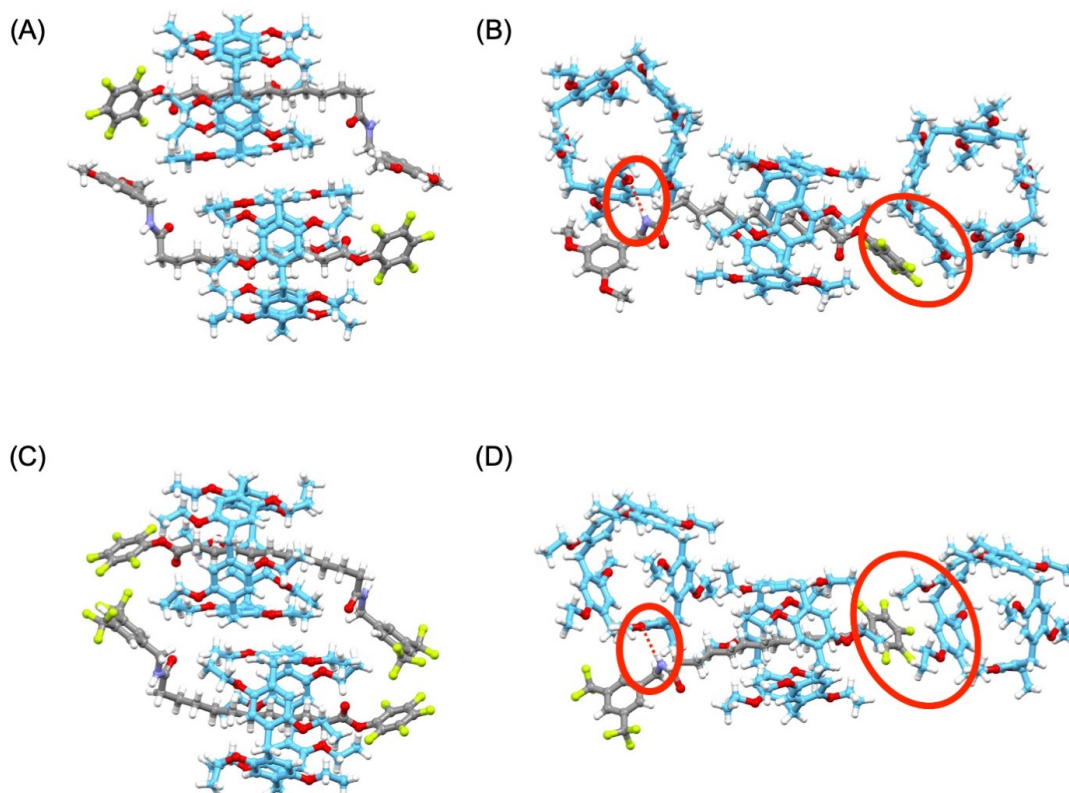


Figure 3. Pairs of enantiomers observed in the X-ray crystal structures of **9a** (A) and **9b** (C). Views highlighting remarkable intermolecular interactions within the crystal lattice of **9a** (B) and **9b** (D); NH \cdots O distances: 2.259 Å for **9a** and 2.365 Å for **9b** (H: white, F: light green, O: red, N: blue, C: grey for the axle and pale blue for the pillar[5]arene moiety).

In both cases, the electron-deficient pentafluorophenyl aromatic ring is interacting with the electron-rich hydroquinone subunit of a neighboring pillar[5]arene. In addition, the amide NH group of the axle of one rotaxane is interacting with the O atom of a pillar[5]arene moiety belonging to another neighboring rotaxane molecule. The establishment of this particular interaction is forcing the $-(\text{CH}_2)_{10}$ - chain of the axle moiety to adopt a tilted conformation. As a result, the pillar[5]arene moiety of the rotaxanes is pushed far from its amide stopper. The peculiar position of the macrocyclic moiety close to the pentafluorophenyl ester subunits

observed in the solid state is therefore not ascribed to an attractive interaction of the pillar[5]arene for its more electro-deficient stopper but is more likely related to packing forces allowing to maximize favorable intermolecular H-bonding and π - π -stacking interactions within the crystal lattice of **9a** or **9b**.

In solution, dynamic gliding motions of the pillar[5]arene subunit along the $-(\text{CH}_2)_{10}$ - chain of the axle moiety of rotaxanes **9a-g** are expected. However, the observed kinetic effects allowing the preferential formation of mono-amides **9a-g** from **5** suggest that the pillar[5]arene is somehow attracted by its pentafluorophenyl ester stopper in **9a-g** thus generating sufficient steric hindrance explaining the reduced kinetic for the second stopper exchange reaction and thus the limited formation of **10a-g** during these stopper exchange reactions. In order to support this hypothesis, the chemical shift observed in the ^1H NMR spectra for the methylene moieties of the $-(\text{CH}_2)_{10}$ - chain of rotaxanes **9a-g** were carefully analyzed. As a typical example, the ^1H NMR spectra recorded at 25°C in CDCl_3 for rotaxane **9b** and the corresponding axle **7b** are shown in Figure 4.

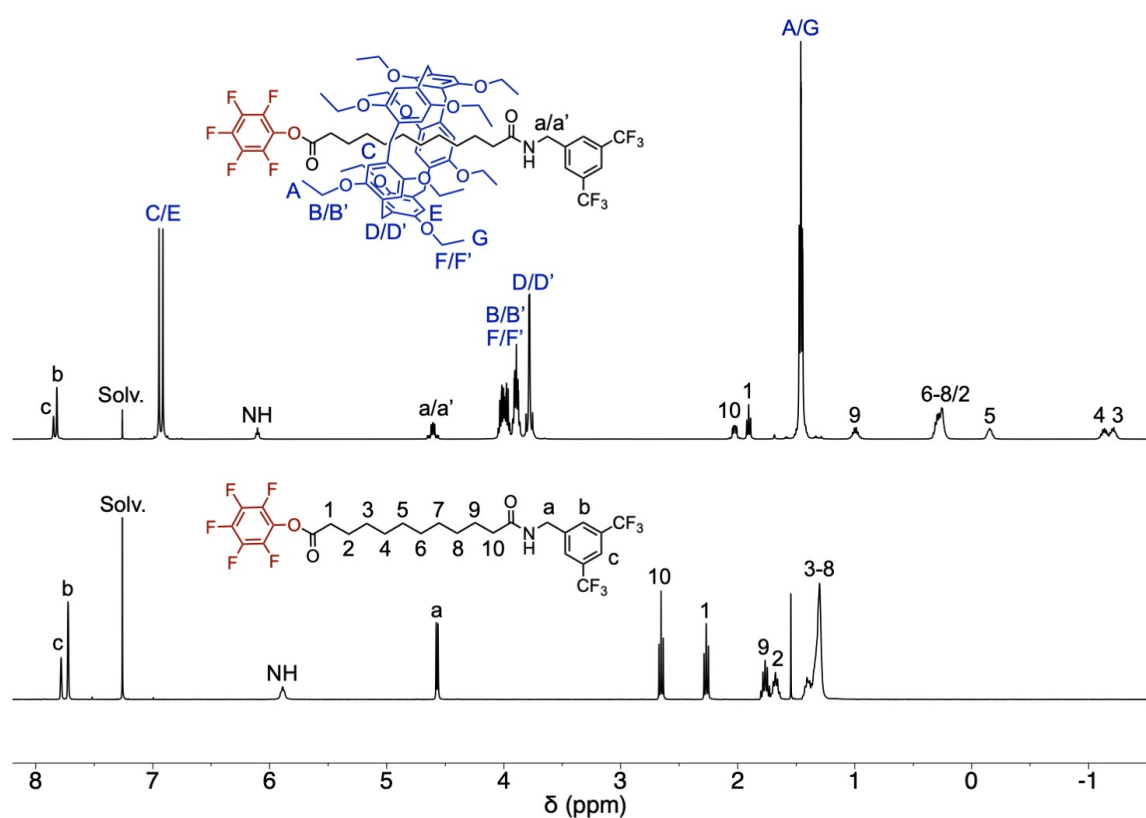


Figure 4. ^1H NMR spectra (500 MHz) recorded for **7b** and **9b** in CDCl_3 at 25°C.

When compared to axle **7a**, a dramatic shielding is observed for all signals arising from the $-(\text{CH}_2)_{10}-$ chain for rotaxane **9b**. This is due to the ring current effect of the pillar[5]arene aromatic moieties on the CH_2 groups of the axle in **9b**. Clearly, all methylene groups are affected thus showing that there is no preferential conformation. In other words, dynamic gliding motions of the pillar[5]arene subunit along the $-(\text{CH}_2)_{10}-$ chain must be very fast on the NMR timescale. However, the shielding effect is more important for H(2), H(3), H(4) and H(5) thus suggesting a higher probability of presence of the pillar[5]arene subunit over these specific positions. Therefore, the electron-rich macrocycle must be on average closer to the most electro-deficient stopper. Similar effects were also evidenced for **9a** and **9c-g**. (Table 2). In all cases, analysis of the chemical shifts observed for the methylene moieties of the $-(\text{CH}_2)_{10}-$ chain in the ^1H NMR of the dissymmetrical rotaxanes were fully consistent with a preferential presence of the macrocycle close to the pentafluorophenyl ester stopper. Favorable donor-acceptor electronic effects may therefore slightly lower the energy of this particular position explaining why it is more populated. As a result, the accessibility of the reactive carbonyl group in **9a-g** by nucleophilic reagents must be more difficult thus explaining well the efficient preparation of mono-amide rotaxanes from building block **1**.

Table 2. Chemical shifts (δ in ppm) of the methylene units of the $-(\text{CH}_2)_{10}-$ chain in the ^1H NMR spectra recorded at 25°C in CDCl_3 for dissymmetrical rotaxanes **9a-g** (for the numbering, see Figure 4).

Compound	H(1)	H(2)	H(3)	H(4)	H(5)	H(6)	H(7)	H(8)	H(9)	H(10)
9a	1.86	-0.05	-1.83	-1.69	-0.38	0.34	0.63	0.86	1.45	2.11
9b	2.02	0.31	-1.18	-1.11	-0.17	0.20	0.20	0.20	0.94	1.87
9c	1.71	-0.31	-2.25	-2.07	-0.56	0.35	0.83	1.08	1.50	2.04
9d	1.86	-0.06	-1.85	-1.70	-0.36	0.37	0.67	0.85	1.36	1.98
9e	1.81	-0.22	-2.13	-1.93	-0.41	0.49	0.97	1.24	1.68	2.26
9f	1.77	-0.27	-2.25	-2.04	-0.44	0.52	1.08	1.35	1.86	2.56
9g	1.69	-0.37	-2.35	-2.11	-0.48	0.50	1.04	1.29	1.69	2.42

Interestingly, detailed analysis of the chemical shifts of the methylene groups of **9a-g** as a function of the amide stopper revealed also some interesting trends. The probability of presence of the macrocycle close to the pentafluorophenyl stopper is increased when the amide stopper is electron-rich (**9a**) or rather bulky (**9c**) as suggested by a more important shielding for the signals ascribed to H(2-5) and a less important one for those corresponding to the resonances of H(6-9). This view is fully consistent with the different relative proportions of starting material, mono- and bis-acylated products obtained in the initial reactions of **1** with primary amines **6a-**

e (Scheme 2, Table 1), the preferential formation of mono-amide rotaxanes being effectively more favorable with primary amine reagents **6a** and **6c** when compared to the other ones.

To fully understand the influence of the different stoppers on the conformational equilibria observed for rotaxanes **9a-g**, the formation of host-guest complexes between pillar[5]arene **3** and model compounds **11a-c** was investigated (Figure 5). The preparation of **11a-c** is shown in the inset of Figure 5. Reaction of amines **6a-b** with undecanoic acid under acylation conditions using 1,1'-carbonyldiimidazole (CDI) afforded model compounds **11a-b** in good yields. Model compound **11c** was prepared from undecanoic acid and pentafluorophenol (**4**) under esterification conditions using *N,N'*-dicyclohexylcarbodiimide (DCC) and 4-dimethylaminopyridine (DMAP).

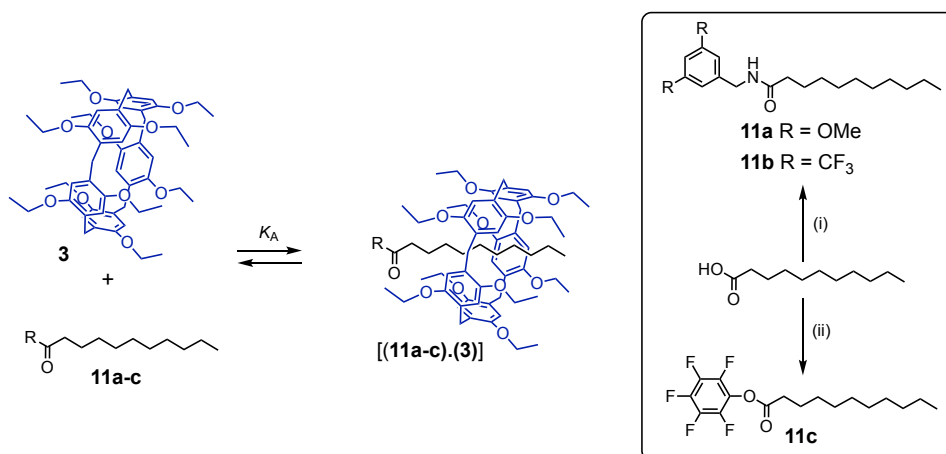
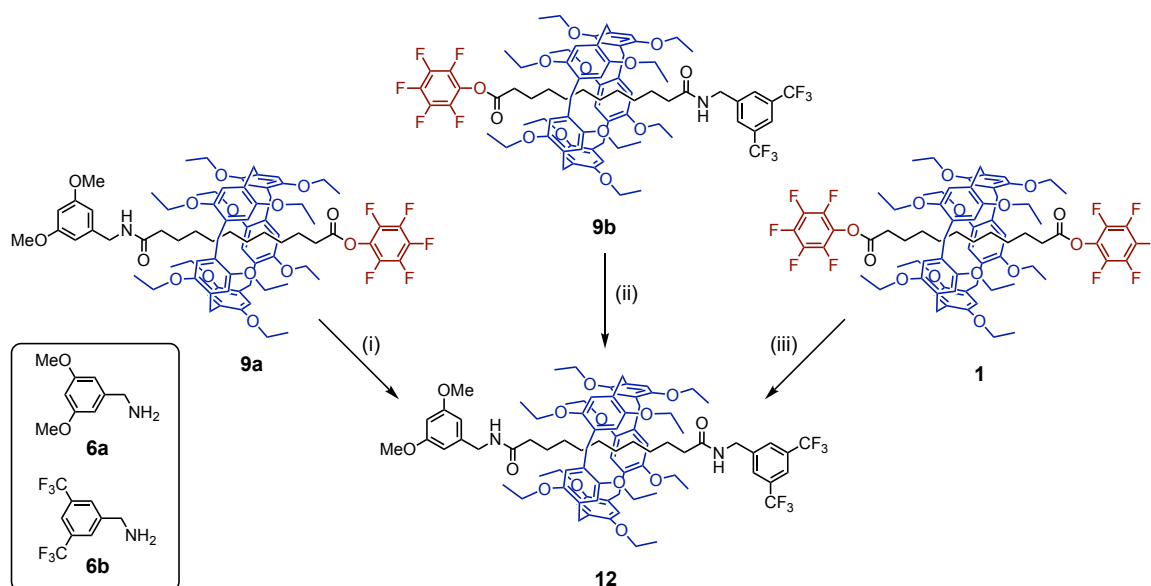


Figure 5. The formation of host-guest complexes from model compounds **11a-c** and pillar[5]arene **3**; the $\log K_A$ values derived from ^1H NMR binding studies in CDCl_3 at 298 K are 0.38(2) for **11a**, 0.82(1) for **11b** and 1.08(2) for **11c**. Inset: synthesis of model compounds **11a-c**; reagents and conditions: (i) **6a-b**, CDI, CHCl_3 , 0°C to rt (**11a**: 98% from **6a**; **11b**: 89% from **6b**); (ii) **4**, DCC, DMAP, CH_2Cl_2 , 0°C to rt (99%).

The ability of **11a-c** to form inclusion complexes with pillar[5]arene **3** was investigated by ^1H NMR binding studies in CDCl_3 at 298 K. The association constants (K_A) for the 1:1 complexes were estimated on the basis of the complexation-induced changes in chemical shift by using curve fitting analysis. The $\log K_A$ values thus obtained are 0.38(2) for **11a**, 0.82(1) for **11b** and 1.08(2) for **11c**. The formation of the host-guest complex is significantly more favorable for guest **11c**. Moreover, the nature of the substituents of the terminal benzylic groups in **11a** and **11b** have also an effect on the K_A values, the formation of the host-guest complex being more favorable for the guest with the electron-deficient bis(trifluoromethyl)benzyl substituent. These

observations are fully consistent with the observed conformational preferences of rotaxanes **9a** and **9b**, and explains well why the peripheral position of the pillar[5]arene close to the pentafluorophenyl ester stopper is favored.

Preparation of dissymmetrical rotaxane 12. Having now in hand an efficient procedure to easily produce dissymmetrical rotaxane building blocks from **5**, we decided to further investigate their possible functionalization to produce rotaxanes with two different amide stoppers. As shown in Scheme 4, treatment of **9a** with amine **4b** in THF at room temperature gave rotaxane **12** with two different amide stoppers. The preparation of **12** was also performed by reversing the order of the successive stopper exchange reactions. Specifically, reaction of **9b** with amine **4a** afforded **12** in a good yield.



Scheme 4. Preparation of compound **12**. *Reagents and conditions:* (i) **6b**, THF, rt (98%); (ii) **6a**, THF, rt (93%); (iii) **6a**, THF, 0°C, then **6b**, THF, rt (89%).

Compound **12** was also directly prepared from **1** by a one-pot approach. In this particular case, the order of addition of the different amine reagents was important. It was decided to use amine **6a** first as this reagent was more selective for the preparation of a mono-amide intermediate (Table 1). Rotaxane **1** was thus first treated with amine **6a** (1 equiv.) in THF at 0°C. Upon 3 hours, **6a** was totally consumed and the second amine reagent, namely **6b**, was added to the reaction mixture and the temperature increased to room temperature. Compound **12** was thus obtained in 89% yield.

Rotaxane **12** was characterized by a combination of different analytical tools. Crystals suitable for X-ray crystal analysis were obtained by slow diffusion of hexane/methanol into a CH_2Cl_2 solution of **12**. As shown in Figure 6, compound **12** co-crystallized with a methanol molecule that is interacting with the O atom of a carbonyl group of the axle moiety of **12** through a H-bond. In addition to the classical intermolecular $\text{C-H}\cdots\pi$ interactions between the aromatic moieties of the pillar[5]arene subunit and the methylene groups of the axle located within its cavity,¹⁰ the occurrence of an intramolecular H-bond between one NH of the axle and an oxygen of the pillar[5]arene subunit is also observed.

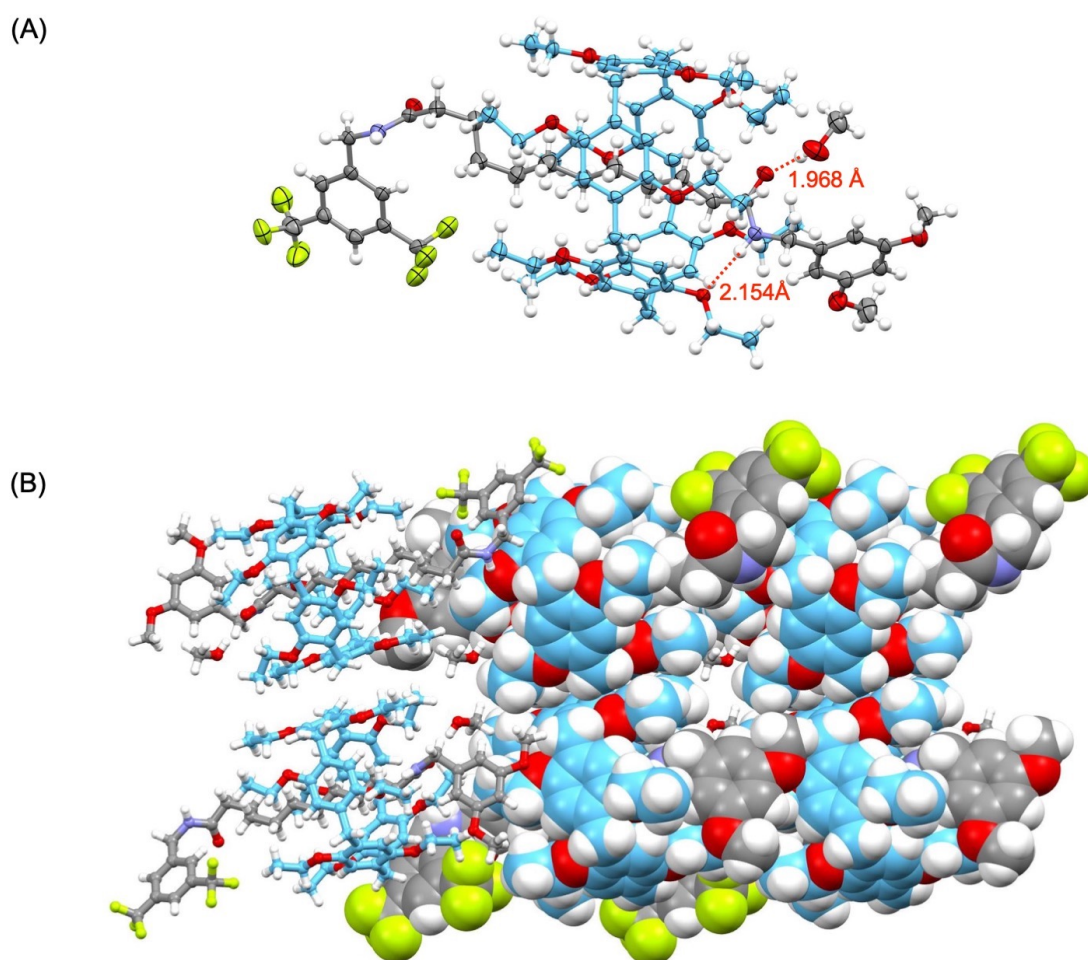
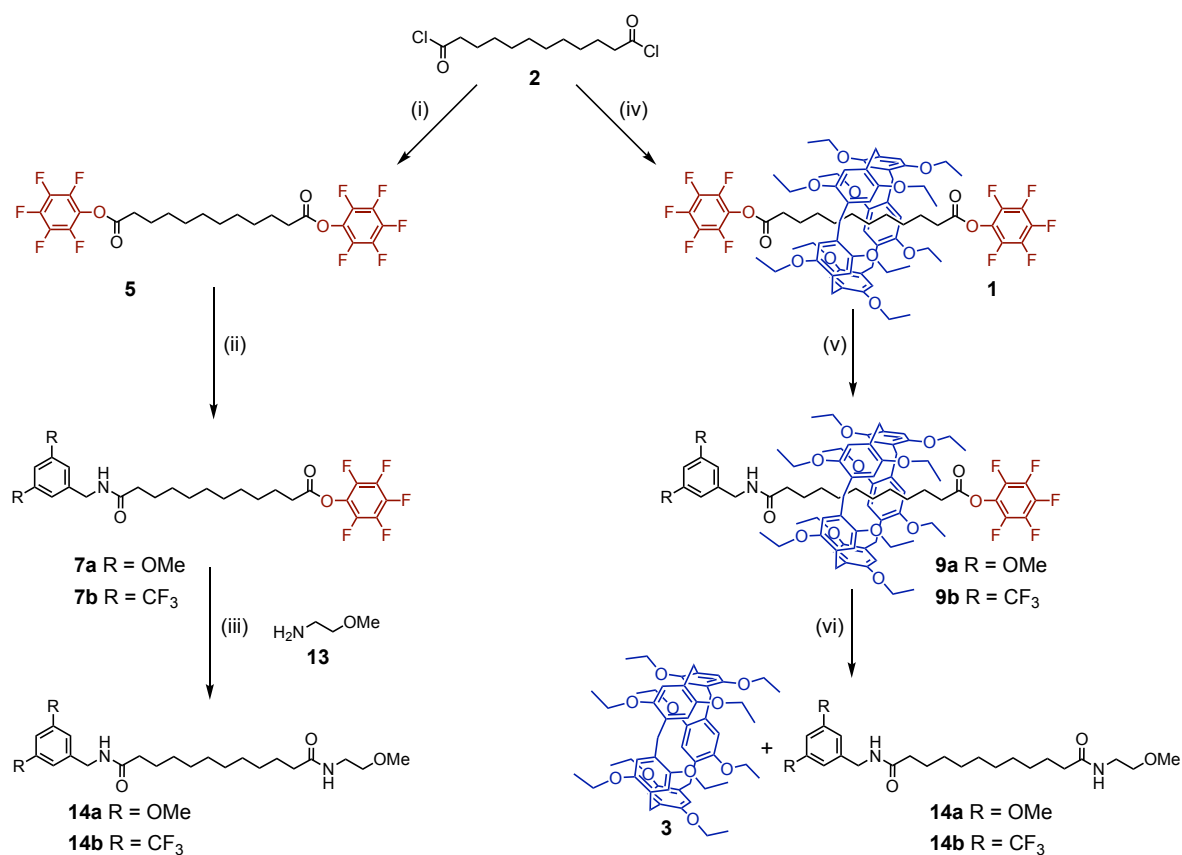


Figure 6. (A) ORTEP plot of the structure of **12**.MeOH highlighting the intramolecular H-bond between the NH group of the axle and an O atom of the macrocycle as well as the H-bond between the axle and the co-crystallized solvent molecule (H: white, F: light green, O: red, N: blue, C: grey for the axle and pale blue for the pillar[5]arene moiety; the disorder of some CF_3 groups has been omitted for clarity; thermal ellipsoids are shown at 50% probability level). (B) Stacking within the **12**.MeOH lattice highlighting the intermolecular π - π interactions between neighboring rotaxanes.

Interestingly, the dodecyl chain of **12** does not adopt a fully extended conformation but is folded. As already observed in the crystal lattice of related rotaxanes,^{12,15} packing forces are likely responsible for the folding of the decyl chain in order to optimize favorable intermolecular contacts. This is fully supported by the observation of intermolecular π - π interactions between the electro-deficient bis(trifluoromethyl)phenyl rings with electron-rich hydroquinone moieties of neighboring pillar[5]arenes leading to the formation of infinite supramolecular chains in the crystal lattice (Figure 5B). Compound **12** is chiral and crystallized as a racemate. Indeed, the two enantiomers are organized in anti-parallel supramolecular chains interacting through π - π interactions between enantiomeric pillar[5]arene moieties.

The pillar[5]arene as a protecting group. The stopper exchange reaction from building blocks **9a-b** is particularly useful to produce rotaxanes with different amide stoppers as shown with the preparation of compound **12**. However, reaction of **9a-b** with a relatively small amine reagent should promote the disassembly of the rotaxane structure and thus provide the corresponding components separately. As the mono-functionalization is by far more efficient and selective for rotaxane building block **1** when compared to model compound **5**, rotaxanes such as **9a-b** appear to be attractive building blocks for the efficient preparation of dissymmetrical axle products. In this case, the pillar[5]arene moiety plays the role of a *recyclable protecting group* allowing the successive introduction of two different terminal amide subunits onto axle **5**. In this respect, amine **13** was selected as the nucleophile (Scheme 5). For comparison purposes, the all synthetic sequence starting from the diacyl chloride starting material is shown in Scheme 5. Compounds **14a-b** were prepared by following two distinct synthetic routes, the first one is using rotaxane intermediates whereas the second one is based on the stepwise functionalization of the axle. The preparation of **7a-b** was achieved in two steps from diacyl chloride **2**. Upon introduction of the pentafluorophenyl ester groups, the mono-functionalization of **5** with amines **6a-b** was poorly selective thus leading to **7a-b** in moderate yield. Moreover, the purification of both **7a** and **7b** by column chromatography on SiO₂ was particularly difficult owing to the formation of significant amounts of bis-amide byproducts (**8a** and **8b**) close in polarity. Finally, treatment of **7a-b** with amine **13** afforded dissymmetrical axle **14a-b** in good yields. These compounds were then prepared by using the rotaxane strategy. In contrast to the first synthesis, high yields were obtained for the two first steps leading to rotaxane building blocks **9a-b**. The selective mono-functionalization of **1** is a clear advantage as it prevents difficult purifications and is thus by far more convenient. Reaction of **9a-b** with

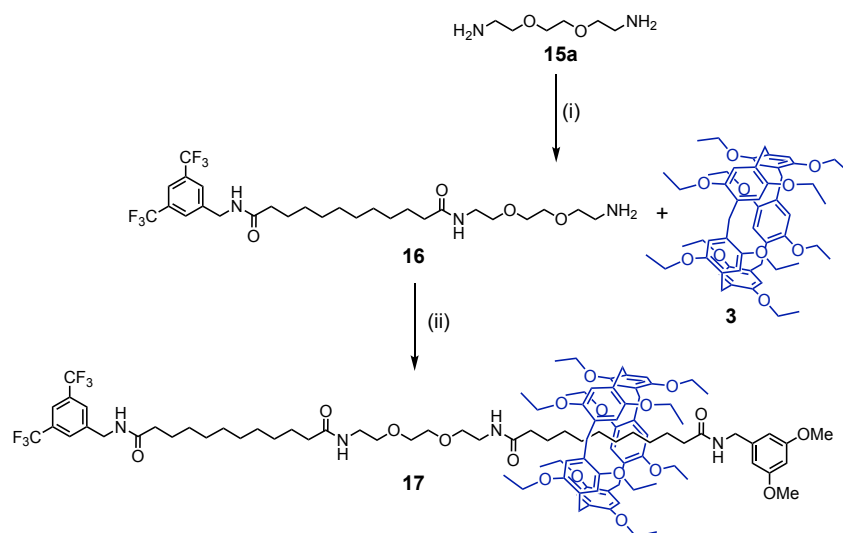
amine **13** finally provided the expected **14a-b** in good yields together with pillar[5]arene **3** that escaped the axle upon reaction with **13** because the methoxyethyl group is too small to act as a stopper to preserve the rotaxane structure. The two products were conveniently separated by column chromatography. Importantly, over 90% of pillar[5]arene **3** was recovered in both cases. Recycling of the pillar[5]arene protecting group is therefore effective. Not only the synthetic route using rotaxane building blocks was more convenient from a practical point of view due to easier purifications, the overall yields for the preparation of **14a-b** from **2** were also much higher (89 vs. 55% for **14a** for the 3 steps and 87 vs. 48% for **14b** for the 3 steps).



Scheme 5. Preparation of dissymmetrical axles **14a-b** by following two different synthetic routes. Reagents and conditions: (i) **4**, Et₃N, CHCl₃, 0°C (87%); (ii) **6a-b** (1 equiv.), **5** (2 equiv.), THF, 0°C (**7a**: 66%; **7b**: 61%); (iii) THF, rt (**14a**: 95%; **14b**: 91%); (iv) **3**, **4**, Et₃N, CHCl₃, -15°C (98%); (v) **6a-b** (1 equiv.), **5** (2 equiv.) THF, 0°C (**9a**: 98%; **9b**: 97%); (vi) **13**, THF, rt (**14a**: 93% and **3**: 92%; **14b**: 92% and **3**: 97%).

This strategy was then applied to prepare a [2]rotaxane with an elongated axle (Scheme 6). Reaction of **9a** with a large excess of diamine **15a** (5 equiv.) in THF gave **16** as well as pillar[5]arene **3**. Compound **16** was then isolated in 69% yield. The pillar[5]arene protecting group was also recovered in 99% yield. It can be noted that the preparation of amine **16** was

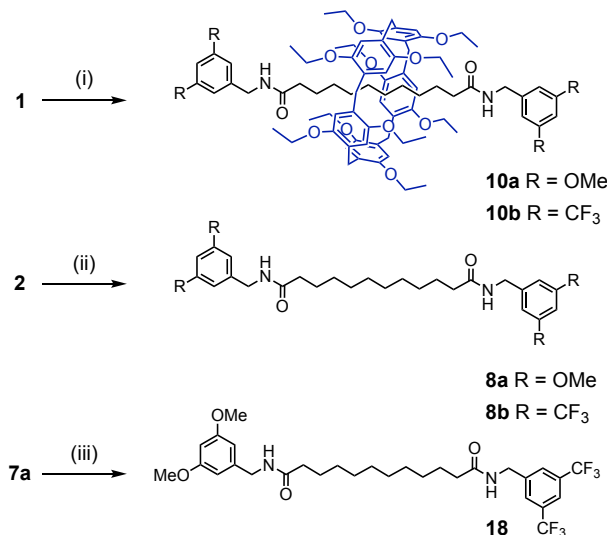
also attempted by direct treatment of **7a** with an excess of **15a** (5 equiv.). In this particular case, the purification of **16** was very difficult owing to the formation of large amounts of diacetylated byproducts and the isolated yield lower (47%). Finally, treatment of amine **16** with building block **9a** in THF at room temperature gave **17** in 98% yield. With its very long axle component, [2]rotaxane **17** is an extended analogue of **12**. With rotaxanes **12** and **17** in hand, the shuttling processes of the pillar[5]arene macrocycle along their axle was then investigated in details.



Scheme 6. Preparation of rotaxane **17** with an elongated axle. Reagents and conditions: (i) **9a**, THF, rt (**16**: 69% and **3**: 99%); (ii) **9b**, THF, rt (98%).

Conformational analysis. In the solid state, the pillar[5]arene subunit of rotaxane **12** is located close to the electron-rich dimethoxyphenyl stopper. As already mentioned for **9a-b**, this peculiar conformation generates the most favorable intermolecular interactions within the crystal lattice of **12** but is not necessarily correlated with the conformational preferences of rotaxane **12** in solution. Obviously, one may expect random gliding motions of the pillar[5]arene moiety all along its decyl axis. However, some specific positions maybe favored owing to the nature of the stopper or through the establishment of H-bonding interactions between one of the NH groups of the axle and an O atom of the pillar[5]arene component. This prompted us to analyze in details the ¹H NMR spectra recorded for rotaxane **12** at different temperatures. In addition, to fully confirm the interpretation of the NMR data, the corresponding symmetrical model compounds (**10a-b**) were prepared by reaction of **1** with the appropriate amine reagent (**6a** or **6b**) in THF at room temperature (Scheme 7). Furthermore, model axles **8a-b** and **18** were also synthesized for comparison purposes. Starting from **2**,

symmetrical axles **8a** and **8b** were obtained by treatment with the appropriate amine reagent (**6a** and **6b**) in CH_2Cl_2 in the presence of Et_3N . Model compound **18** was prepared in 94% yield from amine **6b** and pentafluorophenyl ester **7a**.



Scheme 7. Preparation of model compounds **10a-b**, **8a-b** and **18**. *Reagents and conditions:* (i) **6a-b**, THF, rt (**10a**: 95%; **10b**: 93%); (ii) **6a-b**, Et_3N , CH_2Cl_2 , rt (**8a**: 97%; **8b**: 90%); (iii) **6b**, THF, rt (94%).

The ^1H NMR spectra recorded for rotaxanes **12** and **10a-b** in CD_2Cl_2 at 298K are depicted in Figure 7 and the chemical shifts observed for the methylene moieties of the $-(\text{CH}_2)_{10}-$ chain in the ^1H NMR of **12**, **10a-b**, **8a-b** and **18** are gathered in Table 3. In all cases, 2D NMR COSY and ROESY spectra were analyzed for an unambiguous assignment of all signals.

Table 3. Chemical shifts (δ in ppm) of the methylene units of the $-(\text{CH}_2)_{10}-$ chain in the ^1H NMR spectra recorded at 25°C in CD_2Cl_2 for compounds **12**, **10a-b**, **8a-b** and **18** (for the numbering, see Figure 7).

Compound	H(1)	H(2)	H(3)	H(4)	H(5)	H(6)	H(7)	H(8)	H(9)	H(10)
12	1.81	0.93	0.27	0.17	0.17	-0.03	-0.83	-1.17	-0.13	1.23
10a	1.56	0.51	-0.46	-0.46	0.00					
10b						0.19	-0.29	-0.49	0.37	1.51
8a	2.23	1.62	1.29	1.29	1.29					
8b						1.27	1.27	1.27	1.61	2.16
18	2.23	1.64	1.28	1.28	1.28	1.28	1.28	1.28	1.64	2.18

For all rotaxanes, the characteristic features of the pillar[5]arene moiety are clearly observed. When compared to **10a-b**, the symmetry of **12** is reduced (C_5 vs. D_5) owing to the

unsymmetrical substitution of its axle moiety. Therefore, the two rims of the pillar[5]arene subunit are equivalent in **10a-b** but nonequivalent in **12**. For this reason, two sets of signals are observed for the peripheral ethoxy groups of **12**. Two triplets are effectively observed at $\delta = 1.38$ and 1.44 ppm for the two pairs of five equivalent CH_3 moieties. Moreover, whereas the two protons of the pillar[5]arene CH_2 units are homotopic in **10a-b**, they are diastereotopic in the case of **12**. As a result, protons H(D) give rise to a singlet in the spectra of **10a-b**. In contrast, an AB system ($J = 13$ Hz) is observed for H(D/D')

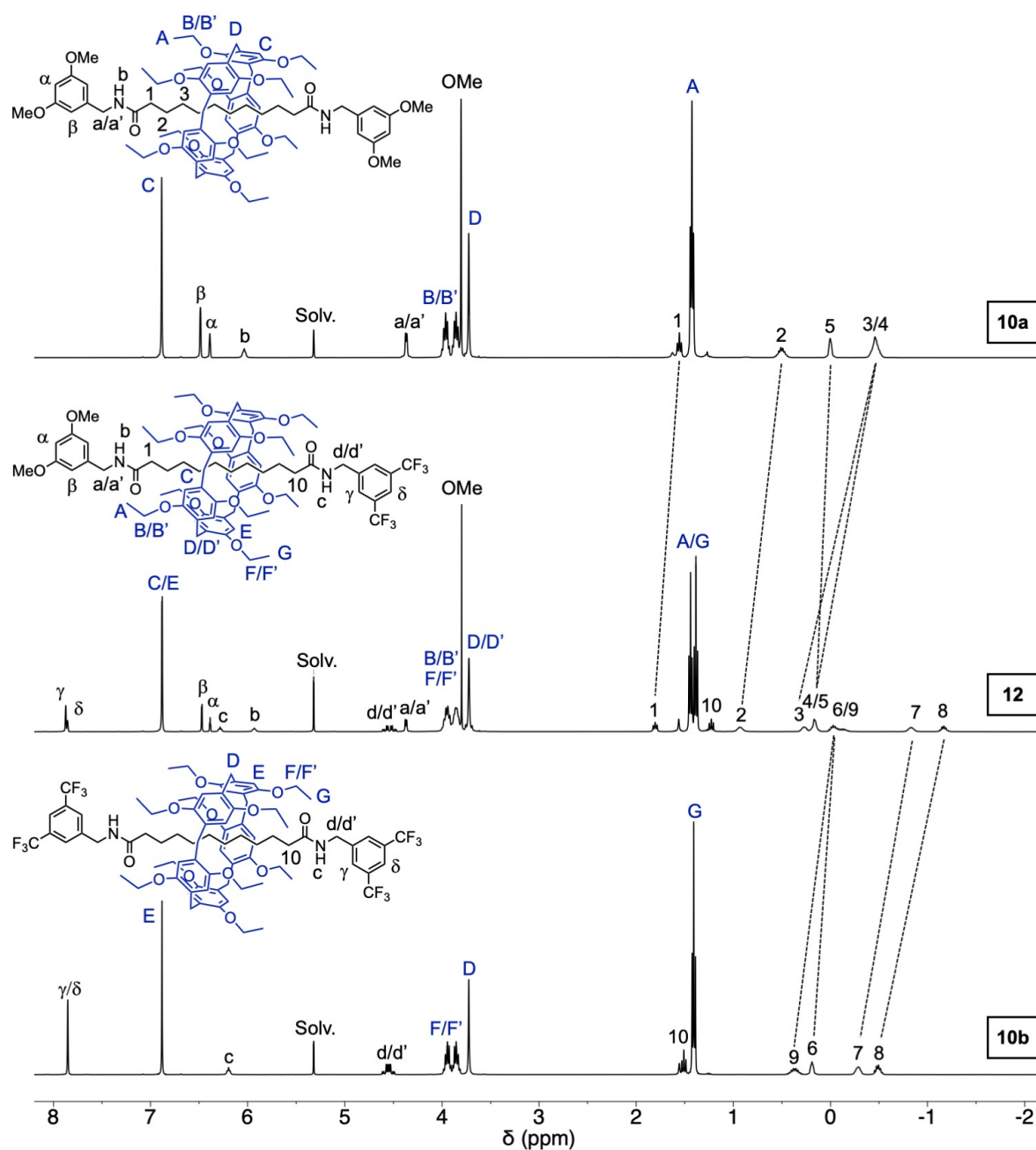


Figure 7. ¹H NMR spectra (400 MHz) recorded for rotaxanes **12** and **10a-b** in CD_2Cl_2 at 298K. For clarity, the proton numbering used for **12** has been kept to assign the corresponding protons in symmetrical rotaxanes **10a-b**.

For rotaxanes **12** and **10a-b**, the resonances arising from their axle moieties are also clearly distinguished. When compared to **8a-b** and **18**, the important shielding observed for the protons of the methylene groups of the $-(\text{CH}_2)_{10}-$ linker (Table 3) provides a diagnostic signature for the interlocked structure of **12** and **10a-b**. For both symmetrical rotaxanes, all signals of the CH_2 units of the decyl chain are affected by the ring current effect of the aromatic ring of their pillar[5]arene component. The shielding is however more important for H(3,4) in the case of **10a** and for H(7,8) in the case of **10b** showing these particular methylene groups a higher probability of presence in the cavity of the macrocycle. In other words, the pillar[5]arene moieties are preferentially located on the periphery of the axle. However, gliding motions of the pillar[5]arene from one end to the other of the axle are faster than the NMR timescale under these conditions as the two stoppers appear as equivalent. It can be also noted that the nature of the stopper has an influence on the preferential positions of the macrocycle. The multiplicity of the two diastereotopic benzylic methylene groups are effectively different in **10a** and **10b**. A doublet of AB is observed for H(d/d') in **10b** showing an effective transfer of the chiral information from the pillar[5]arene to this methylene group in agreement with a high probability of presence of the macrocycle close to the periphery. In contrast, the chiral information transfer is not effective in the case of **10a**. Effectively, H(a/a') appears as a doublet in **12** at room temperature. This observation suggests that the pillar[5]arene has a lower probability of presence in the peripheral positions in **10a** when compared to **10b**. It seems therefore that weak through space interactions between the electron-rich pillar[5]arene moiety and the stopper may also play a role in the distribution of all possible conformers in rotaxanes **10a-b**. These very weak intramolecular dipolar interactions are attractive in the case of the electron-deficient bis(trifluoromethyl)phenyl stopper (**10b**) and repulsive in the case of the electron-rich dimethoxyphenyl stopper (**10a**). In the case of unsymmetrically substituted rotaxane **12**, the most important shielding is observed for the signals arising from the methylene groups H(7,8) of the $-(\text{CH}_2)-$ axle. Therefore, the macrocycle is preferentially located close to the most electro-deficient bis(trifluoromethyl)phenyl stopper. This view is also fully supported by the comparison of the chemical shifts of the methylene groups in **12** with those in **10a-b**. Effectively, when compared to **10b**, the resonances of H(7,8) are significantly upfield shifted in **12**. At the same time, the resonances of H(3,4) are downfield shifted when going from **10a** to **12**. Moreover, a doublet of AB is observed for H(d/d') showing an effective transfer of the chiral information from the pillar[5]arene to this methylene group. In contrast, the chiral information transfer is not effective in the case of H(a/a'). This is also in full agreement for a

higher population of conformers in which the macrocycle is close to the electron-deficient stopper.

To further understand the dynamic conformational equilibrium of **12** and **10a-b**, ^1H NMR spectra were also recorded at different temperatures (Figures 8A and 8B). If there are effectively energetically favored conformations, their population should be increased by lowering the temperature. Additionally, gliding motions should be also slower at low temperature.

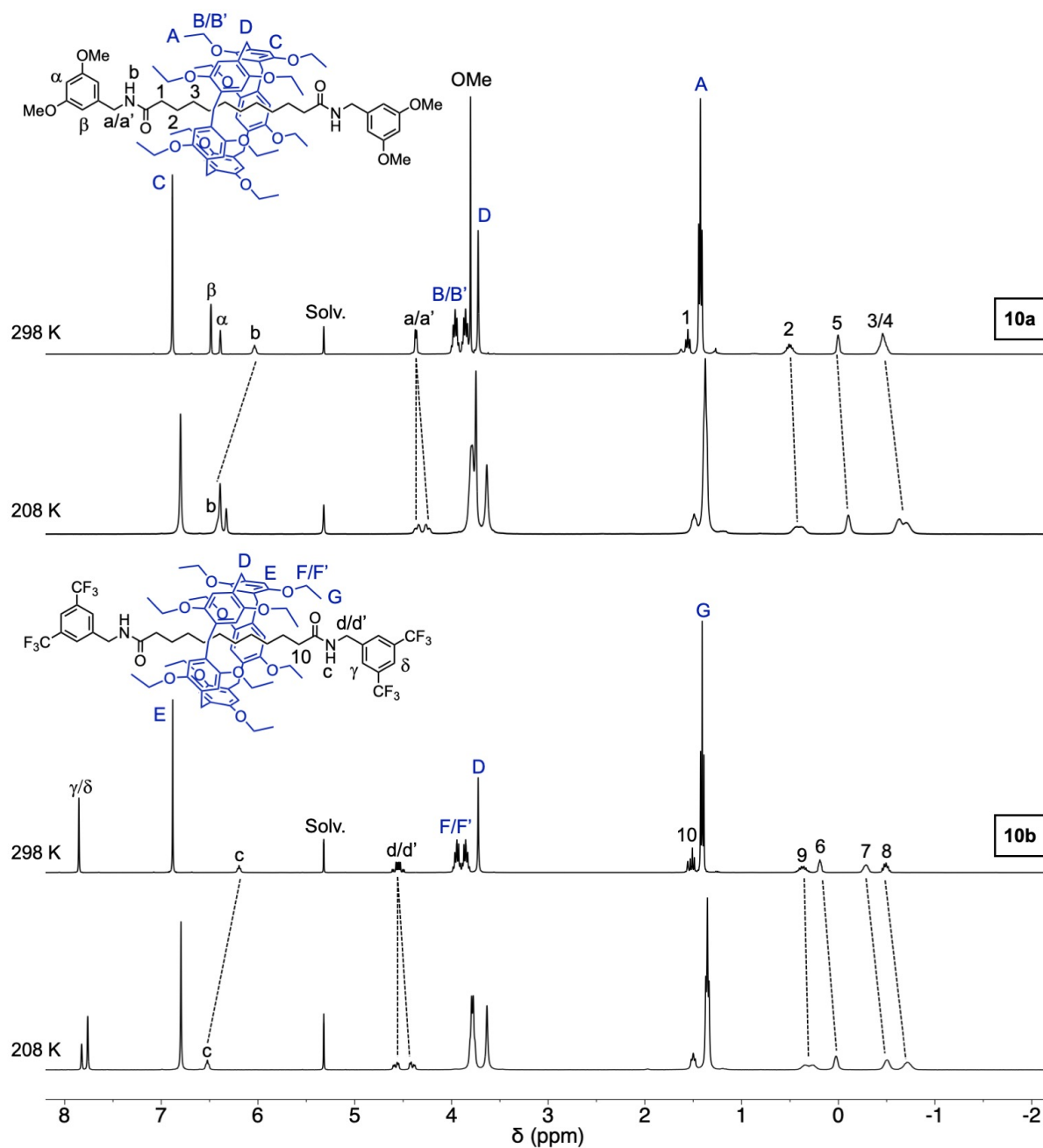


Figure 8A. ^1H NMR spectra (400 MHz) recorded for rotaxanes **10a-b** in CD_2Cl_2 at different temperatures.

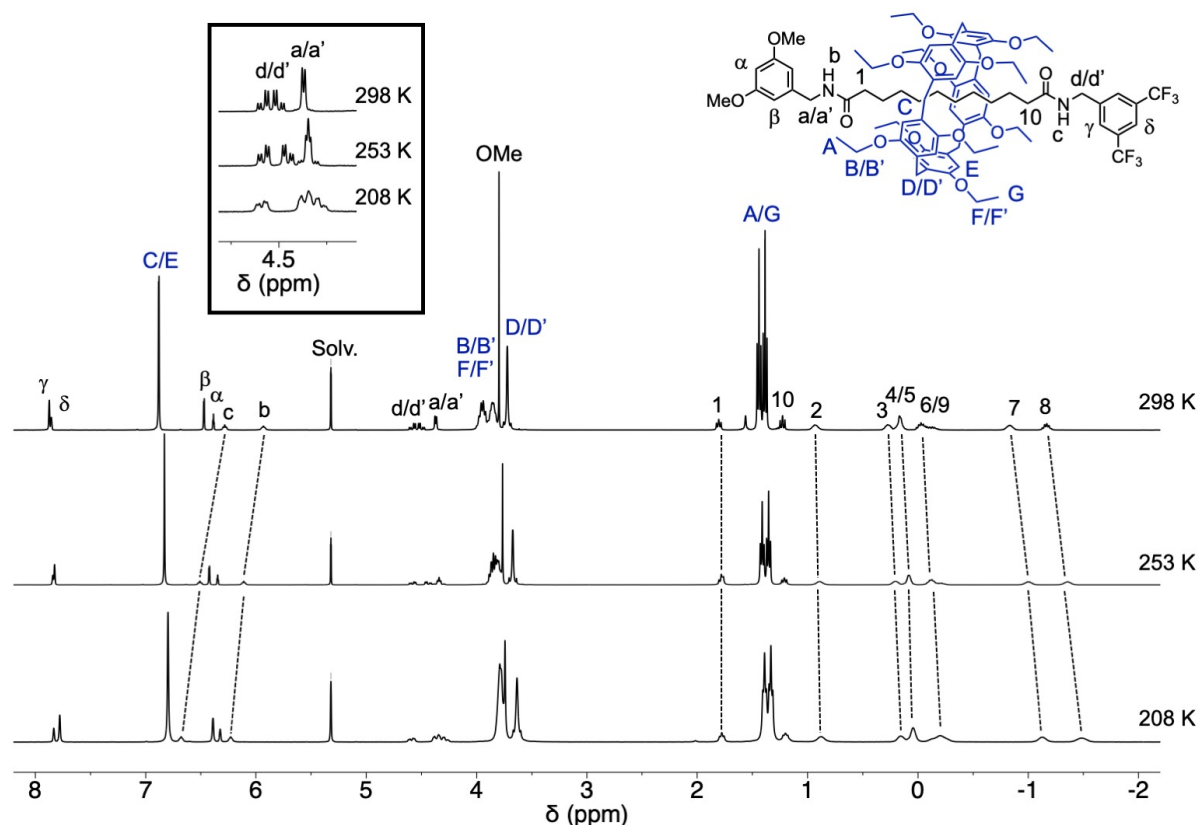


Figure 8B. ^1H NMR spectra (400 MHz) recorded for **12** in CD_2Cl_2 at different temperatures.

In all cases, limited chemical shift changes are observed for the signals of the decyl chain of the axle but the upfield shift observed by lowering the temperature for the resonances of H(7,8) in **12** and **10b** is consistent with a slight preference for conformations in which these particular methylene groups are within the cavity of the pillar[5]arene. Similar upfield shifts are also observed for the resonances of H(3,4) in both **12** and **10a**. Therefore, peripheral positions of the macrocycle are also favored for the electron-rich stopper. Clearly, conformations in which the pillar[5]arene subunit are located close to the stoppers are slightly energetically favored whatever the nature of the stopper. The stabilization is however more pronounced when the stopper is electron-deficient as shown by the difference in chemical shift observed for H(3,4) and H(7,8) in the case of rotaxane **12**. The occurrence of weak H-bond interactions with O atoms of the pillar[5]arene as observed in the X-ray crystal structure of **12** may also play a role in the observed conformational preferences. On the other hand, in all cases, transfer of the chiral information from the pillar[5]arene to the benzylic methylene groups H(a/a') and H(d/d') is more and more effective when lowering the temperature. This is also in complete agreement with a higher probability of presence of the chiral macrocycle on the peripheral positions close

to these diastereotopic CH₂ moieties when lowering the temperature. The energy barrier to switch from one peripheral position to the other is however low as the dynamic exchange is still faster than the NMR timescale at 208 K for all rotaxanes. Overall, detailed analysis of the NMR data recorded in CD₂Cl₂ for compounds **12** and **10a-b** revealed fast dynamic gliding motions of the macrocycle along the decyl chains of the axle. Conformations in which the pillar[5]arene is close to the stopper are slightly stabilized by either stronger dipolar interactions and/or the occurrence of intramolecular H-bonding interactions. In the particular case of **12**, additional weak through space donor-acceptor attractive interactions between the bis(trifluoromethyl)phenyl moiety and the pillar[5]arene contribute to further stabilize conformations in which the macrocycle is close to its electron-deficient stopper. To further support the interpretation of the NMR data, computational studies were carried out in the case of rotaxane **12**. As shown in Figure 9, three possible conformers were optimized at the semi-empirical PM6 level.

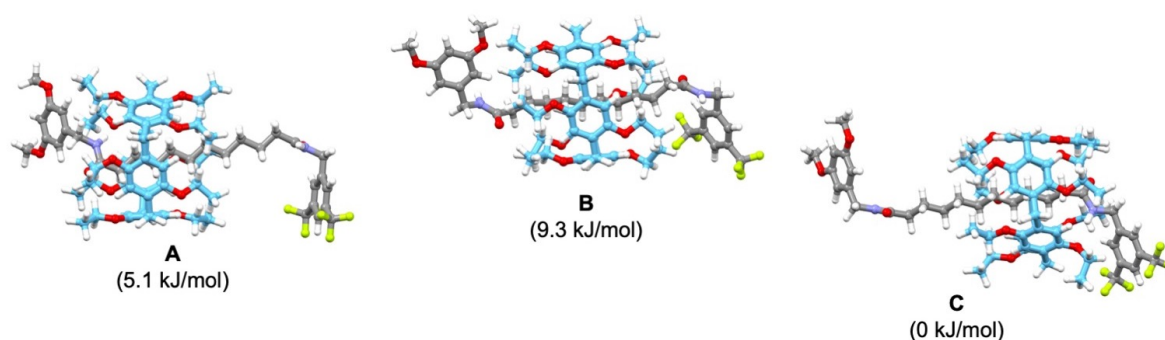


Figure 9. Calculated structures of conformers **A**, **B** and **C** of compound **12** (H: white, F: light green, O: red, N: blue, C: grey for the axle and pale blue for the pillar[5]arene moiety) and relative computed energies. The calculated Gibbs free energy activation barrier for the dynamic exchange between **A** and **C** is 3.8 kJ/mol.

Conformers **A** and **C** were effectively found more stable. The calculated energy difference between **A** and **C** is low (5.1 kJ/mol) but sufficient to explain the slightly preferential position of the pillar[5]arene moiety close to the bis(trifluoromethyl)phenyl stopper. The energy barrier to switch from conformer **A** to **C** was also found low as intermediate conformer **B** is only slightly destabilized. This is fully consistent with the observed fast dynamic exchange between the different possible conformers even at low temperature.

In order to evaluate the role of hypothetical H-bonding interactions between the NH groups of the axle subunit and the O atoms of the pillar[5]arene moiety in rotaxanes **12** and

10a-b, a competitive H-bonding donor/acceptor was added to CD_2Cl_2 solutions of **12** and **10a-b**. As a typical example, the observed changes upon addition of methanol to a CD_2Cl_2 solution of **10a** are shown in Figure 9.

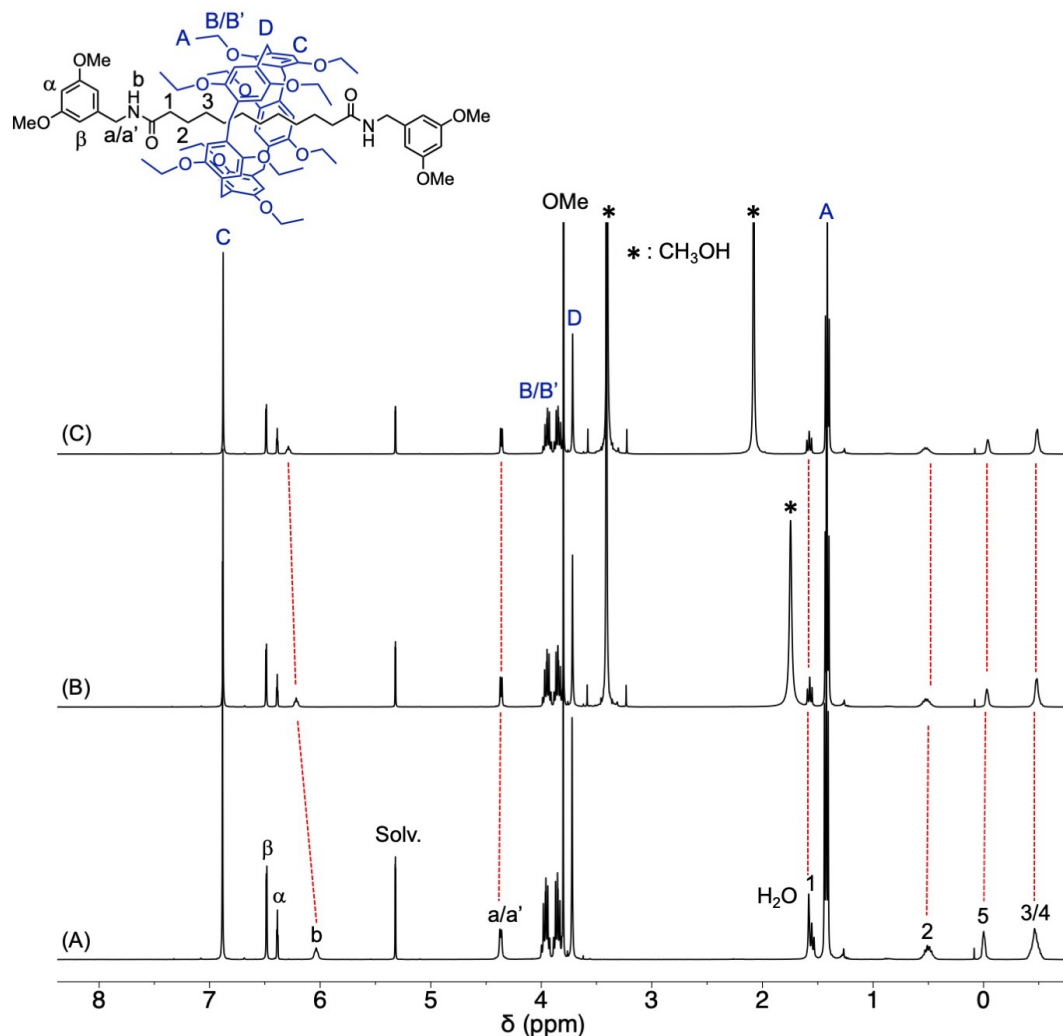


Figure 10. ^1H NMR spectra (CD_2Cl_2 , 400 MHz) recorded for rotaxane **10a** before (A) and after successive additions of methanol [0.05 mL (B); 0.1 mL (C)].

Only minor changes in chemical shifts are detected for the resonances of the methylene moieties of the decyl chains. Therefore, the average position of the macrocycle on the axle of **10a** is not affected by the presence of an excess of methanol thus showing that H-bonding plays only a very minor role if any in the preferential peripheral positions of the macrocyclic component on the axle of rotaxane **10a**. A similar behavior was also evidenced for rotaxanes **12** and **10b**. The position of the pillar[5]arene in rotaxanes **12** and **10a-b** is mainly governed by weak dipole-dipole interactions in a non-polar organic solvent such as methylene chloride. This view is also consistent with the conformational preferences observed for rotaxanes **9a-e**. For all these

compounds, the macrocyclic component is preferentially located close to its pentafluorophenyl ester stopper despite possible additional intercomponent H-bonding interactions between the NH of the other stopper with an O atom of the pillar[5]arene subunit (*vide infra*).

The influence of the different amide stoppers on the conformational equilibria observed for rotaxanes **12** and **10a-b** was also in agreement with the difference observed for the K_A values of the host-guest complexes obtained from model compounds **11a-b** and pillar[5]arene **3** (Figure 5). The *meta*-substituents of the terminal benzylic groups have effectively an effect on the K_A values, the formation of the host-guest complex being more favorable for the guest with the electron-deficient bis(trifluoromethyl)benzyl substituent. This is fully consistent with the influence of the amine stoppers on the conformation observed in the case of rotaxane **12**. The difference in Gibbs free energy ($\Delta\Delta G^0$) between **11a** and **11b** is 2.5 kJ/mol under the experimental conditions used for the binding studies (CDCl_3 , 298 K). This small energy difference is sufficient to significantly influence the Maxwell-Boltzmann distribution of the different possible conformers of **12** and explains well why the peripheral position of the pillar[5]arene close to the bis(trifluoromethyl)benzyl stopper is favored.

To further understand the conformational preferences of rotaxanes of **12** and **10a-b**, ^1H NMR spectra were also recorded in polar organic solvents, namely $\text{DMSO-}d_6$ and/or $\text{DMF-}d_7$. Under these conditions, polar interactions are expected to be disfavored while solvophobic effects are expected to be stronger.¹⁶ The ^1H NMR spectra recorded for **12** and **10a-b** in different solvents are shown in Figure 11. In all cases, dramatic chemical shift changes were observed for the resonances of the methylene groups of the decyl chain when going from a nonpolar to a polar solvent. The position of the pillar[5]arene moiety on its axle moiety is actually highly sensitive to the solvent polarity. Analysis of the relative chemical shifts of the methylene groups in **12** and **10a-b** revealed that the pillar[5]arene moiety is preferentially located in the middle of the decyl chains in polar media. The Maxwell-Boltzmann distribution of all possible conformers is therefore highly sensitive to the solvent polarity. In nonpolar solvents (CH_2Cl_2 or CHCl_3), intramolecular dipole-dipole interactions play a major role. As a result, conformations in which the macrocycle is close to its stoppers are favored. When the two stoppers are different as in the case of **12**, the peripheral position close to the most electron-deficient stopper more populated owing to favorable trough-space donor-acceptor interactions. In contrast, such polar interactions are disfavored in polar solvents (DMSO or DMF). Solvophobic effects are actually dominating the conformational preferences of **12** and **10a-b**.

Obviously, the terminal amide functions of **12** and **10a-b** are well solvated by DMF or DMSO while repulsive interactions between the decyl chain and the polar solvent molecules are expected. As a result, the macrocycle is preferentially located in the middle of the axle subunit to limit unfavorable interactions between the decyl chain and the solvent.

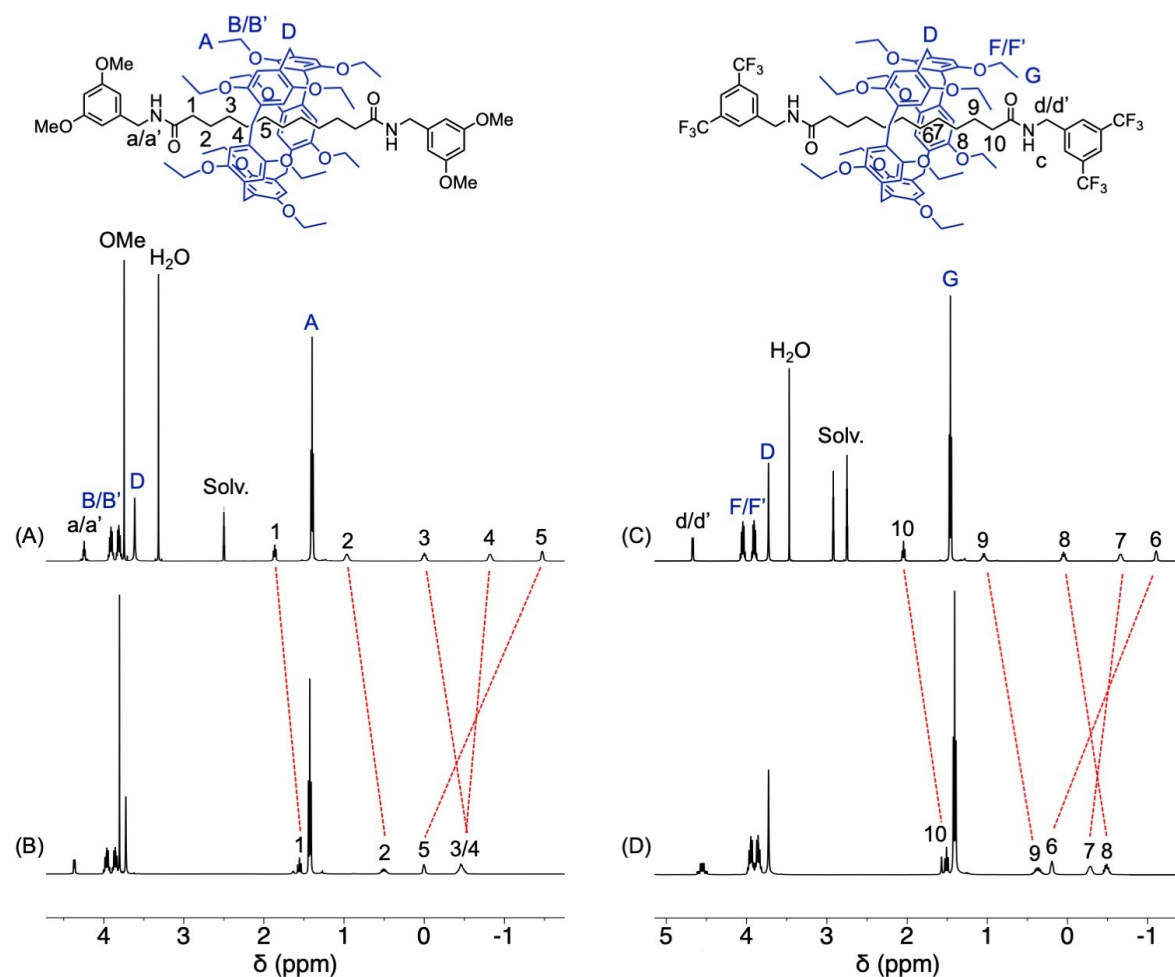


Figure 11A. Aliphatic region of the ^1H NMR spectra (500 MHz, 298 K) recorded for **10a** in $\text{DMSO-}d_6$ (A), **10a** in CD_2Cl_2 (B), **10b** in $\text{DMF-}d_7$ (C) and **10b** in CD_2Cl_2 (D).

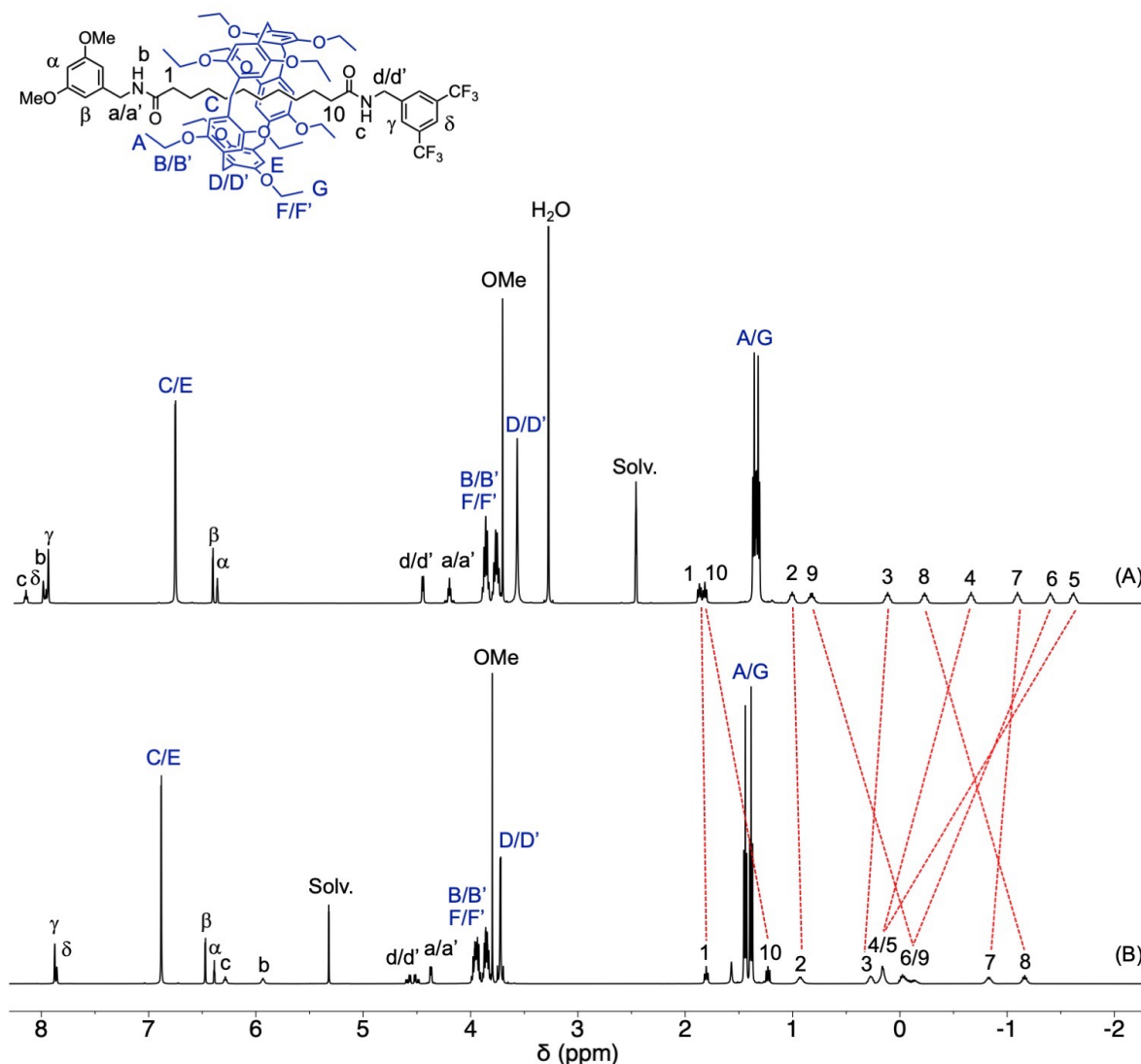


Figure 11B. ^1H NMR spectra (500 MHz, 298 K) recorded for **12** in $\text{DMSO-}d_6$ (A) and CD_2Cl_2 (B).

Conformational analysis of rotaxane **17** with a longer axle was also carried out based on NMR studies. The ^1H NMR spectrum of **17** recorded in CD_2Cl_2 at room temperature is depicted in Figure 12. Considering the shielding effect of the pillar[5]arene moiety on the resonances of the methylene groups located within its cavity, it appears clear that the macrocycle is located over the two decyl subunits of the axle. The dynamic exchange by gliding motions must be however close to the NMR timescale under these conditions as some signals of the decyl chain are broadened. In contrast, the chemical shifts of the CH_2 groups of the triethylene glycol spacer are observed at regular chemical shifts thus showing that the macrocycle is on average not preferentially located on the triethylene glycol station of its axle unit. To fully confirm the fast gliding motions of the macrocycle all over its molecular string,

variable temperature NMR studies were carried out. The ^1H NMR spectra of **17** recorded at various temperature are shown in Figures 13 and 14.

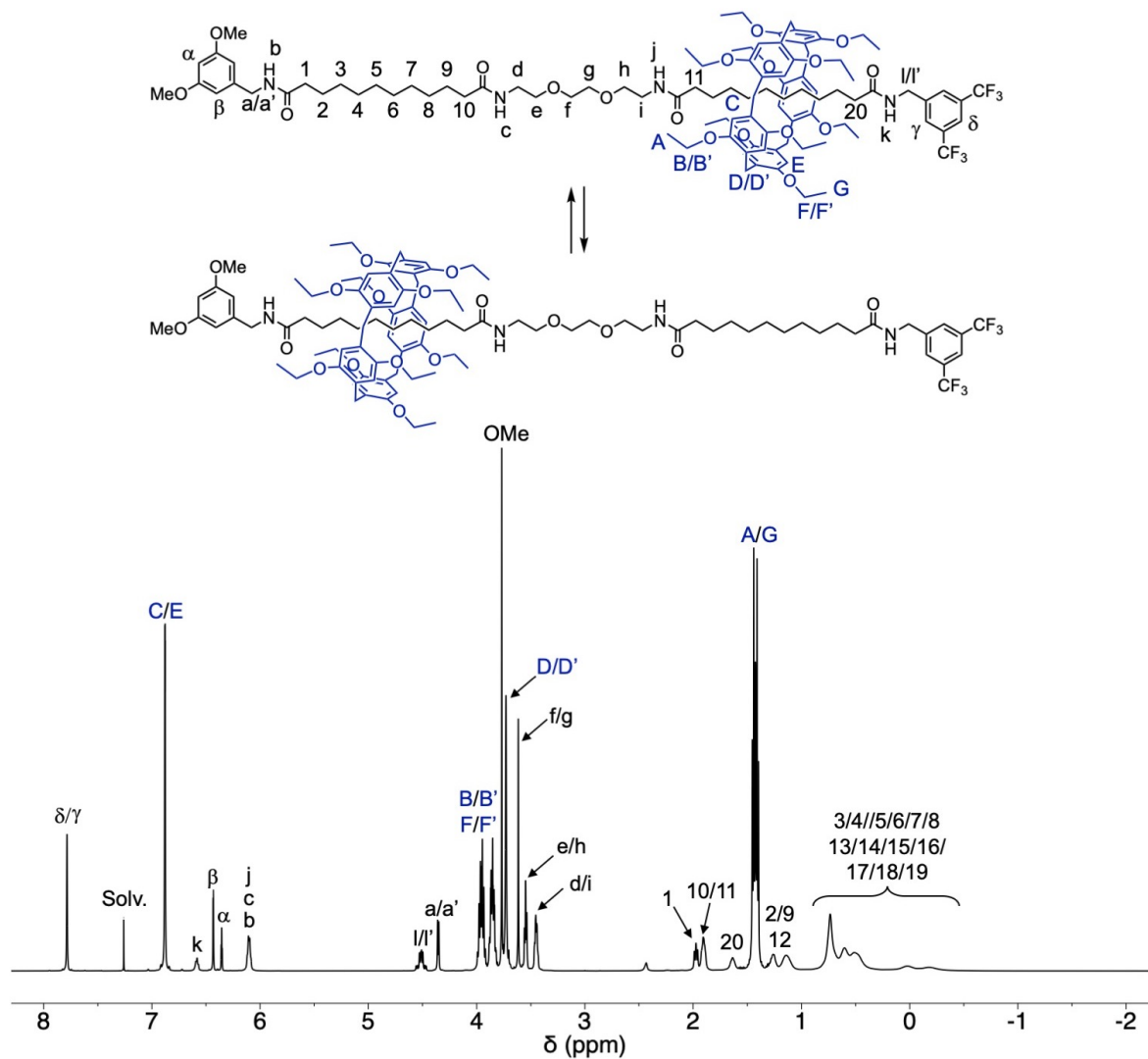


Figure 12. ^1H NMR spectrum (500 MHz) of compound **17** recorded in CD_2Cl_2 at 298 K.

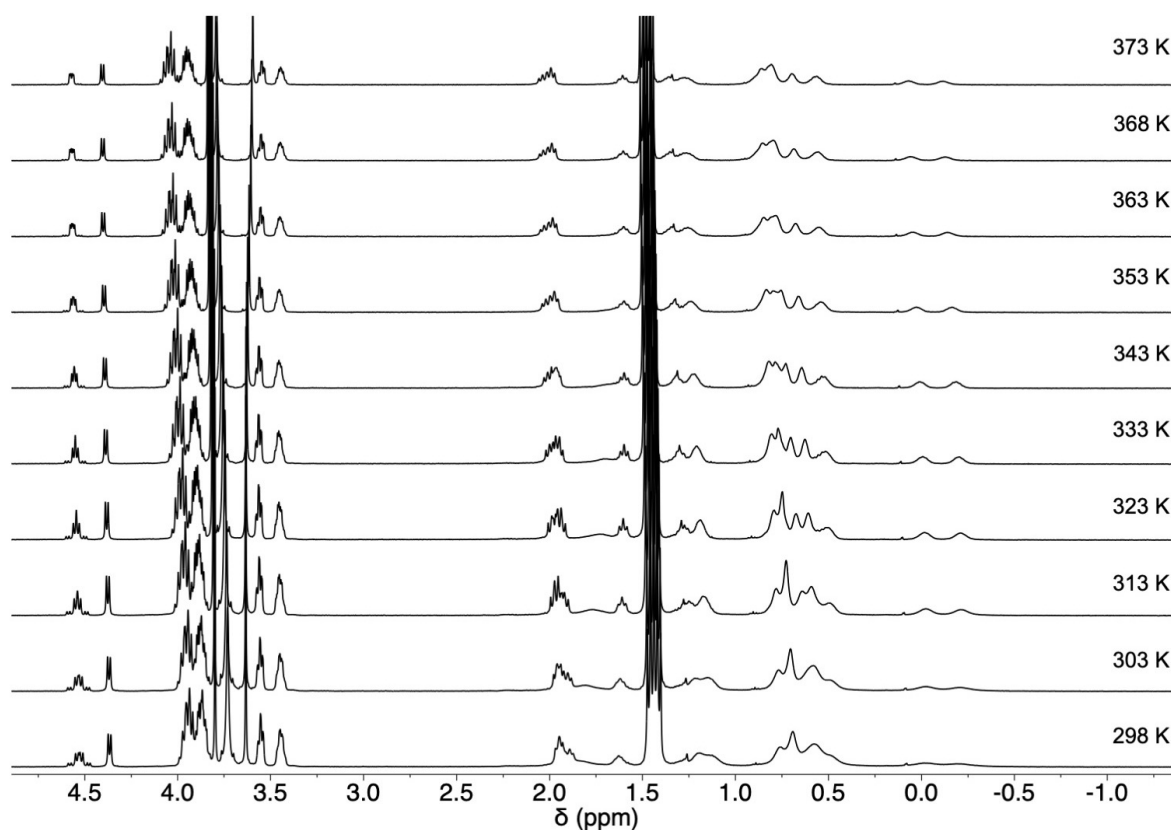


Figure 13. Aliphatic region of the ¹H NMR spectra (400 MHz) of **17** recorded in CDCl₂CDCl₂ at different temperatures.

By increasing the temperature, a perfectly reversible narrowing is observed for the signals of the methylene groups of the decyl moieties. At high temperature, the dynamic exchange between the two possible conformers in which the pillar[5]arene is located over one or the other decyl station is faster than the NMR timescale. In contrast, at low temperature, the dynamic exchange becomes slower than the NMR timescale and the ¹H NMR spectrum recorded at 208 K in CD₂Cl₂ corresponds to the superposition of the spectra of two conformers differing by the position of the pillar[5]arene over its axle. The macrocycle is either located over one or the other decyl station.

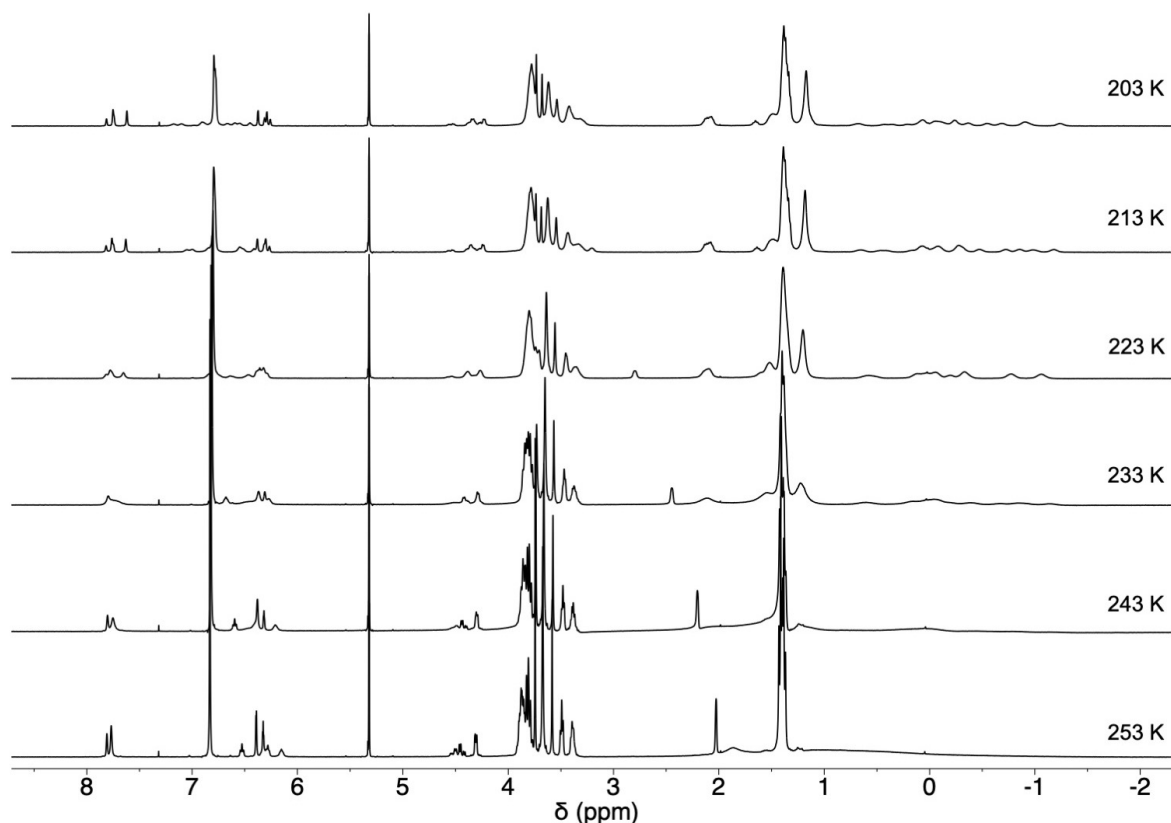


Figure 14. ^1H NMR spectra (400 MHz) of **17** recorded in CD_2Cl_2 at different temperatures.

A detailed analysis of the spectrum recorded at this temperature is depicted in Figure 15. The relative proportion of the two conformers is similar. Based on the integration, a 56:44 ratio is deduced, the major conformer being the one in which the decyl station bearing the bis(trifluoromethyl)benzyl stopper is occupied. Based on a Boltzmann population analysis at 208 K, this corresponds to an average difference of energy lower than 1 kJ/mol between the two conformations. The attractive effect of the electron-deficient stopper is very weak and clearly not sufficient to obtain a perfect conformational control in rotaxane **17**. Moreover, dynamic gliding motions of the macrocycle over the long axle of **17** generate a large number of possible conformations relatively close in energy. Considering the Maxwell-Boltzmann population of all these discrete conformers in dynamic exchange, the multiplication of possible positions for the macrocycle limits also the occupancy of the most energetically favored one when its additional stabilization is weak.

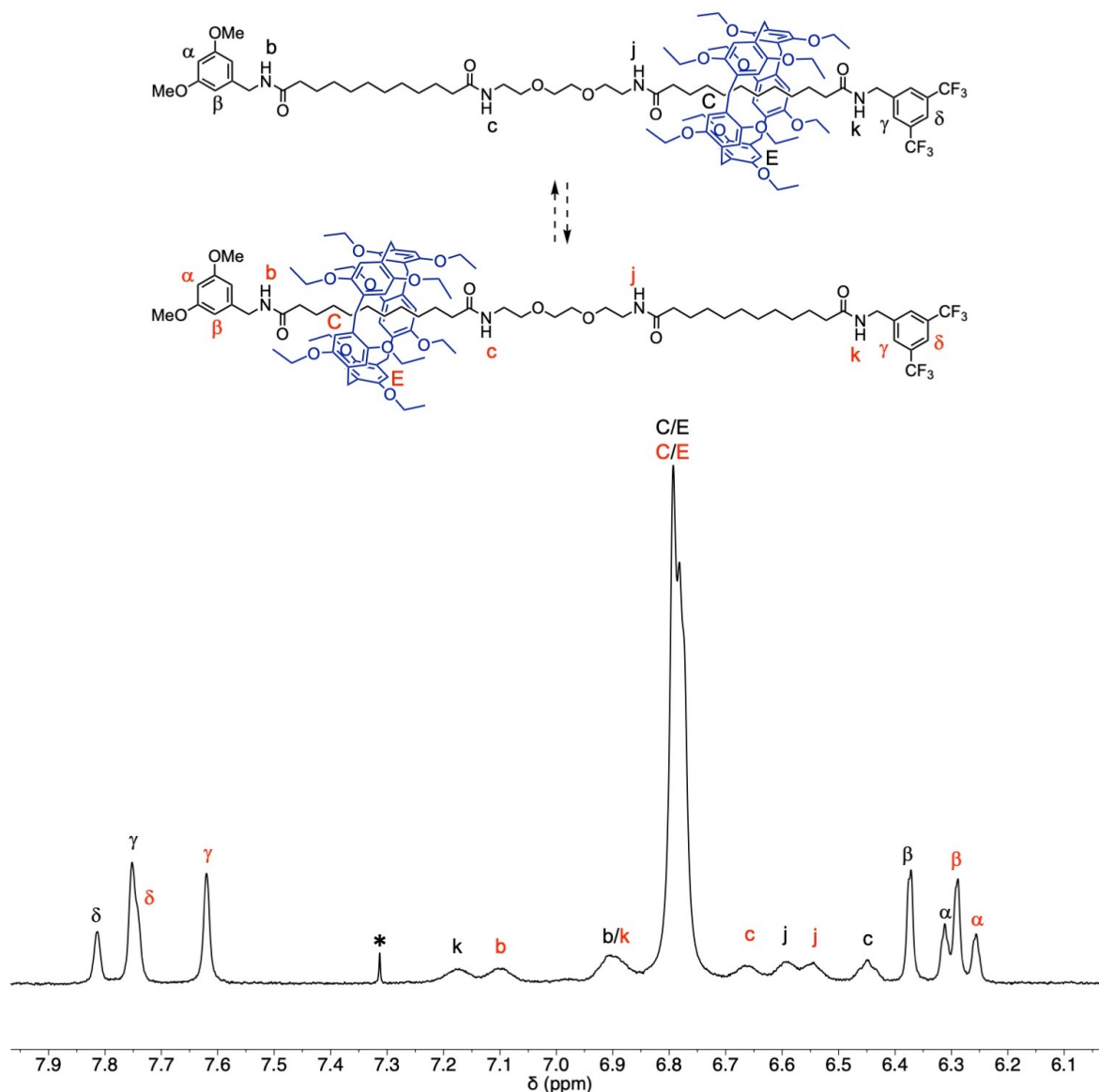


Figure 15. Aromatic region of the ^1H NMR spectra (400 MHz) of **17** recorded in CD_2Cl_2 at 208 K (*: CHCl_3 impurity). Under these conditions, the dynamic exchange of the two conformers in which the macrocycle is located over one or the other decyl station of the axle is slower than the NMR timescale.

An estimation of the rate of the shuttling process can be obtained by using the method described by Günbas and Brouwer.¹⁷ At the coalescence temperature (T_c), there is a simple relationship (Eq. 1) between the rate constant (k) and the chemical shift difference ($\Delta\nu$ for the two exchanging peaks below T_c at slow exchange regime):

$$k = \frac{\pi\Delta\nu}{\sqrt{2}} \quad \text{Eq. 1}$$

The free energy of activation ΔG^\ddagger for the dynamic exchange can be then directly calculated with the Eyring equation (Eq. 2):

$$\Delta G^\ddagger = -R T_c \ln(k h / k_B T_c) \quad \text{Eq. 2}$$

where R is the gas constant, h is Planck's constant, k_B is the Boltzmann constant, T_c is the coalescence temperature, and k is the rate constant of exchange (s^{-1}). The ΔG^\ddagger value thus obtained by analyzing the coalescence of several signals is 47 ± 1 kJ/mol. Overall, the variable temperature NMR studies of rotaxane **17** revealed pillar[5]arene is preferentially located over its two decyl stations (Figure 16). Due to the presence of the bis(trifluoromethyl)benzyl stopper, station 3 is slightly favored but the attractive effect between the electron-rich pillar[5]arene and the electron-deficient stopper is extremely weak.

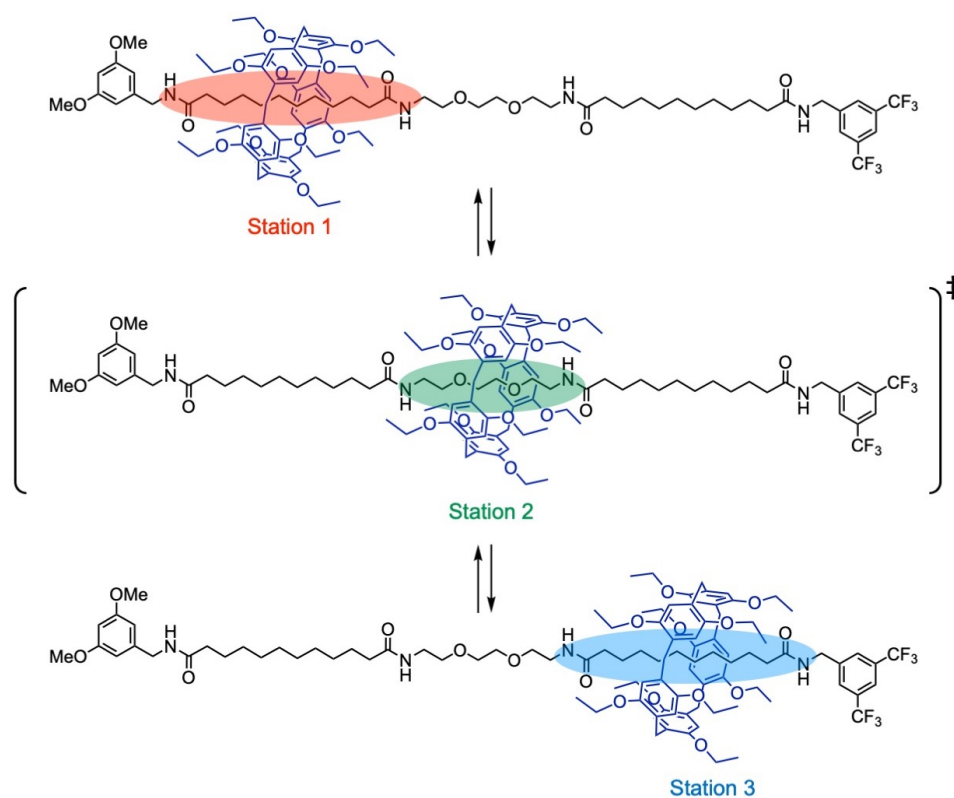


Figure 16. Conformational equilibrium deduced from the variable temperature studies of rotaxane **17**.

In contrast, station 2 is not significantly populated by the macrocycle and can be considered as the transition state for the dynamic exchange allowing the macrocycle to shuttle back and forth between the two different decyl stations. At high temperature, dynamic exchange between the

two degenerate states is faster than the NMR timescale. In contrast, the two conformers are clearly distinguished at low temperature.

II-3. Conclusion

In this second chapter, we have reported detailed investigations on the mono-functionalization of rotaxane building block **1** bearing two equivalent pentafluorophenol ester stoppers. Upon a first stopper exchange, the pillar[5]arene moiety of the mono-acylated product is preferentially located close to its reactive pentafluorophenyl ester stopper. As a result, the accessibility of the reactive carbonyl group by the nucleophilic reagents is more difficult thus allowing the efficient preparation of mono-amide rotaxanes from **1**. The synthetic utility of the resulting building blocks bearing only one activated stopper has been demonstrated with the efficient preparation of dissymmetrical rotaxanes **12** and **17**. Moreover, we have also shown that the pillar[5]arene can play the role of a protecting group for the synthesis of dissymmetrical axles particularly difficult to prepare under statistical conditions. Finally, the conformational analysis of rotaxanes **12** and **17** revealed fast gliding motion of the pillar[5]arene component over its axle subunit. Conformers in which the pillar[5]arene moiety is located close to its most electron-deficient stopper is slightly energetically favored in solution in the case of rotaxane **12** with a relatively short axle unit. Similar effects are however limited in the case of rotaxane **17** with an elongated axle moiety. Weak energy differences resulting from through space donor-acceptor interactions and intramolecular dipole-dipole interactions are actually not sufficient to control the position of the macrocycle onto a very long axle unit. In the case of **17**, a much higher number of conformers is possible. As they are all close in energy, their Maxwell-Boltzmann distribution is not favorable to significantly populate a higher proportion of the conformer in which the macrocycle is close to its electron-deficient stopper.

II-4. References

- 1) a) J.-P. Sauvage, C. Dietrich-Buchecker (Eds.), *Molecular Catenanes, Rotaxanes and Knots – A Journey Through the World of Molecular Topology*, J. Wiley and Sons, **2008**;
b) C. J. Bruns, J. F. Stoddart, *The Nature of the Mechanical Bond – From Molecules to Machines*, J. Wiley & Sons, **2016**.
- 2) R. Brückner, *Eur. J. Org. Chem.* **2019**, 3289-3319.

- 3) a) R. A. Bissell, E. Córdova, A. E. Kaifer, J. F. Stoddart, *Nature* **1994**, *369*, 133-137; b) A. Livoreil, C. O. Dietrich-Buchecker, J.-P. Sauvage, *J. Am. Chem. Soc.* **1994**, *116*, 9399-9400.
- 4) a) J.-P. Sauvage, *Angew. Chem. Int. Ed.* **2017**, *56*, 11080-11093; *Angew. Chem.* **2017**, *129*, 11228-11242; b) J. F. Stoddart, *Angew. Chem. Int. Ed.* **2017**, *56*, 11228-11242; *Angew. Chem.* **2017**, *129*, 11244-11277.
- 5) a) V. Balzani, A. Credi, M. Venturi, *Molecular Devices and Machines – A Journey into the Nano World*, Wiley-VCH, **2003**; b) E. R. Kay, D. A. Leigh, *Angew. Chem. Int. Ed.* **2015**, *54*, 10080-10088; *Angew. Chem.* **2015**, *127*, 10218-10226; c) S. Erbas-Cakmak, D. A. Leigh, C. T. McTernan, A. L. Nussbaumer, *Chem. Rev.* **2015**, *115*, 10081-10206; d) D. A. Leigh, *Angew. Chem. Int. Ed.* **2016**, *55*, 14506-14508; *Angew. Chem.* **2016**, *128*, 14722-14724; e) S.-J. Rao, Q. Zhang, J. Mei, X.-H. Ye, C. Gao, Q.-C. Wang, D.-H. Qu, H. Tian, *Chem. Sci.* **2017**, *8*, 6777-6783; f) S.-J. Rao, K. Nakazono, X. Liang, K. Nakajima, T. Takata, *Chem. Commun.* **2019**, *55*, 5231-5234; g) Q. Zhang, S.-R. Rao, T. Xie, X. Li, T.-Y. Xu, D.-W. Li, D.-H. Qu, Y.-T. Long, H. Tian, *Chem* **2018**, *4*, 2670-2684; h) S. Corra, M. Curcio, M. Baroncini, S. Silvi, A. Credi, *Adv. Mater.* **2020**, *32*, 1906064; i) M. Boroncini, S. Silvi, A. Credi, *Chem. Rev.* **2020**, *120*, 200-268; j) C.-S. Kwan, K. C.-F. Leung, *Mater. Chem. Front.* **2020**, *4*, 2825-2844; k) H.-Y. Zhou, Y. Han, C.-F. Chen, *Mater. Chem. Front.* **2020**, *4*, 12-28.
- 6) P. Waelès, M. Gauthier, F. Coutrot, *Angew. Chem. Int. Ed.* **2021**, *60*, 16778-16799.
- 7) a) S. Anderson, T. D. W. Claridge, H. L. Anderson, *Angew. Chem. Int. Ed.* **1997**, *36*, 1310-1313; *Angew. Chem.* **1997**, *109*, 1367-1370; b) J. E. H. Buston, J. R. Young, H. L. Anderson, *Chem. Commun.* **2000**, 905-906; c) F. Cacialli, J. S. Wilson, J. J. Michels, C. Daniel, C. Silva, R. H. Friend, N. Severin, P. Samorì, J. P. Rabe, M. J. O'Connell, P. N. Taylor, H. L. Anderson, *Nat. Mater.* **2002**, *1*, 160-164; d) M. J. Frampton, H. L. Anderson, *Angew. Chem. Int. Ed.* **2007**, *46*, 1028-1064; *Angew. Chem.* **2007**, *119*, 1046-1083.
- 8) Similar protecting effects have been also reported for squaraine-containing rotaxanes, see: a) E. Arunkumar, C. C. Forbes, B. C. Noll, B. D. Smith, *J. Am. Chem. Soc.* **2005**, *127*, 3288-3289; b) J. Gassensmith, J. M. Baumes, B. D. Smith, *Chem. Commun.* **2009**, 6329-6338.
- 9) a) L. D. Movsisyan, D. V. Kondratuk, M. Franz, A. L. Thompson, R. R. Tykwinski, H. L. Anderson, *Org. Lett.* **2012**, *14*, 3424-3426; b) N. Weisbach, Z. Baranova, S. Gauthier, J. H. Reibenspies, J. A. Gladysz, *Chem. Commun.* **2012**, *48*, 7562-7564; c) H. Sahnoune,

- Z. Baranová, N. Bhuvanesh, J. A. Gladysz, J.-F. Halet, *Organometallics* **2013**, *32*, 6360-6367; d) L. D. Movsisyan, M. D. Peeks, G. M. Greetham, M. Towrie, A. L. Thompson, A. W. Parker, H. L. Anderson, *J. Am. Chem. Soc.* **2014**, *136*, 17996-18008; e) M. Franz, J. A. Januszewski, D. Wendinger, C. Neiss, L. D. Movsisyan, F. Hampel, H. L. Anderson, A. Gçrling, R. R. Tykwinski, *Angew. Chem. Int. Ed.* **2015**, *54*, 6645-6649; *Angew. Chem.* **2015**, *127*, 6746-6750; f) L. D. Movsisyan, M. Franz, F. Hampel, A. L. Thompson, R. R. Tykwinski, H. L. Anderson, *J. Am. Chem. Soc.* **2016**, *138*, 1366-1376; g) D. R. Kohn, L. D. Movsisyan, A. L. Thompson, H. L. Anderson, *Org. Lett.* **2017**, *19*, 348-351; h) D. C. Milan, M. Krempe, A. K. Ismael, L. D. Movsisyan, M. Franz, I. Grace, R. J. Brooke, W. Schwarzacher, S. J. Higgins, H. L. Anderson, C. J. Lambert, R. R. Tykwinski, R. J. Nichols, *Nanoscale* **2017**, *9*, 355-361; i) M. Franz, J. A. Januszewski, F. Hampel, R. R. Tykwinski, *Eur. J. Org. Chem.* **2019**, 3503-3512.
- 10) a) A. H. Parham, B. Windisch, F. Vögtle, *Eur. J. Org. Chem.* **1999**, 1233-1238; b) D. A. Leigh, E. M. Perez, *Chem. Commun.* **2004**, 2262-2263; c) A. Mateo-Alonso, P. Brough, M. Prato, *Chem. Commun.* **2007**, 1412-1414; d) F. Scarel, G. Valenti, S. Gaikwad, M. Marcaccio, F. Paolucci, A. Mateo-Alonso, *Chem. Eur. J.* **2012**, *18*, 14063-14068; e) D. M. D'Souza, D. A. Leigh, L. Mottier, K. M. Mullen, F. Paolucci, S. J. Teat, S. Zhang, *J. Am. Chem. Soc.* **2010**, *132*, 9465-9470; f) N. Kihara, Y. Tachibana, H. Kawasaki, T. Takata, *Chem. Lett.* **2000**, *29*, 506-507; g) J. Winn, A. Pinczewska, S. Goldup, *J. Am. Chem. Soc.* **2013**, *135*, 13318-13321.
- 11) a) I. Nierengarten, E. Meichsner, M. Holler, P. M. Pieper, R. Deschenaux, B. Delavaux-Nicot, J.-F. Nierengarten, *Chem. Eur. J.* **2018**, *24*, 169-177; b) I. Nierengarten, J.-F. Nierengarten, *ChemistryOpen* **2020**, *9*, 393-400.
- 12) M. Rémy, I. Nierengarten, B. Park, M. Holler, U. Hahn, J.-F. Nierengarten, *Chem. Eur. J.* **2021**, *27*, 8492-8499.
- 13) The post-modification of pre-constructed [2]rotaxanes by stopper exchange reactions has been rarely used and only a few examples have been reported so far, see: a) S. J. Rowan, J. F. Stoddart, *J. Am. Chem. Soc.* **2000**, *122*, 164-165; b) S. J. Rowan, S. J. Cantrill, J. F. Stoddart, A. J. P. White, D. J. Williams, *Org. Lett.* **2000**, *2*, 759-762; c) R. J. Bordoli, S. M. Goldup, *J. Am. Chem. Soc.* **2014**, *136*, 4817-4820; d) D. W. Zehnder II, D. B. Smithrud, *Org. Lett.* **2001**, *3*, 2485-2487; e) N. Kihara, S. Motoda, T. Yokozawa, T. Takata, *Org. Lett.* **2005**, *7*, 1199-1202; f) J. S. Hannam, S. M. Lacy, D. A. Leigh, C. G. Saiz, A. M. Z. Slawin, S. G. Stitchell, *Angew. Chem. Int. Ed.* **2004**, *43*,

- 3260-3264; g) S. C. Rajappan, D. R. McCarthy, J. P. Campbell, J. B. Ferrel, M. Sharafi, O. Ambrozaite, J. Li, S. T. Schneebeli, *Angew. Chem. Int. Ed.* **2020**, *59*, 16668-16674.
- 14) R. Milev, A. Lopez-Pacheco, I. Nierengarten, T. M. N. Trinh, M. Holler, R. Deschenaux, J.-F. Nierengarten, *Eur. J. Org. Chem.* **2015**, 479-485.
- 15) a) L. Gao, C. Han, B. Zheng, S. Dong, F. Huang, *Chem. Commun.* **2013**, *49*, 472-474; b) T. M. N. Trinh, I. Nierengarten, M. Holler, J.-L. Gallani, J.-F. Nierengarten, *Chem. Eur. J.* **2015**, *21*, 8019-8022; c) M. Holler, T. Stoerkler, A. Louis, F. Fisher, J.-F. Nierengarten, *Eur. J. Org. Chem.* **2019**, 3401-3405.
- 16) J. L. Cook, C. A. Hunter, C. M. R. Low, A. Perez-Velasco, J. G. Vinter, *Angew. Chem. Int. Ed.* **2007**, *46*, 3706-3709.
- 17) D. D. Günbas, A. M. Brouwer, *J. Org. Chem.* **2012**, *77*, 5724-5735.

Preparation of pillar[5]arene-containing [2] and [3]rotaxanes by a stopper exchange strategy

III-1. Introduction

In the previous section, we have developed efficient conditions for the stepwise functionalization of pillar[5]arene-containing rotaxane building blocks with pentafluorophenyl ester stoppers with different amines. In this section, we now propose to use the mono-functionalized building blocks for the synthesis of [3]rotaxanes and the direct preparation of symmetrical [2]rotaxanes with elongated axles. For this purpose, diamine reagents have been used to functionalize building block **9b** (Figure 1).

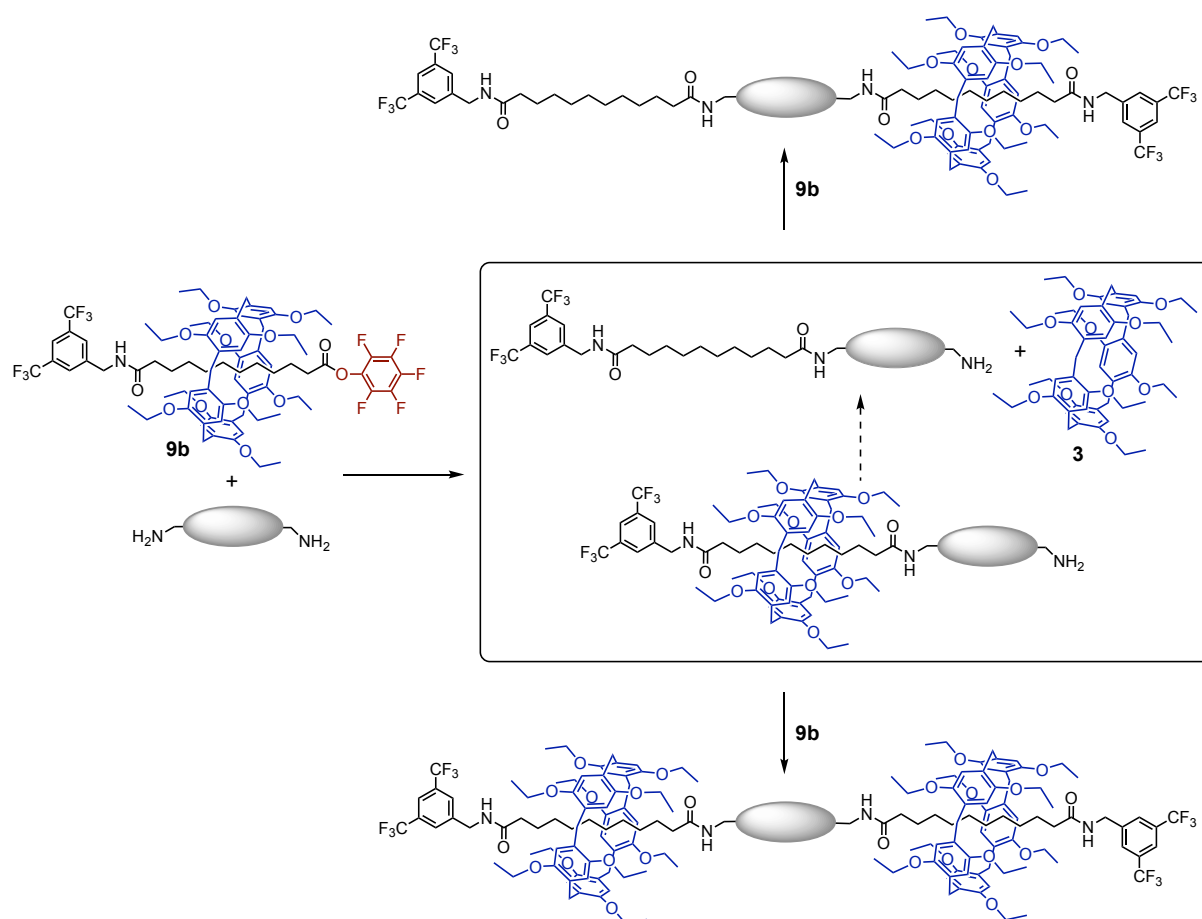
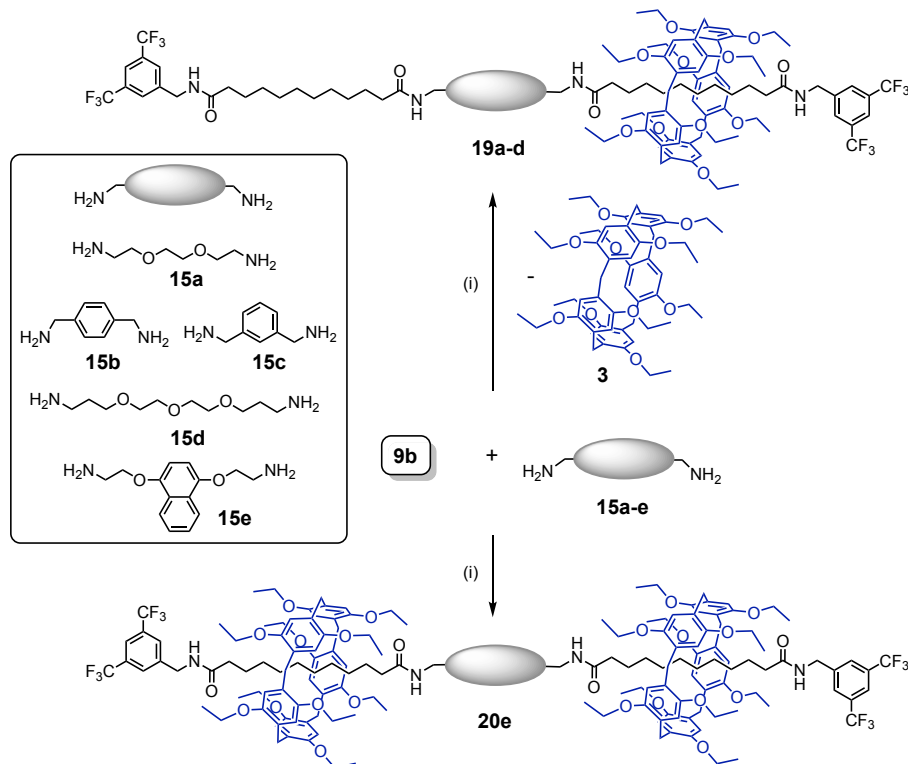


Figure 1. Preparation of [3]rotaxanes and/or [2]rotaxanes with elongated axles from building block **9b** and diamine reagents.

A first acylation of the diamine reagent with **9a** will generate an intermediate [2]rotaxane with a terminal amine function. The outcome of the reaction will then depend on the ability of the pillar[5]arene to escape from its axle. If the newly introduced terminal amide group is large enough to prevent the dissociation of the intermediate, the second acylation will then provide a [3]rotaxane. In contrast, if dissociation is possible, the reaction of the uncomplexed axle intermediate with a second equivalent of **9a** will generate a [2]rotaxane with an elongated axle subunit. In this case, the [3]rotaxane may be obtained if the reaction conditions are appropriate to stabilize the inclusion complex of the mono-amine intermediate and the pillar[5]arene. In solution, dissociation of the intermediate will be most likely favored. In contrast, by performing the stopper exchange under solvent-free conditions,¹⁻⁶ one may expect a significant stabilization of the host-guest complex and therefore the formation of [3]rotaxanes.

III-2. Results and discussion

Stopper exchange with diamine reagents in solution. Building block **9b** was treated with diamines **15a-d** (0.5 equiv.) to form the corresponding [2]rotaxanes (**19a-b**) with an elongated axle moiety (Scheme 1).



Scheme 1. Reaction of [2]rotaxane **9b** with various diamines. *Reagents and conditions:* (i) THF, rt (**19a**: 93% from **15a**; **19b**: 94% from **15b**; **19c**: 89% from **15c**; **19d**: 95% from **15d**; **20e**: 99% from **15e**).

In all cases, a first stopper exchange reaction occurred to generate an intermediate host-guest complex from which the pillar[5]arene unit was liberated thus providing an intermediate axle with a terminal amine function. Subsequent reaction of this intermediate with a second equivalent of **9b** then provided [2]rotaxanes **19a-d**. No traces of [3]rotaxanes could be detected thus showing that dissociation of the intermediate host-guest complexes was always faster than the second stopper exchange reaction. In contrast, when the reaction of **9b** was carried out with amine **15e**, [3]rotaxane **20e** was exclusively obtained as the disubstituted naphthalene moiety is large enough to prevent dissociation of the intermediate obtained after reaction of **9b** with **15e**. In other words, this intermediate is a [2]rotaxane in this particular case. It can be noted that compound **20e** was obtained as a 1:1 mixture of two diastereomers depending on the relative stereochemistry of the two pillar[5]arene moieties (Figure 2). The two macrocycles of the [3]rotaxane have an opposite absolute stereochemistry in the case of the achiral *meso* diastereomer. In contrast, the absolute chemistry of the two pillar[5]arenes is the same in the case of the C_2 -symmetrical diastereomer. The C_s - and C_2 -symmetrical diastereomers of **20e** have an identical polarity and could not be separated.

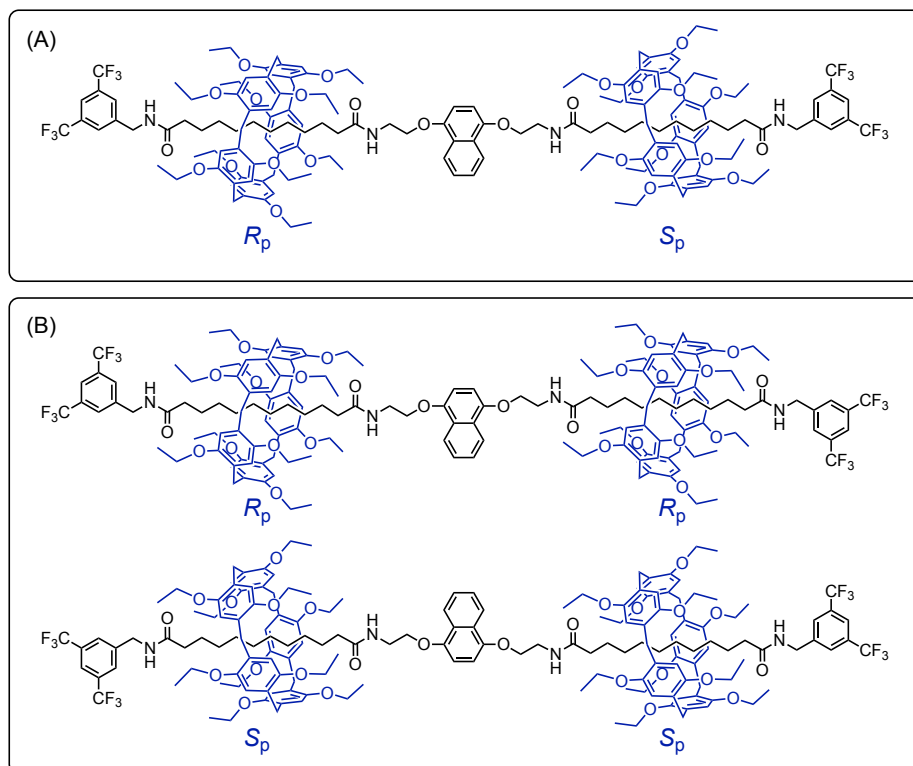
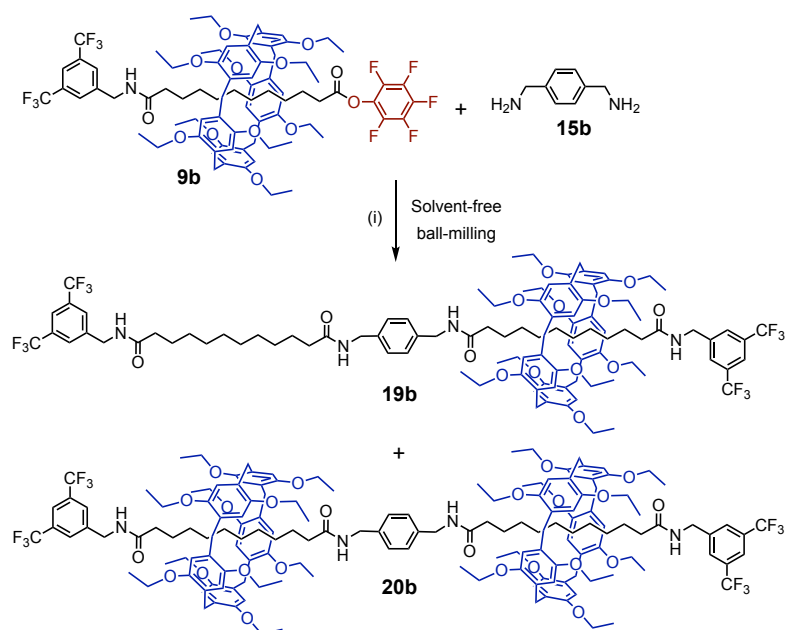


Figure 2. All possible diastereomers of **20e**: the achiral C_s -symmetrical *meso* diastereomer (A) and the two enantiomers of the C_2 -symmetrical diastereomer (B).

Stopper exchange with diamine reagents under solvent-free ball-milling conditions. Mechanochemical solvent-free conditions have been successfully used to prepare rotaxanes.¹⁻³ Our group has shown that such conditions are particularly well suited to obtain pillar[5]arene-containing rotaxanes in good yields.⁴ Indeed, the association between the axle reagent and the pillar[5]arene leading to rotaxane formation is favored in the solid state.⁵ When compared to analogous reactions performed in solution, desolvation energy is totally removed in the solid state. Moreover, the concentration effect is also favorable to generate the inclusion complex in the solid state. Our group has also reported solvent-free conditions for stopper exchange reactions involving pillar[5]arene-containing rotaxane building blocks with pentafluorophenyl ester stoppers and various nucleophiles.⁶ Under such conditions, one may anticipate that the reaction of **9b** with diamine reagents **15a-c** should allow the formation of the corresponding [3]rotaxanes as dissociation of the intermediate host-guest complexes should be limited in the solid state. The mechanochemical solvent-free conditions for the stopper exchange reaction were first optimized with diamine **15b** (Scheme 2, Table 1).



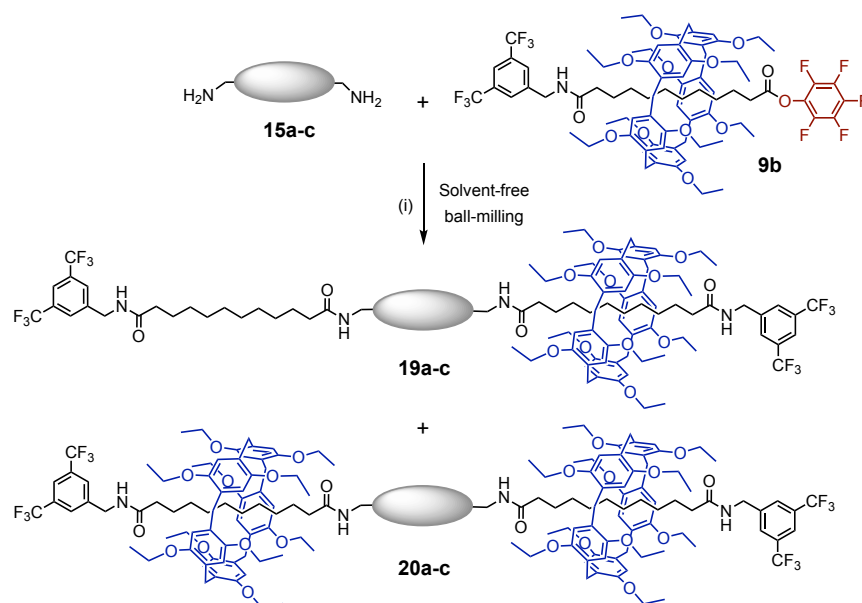
Scheme 2. Optimization of the mechanochemical solvent-free conditions for the reaction of rotaxane **9b** with diamine **15b**. *Reagents and conditions:* (i) additive, mixing in a Retsch MM400 mill at 30 Hz for 2 h (see Table 1 for details).

Table 1. Optimization of the mechanochemical solvent-free conditions for the reaction of **9b** (2.2 equiv.) with diamine **15b** (1 equiv.). All reactions were performed in a 25 mL stainless-steel vial containing four stainless-steel balls that was mixed in a Retsch MM400 mill at 30 Hz for 2 h.

Entry	Additive	Isolated yield in [2]rotaxane 19b	Isolated yield in [3]rotaxane 20b
1	None	9%	8%
2	TBD (1 equiv.)	51%	17%
3	TBD (2 equiv.)	50%	47%
4	TBD (4 equiv.)	55%	41%
5	DMAP (2 equiv.)	46%	37%

The stopper exchange reaction was very slow by mixing diamine **15b** with a slight excess of rotaxane building block **9b** in a Retsch MM400 mill at 30 Hz for 2 hours (Table 1, Entry 1). In this case, acylated products were obtained in low yields together with large amounts of unreacted starting materials. Whereas good yields are typically obtained when using stoichiometric amounts of pentafluorophenyl esters and amine reagents in THF solutions, it has been shown that the use of a large excess of amine reagents (8 equiv.) is mandatory to achieve such reactions in good yields under mechanochemical conditions.⁶ It was however not possible to use an excess of diamine reagent **15b** for the functionalization of **9b** as such conditions would produce large amounts of mono-acetylated byproducts. It was therefore decided to add a base to the mixture. Mixing of **9a** and **15b** was thus carried out in the presence of 1,5,7-triazabicyclo[4.4.0.]dec-5-ene (TBD). The starting materials were not totally consumed after 2 hours when 1 equiv. of TBD was used (Table 1, Entry 2), the reaction was nevertheless much faster than in the absence of additive. By increasing the amount of TBD to 2 equiv. (Entry 3), the starting materials were fully consumed after two hours of mixing. Whereas the reaction of **9b** and **15b** in THF solutions provided exclusively [2]rotaxane **19b**, mechanochemical conditions afforded a mixture of [2] and [3]rotaxanes thus showing that dissociation of the intermediate host-guest complex is significantly prevented in the solid state. Compounds **19b** and **20b** were then conveniently separated by size exclusion chromatography. The isolated yields in **19b** and **20b** were 50 and 47%, respectively. By further increasing the amount of TBD (4equiv.), the overall yield was similar but the formation of [3]rotaxane **20b** was slightly less favorable (Entry 4, Table 1). This observation can be explained by a dilution effect that favors dissociation of the pseudorotaxane intermediate to a greater extent. Alternatively, it was also possible to use 4-dimethylaminopyridine (DMAP) as a base, but the overall yield was not as good as the one obtained with TBD (Entry 5, Table 1).

The mechanochemical reaction conditions optimized with diamine **15b** were then used starting from **15a** and **15c** (Scheme 3). A mixture of the appropriate diamine reagent (1 equiv.), **9b** (2.2 equiv.) and TBD (2 equiv.) was mixed in a Retsch MM400 mill at 30 Hz for 2 hours. The resulting solid was dissolved in CHCl_3 and filtered over a short plug of silica. [2]Rotaxane **19a-c** and [3]rotaxane **20a-c** were then separated by gel permeation chromatography (Biobeads SX-1, CHCl_3).



Scheme 2. Preparation of [2] and [3]rotaxanes under optimized mechanochemical solvent-free conditions.

Reagents and conditions: (i) TBD (2 equiv.), mixing in a Retsch MM400 mill at 30 Hz for 2 h [**19a**: 72% and **20a**: 24% (from **15a**); **19b**: 50% and **20b**: 47% (from **15b**); **19c**: 29% and **20c**: 68% (from **15c**)].

The overall yield in rotaxane was the same whatever the diamine reagent (96-97%), however the relative proportion of [2] and [3]rotaxane was significantly affected by the nature of the linker between the two amine functions of **15a-c**. Diamine reagents **15b-c** with phenylene spacers gave effectively higher yields in [3]rotaxane when compared to triethylene glycol diamine (**15a**). Structural factors play obviously an important role on the stability of the intermediate pseudorotaxane obtained after the first acylation. The nature of the spacer may influence the dissociation kinetics. The energy barrier required for the unthreading process actually depends on the size of the spacer. This effect is consistent with the better yields in [3]rotaxane obtained from **15c**, the dethreading of the pillar[5]arene macrocycle through the *meta*-phenylene linker being significantly more difficult (*vide supra*). On the other hand, the system is likely dynamic and association/dissociation of the pseudorotaxane intermediate is

expected to take place during the reaction.⁵ Owing to the very poor affinity of oligoethylene glycol for the pillar[5]arene, the threading process of the axle component terminated with the ethylene glycol amine is likely not very favorable. This view is supported by the different binding constant values derived from ¹H NMR titration experiments performed in CDCl₃ at 298 K for the formation of host-guest complexes from pillar[5]arene **3** and model compounds **11b** and **14b** (Figure 3). When compared to **11b**, the presence of the terminal methoxyethyl unit in **14b** reduced significantly the affinity of the pillar[5]arene host.

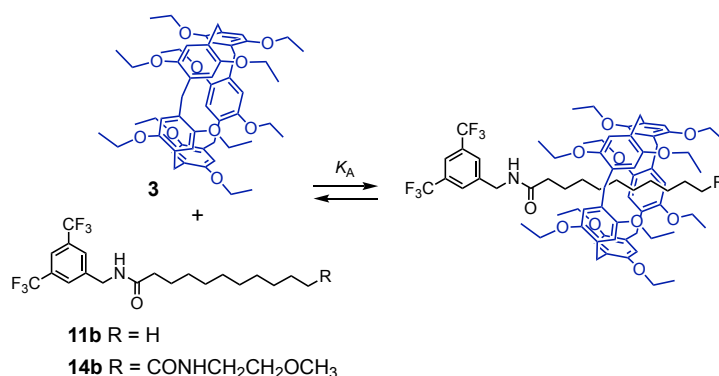


Figure 3. The formation of host-guest complexes from pillar[5]arene **3** and model compounds **11b** and **14b**; the $\log K_A$ values derived from ¹H NMR binding studies in CDCl₃ at 298 K are 0.82(1) for **11b** and 0.2(1) for **14b**.

Characterization of the rotaxanes. Compounds **19a-d**, **20a-c** and **20e** were characterized by a combination of different analytical techniques. Matrix-assisted laser desorption – time of flight (MALDI-TOF) mass spectrometry confirmed the proposed structures of **19a-d**, **20a-c** and **20e**. As typical examples, the mass spectra recorded for compounds **19a-b** and **20a-b** in the positive mode are depicted in Figure 4. In all cases, only the singly charged molecular ion peak corresponding to $[M+H]^+$ was observed. Under these experimental conditions, no fragmentation occurred thus showing that MALDI-TOF mass spectrometry is an ideal tool for the characterization of such rotaxanes.

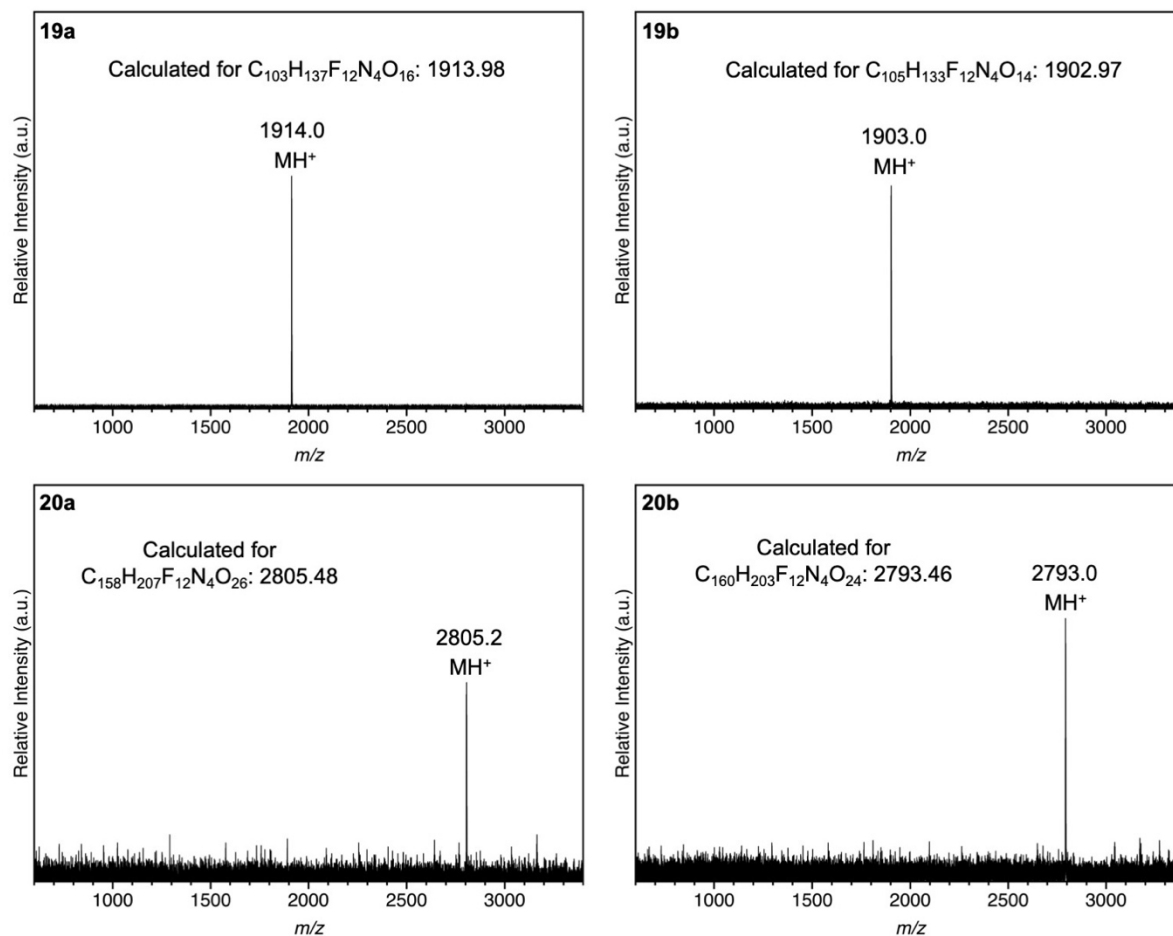


Figure 4. MALDI-TOF mass spectra of compounds **19a-b** and **20a-b** recorded in the positive mode.

Compounds **19a-d** were also characterized by NMR spectroscopy. As shown in Figure 5, the ^1H NMR spectrum of **19b** recorded in CDCl_3 at room temperature revealed that the two 3,5-bis(trifluoromethyl)benzyl stoppers of **19b** appear as equivalent suggesting fast dynamic gliding motions of the pillar[5]arene moiety along the molecular string of the rotaxane. The dynamic shuttling must be however close to the NMR timescale under these conditions as the signals arising from the two decyl chains are broad. This prompted us to perform temperature-dependent NMR measurements.

At low temperature, the dynamic gliding motions became slower than the NMR timescale and the two moieties of the axle of **19b** appeared as non-equivalent in the ^1H NMR spectrum recorded at 218 K in CDCl_3 (Figure 5). Considering the dramatic shielding effect of the pillar[5]arene moiety on the resonances of the groups located within its cavity, it appears clear that the macrocycle is located over one decyl station of the axle, the second one remaining

unoccupied. In contrast, the dynamic exchange allowing the macrocycle to shuttle back and forth between the two decyl moieties is faster than the NMR timescale at high temperature (Figure 6). The ^1H NMR spectrum of **19b** recorded in $\text{CDCl}_2\text{CDCl}_2$ revealed effectively one set of signals for the two decyl chains at 378 K.

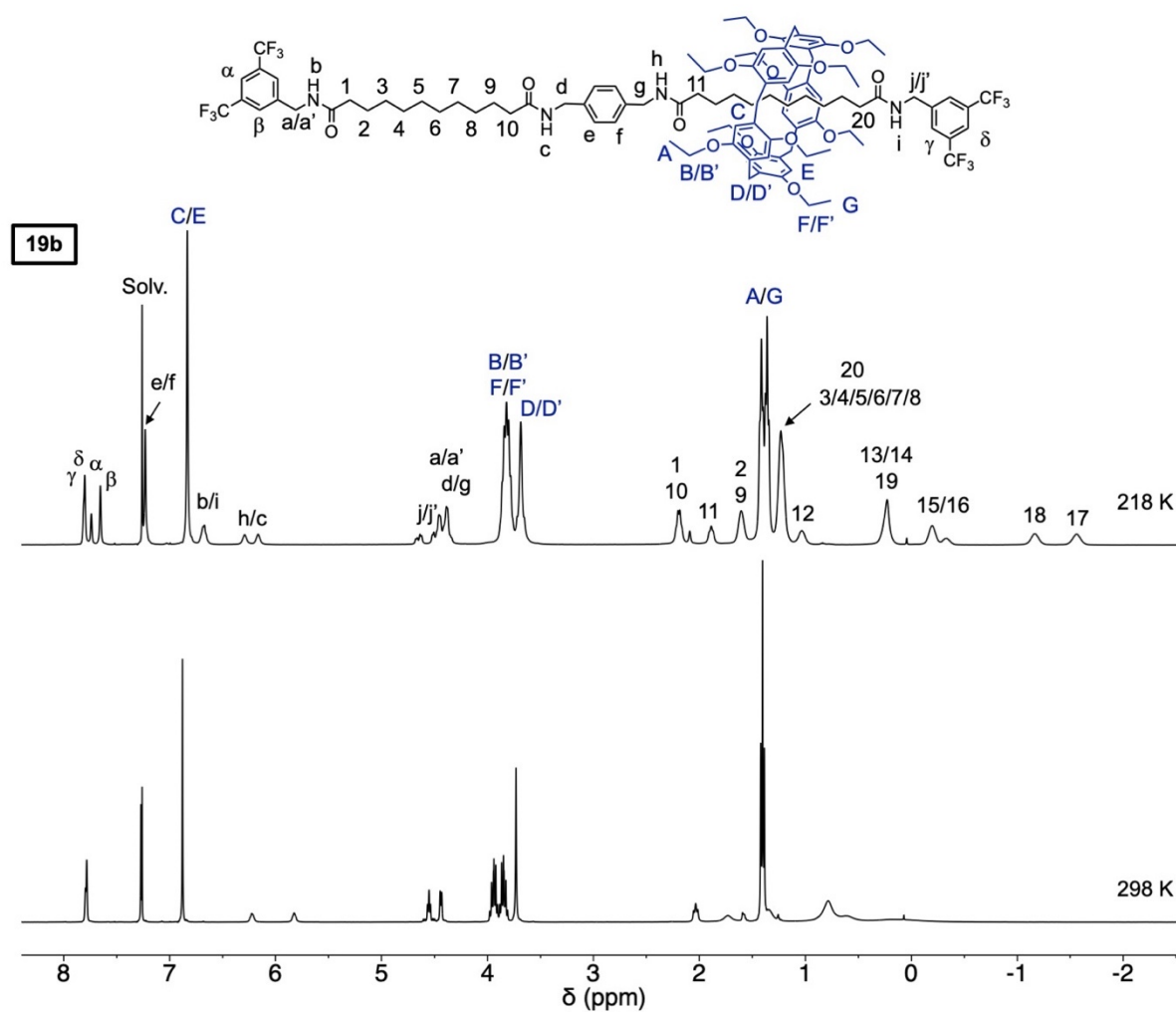


Figure 5. ^1H NMR spectra (400 MHz) of [2]rotaxane **19b** recorded in CDCl_3 at different temperatures.

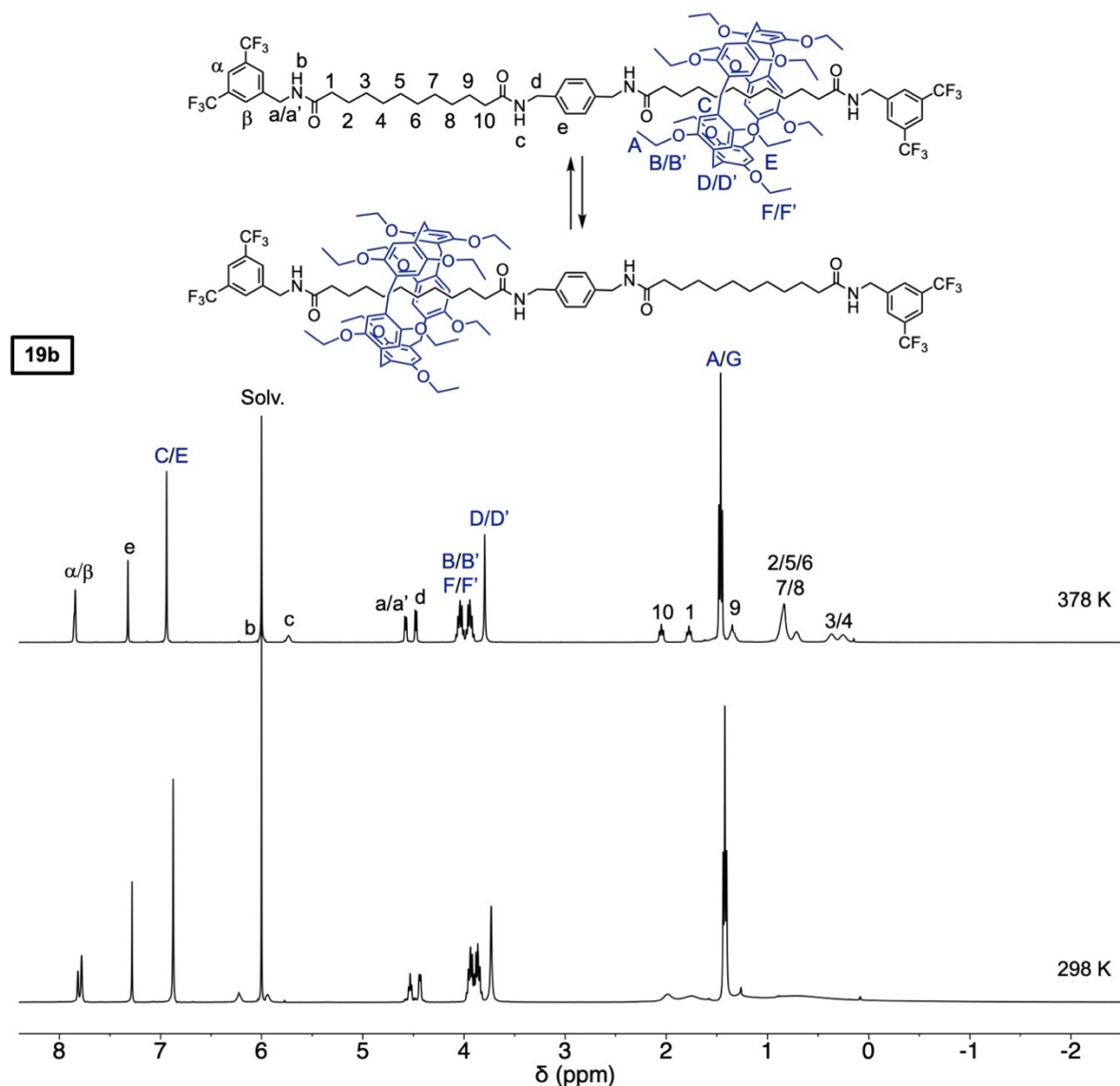


Figure 6. ^1H NMR spectra (400 MHz) of [2]rotaxane **19b** recorded in $\text{CDCl}_2\text{CDCl}_2$ at different temperatures.

The chemical shift and the shape of the signal arising from the aromatic protons of the central *para*-phenylene moiety of **19b** are only slightly affected by the temperature changes. Indeed, the central station of **19b** is not significantly occupied by the pillar[5]arene subunit and can be considered as the transition state for the dynamic exchange. This view is fully supported by the difference in coalescence temperature observed between isomers **19b** and **19c**. The gliding motions of the pillar[5]arene are indeed slower than the NMR timescale at room temperature in the case of **19c** with the *meta*-phenylene linker. Effectively, the ^1H NMR spectrum of **19c** recorded at 298 K revealed non-equivalent decyl moieties (Figure 7).

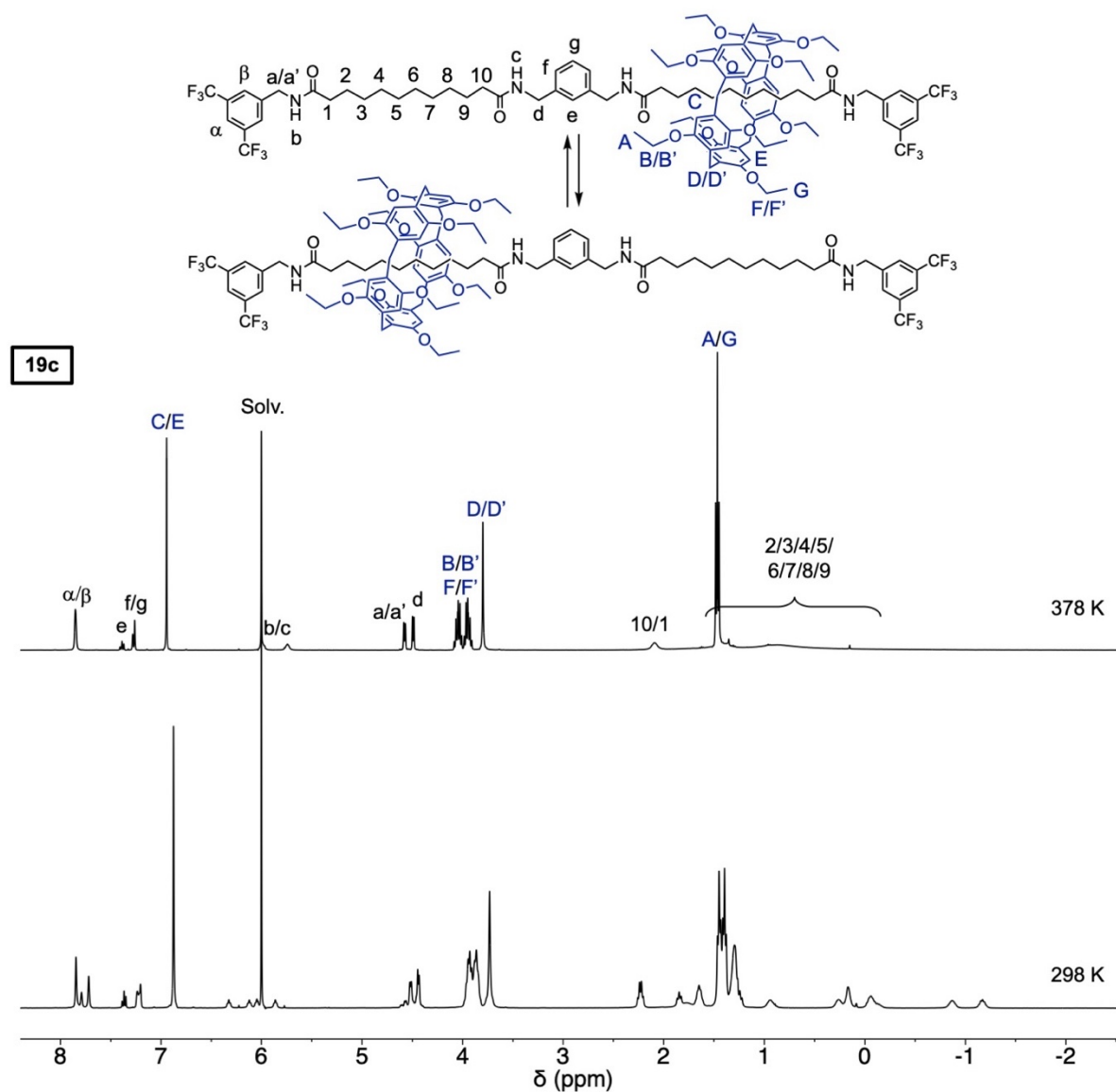


Figure 7. ^1H NMR spectra (400 MHz) of [2]rotaxane **19c** recorded in $\text{CDCl}_2\text{CDCl}_2$ at different temperatures.

By increasing the temperature, a clear coalescence was observed but the dynamic exchange is still not fast enough to obtain an average spectrum with narrow signals at the highest possible temperature that can be reached with our spectrometer (378 K). The energy barrier allowing the pillar[5]arene to shuttle back and forth between the two decyl moieties is therefore higher in the case of **19c** when compared to **19b**. Obviously, the *meta*-phenylene spacer in **19c** is larger when compared to the *para*-phenylene linker in its isomer **19b** and crossing the central part of the axle becomes more difficult for the pillar[5]arene moiety.

Variable temperature NMR investigations were also carried out for **19a** and **19d**. The ^1H NMR spectra recorded at different temperatures for [2]rotaxanes **19a** and **19d** are shown in Figures 8 and 9, respectively. As discussed for compound **19b**, dynamic gliding motions of the macrocyclic moiety along the molecular string of **19a** and **19d** is faster than the NMR timescale at 298 K. The two 3,5-bis(trifluoromethyl)benzamide terminated decyl chains appear effectively as equivalent under these conditions.

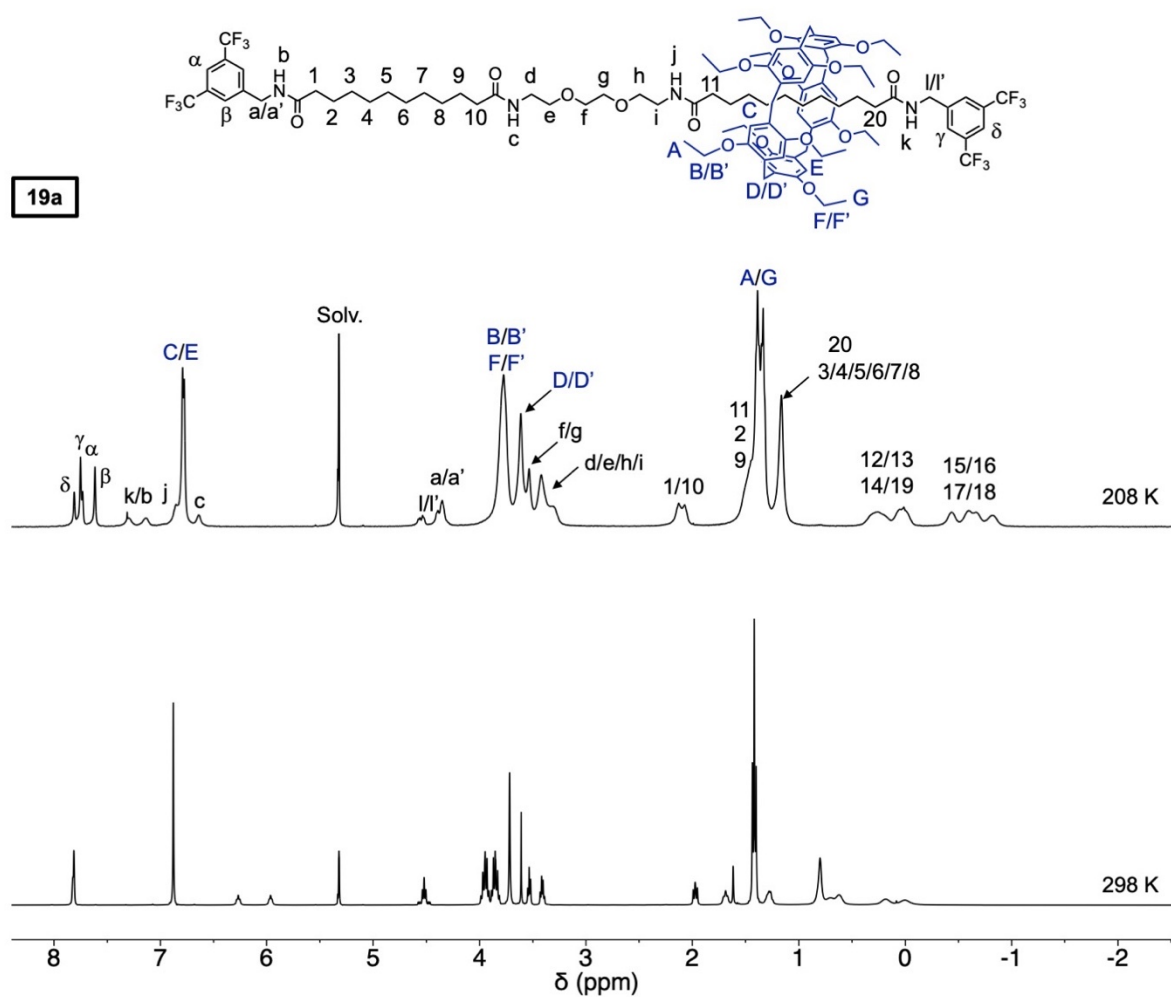


Figure 8. ^1H NMR spectra (400 MHz) of [2]rotaxane **19a** recorded in CD_2Cl_2 at different temperatures.

By lowering the temperature, the dynamic gliding motions became slower than the NMR timescale for both **19a** and **19d**. As observed for **19b**, two 3,5-bis(trifluoromethyl)benzamide terminated decyl chains appeared effectively as non-equivalent in the ^1H NMR spectra recorded

at low temperatures. In both cases, the macrocycle is located over one decyl chain of the axle and the central station is not significantly occupied.

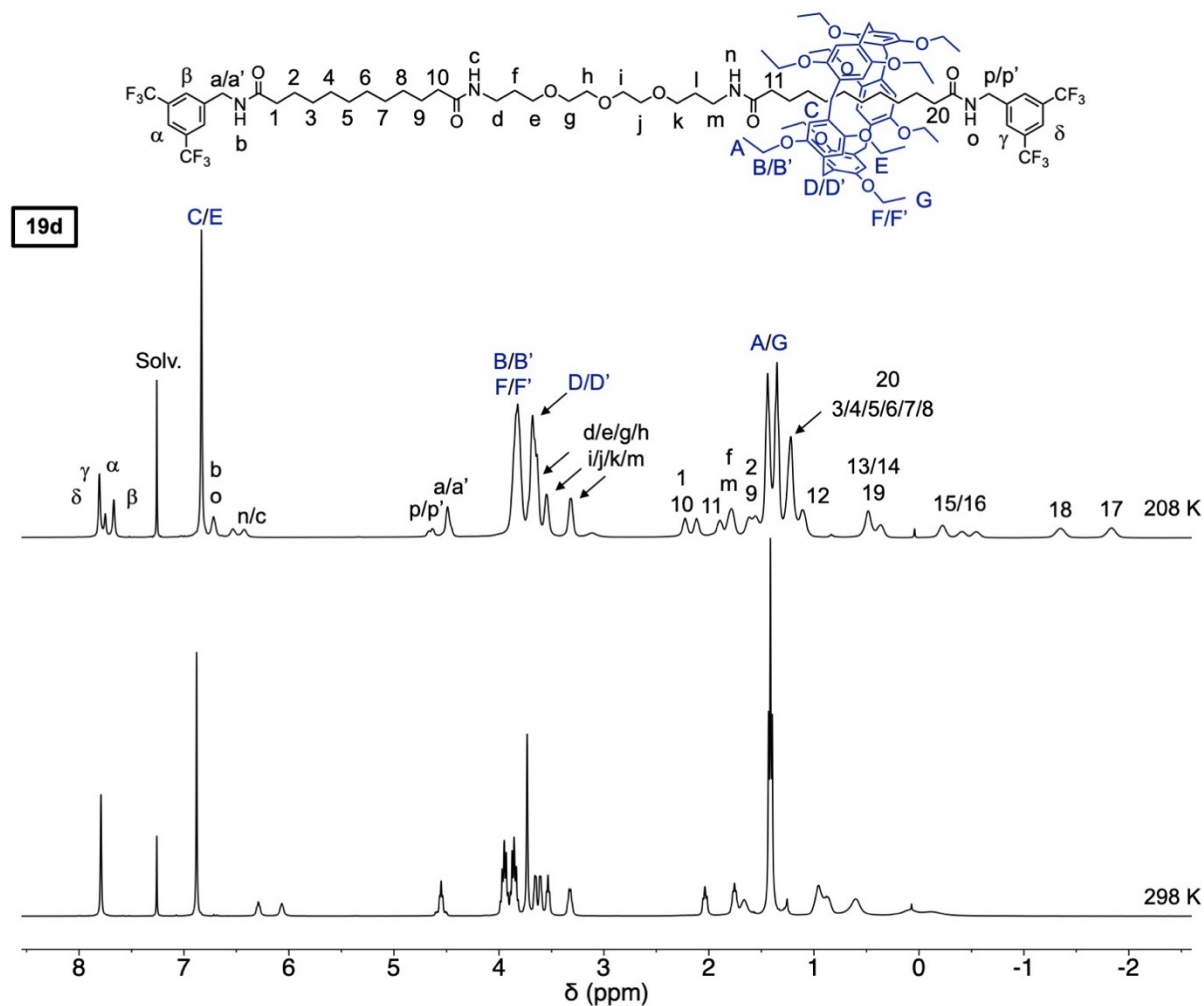


Figure 9. ^1H NMR spectra (400 MHz) of [2]rotaxane **19d** recorded in CDCl_3 at different temperatures.

Overall, variable temperature ^1H NMR investigations revealed that the pillar[5]arene is preferentially located over its two decyl stations in [2]rotaxanes **19a-d**. In contrast, the conformer in which the macrocyclic subunit of **19a-d** is located over the central moiety of the axle is not significantly populated. Indeed, this central station can be considered as the transition state for the dynamic exchange allowing the macrocycle to shuttle back and forth between the two different decyl stations (Figure 10). The coalescence temperatures were found significantly different indicating changes in the activation free energy (ΔG^\ddagger) of the shuttling process with the

nature of the central linkers in **19a-d**. At the coalescence temperature (T_c), the rate constant (k) of the dynamic exchange is related to the chemical shift difference ($\Delta\nu$) for the two exchanging peaks below T_c at slow exchange regime (Eq. 1):

$$k = \frac{\pi\Delta\nu}{\sqrt{2}} \quad \text{Eq. 1}$$

The free energy of activation ΔG^\ddagger for the dynamic exchange can be then directly evaluated with the Eyring equation (Eq. 2):

$$\Delta G^\ddagger = -R T_c \ln(k h / k_B T_c) \quad \text{Eq. 2}$$

where R is the gas constant, h is Planck's constant, k_B is the Boltzmann constant, T_c is the coalescence temperature, and k is the rate constant of exchange (s^{-1}). The ΔG^\ddagger values derived from the coalescence of the signals arising from the aromatic protons of the 3,5-bis(trifluoromethyl)benzyl stoppers are reported in Table 2.

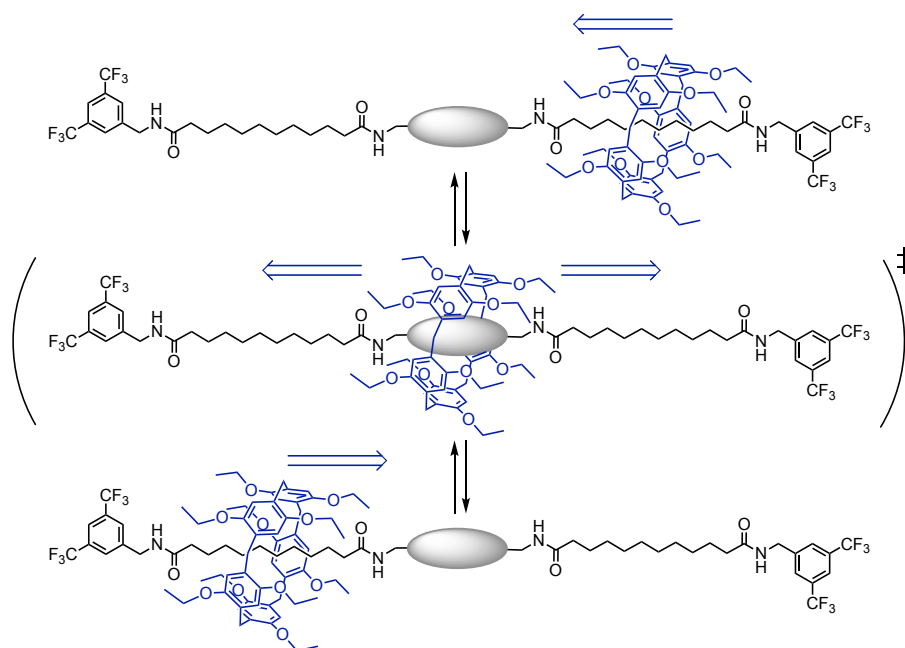


Figure 10. Variable temperature ^1H NMR investigations revealed that the pillar[5]arene is preferentially located over its two decyl stations in [2]rotaxanes **19a-d**. The central station can be considered as the transition state for the dynamic exchange allowing the macrocycle to switch from one decyl station to the other one.

Table 2. Coalescence temperature (T_c), rate constant (k), chemical shift difference ($\Delta\nu$) and activation free energy (ΔG^\ddagger) deduced from the ^1H NMR spectra recorded at different temperatures for [2]rotaxanes **19a-d**.

[2]Rotaxane		T_c (K)	$\Delta\nu$ (Hz)	k (s^{-1})	ΔG^\ddagger (kJ/mol)
19a ^[a]	H(α)	233	31.3	69.4	48(1)
	H(β)	233	54.3	120.5	47(1)
19b ^[b]	H(α)	243	29.4	65.3	51(1)
	H(β)	253	58.9	130.8	51(1)
19c ^[c]	H(α)	323	28.5	63.2	68(1)
	H(β)	333	50.5	112.1	68(1)
19d ^[b]	H(α)	233	22.3	49.5	49(1)
	H(β)	243	55.0	122.2	49(1)

[a] From the ^1H NMR spectra recorded in CD_2Cl_2 . [b] From the ^1H NMR spectra recorded in CDCl_3 . [c] From the ^1H NMR spectra recorded in $\text{CDCl}_2\text{CDCl}_2$.

The ΔG^\ddagger values were also conveniently derived from variable temperature ^{19}F NMR studies. In this case, [2]rotaxanes **19a-d** were all investigated in the same solvent (CDCl_3). As shown in Figure 11, the ^{19}F NMR spectra recorded in CDCl_3 at room temperature for **19a-d** revealed only one singlet. In all cases, the CF_3 groups of both stoppers appear as equivalent as the shuttling of the macrocycle between its two decyl stations is faster than the NMR timescale. In contrast, by lowering the temperature, the two stoppers are not anymore equivalent and two singlets are observed. In this case, position exchange of the macrocycle between its two decyl stations is slower than the NMR timescale. The ΔG^\ddagger values obtained by analyzing the coalescence of the ^{19}F NMR signals of **19a-d** are similar to the ones derived from the analysis of the ^1H NMR data (Table 3).

Table 3. Coalescence temperature (T_c), rate constant (k), chemical shift difference ($\Delta\nu$) and activation free energy (ΔG^\ddagger) deduced from the ^{19}F NMR spectra recorded in CDCl_3 at different temperatures for [2]rotaxanes **19a-d**.

[2]Rotaxane	T_c (K)	$\Delta\nu$ (Hz)	k (s^{-1})	ΔG^\ddagger (kJ/mol)
19a	233	10.0	22.3	51(1)
19b	233	9.2	20.4	51(1)
19c	293	15.7	34.8	63(1)
19d	233	9.0	20.1	51(1)

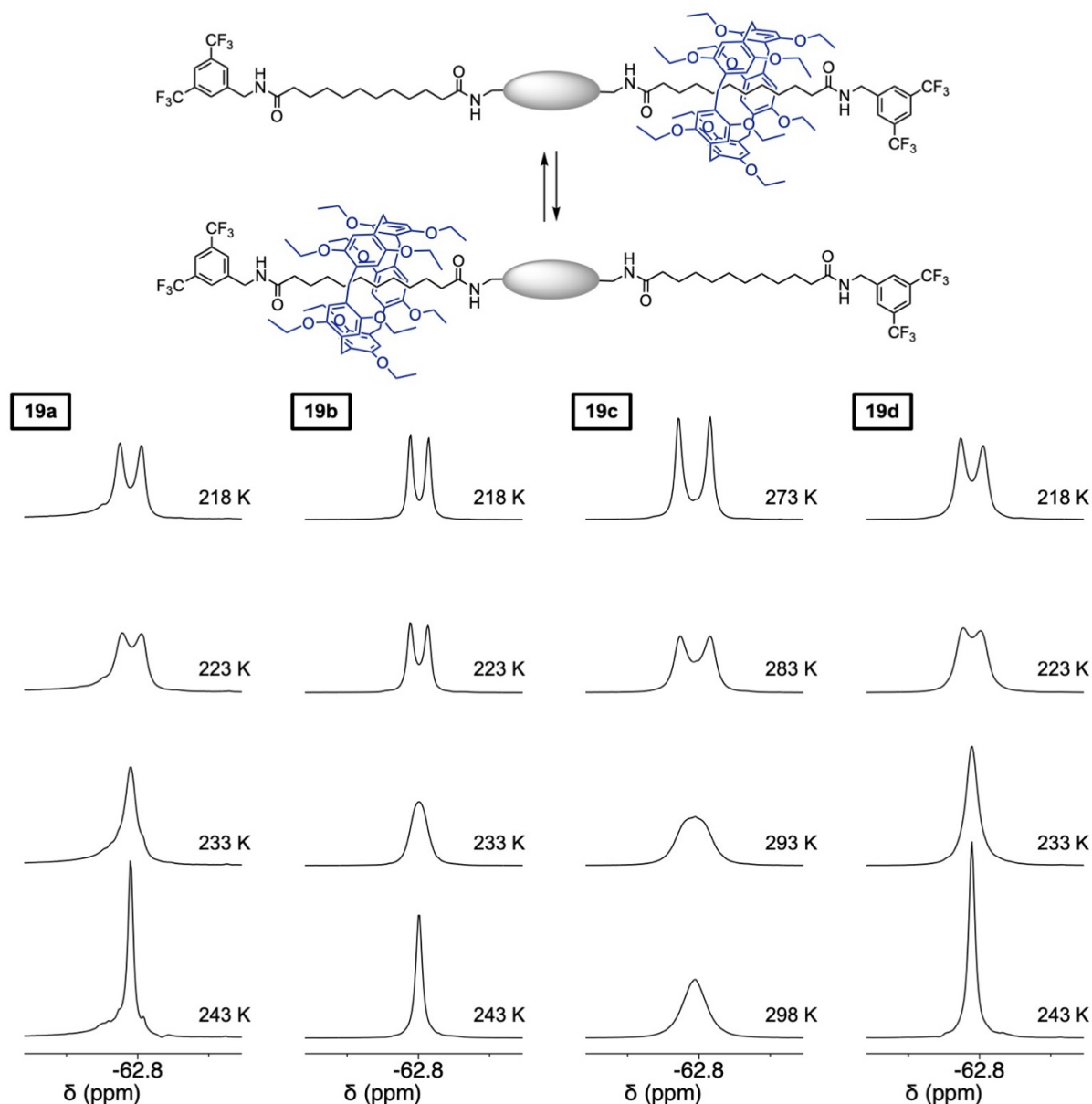


Figure 11. ^{19}F NMR spectra (376 MHz) of [2]rotaxanes **19a-d** recorded in CDCl_3 at different temperatures.

The energy barrier for the shuttling of the pillar[5]arene moiety over the central linker in **19a-d** results from an interplay between electronic and steric effects. In the case of **19a** and **19d**, steric effects are limited and unfavorable interactions between the triethylene glycol spacer⁵ and the pillar[5]arene subunit in **19a** and **19d** are most likely at the origin of the energy barrier for the shuttling of the macrocycle between its two decyl stations. In the case of **19b-c**, the cavity of the pillar[5]arene is probably slightly too small to accommodate the central phenylene linker despite possible favorable van der Waals interactions. Effectively, the cavity size of the pillar[5]arene⁸ is *ca.* 4.7 Å and the size of a phenyl ring calculated by van der Waals radii⁹ *ca.*

5 to 6 Å (Figure 12). Obviously, substantial distortion of the pillar[5]arene scaffold is necessary to allow the phenyl group to pass through the cavity of the macrocycle. As a result, steric effects may play a major role for the shuttling of the macrocycle between the two decyl stations in the case of **19b-c**.

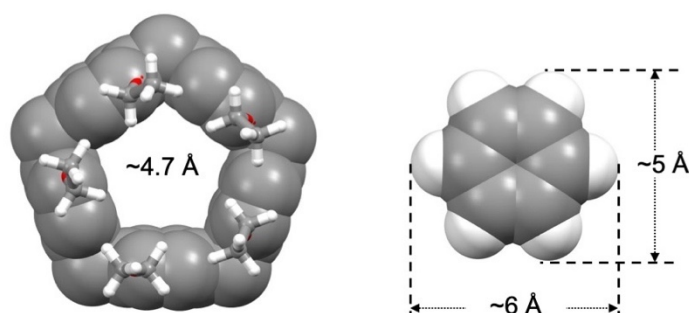


Figure 12. Calculated structure of pillar[5]arene **3** showing the size of its cavity together with the calculated structure of benzene highlighting its molecular size calculated by van der Waals radii.

DFT calculations. In order to visualize how the pillar[5]arene moiety slides over the phenylene stations in [2]rotaxanes **19b** and **19c**, density functional theory (DFT) calculations were carried out with appropriate fragments (Figures 13 and 14). Specifically, the structure of the host-guest complexes resulting from the association of methoxypillar[5]arene (**H**) with phenylene-based model guests **G1-2** were optimized at the B3LYP/6-31G* level of theory.¹⁰ Starting from the optimized structures of inclusion complexes (**H.G1**) and (**H.G2**), the distance between one C atom of the phenylene moiety of the guest and an oxygen atom of the host located on the opposite side of the cavity was constrained in order to program the slipping of the guest through the macrocyclic host in a stepwise manner. As shown in Figure 13, the pillar[5]arene host has to tilt one of its hydroquinone unit to accommodate part of the phenylene ring of guest **G1** within its cavity. The energy then gradually increases as the phenylene moiety of **G1** begins to pass through the cavity of **H**. Near the transition state, the entire cyclophane scaffold of **H** bends slightly and the tilted hydroquinone subunit of **H** then swings over the phenyl ring of the guest thus allowing the guest to escape on the other side. The energy profile shows an abrupt drop after the transition state. Indeed, as soon as the phenylene group has sufficiently crossed the median plane of the cavity, the system directs the distance constraint towards the outside of the cavity and no longer towards the inside.

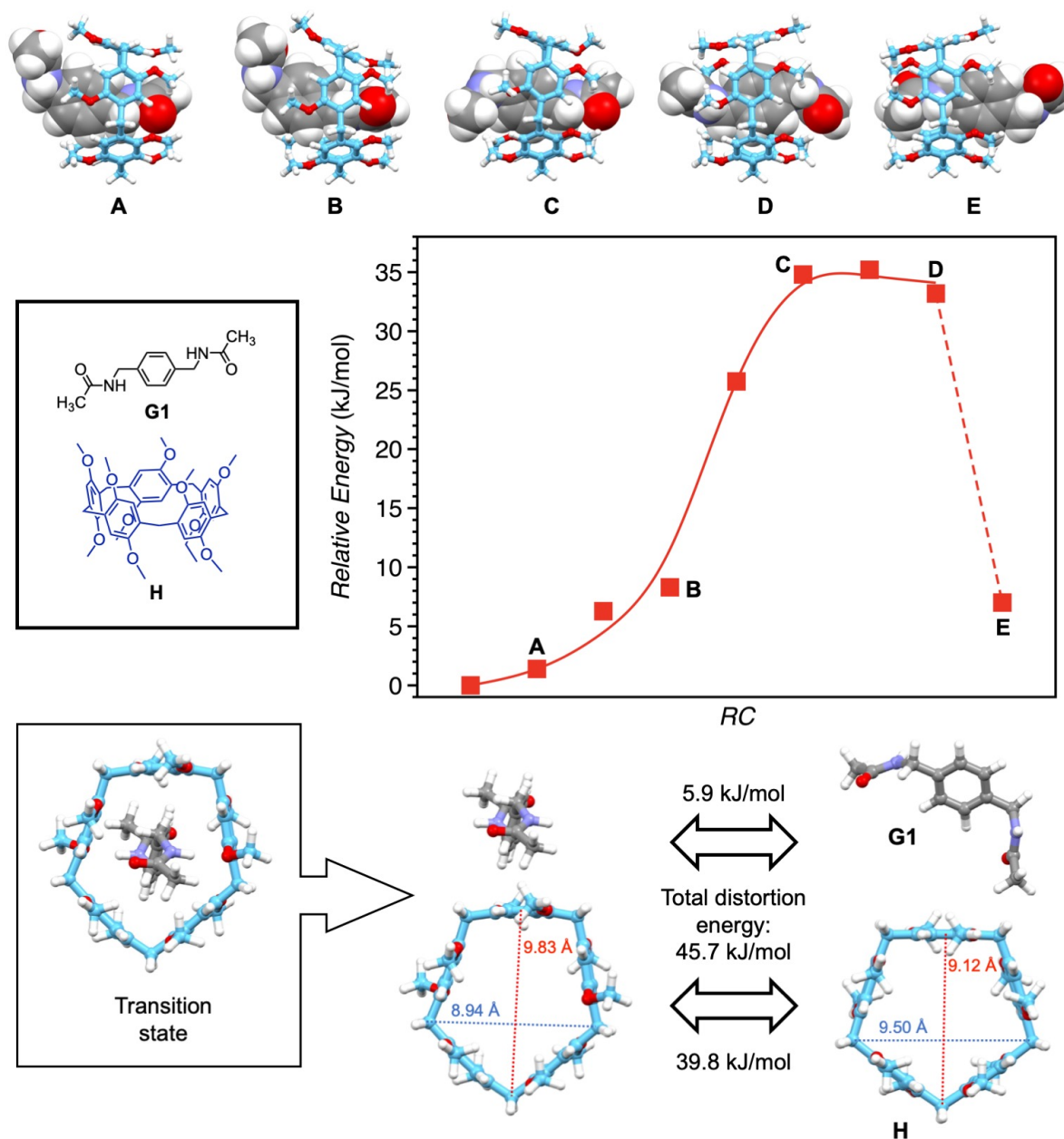


Figure 13. Energy profile calculated for host-guest complex (**H.G1**) for the slipping of the guest through the macrocyclic host and five calculated structures (B3LYP/6-31G* in the gas phase). Bottom: detailed view of the transition state; the distortion energy corresponds to the difference between the electronic energy calculated for the **H** and **G1** moieties of (**H.G1**) and the electronic energy of **H** and **G1** optimized at the same level (H: white, O: red, N: blue, C: grey for **G1** and pale blue for **H**).

The calculations done with host **G2** show the same qualitative trends (Figure 14). Steric constraints are however more important due to the *meta*-substitution pattern of the phenylene moiety of **G2**. Indeed, the aromatic subunit of **G2** is forced to cross the cavity with two *para*-

CH groups parallel to the plane of the cavity of the pillar[5]arene. As a result, the width of the phenylene is greater than in the case of the *para* analogue (**G1**) which can cross the cavity with a more favorable orientation.

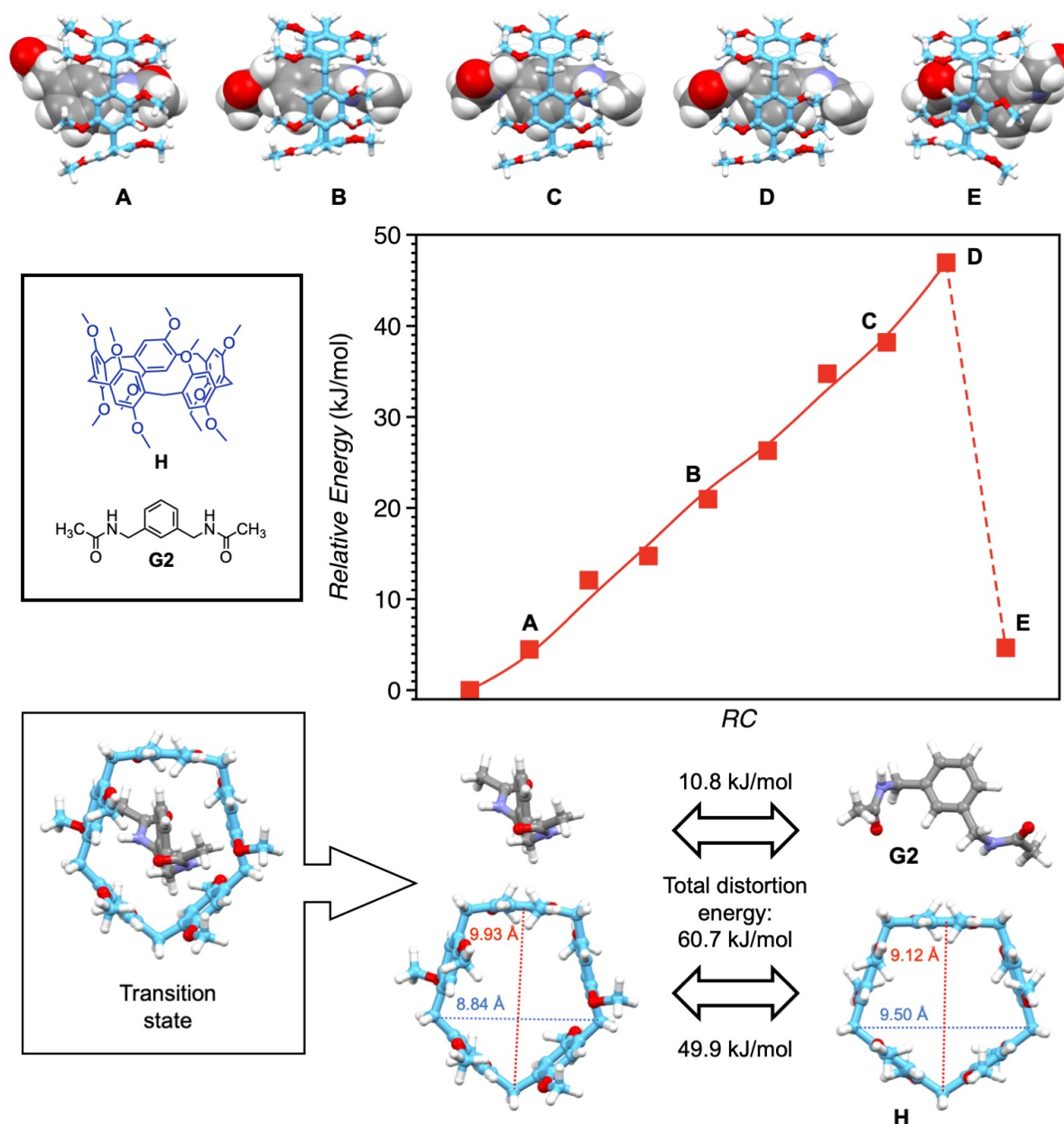


Figure 14. Energy profile calculated for host-guest complex (**H.G2**) for the slipping of the guest through the macrocyclic host and five calculated structures (B3LYP/6-31G* in the gas phase). Bottom: detailed view of the transition state; the distortion energy corresponds to the difference between the electronic energy calculated for the **H** and **G2** moieties of (**H.G2**) and the electronic energy of **H** and **G2** optimized at the same level of theory (H: white, O: red, N: blue, C: grey for **G2** and pale blue for **H**).

Close analysis of the transition states found for the slipping of guest **G1-2** through the macrocyclic host **H** shows a substantial deformation of the cyclophane core. The pillar[5]arene is shrinking its structure in one direction to increase the height of its cavity in the perpendicular direction. In this way, the cavity is able to accommodate the phenylene moiety of the host. When compared to the optimized structure of **H** for which the height is 9.12 Å, an increase of 0.71 and 0.81 Å is observed in the transition states (**H.G1**)[‡] and (**H.G2**)[‡], respectively. Clearly, the distortion of the pillar[5]arene is more important in the case of (**H.G2**)[‡]. The structural factors controlling the slippage of the pillar[5]arene over the phenylene moieties of **G1** and **G2** were further elucidated by evaluating the energy required for the deformation of their individual components (**H** and **G1-2**) in transition states (**H.G1**)[‡] and (**H.G2**)[‡]. The distortion energy (ΔE_{dist})¹¹ is obtained from Eq. 3:

$$(\Delta E_{\text{dist}}) = (E_{\text{Frag}}^{\text{H}} + E_{\text{Frag}}^{\text{G}}) - (E^{\text{H}} + E^{\text{G}}) \quad (\text{Eq. 3})$$

where $E_{\text{Frag}}^{\text{H}}$ is the electronic energy of the pillar[5]arene fragment in (**H.G1-2**)[‡], $E_{\text{Frag}}^{\text{G}}$ is the electronic energy of the guest fragment in (**H.G1-2**)[‡], E^{H} is the electronic energy of **H** and E^{G} is the electronic energy of **G1-2**. The ΔE_{dist} values thus obtained for (**H.G1**)[‡] and (**H.G2**)[‡] are 45.7 and 60.7 kJ/mol, respectively. The distortion energy difference determined for the *para*- and *meta*-phenylene-containing model systems **G1** and **G2** are fully consistent with the difference in free energy of activation experimentally determined by analyzing the coalescence of the NMR signals of **19b** and **19c**. The ΔE_{dist} values are also close to the experimental ΔG^{\ddagger} values thus showing that the shuttling of the macrocycle between the two decyl stations in **19b** and **19c** are mainly dominated by steric effects.

For comparison purposes, the inclusion complexes of **H** with *n*-hexane (**G3**) and 1,2-dimethoxyethane (**G4**) were also computed (Figure 15). Evaluation of the distortion energies revealed limited deformation of their individual components in both cases thus showing that steric effects play only a very minor role in the energy barrier observed for the shuttling of the pillar[5]arene subunit for rotaxanes **19a** and **19d**. Indeed, the preferential position of the pillar[5]arene over the decyl stations of **19a** and **19d** results from more favorable dispersive interactions between the pillar[5]arene and a linear alkyl chain when compared to a triethylene glycol subunit. The energy barrier therefore accounts mainly for the energy necessary to overcome the enthalpic changes when going from a decyl station to the triethylene glycol one.

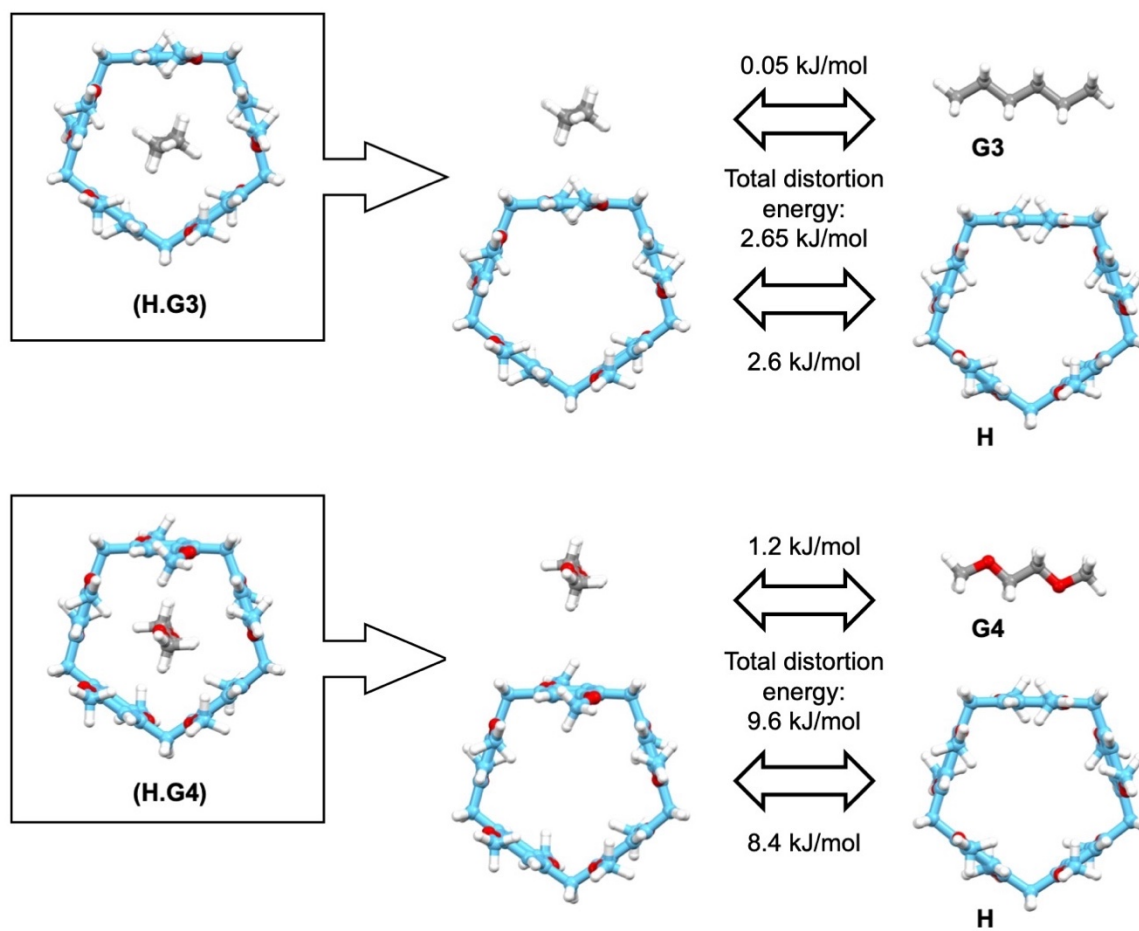


Figure 15. Structures of (H.G3) and (H.G4) optimized in the gas phase at the B3LYP/6-31G* level; the distortion energy corresponds to the difference between the electronic energy calculated for the H and G2 moieties of (H.G3-4) and the electronic energy of H and G3-4 optimized at the same level of theory (H: white, O: red, N: blue, C: grey for G3-4 and pale blue for H).

Computational studies were also carried out in order to evaluate the distance over which the gliding motions of the pillar[5]arene moiety are possible in the case of [2]rotaxanes **19a-d**. Geometry optimizations were performed at the semi-empirical level (PM6). The calculated structures are shown in Figure 16. The length of the decyl stations of the rotaxanes is *ca.* 1.39 nm. The width of the pillar[5]arene moiety is *ca.* 1 nm if one considers its ethoxy substituents. Gliding motions of the pillar[5]arene component over its axle subunit occurs over a distance of *ca.* 3.8-4.2 nm depending on the nature of the central spacer. Despite the relatively large length of the axle, the dynamic exchange allowing the macrocycle to shuttle back and forth between the two different decyl stations remains faster than the NMR timescale at room temperature in the case of **19a-b** and **19d**. In the particular case of **19c**, higher temperature are necessary to allow motions of the pillar[5]arene over the entire length of the axle due to a greater energy barrier to cross the substantially larger central subunit.

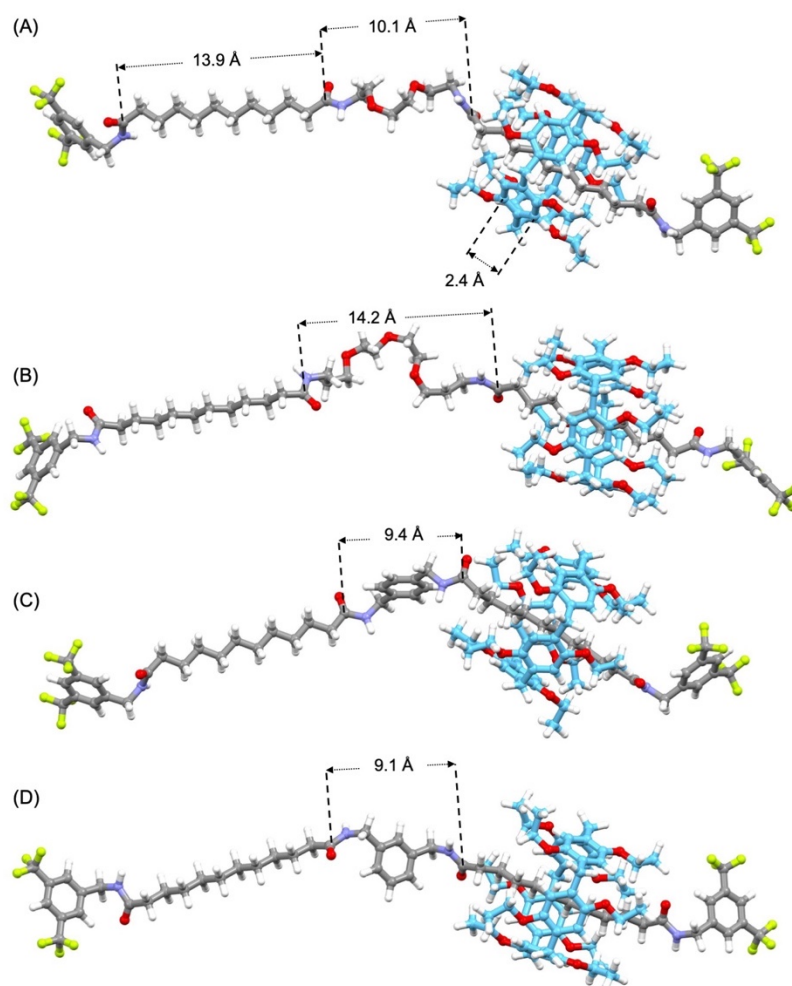


Figure 16. Calculated structures of compounds **19a** (A), **19d** (B), **19b** (C) and **19c** (D) highlighting the distances between the C atoms of the C=O moieties of the axle component and the C-C distance between two aromatic C atoms of the pillar[5]arene moiety (H: white, F: light green, O: red, N: blue, C: grey for the axle and pale blue for the pillar[5]arene moiety).

Characterization of the [3]rotaxanes. Compounds **20a-c** and **20e** were also characterized by NMR spectroscopy. As a typical example, the ^1H NMR spectra recorded for [3]rotaxane **20b** in CDCl_3 and $\text{DMSO}-d_6$ are depicted in Figure 17. Considering the shielding effect of the pillar[5]arene moiety on the resonances of the methylene groups located within its cavity, each macrocycle is clearly located over a decyl subunit of the axle. All signals of the CH_2 units of the decyl chain are affected by the ring current effect of the aromatic ring of their pillar[5]arene component thus showing that gliding motions of the pillar[5]arenes all over their decyl station are faster than the NMR timescale under these conditions. In CDCl_3 , the shielding is more important for H(3,4) showing that these particular methylene groups have a higher probability of presence in the cavity of the macrocycle. As already discussed in the previous chapter,

intramolecular dipole-dipole interactions play a major role in nonpolar solvents and conformations in which the macrocycle is close to its bis(trifluoromethyl)phenyl stoppers are favored.

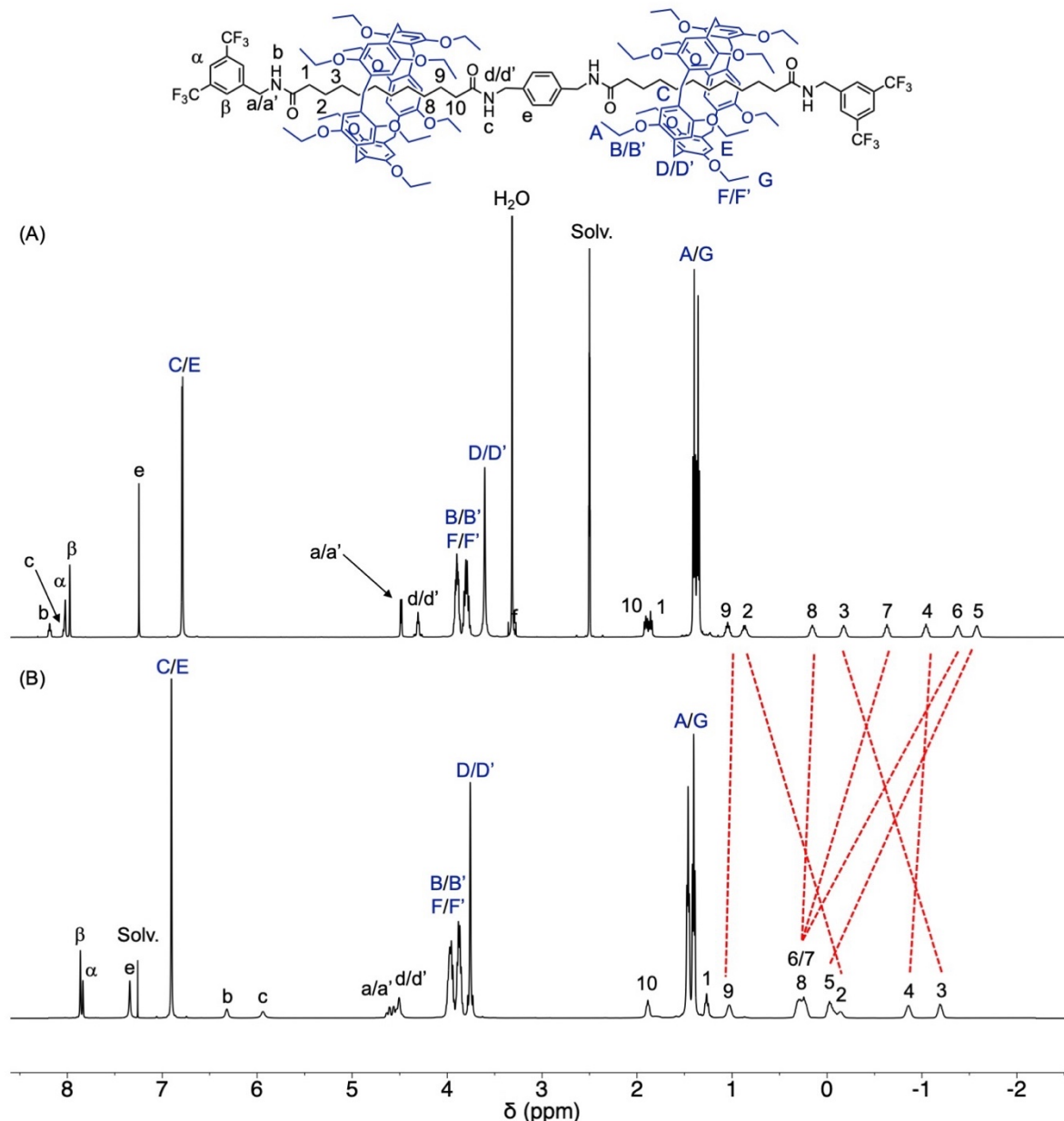


Figure 17. ^1H NMR spectra (500 MHz, 298 K) recorded for [3]rotaxane **20b** in DMSO- d_6 (A) and CDCl_3 (B).

When going from CDCl_3 to DMSO- d_6 , dramatic chemical shift changes are observed for the resonances of the methylene groups of the decyl chains. Analysis of the relative chemical shifts of the methylene groups revealed that the pillar[5]arene moiety is preferentially located in the middle of the decyl chains in DMSO. Under these conditions, the conformational preferences of rotaxane **20b** result from solvophobic effects. Obviously, the amide functions of **20b** are well

solvated by DMSO while repulsive interactions between the decyl chain and the polar solvent molecules are expected. As a result, the macrocycle is preferentially located in the middle of the axle subunit to limit unfavorable interactions between the decyl chain and the solvent. A similar behavior was also observed for [3]rotaxanes **20a**, **20c** and **20e**. Finally, it should be added that compounds **20a-c** and **20e** were all obtained as a mixture of two diastereomers as shown in Figure 2 for **20e**. However, the NMR spectra of the two diastereomers recorded at room temperature are identical in all cases. Actually, it was necessary to record the spectra at low temperature to distinguish the two diastereomers. This is shown in Figure 18 for compound **20e**.

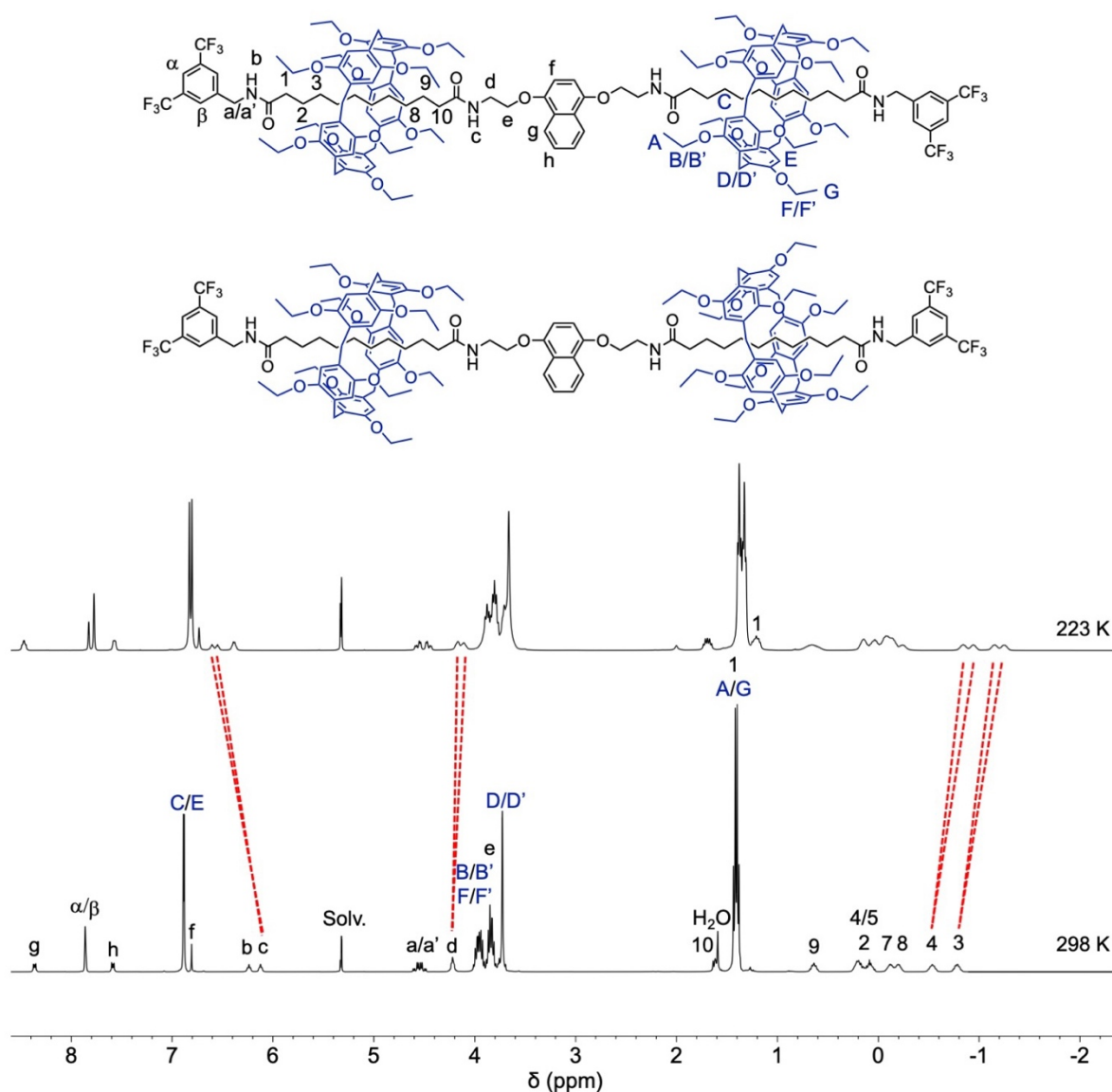


Figure 18. ^1H NMR spectra (400 MHz) of [3]rotaxane **20e** recorded in CD_2Cl_2 at different temperatures. While the two diastereomers cannot be distinguished at 298 K, they are clearly observed at 223 K as highlighted for the signals of H(3), H(4), H(c) and H(d).

At room temperature, dynamic exchanges are fast and thermal agitation prevents the transfer of the chiral information.¹² By lowering the temperature, molecular motions are more limited and the exchange of the chiral information occurs effectively. As a matter of fact, the ¹H NMR spectra recorded at low temperatures revealed the presence of the two diastereomers in all cases.

III-3. Conclusion

In this chapter, the functionalization of a rotaxane building block bearing an activated pentafluorophenyl ester stopper with diamine reagents has been investigated. When the diamine reagent is large enough to prevent dissociation of the monoacylated intermediate, reaction with a second equivalent of the rotaxane building block provides the corresponding [3]rotaxane in excellent yields. In contrast, when the diamine reagent is smaller, the monoacylated intermediate is an inclusion complex. When the reaction is carried out in THF solutions, complete dissociation of the inclusion complex occurred. The amine function of the molecular thread thus generated with the pentafluorophenyl ester stoppered rotaxane affords the corresponding [2]rotaxane with an elongated axle unit. In contrast, when the reaction is performed under solvent-free mechanochemical conditions, dissociation of the intermediate inclusion complex is partially prevented thus allowing the formation of [3]rotaxanes.

III-4. References

- 1) For reviews on supramolecular concepts in mechanochemistry, see: (a) T. Friščić, *Chem. Soc. Rev.* **2012**, *41*, 3493-3510. (b) A. Inthassot, T.-Y. Tai, S.-H. Chiu, *J. Chin. Chem. Soc.* **2019**, *66*, 134-145.
- 2) For previous examples of rotaxane synthesis under mechanochemical solvent-free conditions, see: (a) A. Orita, J. Okano, Y. Tawa, L. Jiang, J. Otera, *Angew. Chem. Int. Ed.* **2004**, *43*, 3724-3728. (b) S. Y. Hsueh, K. W. Cheng, C.-C. Lai, S.-H. Chiu, *Angew. Chem. Int. Ed.* **2008**, *47*, 4436-4439. (c) C.-C. Hsu, N. C. Chen, C.-C. Lai, Y.-H. Liu, S.-M. Peng, S.-H. Shiu, *Angew. Chem. Int. Ed.* **2008**, *47*, 7475-7478. (d) C.-C. Hsu, C.-C. Lai, S.-H. Chiu, *Tetrahedron* **2009**, *65*, 2824-2829. (e) P.-N. Chen, C.-C. Lai, S.-H. Chiu, *Org. Lett.* **2011**, *13*, 4660-4663. (f) K.-D. Wu, Y.-H. Lin, C.-C. Lai, S.-H. Chiu, *Org. Lett.* **2014**, *16*, 1068-1071.

- 3) For examples of rotaxane synthesis under solvent-assisted ball-milling conditions, see: H.-G. Li, G.-W. Wang, *J. Org. Chem.* **2017**, *82*, 6341-6348.
- 4) M. Holler, T. Stoerkler, A. Louis, F. Fisher, J.-F. Nierengarten, *Eur. J. Org. Chem.* **2019**, 3401-3405.
- 5) T.w. Kwon, B. Song, K. W. Nam, J. F. Stoddart, *J. Am. Chem. Soc.* **2022**, *144*, 12595-12601.
- 6) M. Rémy, I. Nierengarten, B. Park, M. Holler, U. Hahn, J.-F. Nierengarten, *Chem. Eur. J.* **2021**, *27*, 8492-8499.
- 7) D. D. Günbas, A. M. Brouwer, *J. Org. Chem.* **2012**, *77*, 5724-5735.
- 8) N. Song, T. Kakuta, T.-a. Yamagishi, Y.-W. Yang, T. Ogoshi, *Chem* **2018**, *4*, 2029-2053.
- 9) (a) X. Zhang, F. Rösicke, V. Syritski, G. Sun, J. Reur, K. Hinrichs, S. Janietz, J. Rappich, *Z. Phys. Chem.* **2014**, *228*, 557-573. (b) A. Bondi, *J. Phys. Chem.* **1964**, *68*, 441-451.
- 10) For examples of DFT calculations on pillar[5]arene host-guest complexes, see: (a) S. V. Athare, S. P. Gejji, *J. Phys. Chem. A* **2019**, *123*, 8391-8396. (b) M. Panneerselvam, M. D. Kumar, M. Jaccob, R. V. Solomon, *ChemistrySelect* **2018**, *3*, 1321-1334.
- 11) J.-F. Nierengarten, *J. Porphyrins Phthalocyanines* **2023**, *27*, 1253-1262.
- 12) I. Nierengarten, K. Buffet, M. Holler, S. P. Vincent, J.-F. Nierengarten, *Tetrahedron Lett.* **2013**, *54*, 2398-2402.

Pillar[5]arene-containing molecular shuttles

IV-1. Introduction

In the previous section, we have prepared several pillar[5]arene-containing [2]rotaxanes. The uncontrolled dynamic gliding motions of their macrocyclic subunit along the axle unit have been investigated in details. Based on all the knowledge acquired with these systems, we now propose to use our building blocks for the preparation of [2]rotaxanes in which the position can be controlled by an external stimulus. So far, only a few examples of pillar[5]arene-based molecular shuttles have been reported and their behavior only superficially investigated.¹ Actually, when compared to related systems prepared with other macrocycles,² a full control is by far more difficult to achieve owing to the low interaction energies between the different stations of the axle and the pillar[5]arene subunit. For the design of our molecular shuttles we have decided to combine a decyl station with a protonable aromatic subunit (Figure 1).

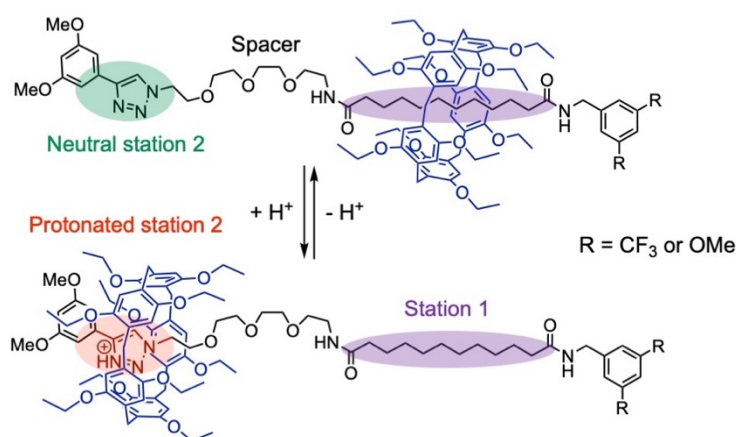


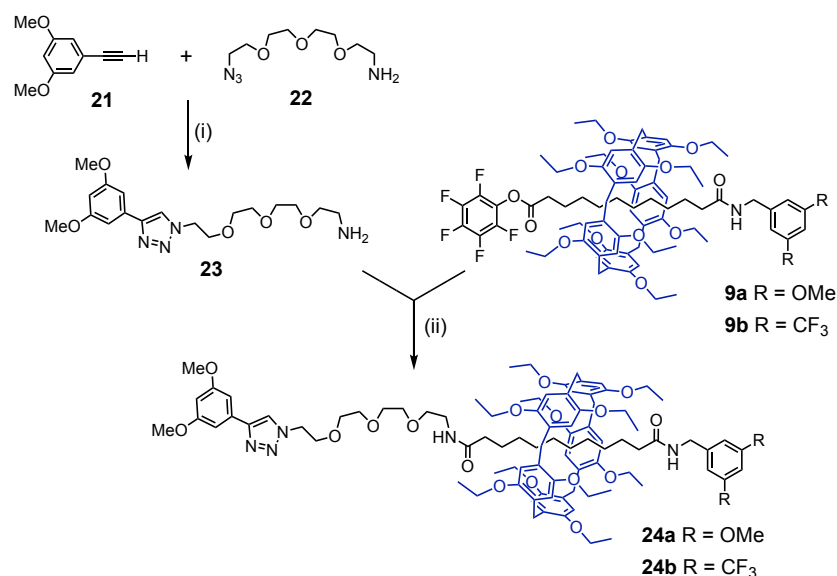
Figure 1. Proposed molecular design for the pillar[5]arene-based molecular shuttles.

Ideally, the pillar[5]arene moiety should form a charge transfer complex with the protonated cationic aromatic moiety while repulsive interactions should occur in the neutral state. The interaction energy of the pillar[5]arene with the cationic station is expected to be higher than the one between the pillar[5]arene and the decyl station. Therefore, the protonated aromatic

station should be preferentially populated. In contrast, in the neutral state, the pillar[5]arene should be preferentially located on the decyl station. For this purpose, we have selected a 1,2,3-triazole unit. Based on preliminary computational studies, this five-membered ring system has an appropriate size to fit within the pillar[5]arene cavity. On the other hand, 1,2,3-triazoles are conveniently prepared by copper-catalyzed alkyne-azide cycloadditions (CuAAC), the so-called click reaction.³ Concerning the decyl station, the stopper is in principle able to affect its affinity for the pillar[5]arene as shown in the previous sections of the present thesis. For this reason, equivalent systems with different electronic properties have been prepared in order to further evaluate the influence of this structural parameter. Finally, it has been decided to incorporate a tetraethylene glycol spacer between the two stations. As shown in the previous sections, the pillar[5]arene has effectively no affinity for oligoethylene glycol chains.

IV-2. Results and discussion

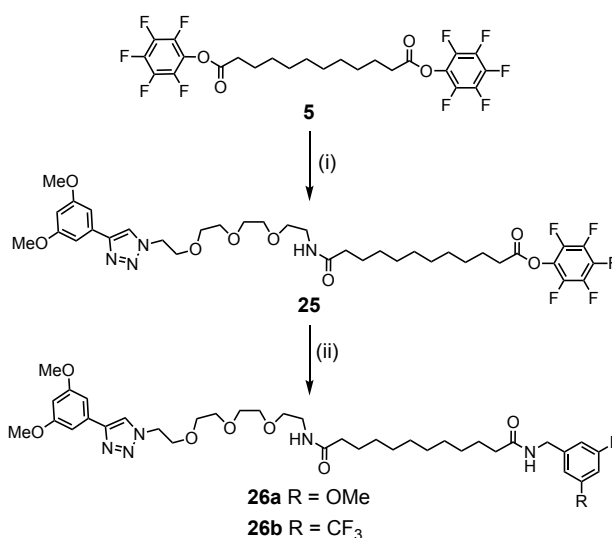
Synthesis. The preparation of the pillar[5]arene-containing molecular shuttles is depicted in Scheme 1.



Scheme 1. Preparation of molecular shuttles **24a-b**. *Reagents and conditions:* (i) CuBr.SMe₂, CH₂Cl₂, rt (85%); (ii) THF, rt (**24a**: 93%; **24b**: 79%).

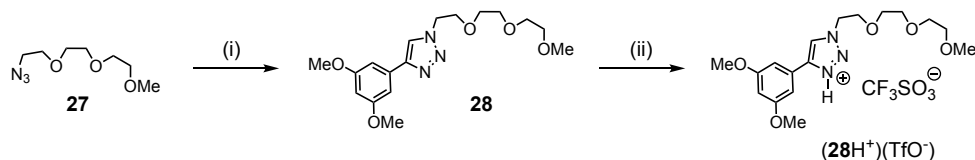
The synthetic approach to prepare **24a** and **24b** relies on the stopper exchange reaction between readily available rotaxane building blocks bearing an activated pentafluorophenyl ester group⁴⁻

⁵ and an amine reagent equipped with the protonable 1,2,3-triazole subunit. For this purpose, the necessary amine building block **23** was prepared by a copper-catalyzed 1,3-dipolar cycloaddition³ reaction to generate the 1,2,3-triazole subunit. Treatment of alkyne **21** with azide **22** in the presence of CuBr.SMe₂ in CH₂Cl₂ at room temperature afforded the desired amine reagent (**23**) in 85% yield. Subsequent reaction with rotaxanes **9a** and **9b** in THF at room temperature gave the targeted molecular shuttles **24a** and **24b** in 93 and 79% yields, respectively. As the stopper exchange reaction occurred through an addition-elimination mechanism, the rotaxane structure is fully preserved during these chemical transformations.⁴ For comparison purposes, the corresponding axle model compounds were also prepared (Scheme 2). Treatment of amine **23** with a large excess of **5** (4 equiv.) gave the monoacylated product (**25**) in 72% yield. Compounds **26a** and **26b** were then obtained by reaction of **25** with **6a** and **6b**, respectively.



Scheme 2. Preparation of axles **26a-b**. *Reagents and conditions:* (i) **23** (0.25 equiv.), THF, rt (72%); (ii) **6a-b**, THF, rt (**26a**: 97% from **6a**; **26b**: 93% from **6b**).

Finally, a model compound of station 2 was also prepared. The synthesis of **28** is shown in Scheme 3. Reaction of alkyne **21** with azide **27**⁶ in the presence of CuSO₄·5H₂O and sodium ascorbate (NaAsc) in CH₂Cl₂/H₂O gave model compound **28** in 83% yield. This compound was also protonated by treatment with a strong acid, namely triflic acid (TfOH), to afford triflate salt (**28H**⁺)(TfO⁻).



Scheme 3. Preparation of model compounds **28** and $(28\text{H}^+)(\text{TfO}^-)$. *Reagents and conditions:*

(i) $\text{CuSO}_4 \cdot 5\text{H}_2\text{O}$, NaAsc, $\text{CH}_2\text{Cl}_2/\text{H}_2\text{O}$, rt (83%); (ii) TfOH, CHCl_3 (quantitative).

Characterization of the new compounds in the neutral state. The structure and purity of compounds **24a-b** and **26a-b** were confirmed by NMR spectroscopy, mass spectrometry and elemental analysis. For all these compounds, the expected molecular ion peak was observed in their MALDI-TOF mass spectrum. The ¹H NMR spectra of compounds **24a-b** and **26a-b** recorded in CD_2Cl_2 at 298 K are shown in Figures 2 and 3. In the ¹H NMR spectra of **24a-b**, the diagnostic signals of the macrocyclic subunit are clearly distinguished. Owing to the unsymmetrical substitution of the axle component, the two rims of the pillar[5]arene moiety are non-equivalent in **24a-b**. As a result, distinct sets of signals are observed the aromatic protons of the pillar[5]arene subunit [H(C/E)]. Two triplets are also observed for the peripheral CH₃ groups [H(A/G)]. In addition to the signals corresponding to the pillar[5]arene moiety of rotaxanes **24a-b**, the characteristic features of the axle component are also clearly observed. When compared to axles **26a-b**, a dramatic shielding of all signals arising from the decyl chain is observed in the corresponding rotaxanes (**24a-b**) due to the ring current effect of the pillar[5]arene hydroquinone subunits on the CH₂ moieties of the axle. Comparison of **24a** and **24b** reveals significant differences in chemical shifts for the signals of H(1-10). The average position of the macrocyclic component on its decyl chain must be therefore different in **24a** and **24b**. On average, the shielding effect is more important for the resonances of H(1-5) in **24b** when compared to **24a** while an opposite trend is observed for H(6-10). As recently shown with related pillar[5]arene-containing rotaxanes, the average position of the electron-rich pillar[5]arene on the decyl station is sensitive to the nature of the benzylic stopper.⁵ Weak through-space donor-acceptor interactions between the bis(trifluoromethyl)phenyl moiety and the pillar[5]arene contribute to stabilize conformations in which the macrocycle is close to its electron-deficient stopper in **24b**. In contrast, the attractive interactions are weaker if any in the case of **24a** with an electron-rich terminal stopper. As a result, the position of the macrocycle is distributed more homogeneously over its decyl station in the case of **24a**.

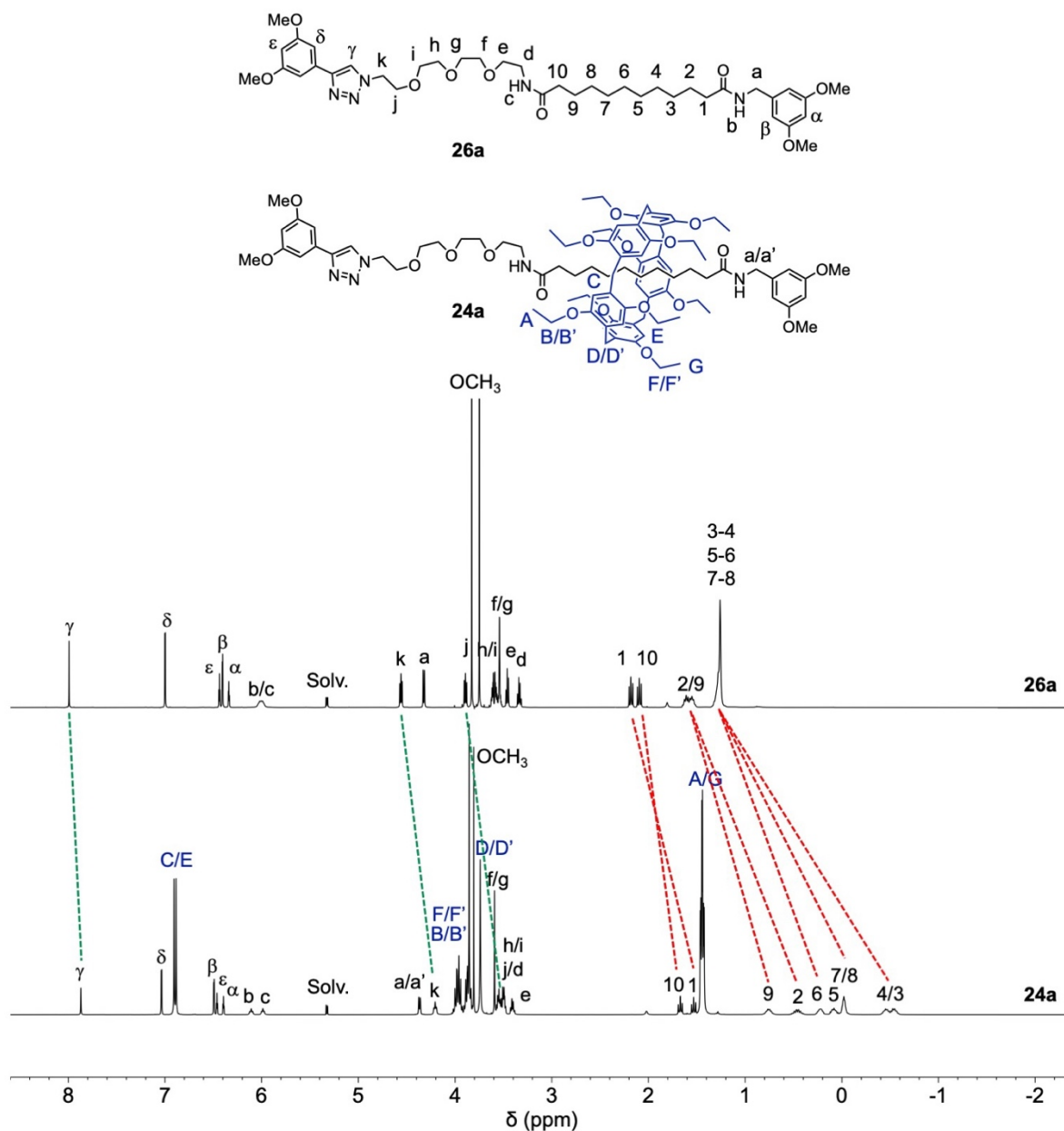


Figure 2. ^1H NMR spectra (CD_2Cl_2 , 500 MHz) recorded for **24a** and **26a** at 298 K. Changes in chemical shifts for the signals arising from the decyl station are highlighted with red lines and from the triazole station with green lines.

All these observations suggest a preferential position of the pillar[5]arene over the decyl chain station in both **24a** and **24b**. However, close inspection of the chemical shifts of some signals arising from protons of the triazole station in **24a-b** and **26a-b** revealed also an upfield shift. Nevertheless, the shielding effect is by far less important than the one observed for the signals of the methylene groups of the decyl station. This observation suggests however that the triazole station is likely partially occupied in **24a-b** under these conditions (CD_2Cl_2 , 298 K). This

prompted us to record the ^1H NMR spectra of **24a-b** at different temperatures. For comparison purposes, the ^1H NMR spectra of **26a-b** were also recorded at different temperatures.

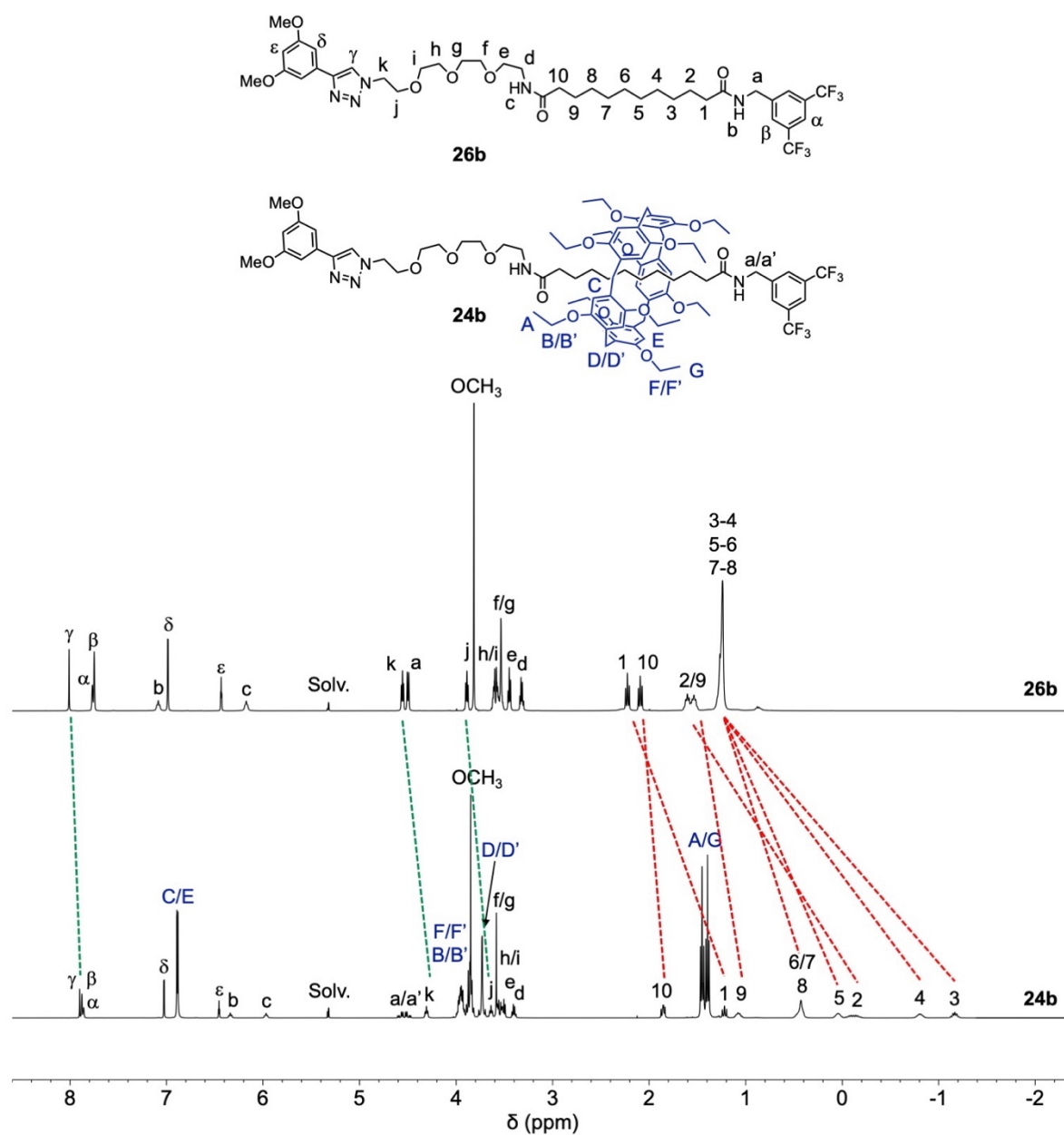


Figure 3. ^1H NMR spectra (CD_2Cl_2 , 500 MHz) recorded for **24b** and **26b** at 298 K. Changes in chemical shifts for the signals arising from the decyl station are highlighted with red lines and from the triazole station with green lines.

While no changes of chemical shift could be observed for the signals of axes **26a-b** as a function of the temperature between 298 and 208 K, significant changes were detected for rotaxanes **24a-b** (Figure 4).

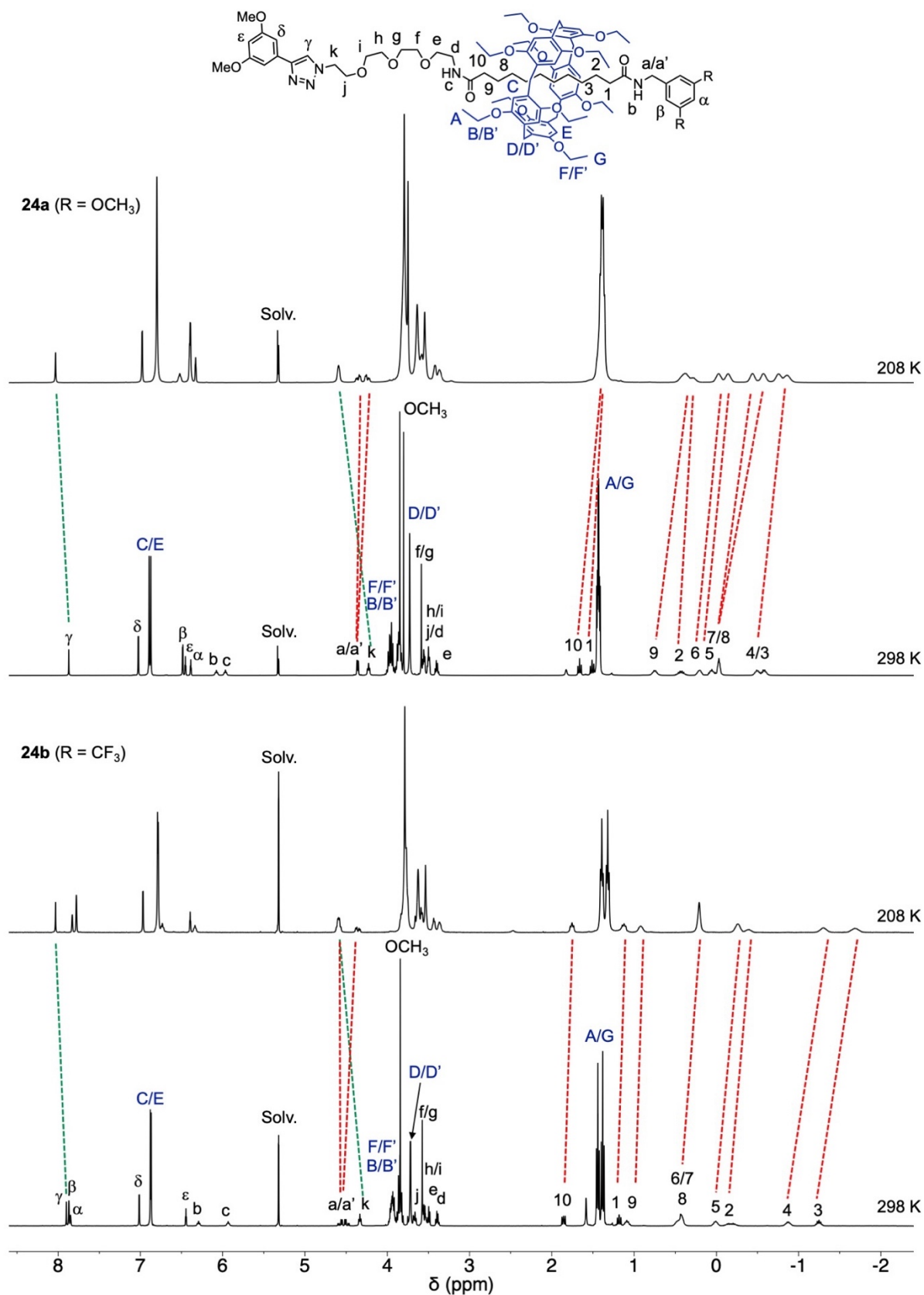


Figure 4. ^1H NMR spectra (CD $_2$ Cl $_2$, 400 MHz) of **24a** and **24b** recorded at different temperatures. Changes in chemical shifts for the signals arising from the decyl station are highlighted with red lines and from the triazole station with green lines.

For both **24a** and **24b**, the signals arising from the triazole station are downfield shifted by lowering the temperature. At the same time, the signals of the decyl station are upfield shifted. These observations suggest that the decyl station is more and more populated by decreasing the temperature. By following the chemical shift of the signals observed for the protons of both stations as a function of the temperature, it appears that no changes could be observed for temperatures below 223 K (Figure 5). Therefore, the pillar[5]arene moiety does not exchange its position between the decyl and the triazole stations by gliding motions below this temperature. On the other hand, transfer of the chiral information from the macrocycle to the benzylic methylene group H(a/a') is more and more effective for both **24a** and **24b** when decreasing the temperature. This is also in complete agreement with a higher probability of presence of the chiral macrocycle on the decyl station close to H(a/a') when the temperature is decreased.

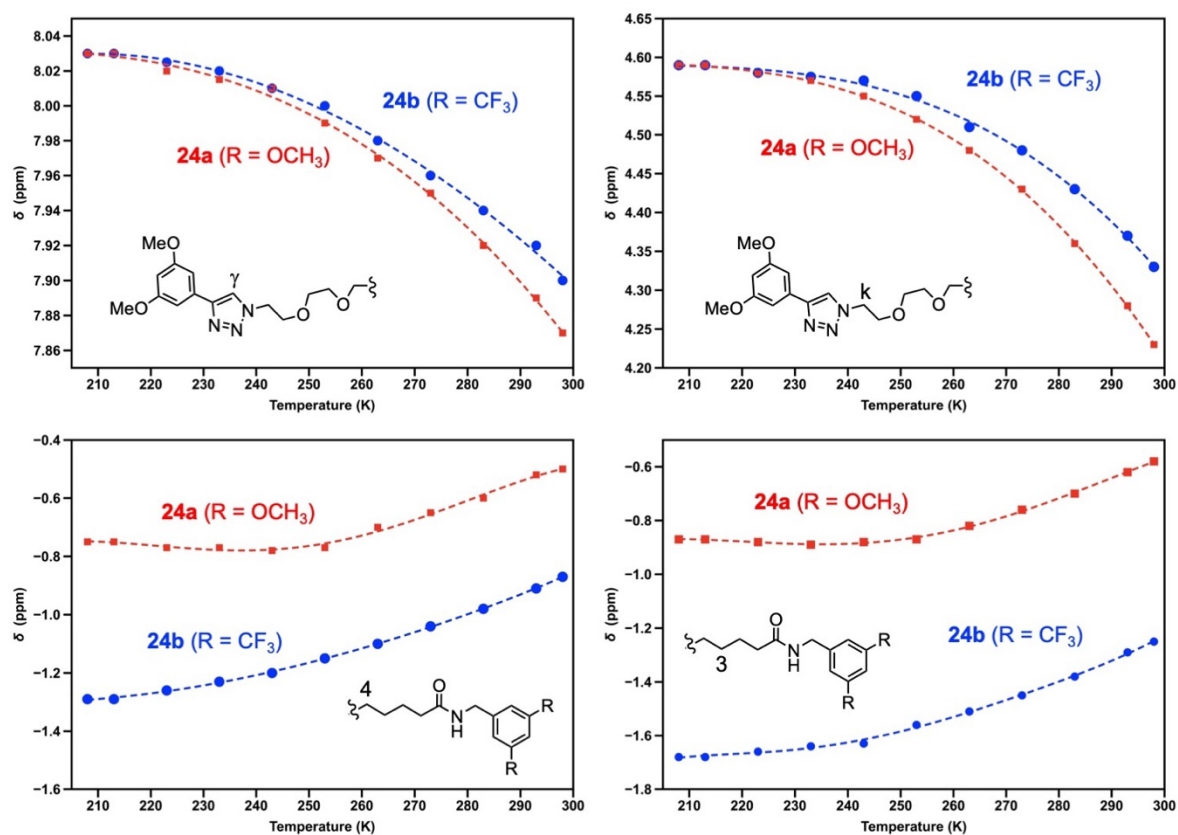


Figure 5. Chemical shift of the signals of H(γ), H(k), H(4) and H(3) in the ^1H NMR spectra (CD_2Cl_2 , 400 MHz) of **24a** and **24b** as a function of the temperature.

The chemical shifts of the resonances observed for H(γ) and H(k) are also the same below 223 K for both **24a** and **24b**. The δ values correspond exactly to the one observed for the same protons in the ^1H NMR spectra of axes **26a** and **26b** recorded under the same conditions.

Obviously, the triazole station is not occupied anymore at temperature below 223 K. The pillar[5]arene is therefore totally located over the decyl station of **24a-b** under these conditions. From an energetic point of view, the difference of energy between the two conformers can be estimated higher than 10 kJ/mol which correspond to a 99.5:0.5 relative population at 223 K based on a Maxwell-Boltzmann analysis. By increasing the temperature, the shielding observed for the resonances of H(γ) and H(k) is less important for **24b** when compared to **24a** thus indicating a lower population of conformers in which the pillar[5]arene is located over the triazole station in **24b**. This is in perfect agreement with stronger attractive interactions between the pillar[5]arene and the bis(trifluoromethyl)phenyl stopper when compared to the dimethoxyphenyl one. These conclusions are also supported by following the chemical shifts of H(3) and H(4) as a function of the temperature. Effectively, the continuous downfield shifted resonances of H(3,4) are fully consistent with an increased population of conformers in which the macrocycle is located over the decyl station in **24a-b** when decreasing the temperature. Moreover, the most important shielding observed for the resonances of H(3,4) in **24b** when compared to **24a** further confirms the attractive interactions between the electron-rich macrocycle and the bis(trifluoromethyl)phenyl stopper. Finally, based on the pseudo-coalescence observed for the signals of H(B-B', F-F'), it was possible to estimate the free energy of activation (ΔG^\ddagger) for the dynamic exchange at the coalescence temperature (223 K). The ΔG^\ddagger values thus obtained were found similar for **24a** and **24b** (46 ± 1 kJ/mol).

Binding studies. To fully understand the behavior of molecular shuttles **24a-b**, the formation of host-guest complexes between pillar[5]arene **3** and appropriate model compounds was also investigated (Figure 6). Compounds **11a-b** were prepared as reported in the literature.⁵ The ability of pillar[5]arene **3** to form inclusion complexes with the different model guests was investigated by ¹H NMR binding studies in CDCl₃ at 298 K. The association constants (K_A) for the 1:1 complexes were estimated on the basis of the complexation-induced changes in chemical shift by using curve fitting analysis. While no binding could be evidenced under these experimental conditions for model triazole **28**, the formation of inclusion complexes was clearly evidenced for **11a-b** and (**28H⁺**)(TfO⁻). The log K_A values derived from ¹H NMR binding studies are listed in the table depicted in Figure 6. As already reported,⁵ the nature of the substituents of the terminal benzylic groups of guests **11a** and **11b** have an influence on the K_A values. The formation of the host-guest complex is effectively more favorable for the guest with the electron-deficient bis(trifluoromethyl)benzyl substituent owing to the occurrence of attractive

interactions with the electron-rich pillar[5]arene host. As the pillar[5]arene host has no affinity for triazole **28**, the preferential position observed for the macrocyclic moiety over the decyl station in **24a-b** is clearly explained. In contrast, the affinity of the model guest for the pillar[5]arene is switched on upon protonation. Based on the relative K_A values obtained for the binding of host **3** with guests $(\mathbf{28H}^+)(\text{TfO}^-)$ and **11a-b**, protonation of molecular shuttles **24a-b** should dramatically influence their conformational equilibria.

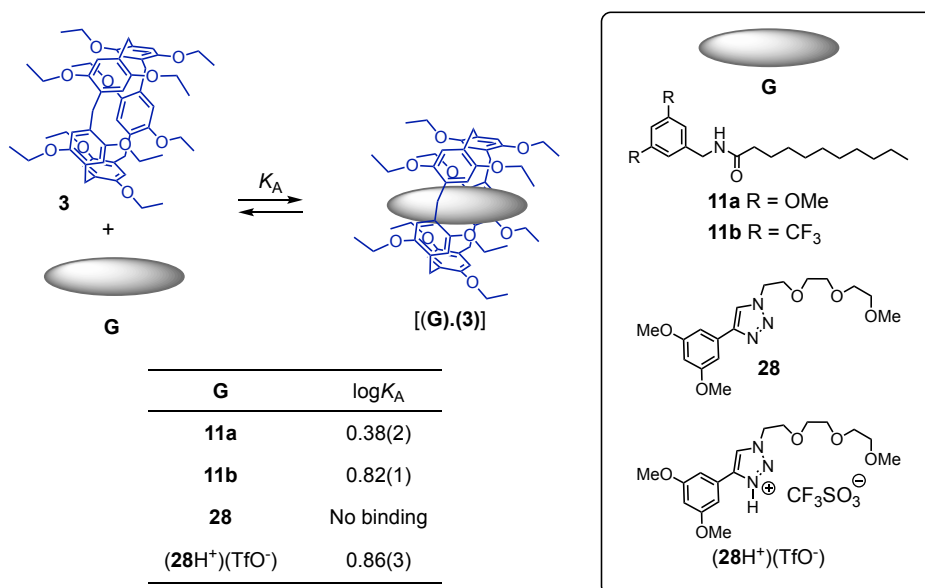


Figure 6. Formation of host-guest complexes between pillar[5]arene **3** and model compounds **11a-b**, **28** and $(\mathbf{28H}^+)(\text{TfO}^-)$. The log K_A values derived from ^1H NMR binding studies in CDCl_3 at 298 K are summarized in the table.

Protonation of model compounds. Before investigating the protonation of **24a-b**, the $\text{p}K_a(\text{BH}^+)$ value of the 1,2,3-triazole station present in **24a-b** and **26a-b** was estimated by following a theoretical method successfully applied to a series of aromatic *N*-heterocyclic compounds.⁷ The neutral and the protonated form of 1-methyl-4-(3,5-dimethoxyphenyl)-1,2,3-triazole (**B3**) were calculated at the B3LYP/6-311+G(2df,2p) level using the conductor-like polarizable model (CPCM) approach⁸ with the dielectric constant of water (Figure 7). Calculations were also performed on 1-methyl-4-phenyl-1,2,3-triazole (**B2**) for which a $\text{p}K_a$ value is available in the literature⁹ and for pyridine (**B1**) used as a reference compound. Whereas only one protonable nitrogen atom is present in **B1**, the situation is more complex for **B2** and **B3** as two protonated forms are possible. The 1,2,3-triazole ring contains effectively two basic sp^2 -hybridized nitrogen atoms. For both **B2** and **B3**, close inspection of the atomic charge in the calculated

structures revealed more negative values for N(3) when compared to N(2). Protonation is expected to be more favorable on the more electron-rich N(3) position. Calculations revealed effectively that the triazoliums protonated in the N(3) position are more stable for both **B2** and **B3** (Figure 7). This is fully consistent with experimental and theoretical data reported in the literature for related 1,2,3-triazole derivatives.⁸⁻⁹ The difference in free energy between the two triazolium isomers of **B2** and **B3** is 32.5 and 32.3 kJ/mol, respectively. At 298.15 K, the Boltzmann population of the less stable isomer is therefore negligible (*ca.* 0.00012%) and only the most stable protonated forms of **B2** and **B3** were considered for the $pK_a(BH^+)$ calculations.

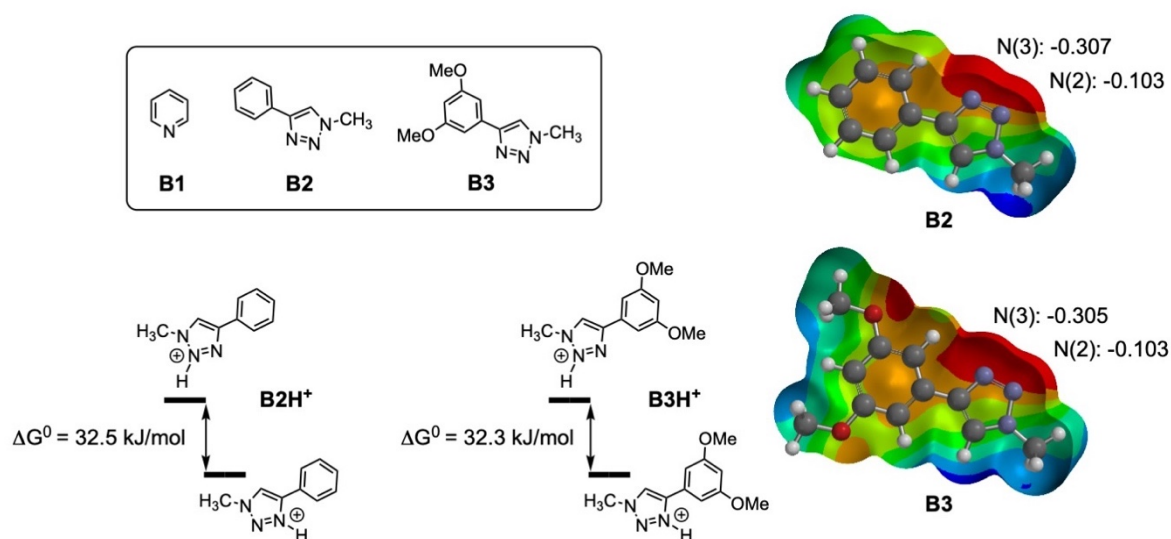


Figure 7. Relative Gibbs free energy at 298.15 K (ΔG^0) calculated at the B3LYP/6-311+G(2df,2p) level in water for the isomeric protonated forms of **B2** and **B3**. Electrostatic potential map of **B2-3** and natural atomic charge of their unsubstituted sp^2 -hybridized nitrogen atoms calculated at the B3LYP/6-31G* level in water.

For **B1-3**, the following equilibrium was considered to calculate the $pK_a(BH^+)$ values:



The pK_a of BH^+ was calculated from

$$\Delta G_{aq} = G(B)_{aq} + G(H^+)_{aq} - G(BH^+)_{aq} \quad (\text{Eq. 2})$$

$$pK_a(BH^+) = \Delta G_{aq} / 2.303RT \quad (\text{Eq. 3})$$

where R is the gas constant, T is the temperature, and ΔG_{aq} is the free energy of the reaction. For the calculations, the Gibbs free energy of the solvated proton ($G(\text{H}^+)_{\text{aq}} = -1130.85$ kJ/mol) reported by Coe and co-workers has been used.¹⁰ An error of at least 8 kJ/mol is usually assumed corresponding to *ca.* 1.5 pK_a units. In order to avoid the uncertainties related to the proton free energy, the $\text{pK}_a(\text{BH}^+)$ values were also computed by using isodesmic reactions and the experimental pK_a data of a reference system (pyridine, $\text{pK}_a(\text{pyridineH}^+)_{\text{exp}} = 5.23$):



$$\Delta G_{\text{exchange}} = G(\text{B})_{\text{aq}} + G(\text{pyridineH}^+)_{\text{aq}} - G(\text{BH}^+)_{\text{aq}} - G(\text{pyridine})_{\text{aq}} \quad (\text{Eq.5})$$

$$\text{pK}_a(\text{BH}^+) = (\Delta G_{\text{exchange}} / 2.303RT) + \text{pK}_a(\text{pyridine})_{\text{exp}} \quad (\text{Eq.6})$$

The values thus obtained are reported in Table 1. Triazole ligands **B2** and **B3** are significantly less basic when compared to pyridine. The direct calculations of the pK_a values with Eq. (3) gave a correct trend but comparison with the experimental values reveals large errors. In contrast, the difference between the calculated and the experimental $\text{pK}_a(\text{BH}^+)$ value of **B2** is by far less important by using the isodesmic reaction with pyridine as a reference system.

Table 1. Experimental and calculated $\text{pK}_a(\text{BH}^+)$ values of pyridine (**B1**), 1-methyl-4-phenyl-1,2,3-triazole (**B2**) and 1-methyl-4-(3,5-dimethoxyphenyl)-1,2,3-triazole (**B3**). The Gibbs free energy values calculated at the B3LYP/6-311+G(2df,2p) level in water have been used for the $\text{pK}_a(\text{BH}^+)$ calculations.

Compound	$\text{pK}_a(\text{BH}^+)$	$\text{pK}_a(\text{BH}^+)$	$\text{pK}_a(\text{BH}^+)$
	Calculated from Eq. 3	Calculated from Eq. 6	Experimental value
B1	4.32 ^[a]		5.23 ^[b]
B2	-0.86	0.01	0.05 ^[b]
B3	-0.96	0.01	

[a] From ref. 7. [b] From ref. 9

The basicity of **B2** and **B3** are similar thus showing that the *meta*-substituents of the phenyl group are only playing a minor role. Importantly, the $\text{pK}_a(\text{BH}^+)$ of **B3** is one to two orders of magnitude higher when compared to $\text{pK}_a(\text{BH}^+)$ values experimentally determined for aliphatic amides in aqueous H_2SO_4 .¹¹ As a result, the first protonation of molecular shuttles **24a-b** and axles **26a-b** containing one triazole moiety and two amide subunits should selectively occur on the triazole station. To fully confirm this selectivity, the protonation of axles **26a-b** and model

compound **28** lacking the amide functions was investigated by ^1H NMR and UV/vis spectroscopies. As shown in Figure 8, successive addition of trifluoroacetic acid (TFA) to a CDCl_3 solutions of **26b** and **28** resulted in similar chemical shift changes for the signals of the 4-(3,5-dimethoxyphenyl)-1,2,3-triazole moiety. In particular, continuous upfield shifts of the resonance of H(δ) and downfield shifts of the resonances of H(γ) and H(ϵ) were evidenced in both cases during the titrations. In contrast, the signals of the CH_2 groups neighboring the amide functions of **26b** were only marginally affected by the addition of TFA. All these observations suggest that protonation of **26b** occurs effectively at the triazole N(3) atom as in the case of **28**.

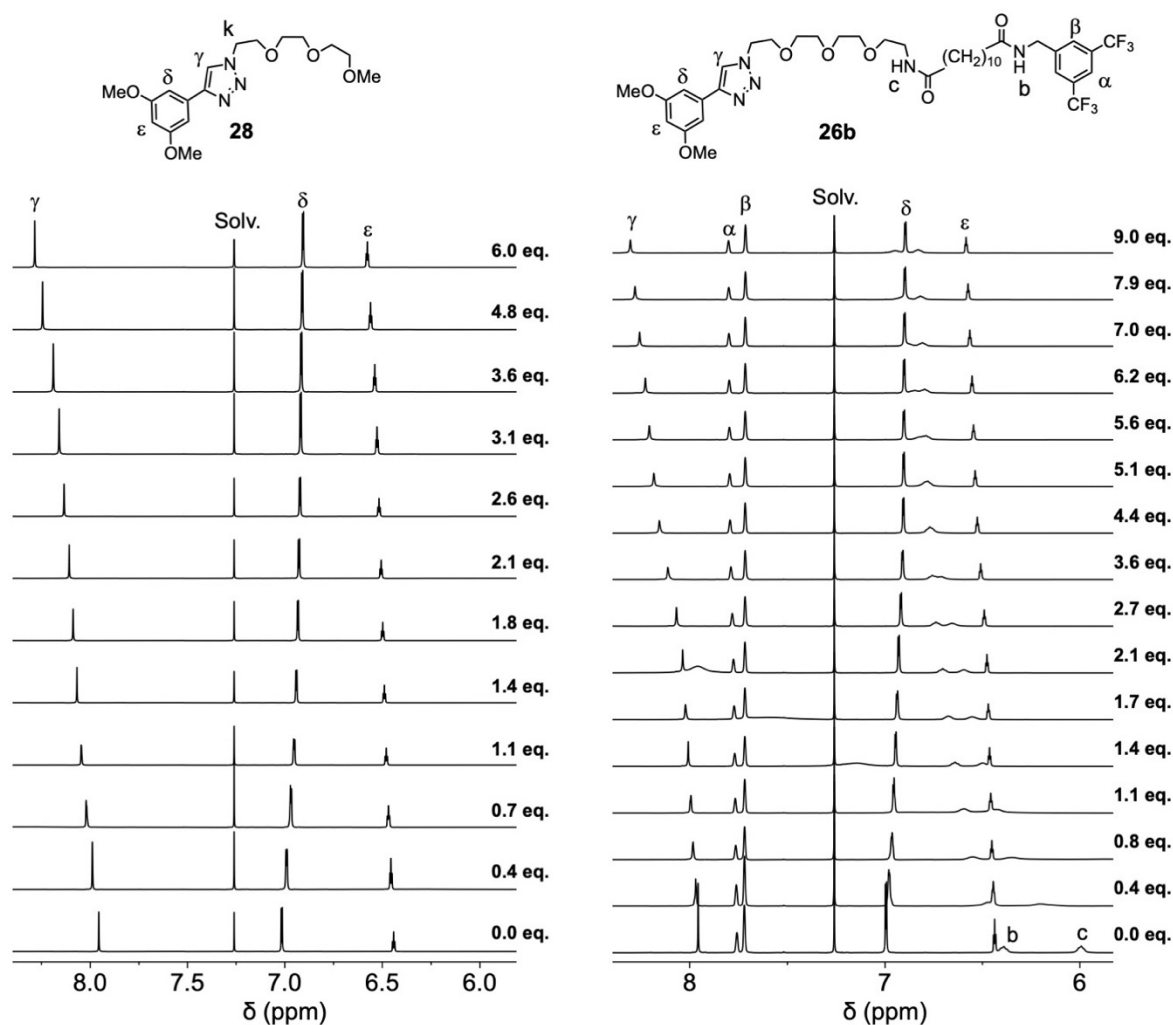


Figure 8. Spectral changes in the aromatic region of the ^1H NMR spectra (CDCl_3 , 400 MHz, 298 K) of **28** (28.4 mM) and **26b** (17.8 mM) upon successive addition of TFA.

Protonation of **28** and **26a-b** was further investigated by UV/vis spectrophotometric titrations. As shown in Figure 9, the UV/vis spectra of **28** and **26b** changed substantially upon addition of TFA. A clear isosbestic point is observed for **28** and **26b** thus revealing an equilibrium between two well-defined species in both cases. The similar behavior observed for **28** and **26b** upon addition of TFA further supports the selective protonation of **26b** at the triazole N(3) atom.

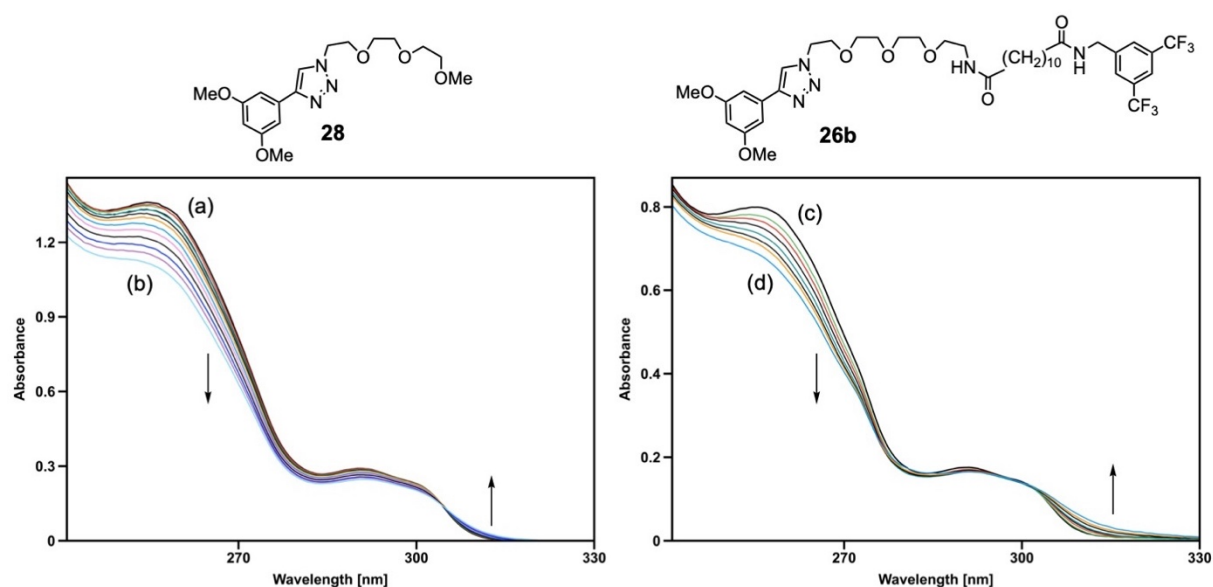


Figure 9. UV/vis spectrophotometric titrations of **28** and **26b** with TFA in CHCl_3 at 25°C ($d = 0.1$ cm); (a) $[\mathbf{28}] = 5.07 \times 10^{-4}$ M; (b) $[\text{TFA}]/[\mathbf{28}] = 65$; (c) $[\mathbf{26b}] = 6.10 \times 10^{-4}$ M; (d) $[\text{TFA}]/[\mathbf{26b}] = 227$.

Protonation of molecular shuttles 24a-b. ^1H NMR titrations of **24a** and **24b** were carried out with TFA in CDCl_3 at 298 K. The spectra recorded during the titration of **24b** are shown in Figure 10. Continuous changes in chemical shifts were evidenced for most of the signals upon the successive additions of TFA. At the same time, a substantial broadening was also observed, in particular for the signals arising from the triazole and the decyl stations. The apparent downfield shift of all signals of the decyl chain upon protonation of the triazole moiety suggest that the pillar[5]arene moiety has a lower probability of presence over the decyl station upon protonation of **24b**. This view is also supported by the evolution of the signal of the benzylic diastereotopic protons during the titration. In the neutral state a doublet of AB is observed owing to the proximity of the chiral pillar[5]arene subunit. At the end of the titration, the transfer of the chiral information is vanished and a doublet is seen for H(a/a'). Obviously, the probability of presence of the macrocycle near H(a/a') is significantly reduced upon protonation of the triazole station.

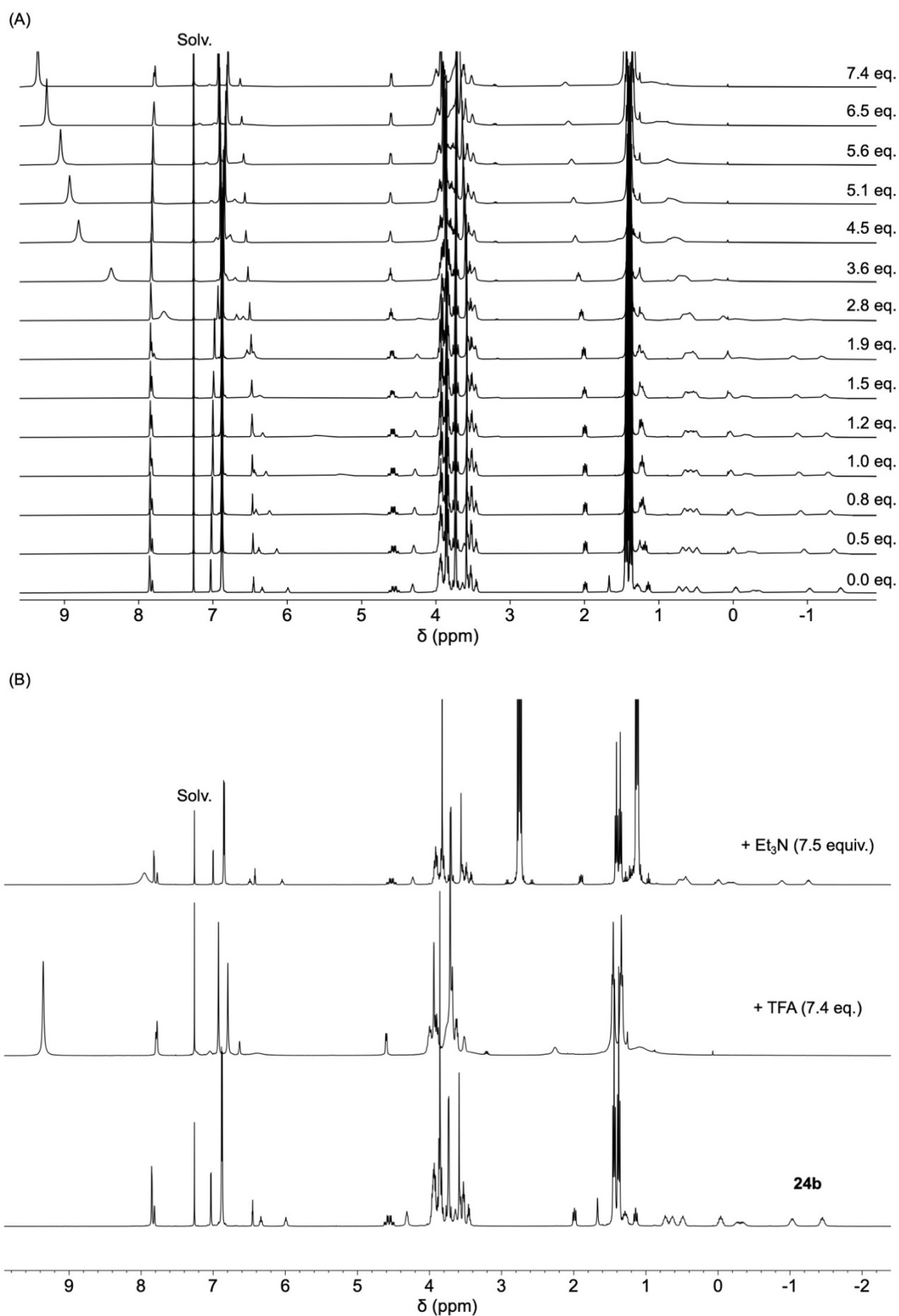
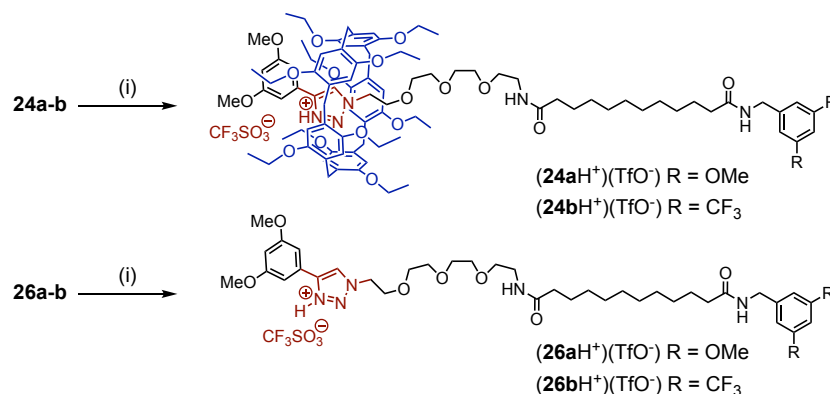


Figure 10. (A) Spectral changes in the ^1H NMR spectra (CDCl_3 , 400 MHz, 298 K) of **24b** (28.4 mM) upon successive addition of TFA. (B) ^1H NMR spectra (CDCl_3 , 400 MHz, 298 K) of **24b**, **24b** after addition of TFA (7.4 equiv.) and neutralization by addition of Et_3N showing the reversibility of the conformational changes.

All these observations are consistent with a conformational change of **24b** upon protonation. Importantly, addition of an excess of triethylamine (Et_3N) at the end of the titration restored the initial state of **24b** thus showing the reversibility of the process (Figure 10B). The minor differences observed for the signals of the decyl chain are explained by the change in polarity. It has been effectively shown that the position of the pillar[5]arene moiety of related rotaxanes with a diamide-stoppered decyl chain is highly sensitive to the polarity of the medium.⁵ Owing to the broadening of the signals of **24a-b** during the titrations with TFA, it was difficult to derive clear information about their conformations in the protonated state. This prompted us to prepare the triflate salts of **24a-b** by treatment with a stoichiometric amount of TfOH (Scheme 4). For comparison purposes, (**26aH⁺**)(TfO⁻) and (**26bH⁺**)(TfO⁻) were also prepared from **26a** and **26b**, respectively. The use of a strong acid like TfOH allows the total protonation of the triazole station of **24a-b** and **26a-b**. This is essential for a non-ambiguous conformational analysis of (**24aH⁺**)(TfO⁻) and (**24bH⁺**)(TfO⁻).



Scheme 4. Preparation of (**24a-bH⁺**)(TfO⁻) and (**26a-bH⁺**)(TfO⁻). *Reagents and conditions:* (i) TfOH, CHCl_3 (quantitative).

The ^1H NMR spectra of (**24aH⁺**)(TfO⁻) and (**26aH⁺**)(TfO⁻) recorded in CDCl_3 at 298 K are depicted in Figure 11. While all signals of protonated axle (**26aH⁺**)(TfO⁻) are well resolved under these conditions, the spectrum recorded for rotaxane (**24aH⁺**)(TfO⁻) is characterized by the broadening of the signals arising from the CH_2 moieties of the decyl station [H(1-10)]. Similarly, resonances of H(i-k) and H(γ, δ, ϵ) are particularly broad and could not be clearly detected in the ^1H NMR spectrum of (**24aH⁺**)(TfO⁻) recorded at room temperature. These observations suggest that the pillar[5]arene is exchanging his position between the decyl and the triazolium stations in (**24aH⁺**)(TfO⁻) at a rate close to the NMR timescale at 298 K.

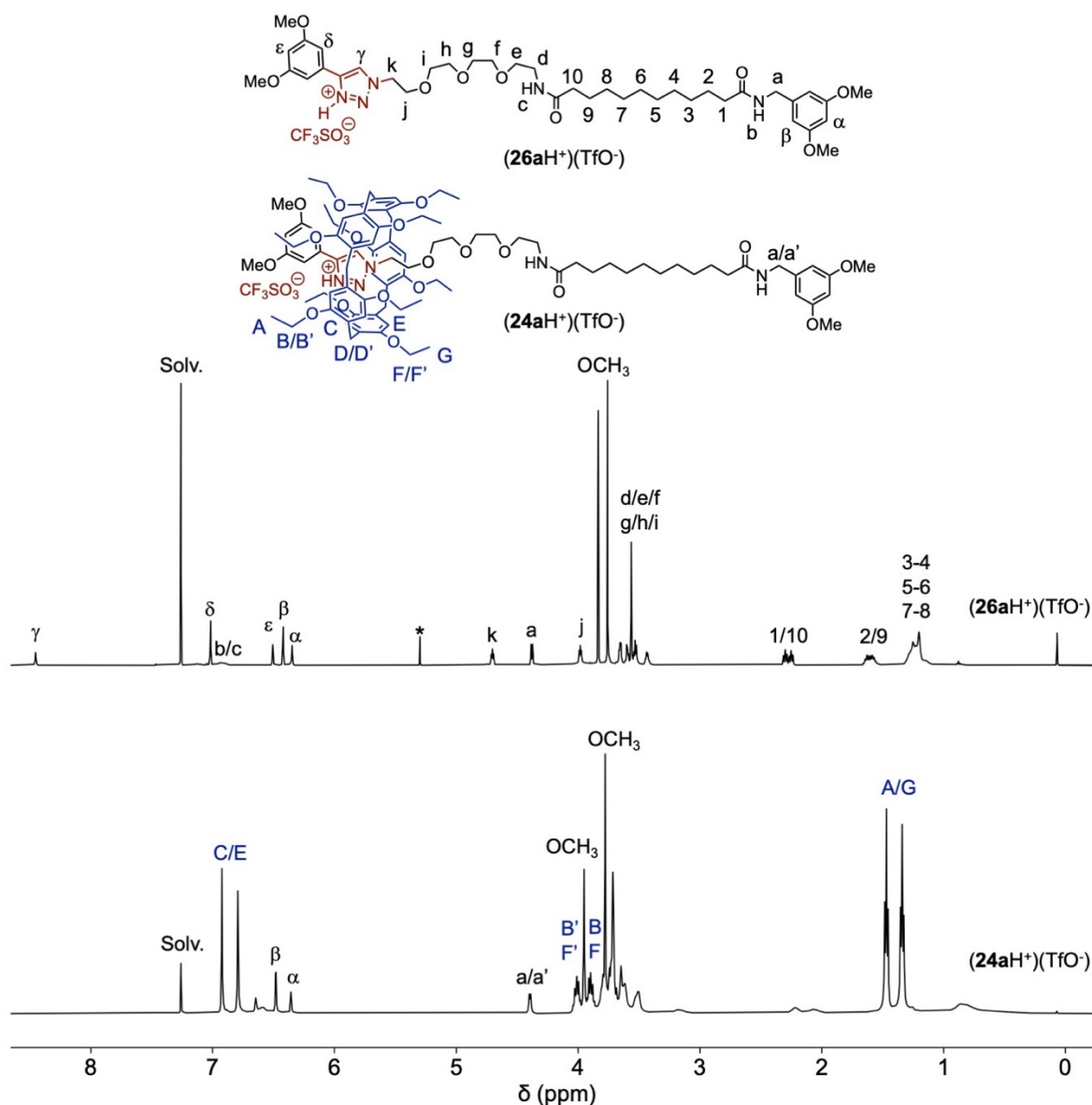


Figure 11. ^1H NMR spectra (CDCl_3 , 500 MHz, 298 K) of $(\mathbf{24aH}^+)(\text{TfO}^-)$ and $(\mathbf{26aH}^+)(\text{TfO}^-)$; *: CH_2Cl_2 impurity.

As shown in Figure 12, a similar behavior was also evidenced for $(\mathbf{24bH}^+)(\text{TfO}^-)$. Clearly, the triazolium station plays a major role in the conformational scenario of protonated molecular shuttles $(\mathbf{24aH}^+)(\text{TfO}^-)$ and $(\mathbf{24bH}^+)(\text{TfO}^-)$. To fully understand their behavior, variable temperature NMR studies were carried out. A reversible narrowing of most of the broad signals was observed by increasing the temperature and the ^1H NMR spectra of $(\mathbf{24aH}^+)(\text{TfO}^-)$ and $(\mathbf{24bH}^+)(\text{TfO}^-)$ recorded in $\text{CDCl}_2\text{CDCl}_2$ at 373 K are well resolved. Under these conditions, dynamic gliding motions allowing the macrocycle to shuttle back and forth between the two stations are faster than the NMR timescale. While confirming the dynamic exchange, the ^1H

NMR spectra recorded at high temperature are not very informative concerning the population of the different possible conformers.

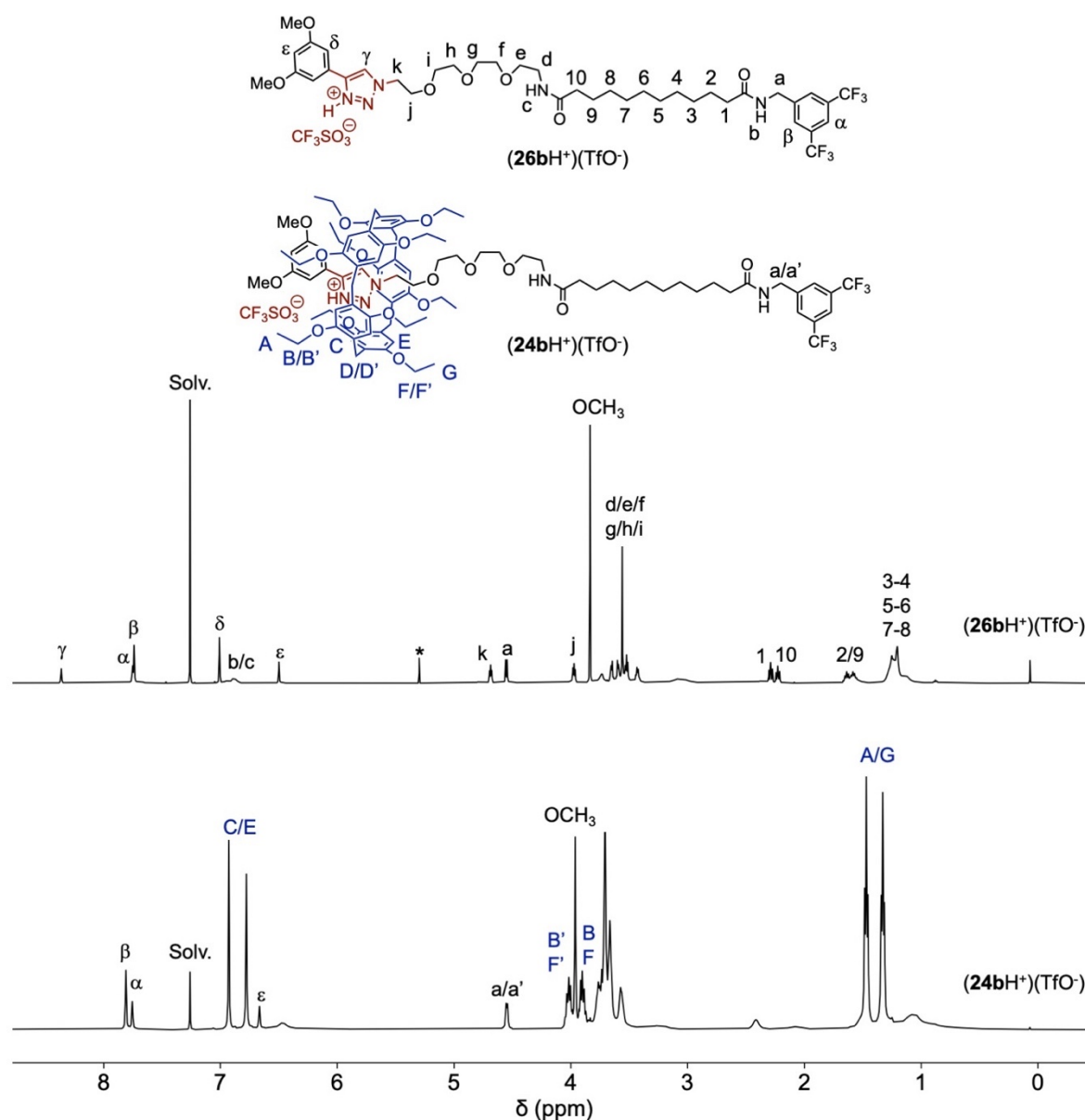


Figure 12. ^1H NMR spectra (CDCl_3 , 500 MHz, 298 K) of $(\mathbf{24bH}^+)(\text{TfO}^-)$ and $(\mathbf{26bH}^+)(\text{TfO}^-)$; *: CH_2Cl_2 impurity.

^1H NMR spectra of $(\mathbf{24aH}^+)(\text{TfO}^-)$ and $(\mathbf{24bH}^+)(\text{TfO}^-)$ were also recorded in CD_2Cl_2 at low temperature. As shown in Figure 13, a clear coalescence is observed at 243 K and the two conformers of $(\mathbf{24aH}^+)(\text{TfO}^-)$ are clearly distinguished at lower temperatures. In other words, the dynamic exchange between conformers A and B is slower than the RMN timescale under

these conditions. The ΔG^\ddagger value derived from the coalescence of the signals arising from the aromatic protons of the pillar[5]arene moiety is 49 ± 1 kJ/mol. Based on the integration, the relative proportion of the two conformers is 67:33 at 223 K; the major conformer being the one in which the triazolium station is occupied (conformer B). A Boltzmann population analysis at 223 K revealed a difference of energy of 1 kJ/mol between the two conformations.

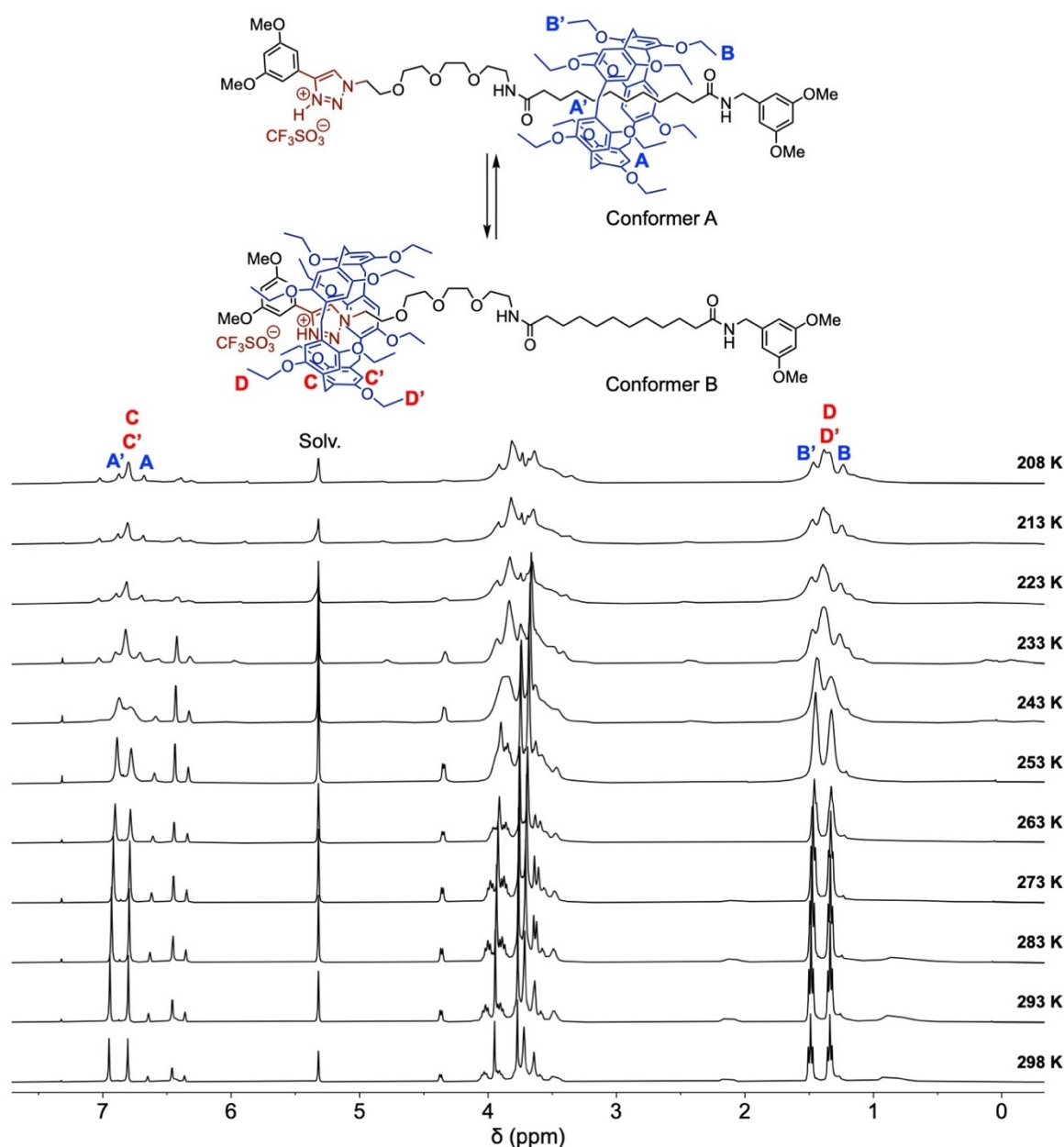


Figure 13. ^1H NMR spectra (CD_2Cl_2 , 400 MHz, 298 K) of $(\mathbf{24aH}^+)(\text{TfO}^-)$ recorded at different temperatures.

As shown in Figure 14, a similar behavior was also evidenced for $(\mathbf{24bH}^+)(\text{TfO}^-)$. However, conformer A is favored in this particular case. At 223 K, a 62:38 ratio was deduced from the

integration corresponding to a difference of energy of 0.9 kJ/mol. Based on the coalescence of the signals arising from the aromatic protons of the pillar[5]arene moiety, a ΔG^\ddagger value of 50 ± 1 kJ/mol was obtained for the dynamic exchange between conformers A and B.

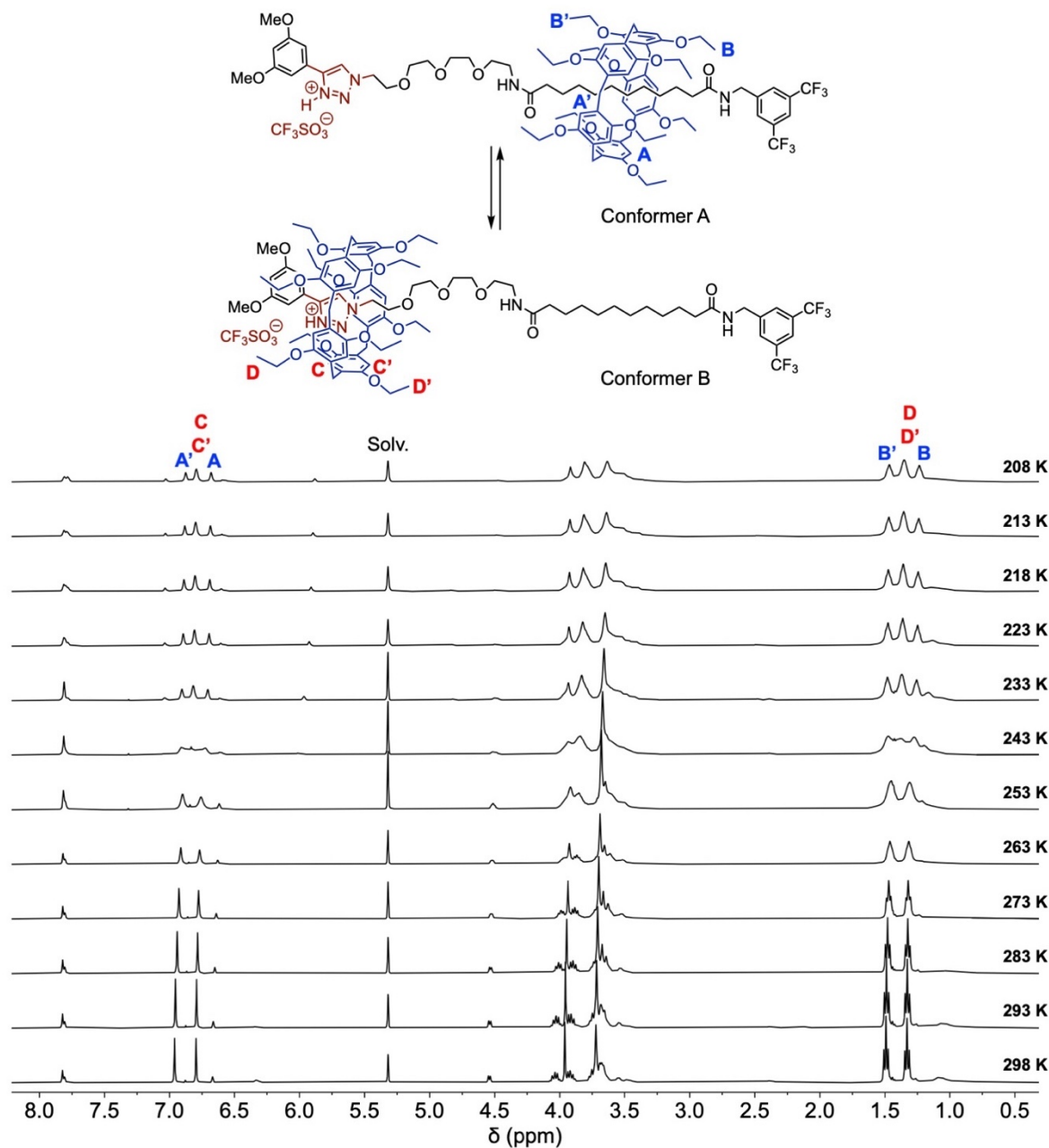


Figure 14. ^1H NMR spectra (CD_2Cl_2 , 400 MHz, 298 K) of $(24\text{bH}^+)(\text{TfO}^-)$ recorded at different temperatures.

Finally, deprotonation of $(24\text{a-bH}^+)(\text{TfO}^-)$ and $(26\text{a-bH}^+)(\text{TfO}^-)$ was investigated by UV/vis spectrophotometric titrations with Et_3N as a base. As a typical example, the titration of $(24\text{bH}^+)(\text{TfO}^-)$ carried out in CHCl_3 is shown in Figure 15. Continuous changes were observed in the UV/vis spectra upon addition of Et_3N . A clear isosbestic point is also observed at 264 nm

thus revealing an equilibrium between two well-defined species, namely $(\mathbf{24bH}^+)(\text{TfO}^-)$ and $\mathbf{24b}$. The absorption spectrum obtained at the end of the titration is effectively the same as the one recorded for compound $\mathbf{24}$ in the same solvent.

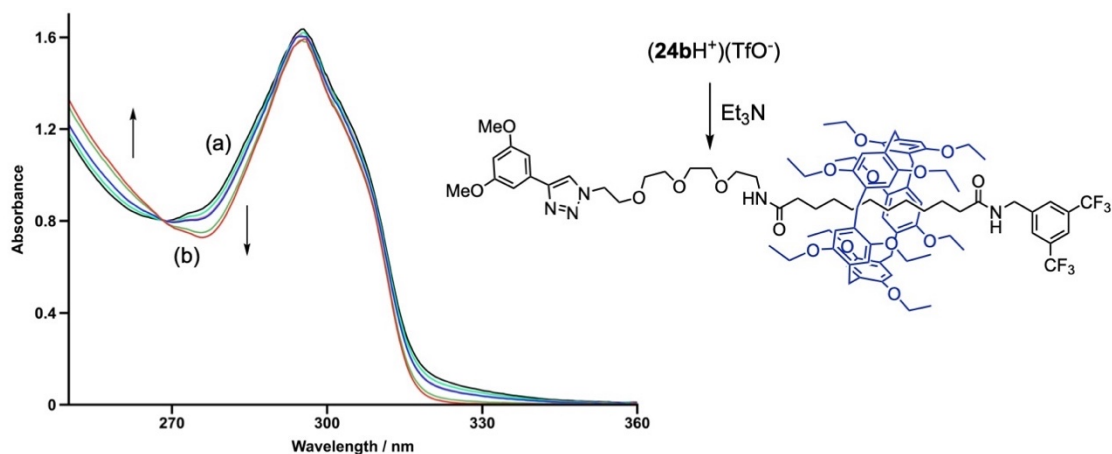


Figure 15. UV/vis spectrophotometric titrations of $(\mathbf{24bH}^+)(\text{TfO}^-)$ with Et_3N in CHCl_3 at 25°C ($d = 0.1$ cm); (a) $[(\mathbf{24bH}^+)(\text{TfO}^-)] = 6.05 \times 10^{-4}$ M; (b) $[\text{Et}_3\text{N}]/[(\mathbf{24bH}^+)(\text{TfO}^-)] = 1.5$).

The conformational equilibria of molecular shuttles $\mathbf{24a-b}$ in their neutral and protonated state were fully elucidated by variable temperature NMR studies. A summary of all experimental findings is depicted in Figure 16. In their neutral state, the decyl station of $\mathbf{24a-b}$ is largely favored over the triazole one. Upon protonation of $\mathbf{24a-b}$, the affinity of the resulting triazolium station for the pillar[5]arene is significantly increased. As a result, protonation triggers significant conformational changes. Actually, the pillar[5]arene is exchanging its position between the two available stations at temperatures higher than 243 K and the relative population of the two possible conformers of $(\mathbf{24a-bH}^+)$ is significantly influenced by the *meta*-substituents of the terminal benzylic amide group of the decyl station. This is fully consistent with the influence of the amine stoppers on the K_A values obtained from the binding studies of pillar[5]arene $\mathbf{3}$ and model compounds $\mathbf{11a-b}$. The formation of the inclusion complex is effectively more favorable for guest $\mathbf{11b}$ with the electron-deficient bis(trifluoromethyl)benzyl substituent. The difference in Gibbs free energy ($\Delta\Delta G^0$) between $\mathbf{11a}$ and $\mathbf{11b}$ is 2.5 kJ/mol under the experimental conditions used for the binding studies (CDCl_3 , 298 K). This quite small energy difference is however sufficient to significantly influence the Maxwell-Boltzmann distribution of the different possible conformers of $(\mathbf{24a-bH}^+)$ and is consistent with a higher population of the decyl station in the case of $(\mathbf{24bH}^+)$ when compared to $(\mathbf{24aH}^+)$. The effect of

such a subtle structural difference could be evidenced because the triazolium station has an affinity similar to that of the different decyl stations. This is fully consistent with the K_A values derived for the binding of pillar[5]arene **3** with model compounds **11a-b** and (**28H**⁺). Overall, the gliding motions of the pillar[5]arene occur over the full length of its molecular axle in protonated (**24a-bH**⁺) while such molecular motions are largely limited over the decyl stations in unprotonated **24a-b**. The perfectly reversible protonation/deprotonation of these molecular shuttles allows therefore to control the amplitude of the oscillations of the macrocyclic component along its axle moiety.

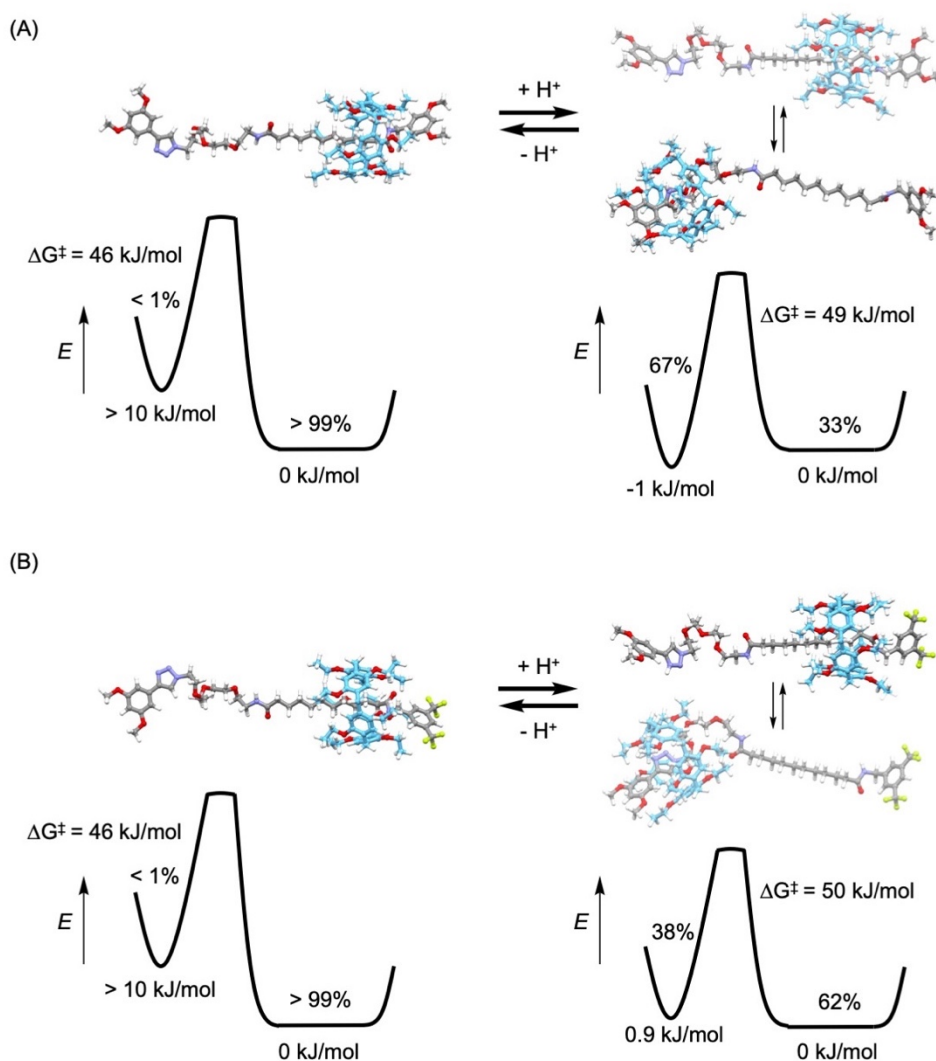


Figure 16. Potential energy diagrams of **24a** (A) and **24b** (B) in both the neutral and the protonated states deduced from the variable temperature ¹H NMR studies; the energy levels and the proportion of the conformers are given at 223 K; the free energy of activation (ΔG^\ddagger) values for the dynamic exchange are those obtained at the coalescence temperature (223 K in the neutral state and 243 K in the protonated state).

DFT calculations. In order to fully understand the interactions of the pillar[5]arene moiety with its different stations in **24a-b**, density functional theory (DFT) calculations were carried out with appropriate fragments. Specifically, the structure of the host-guest complexes resulting from the association of ethoxypillar[5]arene (**P**) with octane (**Oct**), 1-methyl-4-(3,5-dimethoxyphenyl)-1,2,3-triazole (**B3**) and triazolium (**B3H⁺**) were optimized at the ω B97X-D/6-31G* level. The ω B97X-D functional was selected as it includes empirical corrections for long-range dispersive interactions.¹² Calculations were done with the conductor-like polarizable continuum model (CPCM) using the dielectric constant of THF. The CPCM does not account for explicit solvent-solute interactions such as H-bonds or hydrophobic effects. However, such simple continuum calculations provide typically good qualitative trends for the investigated systems.⁸ The optimized structures of **P**, **Oct**, **B3** and (**B3H⁺**)(TfO⁻) are shown in Figure 17 together with their electrostatic potential maps. The cavity of pillar[5]arene is clearly electron-rich and interactions with an electron-deficient guest such as (**B3H⁺**) appears electronically favorable to form a charge-transfer complex. In contrast, π - π interactions with guest **B3** are likely less favorable owing to the presence of its electron-rich nitrogen atoms. On the other hand, only dispersive interactions are expected between the pillar[5]arene host and the octane guest.

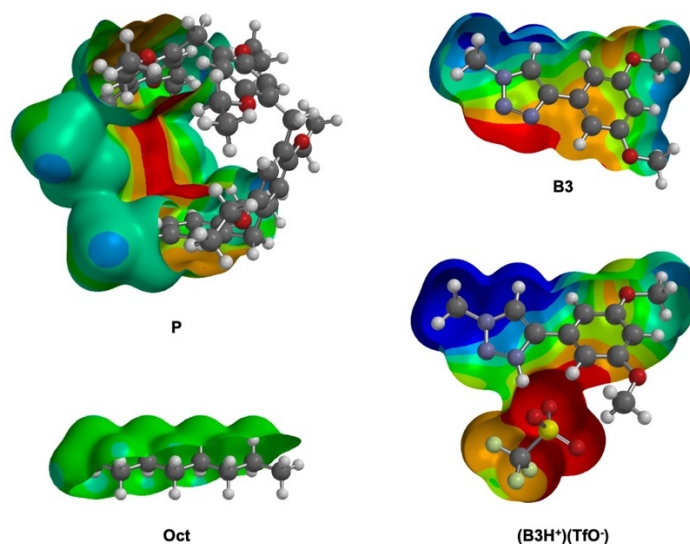


Figure 17. Electrostatic potential map of **P**, **Oct**, **B3** and (**B3H⁺**)(TfO⁻) calculated at the ω B97X-D/6-31G* level using the CPCM with the dielectric constant of THF.

The frontier molecular orbitals (FMOs) of **P**, (**P.Oct**), (**P.B3**), (**P.B3H⁺**), **Oct**, **B3** and **B3H⁺** are depicted in Figure 18.

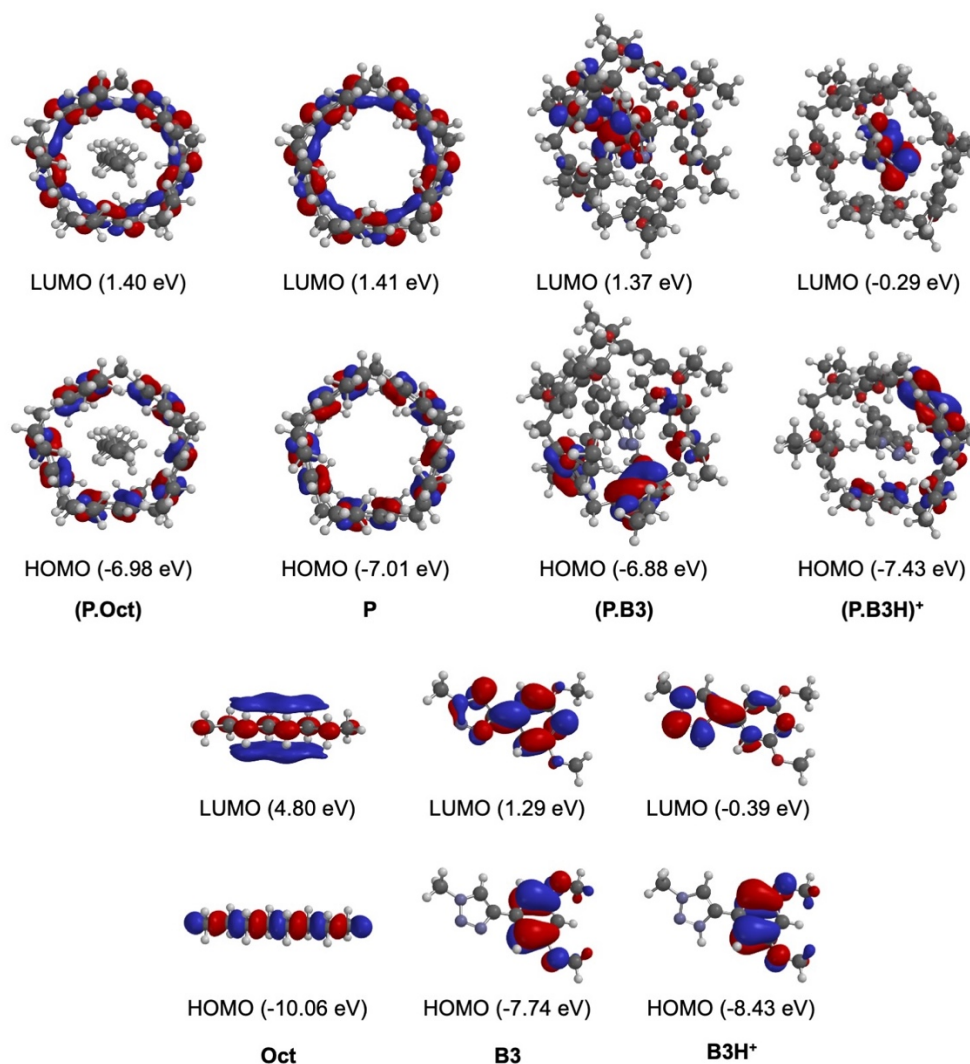


Figure 18. FMOs of (**P.Oct**), **P**, (**P.Oct**), (**P.B3**), (**P.B3H⁺**), **Oct**, **B3** and **B3H⁺** calculated at the ω B97X-D/6-31G* level using the CPCM model with the dielectric constant of THF.

Comparison of the FMOs of **P** and (**P.Oct**) revealed only a marginal effect of the complexation of **Oct** host by the pillar[5]arene. This is consistent with the absence of strong electronic interactions between **P** and **Oct** in the inclusion complex and the binding is totally dominated by dispersive interactions. In the case of (**P.B3**), the lowest unoccupied molecular orbital (LUMO) of (**P.B3**) is distributed over the 3,5-dimethoxyphenyl subunit of **B3** and the aromatic subunits of **P**. While the LUMO level centered on **B3** is destabilized, the part centered on the pillar[5]arene is stabilized. The highest occupied molecular orbital (HOMO) totally localized on the pillar[5]arene moiety is substantially destabilized ($\Delta E = +0.13$ eV). Overall, these observations revealed rather unfavorable electronic interactions between the host and the guest

in (**P.B3**), therefore the binding of **B3** is mainly governed by dispersive interactions as observed in the case of **Oct**. The situation is totally different for (**P.B3H⁺**). In this case, favorable electronic interactions are effectively evidenced by a significative stabilization of the HOMO of **P** ($\Delta E = -0.42$ eV) and a destabilization of the LUMO of **B3H⁺** ($\Delta E = +0.10$ eV) in the host-guest complex. Moreover, with its HOMO fully localized over the pillar[5]arene moiety and its LUMO totally centered on the **B3H⁺** host, (**P.B3H⁺**) is a charge transfer complex.

The factors controlling the affinity of guest **P** with the different hosts were further analyzed by using the interaction energy decomposition method (Figure 19).^{7,13} The electronic energy of the host-guest complexes was decomposed into two terms: (i) the distortion energy which corresponds to the energy required for the deformation of the individual components [guest **P** and host **Oct**, **B3** or (**B3H⁺**)] to form the inclusion complex; and (ii) the interaction energy which corresponds to the difference between the electronic energies of the two distorted components and the supramolecular complex. The overall energy gain for the formation of the host-guest complex was then evaluated by adding the positive distortion energy to the negative interaction energy. The lowest interaction energy was obtained for inclusion complex (**P.Oct**) in which only van der Waals interactions are possible. For neutral guest **B3**, the interaction energy was found 17 kJ/mol stronger when compared to (**P.Oct**) thus showing more favorable dispersive interactions between the host and the guest in (**P.B3**) despite their poor electronic complementarity suggested by the FMOs analysis. However, the overall energy gain is substantially penalized by an important distortion energy (46.4 kJ/mol). As a result, steric factors explain the more favorable complexation of the octane guest. In the case of molecular shuttles **24a-b**, the preferred conformation in which the pillar[5]arene moiety is located over the alkyl station results therefore mainly from the limited distortion of the macrocyclic component and electronic factors play only a very minor role. In the case of guest (**B3H⁺**), the formation of the host-guest complex with **P** requires also an important distortion of the macrocyclic scaffold. However, the significantly increased interaction energy in (**P.B3H⁺**) provides a higher energy gain (-204.6 kJ/mol). This value certainly overestimates the real energy gain as intimate ion pairs are most likely interacting with the pillar[5]arene guest in nonpolar solvents thus generating an increased distortion of the guest moiety. Overall, the position of the pillar[5]arene subunit on its axle moiety in **24a-b** and (**24a-bH⁺**) results from an interplay between electronic interactions and steric effects. In the neutral state, the conformational preferences are totally dominated by dispersive interactions and steric effects largely prevent occupation of the triazole station in **24a-b**. In contrast, favorable electronic interactions between the protonated triazole moiety and the pillar[5]arene in (**24a-bH⁺**) are able

to compensate, at least in part, the substantial energy required for the distortion of the macrocyclic scaffold when the triazolium station is populated. As a result, the triazolium station becomes competitive with the decyl station in (**24a-bH**⁺).

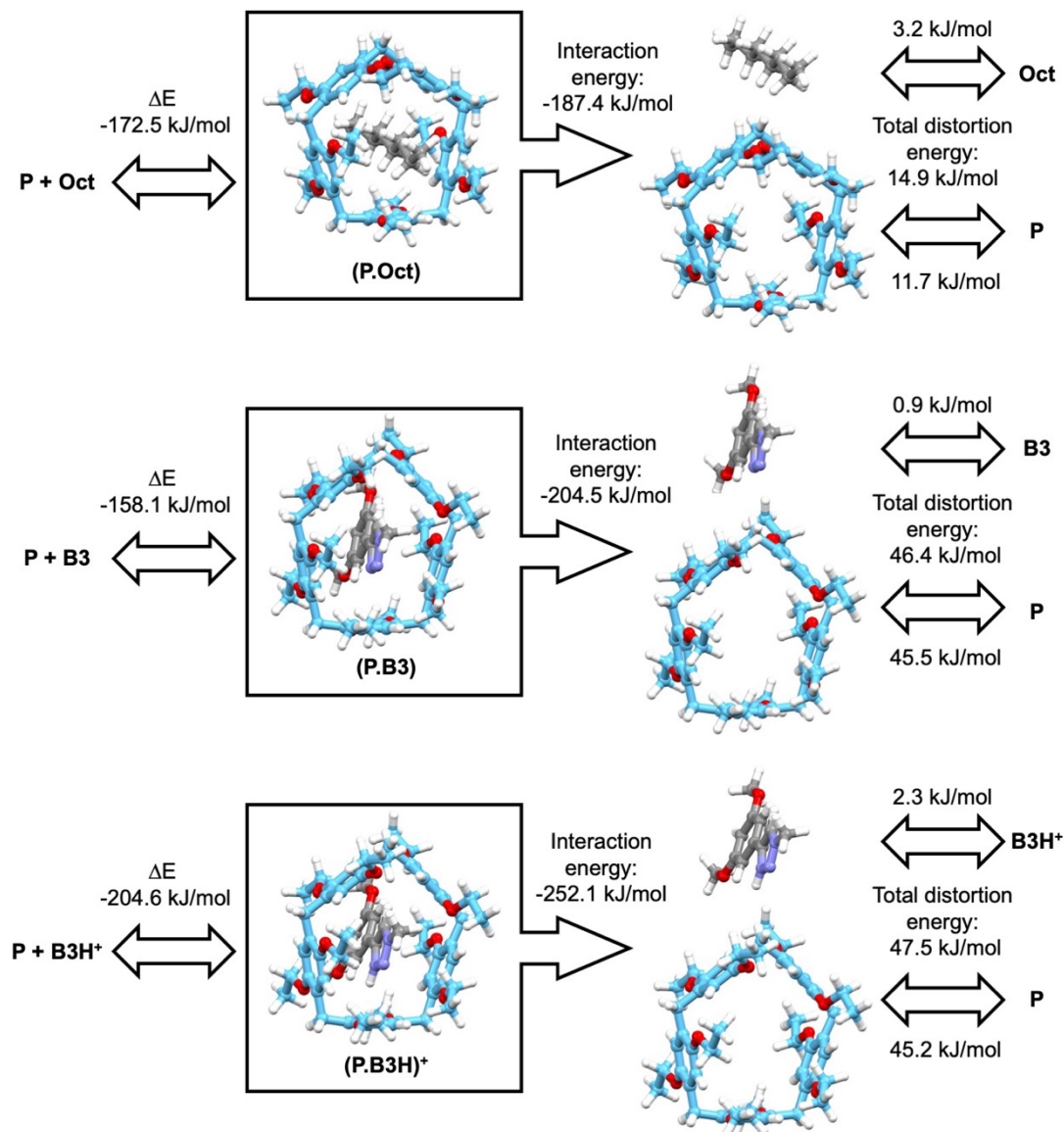


Figure 19. Structures of (**P.Oct**), (**P.B3**) and (**P.B3H**)⁺ optimized at the ω B97X-D/6-31G* level using the CPCM with the dielectric constant of THF and their distortion/interaction analysis (H: white, O: red, N: blue, C: grey for the guests and pale blue for host **P**).

Finally, the UV/vis spectra of **P**, **B3**, **B3H**⁺, (**P.Oct**), (**P.B3**) and (**P.B3H**)⁺ were also calculated in the gas-phase at the TD- ω B97X-D/6-31G* level of theory. The calculated UV/vis allowed transitions are summarized in Table 2.

Table 2. UV/vis allowed transitions of **B3H⁺** and (**P.B3H⁺**) calculated in the gas-phase at the TD- ω B97X-D/6-31G* level of theory.

Wavelength (nm)	Strength	MO component
----- Guest P -----		
222.58	0.0754	HOMO-5 \rightarrow LUMO (17%) HOMO \rightarrow LUMO (12%)
249.36	0.0000	HOMO-4 \rightarrow LUMO (19%)
249.37	0.0000	HOMO-3 \rightarrow LUMO (19%)
253.73	0.2598	HOMO \rightarrow LUMO+2 (20%) HOMO-1 \rightarrow LUMO (16%) HOMO-2 \rightarrow LUMO (15%)
253.92	0.2633	HOMO \rightarrow LUMO+1 (21%) HOMO-2 \rightarrow LUMO (16%) HOMO-1 \rightarrow LUMO (16%)
263.56	0.0275	HOMO \rightarrow LUMO (40%) HOMO-1 \rightarrow LUMO+1 (15%) HOMO-2 \rightarrow LUMO+2 (15%)
----- Host-guest complex (P.Oct) -----		
223.28	0.0639	HOMO-5 \rightarrow LUMO (17%) HOMO \rightarrow LUMO (12%) HOMO-3 \rightarrow LUMO+3 (11%)
249.80	0.0018	HOMO-4 \rightarrow LUMO (26%) HOMO-3 \rightarrow LUMO+4 (12%)
250.71	0.0007	HOMO-3 \rightarrow LUMO (23%) HOMO \rightarrow LUMO+3 (16%)
255.29	0.2331	HOMO-1 \rightarrow LUMO (32%) HOMO \rightarrow LUMO+2 (22%)
255.45	0.2038	HOMO-2 \rightarrow LUMO (32%) HOMO \rightarrow LUMO+1 (23%)
264.81	0.0237	HOMO \rightarrow LUMO (41%) HOMO-2 \rightarrow LUMO+1 (20%) HOMO-1 \rightarrow LUMO+2 (18%)
----- Host B3 -----		
191.91	0.0022	HOMO-3 \rightarrow LUMO (88%)
199.36	0.5864	HOMO-1 \rightarrow LUMO+1 (34%) HOMO \rightarrow LUMO+2 (29%) HOMO \rightarrow LUMO+1 (19%)
202.56	0.2093	HOMO-1 \rightarrow LUMO+1 (46%) HOMO \rightarrow LUMO+1 (20%) HOMO \rightarrow LUMO+2 (16%)

205.47	0.0082	HOMO-3 → LUMO+1 (82%)
225.67	0.3120	HOMO-1 → LUMO (88%)
253.41	0.0494	HOMO → LUMO (77%)
----- Host-guest complex (P.B3) -----		
244.83	0.0267	HOMO-3 → LUMO+2 (20%)
247.00	0.0861	HOMO-3 → LUMO+1 (17%) HOMO-3 → LUMO (16%)
249.07	0.0342	HOMO-7 → LUMO (18%) HOMO-6 → LUMO (15%) HOMO-7 → LUMO+1 (11%) HOMO-6 → LUMO+1 (10%)
253.80	0.0681	HOMO-1 → LUMO+5 (13%)
256.15	0.1424	HOMO-2 → LUMO +4 (11%)
262.98	0.0508	HOMO → LUMO+4 (21%) HOMO → LUMO+5 (13%)
----- Host B3H⁺ -----		
199.30	0.0303	HOMO → LUMO+3 (48%) HOMO-1 → LUMO+2 (42%)
203.06	0.6611	HOMO → LUMO+2 (85%)
223.00	0.0199	HOMO-1 → LUMO+1 (69%)
251.57	0.2243	HOMO-1 → LUMO (76%)
262.79	0.0219	HOMO → LUMO+1 (69%) HOMO → LUMO (24%)
309.03	0.0323	HOMO → LUMO (75%) HOMO → LUMO+1 (22%)
----- Host-guest complex (P.B3H⁺) -----		
270.98	0.0043	HOMO → LUMO+1 (55%)
272.24	0.0236	HOMO-3 → LUMO (40%) HOMO → LUMO+1 (18%) HOMO-1 → LUMO+1 (10%)
277.56	0.0171	HOMO-3 → LUMO (38%) HOMO-6 → LUMO (21%) HOMO-7 → LUMO (14%)
305.54	0.0058	HOMO-2 → LUMO (91%)
326.26	0.0059	HOMO-1 → LUMO (84%)
334.67	0.0013	HOMO → LUMO (85%)

The calculated UV/vis features of **P** and (**P.Oct**) are nearly identical thus showing the weak effect of the **Oct** host on the π - π^* transition of the pillar[5]arene in the host-guest complex.

The calculated wavelength of the lowest allowed transitions values are 263.56 and 264.81 nm for **P** and (**P.Oct**), respectively. In the case of (**P.B3**), the calculated transitions are reminiscent from its constitutive moieties as expected based on the absence of significant electronic interactions between **P** and **B3** in the supramolecular ensemble. All these theoretical results are consistent with the experimental UV/vis spectrum recorded for compound **24a-b** showing an end-absorption identical to the one observed for pillar[5]arene **3**. As typical examples, the absorption spectra of **3**, **24b** and **26b** are shown in Figure 20. Some differences are observed between the spectrum of **24b** and the sum of the spectra of its constitutive components (**3** and **26b**). This indicates the occurrence of electronic interactions between the axle and the macrocycle in rotaxane **24b** which are likely occurring between the electron-deficient benzylic stopper and the electron-rich pillar[5]arene.

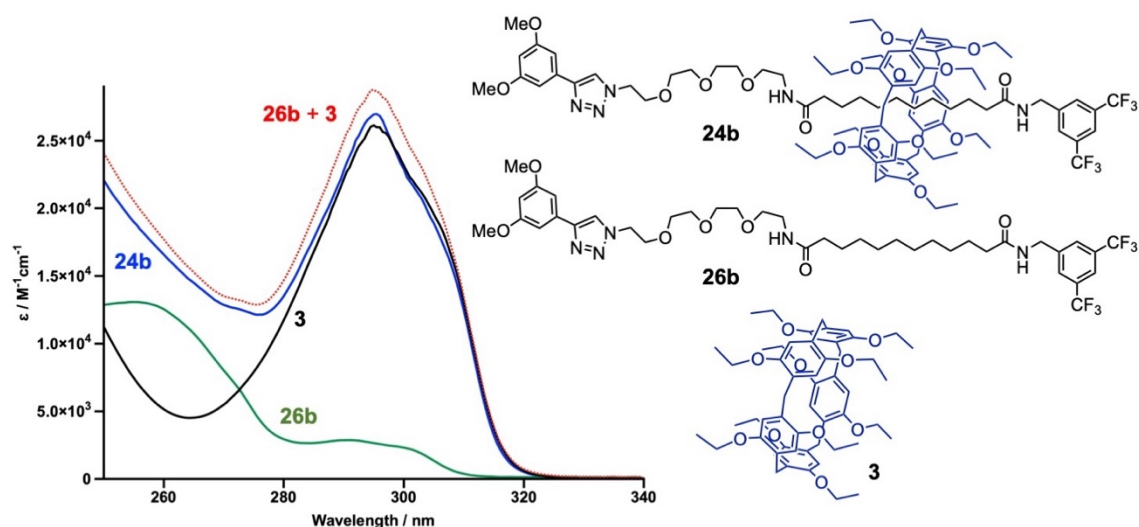


Figure 20. UV/vis spectra of **3**, **24b** and **26b** recorded in CHCl_3 at 25°C . The calculated spectrum corresponding to the sum of the spectra of **3** and **26b** is represented in red.

Upon protonation of **B3**, significant changes are observed. The calculations revealed that the two lowest allowed UV/vis transitions of **B3H⁺** are associated with a substantial delocalization of the electronic density from the electron-rich 3,5-dimethoxyphenyl moiety to the electron-deficient triazolium ring. This charge transfer is fully consistent with the red-shifted end-absorption observed upon protonation of **26a-b** and **28**. The value calculated for the first allowed π - π^* transition of **B3** is effectively higher in energy (253.41 nm; HOMO \rightarrow LUMO). The low strength of the charge transfer band is also in agreement with the weak intensity of the absorption of **26a-b** and **28** in the 310-330 nm region (Figure 9). The calculated UV/vis spectra of (**P.B3H⁺**) revealed intercomponent charge transfer bands. The three lowest allowed UV/vis

transitions correspond effectively to transitions from HOMO levels totally centered on the pillar[5]arene moiety to the LUMO fully localized on the triazolium guest. The weak absorption that appeared in the 310-360 nm region upon protonation of **24a-b** are actually associated to the apparition of an intercomponent charge transfer band when the pillar[5]arene is located over its triazolium station or to an intramolecular charge transfer band centered on the triazolium unit when the macrocycle is located over its decyl station. As typical examples, the absorption spectra recorded for **3**, (**24bH⁺**)(TfO⁻) and (**26bH⁺**)(TfO⁻) are depicted in Figure 21. When compared to (**26bH⁺**)(TfO⁻), the slightly increased absorption observed for (**24bH⁺**)(TfO⁻) in the 310-360 nm region suggests a contribution of the intercomponent charge transfer band thus supporting the significative population of conformers in which the pillar[5]arene is located over the triazolium station as deduced from the NMR studies. The differences observed between the spectrum of (**24bH⁺**)(TfO⁻) and the sum of the spectra of its constitutive components are also consistent with the occurrence of intercomponent electronic interactions.

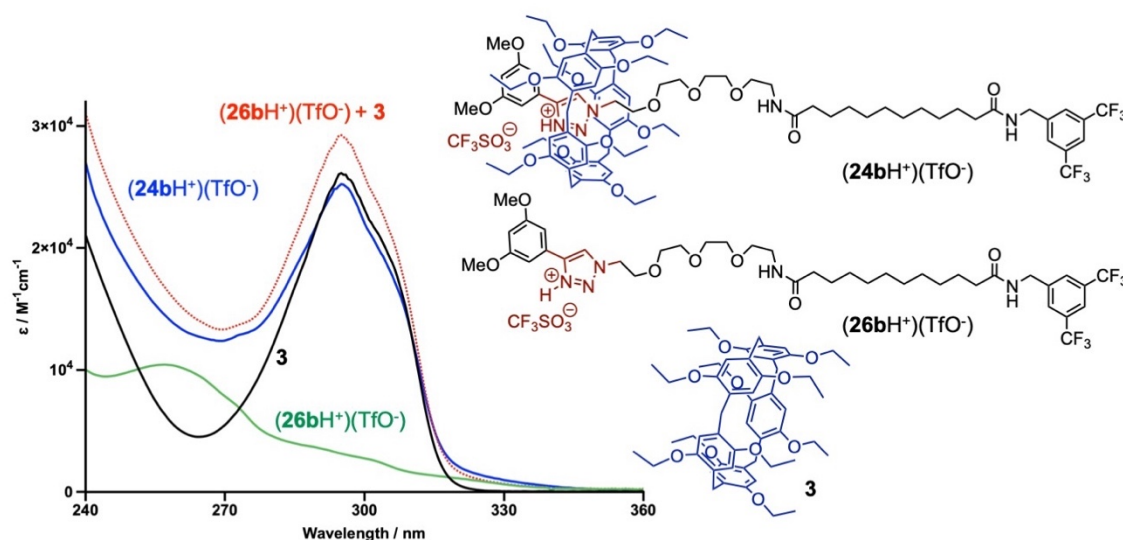


Figure 21. UV/vis spectra of **3**, (**24bH⁺**)(TfO⁻) and (**26bH⁺**)(TfO⁻) recorded in CHCl₃ at 25°C. The calculated spectrum corresponding to the sum of the spectra of **3** and (**26bH⁺**)(TfO⁻) is represented in red.

Electrochemistry. The electrochemical properties of compounds **24a-b** and (**24a-bH⁺**)(TfO⁻) were determined by cyclic voltammetry (CV) and Osteryoung Square Wave Voltammetry (OSVW).¹⁴ For the sake of comparison, electrochemical measurements were also carried out with model compounds **3**, **10a-b**, **12**, **28** and (**28H⁺**)(TfO⁻). All experiments were performed at room temperature in CH₂Cl₂ solutions containing *n*Bu₄NBF₄ (0.10 M) as supporting electrolyte and ferrocene (Fc) as internal reference, with a Pt wire as the working electrode and a saturated

calomel electrode (SCE) as a reference. Potential data for all compounds are collected in Table 3. Selected voltammograms are depicted in Figures 22-25.

Table 3. Electrochemical data of compounds **3**, **10a-b**, **12**, **28**, **24a-b**, **(28H⁺)(TfO⁻)** and **(24a-bH⁺)(TfO⁻)** determined by OSWV on a Pt working electrode in CH₂Cl₂ + 0.1 M *n*Bu₄BF₄ at room temperature. Ferrocene is used as internal reference.^[a,b]

Compound	E^5_{Ox}	E^4_{Ox}	E^3_{Ox}	E^2_{Ox}	E^1_{Ox}	E^1_{Red}
3 ^[c]		+1.72	+1.35	+1.27 ^[d]	+1.11 ^[d]	
10a		+1.63	+1.48 ^[d]	+1.28 ^[d]	+1.09 ^[d]	
12		+1.65	+1.46	+1.25 ^[d]	+1.07 ^[d]	
10b		+1.68	+1.48	+1.24 ^[d]	+1.09 ^[d]	
28				+1.91	+1.66	
(28H⁺)(TfO⁻)					+1.90	-0.11 ^[e]
24a		+1.65	+1.47 ^[d]	+1.28 ^[d]	+1.07 ^[d]	
(24aH⁺)(TfO⁻)		+1.64	+1.47	+1.27	+1.11	-0.02 ^[e]
24b		+1.68	+1.48	+1.28 ^[d]	+1.09 ^[d]	
(24bH⁺)(TfO⁻)	+1.68	+1.47	+1.36	+1.25	+1.12	-0.10 ^[e]

^[a] OSWVs were obtained using a sweep width of 20 mV, a frequency of 20 Hz, and a step potential of 5 mV.

^[b] Potential values in oxidation (E_{Ox}) and reduction (E_{Red}) in Volt vs. SCE (Fc⁺/Fc is observed at 0.55 ± 0.01

V vs. SCE). ^[c] From ref. 15. ^[d] Quasi-reversible processes in cyclic voltammetry. ^[e] Broad signal.

For compounds **3**, **10a-b** and **12**, no redox processes could be detected in the cathodic region. In contrast, successive oxidations are observed for all these compounds during the anodic scans. The two first anodic processes observed in the CV of pillar[5]arene **3** are quasi-reversible and correspond to the stepwise one electron-transfer to two of the five hydroquinone subunits of the macrocycle. Additional oxidations are observed by scanning at more positive potentials, these processes are however complex due to adsorption phenomena and the formation of oxidation side products. The electrochemical properties of the corresponding methylated pillar[5]arene derivative have been investigated in details.¹⁶ The third oxidation peak involves three electrons to generate the pentacationic pillar[5]arene and the fourth peak is a five-electron process related to the oxidation of the pentacation towards quinone products. The electrochemical features of the model [2]rotaxanes **10a-b** and **12** are characterized by four successive pillar[5]arene-centered oxidations. Typical examples of CVs recorded for compound **10a** are shown in Figure 22. While the three first oxidations (i, ii, iii) correspond to a one-electron transfer, the last oxidation wave (iv) involves two electrons. Overall, the five hydroquinone subunits of the pillar[5]arene moiety of the rotaxanes are oxidized in a step-wise manner to generate a

pentacationic species. The redox potentials of the different oxidations of **10a-b** and **12** are quite similar thus showing a limited influence of the amide stopper on the redox properties of the pillar[5]arene moieties. When compared to parent pillar[5]arene **3**, the two first oxidation processes (i and ii) of **10a-b** and **12** are only poorly affected by the presence of the alkyl chain in the cavity of the macrocycle. This is fully consistent with the poor influence of the alkyl chain present in the cavity on the FMOs of the pillar[5]arene as evidenced by the DFT calculations. In contrast, the following oxidations (iii and iv) suggest a substantial stabilization of the polycationic species in the case of the rotaxanes and the formation of quinone products seen for **3** is not observed anymore for **10a-b** and **12**.

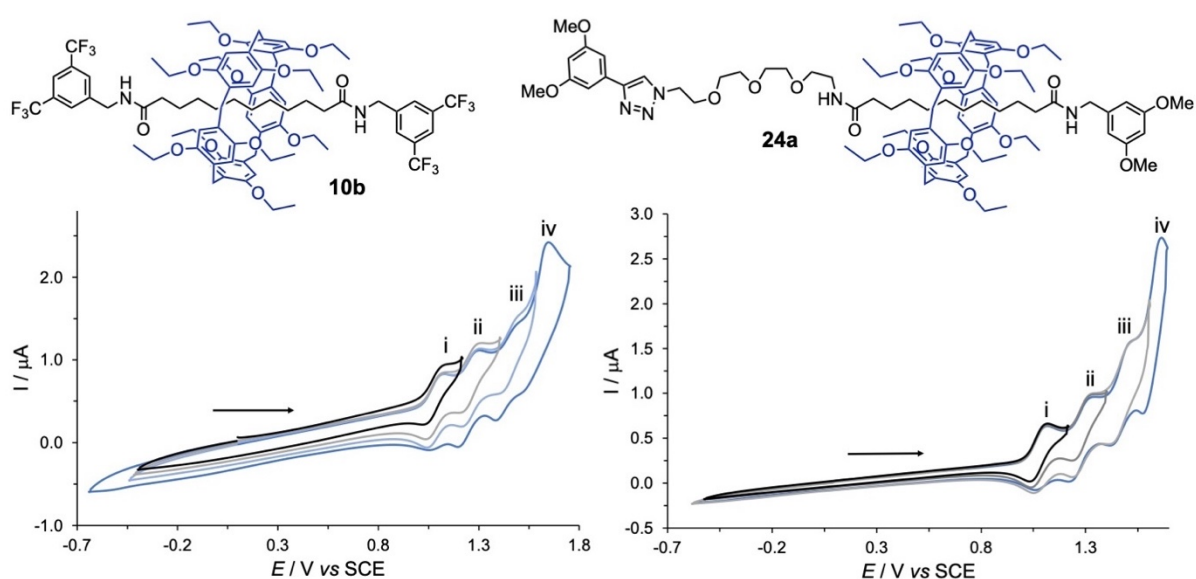


Figure 22. Cyclic voltammograms recorded for compounds **10b** and **24a** on a Pt electrode in $\text{CH}_2\text{Cl}_2 + 0.1 \text{ M } n\text{Bu}_4\text{BF}_4$ at a scan rate of 0.1 Vs^{-1} .

The electrochemical behavior of molecular shuttles **24a-b** is similar to the one observed for model rotaxanes **10a-b** and **12** (Figure 22). Four successive oxidation waves are effectively observed at similar redox potentials. The presence of both the triazole station and the tetraethylene glycol linker has no particular influence. This suggests that the pillar[5]arene moiety remains located over the decyl station in **24a** and **24b** upon the successive oxidations of the macrocyclic subunit and confirms the stabilization of the polycationic species when an alkyl chain is present in the cavity.

To fully understand the electrochemical properties of protonated molecular shuttles (**24a-bH⁺**)(TfO⁻), it was important to also investigate the electrochemical properties of model

compounds **28** and $(28\text{H}^+)(\text{TfO}^-)$. The cyclic voltammograms recorded for these two compounds are shown in Figure 23. Two oxidation waves are observed at high potential for the neutral compound. Upon protonation of the triazole ring, the system becomes electron-deficient and a reduction is effectively observed at -0.11 V vs. SCE for the triazolium moiety of $(28\text{H}^+)(\text{TfO}^-)$. On the other hand, only one oxidation wave is evidenced at high potential for $(28\text{H}^+)(\text{TfO}^-)$.

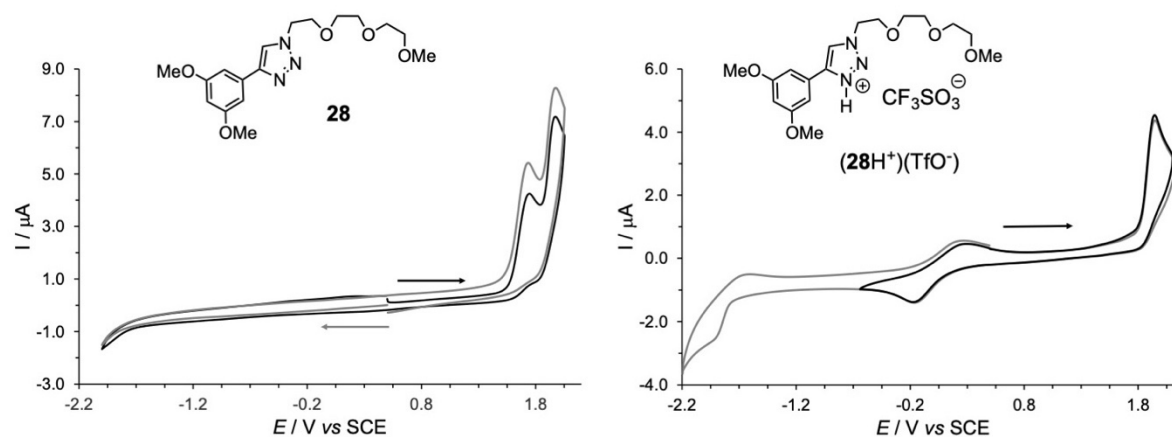


Figure 23. Cyclic voltammograms recorded for compounds **28** and $(28\text{H}^+)(\text{TfO}^-)$ on a Pt electrode in $\text{CH}_2\text{Cl}_2 + 0.1 \text{ M } n\text{Bu}_4\text{BF}_4$ at a scan rate of 0.1 Vs^{-1} .

Cyclic voltammograms recorded for molecular shuttles $(24\text{aH}^+)(\text{TfO}^-)$ and $(24\text{bH}^+)(\text{TfO}^-)$ are shown in Figure 24. Importantly, the diagnostic reduction wave of their triazolium moiety is clearly observed thus confirming the protonation of their *N*-heteroaromatic subunit.

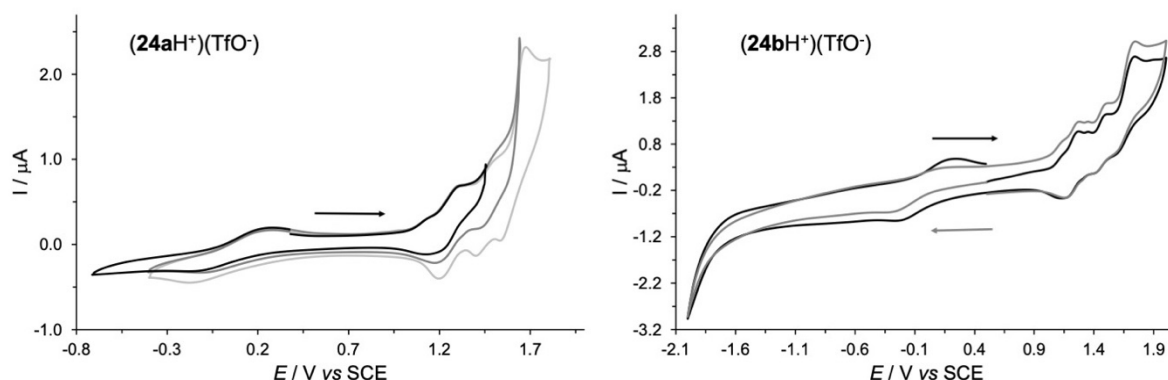


Figure 24. Cyclic voltammograms recorded for compounds $(24\text{aH}^+)(\text{TfO}^-)$ and $(24\text{bH}^+)(\text{TfO}^-)$ on a Pt electrode in $\text{CH}_2\text{Cl}_2 + 0.1 \text{ M } n\text{Bu}_4\text{BF}_4$ at a scan rate of 0.1 Vs^{-1} .

Cyclic voltammograms and OSWVs recorded for $(\mathbf{24aH}^+)(\text{TfO}^-)$ and $(\mathbf{24bH}^+)(\text{TfO}^-)$ in the anodic region are shown in Figure 25. For comparison purposes, the OSWV of $\mathbf{24a-b}$ are also represented in Figure 25.

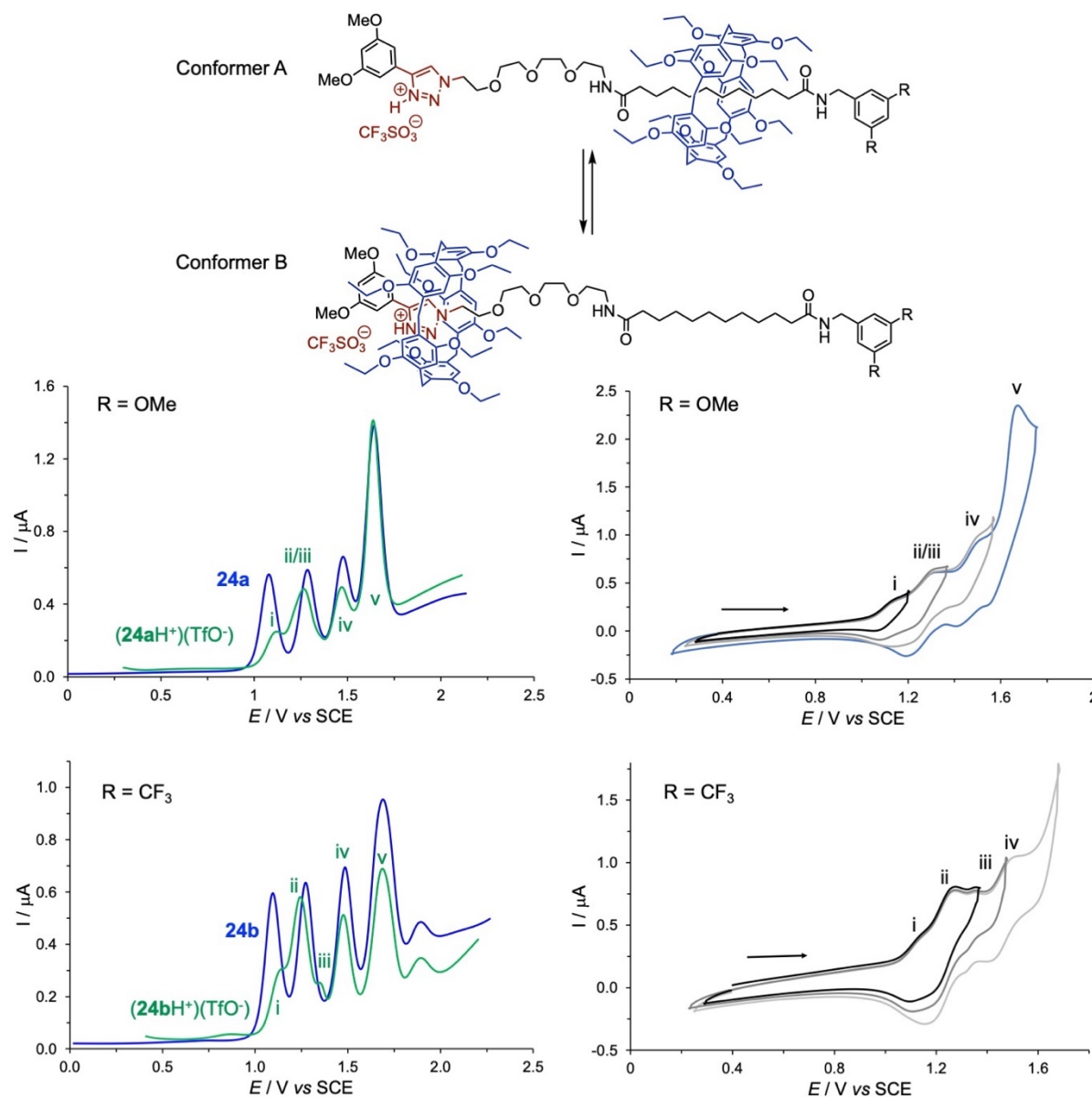


Figure 25. OSWVs (anodic scan; frequency 20 Hz, amplitude 20 mV, step potential 5 mV) of compounds $\mathbf{24a-b}$ and $(\mathbf{24aH}^+)(\text{TfO}^-)$ as well as cyclic voltammograms recorded for compounds $(\mathbf{24aH}^+)(\text{TfO}^-)$ and $(\mathbf{24bH}^+)(\text{TfO}^-)$ on a Pt electrode in $\text{CH}_2\text{Cl}_2 + 0.1 \text{ M } n\text{Bu}_4\text{BF}_4$ at a scan rate of 0.1 Vs^{-1} .

Owing to the coexistence of two conformers for both $(\mathbf{24aH}^+)(\text{TfO}^-)$ and $(\mathbf{24bH}^+)(\text{TfO}^-)$, their electrochemical behavior is more complicated when compared to $\mathbf{24a}$ and $\mathbf{24b}$. Actually, the first oxidation of the two conformers occurs at different potentials. For both protonated

molecular shuttles, the first wave (i) is ascribed to the one-electron oxidation of the pillar[5]arene subunit of conformer A and the second one (ii) to the simultaneous first pillar[5]arene-centered oxidation of conformer B and the oxidation of the pillar[5]arene radical cation of conformer A. The two first oxidations are indeed observed at almost the same redox potential for conformer A of $(\mathbf{24a-bH}^+)(\text{TfO}^-)$ and the corresponding unprotonated compounds $\mathbf{24a-b}$. On the other hand, the first pillar[5]arene-centered oxidation of conformer B is shifted to more positive potentials by *ca.* 130 and 160 mV for $(\mathbf{24aH}^+)(\text{TfO}^-)$ and $(\mathbf{24bH}^+)(\text{TfO}^-)$, respectively. This change is fully consistent with the presence of a positively charged triazolium subunit in the cavity of the pillar[5]arene moiety of conformer B. It can be noted that similar positive shifts have been already reported for the first oxidation of pillar[5]arene-containing rotaxane in which an imidazolium moiety is located within the cavity of the macrocycle.¹⁷ Upon the first oxidation, the pillar[5]arene radical cation is most likely expelled from the triazolium station due to electrostatic repulsion. In the particular case of $(\mathbf{24bH}^+)(\text{TfO}^-)$, the wave (iii) detected at +1.36 V vs. SCE corresponds to the subsequent oxidation of the radical cationic pillar[5]arene. In contrast, no peak separation could be observed in the case of $(\mathbf{24aH}^+)(\text{TfO}^-)$ as the two first oxidations of the pillar[5]arene moiety of conformer B occur at very close redox potentials. The triazolium station is totally unoccupied after these oxidations and the dicationic pillar[5]arene moiety is exclusively located on the decyl station whatever the starting conformation (Figure 26).

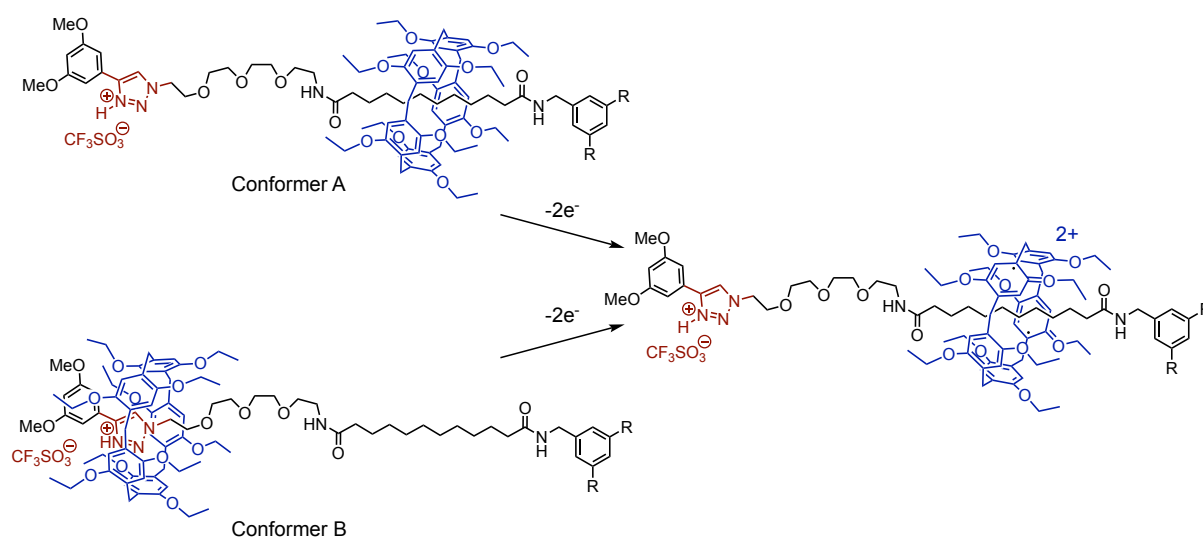


Figure 26. Upon oxidation of conformer B, the oxidized macrocycle is expelled from the triazolium station. For this reason, whatever the initial state (conformer A or conformer B), only one conformer is present after the first oxidations.

Finally, the two last oxidations (iv and v) are observed at the typical redox potentials of a pillar[5]arene moiety located onto a decyl station. This observation is in full agreement with the proposed conformational reorganization of conformer B upon the two first oxidations.

IV-3. Conclusion

In this chapter, the functionalization of a rotaxane building block bearing an activated pentafluorophenyl ester stopper with an amine bearing a triazole subunit allowed us to prepare new molecular shuttles. Detailed spectroscopic investigations supported by DFT calculations allowed us to fully understand the conformation of these systems. In the neutral state, the pillar[5]arene is almost exclusively located over the decyl station of the rotaxanes. In contrast, upon protonation, the affinity of the triazolium station for the pillar[5]arene is significantly increased. Protonation therefore triggers significant conformational changes. Actually, the pillar[5]arene is exchanging its position between the two available stations and the relative population of the two possible conformers is significantly influenced by the terminal stopper of the decyl station. Overall, the gliding motions of the pillar[5]arene occur over the full length of its molecular axle in the protonated state while such molecular motions are largely limited over the decyl stations in the neutral state. The perfectly reversible protonation/deprotonation of these molecular shuttles allows therefore to control the amplitude of the oscillations of the macrocyclic component along its axle moiety.

IV-4. References

- 1) K. Kato, S. Fa, S. Ohtani, T.-h. Shi, A. M. Brouwer, T. Ogoshi, *Chem. Soc. Rev.* **2022**, *51*, 3648-3687.
- 2) a) V. Balzani, A. Credi, M. Venturi, *Molecular Devices and Machines – A Journey into the Nano World*, Wiley-VCH, **2003**; b) E. R. Kay, D. A. Leigh, *Angew. Chem. Int. Ed.* **2015**, *54*, 10080-10088; *Angew. Chem.* **2015**, *127*, 10218-10226; c) S. Erbas-Cakmak, D. A. Leigh, C. T. McTernan, A. L. Nussbaumer, *Chem. Rev.* **2015**, *115*, 10081-10206; d) D. A. Leigh, *Angew. Chem. Int. Ed.* **2016**, *55*, 14506-14508; *Angew. Chem.* **2016**, *128*, 14722-14724; e) S.-J. Rao, Q. Zhang, J. Mei, X.-H. Ye, C. Gao, Q.-C. Wang, D.-H. Qu, H. Tian, *Chem. Sci.* **2017**, *8*, 6777-6783; f) S.-J. Rao, K. Nakazono, X. Liang, K. Nakajima, T. Takata, *Chem. Commun.* **2019**, *55*, 5231-5234; g) Q. Zhang, S.-R. Rao, T.

- Xie, X. Li, T.-Y. Xu, D.-W. Li, D.-H. Qu, Y.-T. Long, H. Tian, *Chem* **2018**, *4*, 2670-2684; h) S. Corra, M. Curcio, M. Baroncini, S. Silvi, A. Credi, *Adv. Mater.* **2020**, *32*, 1906064; i) M. Boroncini, S. Silvi, A. Credi, *Chem. Rev.* **2020**, *120*, 200-268; j) C.-S. Kwan, K. C.-F. Leung, *Mater. Chem. Front.* **2020**, *4*, 2825-2844; k) H.-Y. Zhou, Y. Han, C.-F. Chen, *Mater. Chem. Front.* **2020**, *4*, 12-28.
- 3) H. C. Kolb, M. G. Finn, K. B. Sharpless, *Angew. Chem. Int. Ed.* **2001**, *40*, 2004-2021.
 - 4) M. Rémy, I. Nierengarten, B. Park, M. Holler, U. Hahn, J.-F. Nierengarten, *Chem. Eur. J.* **2021**, *27*, 8492-8499.
 - 5) N. Becharguia, E. Wasielewski, R. Abidi, I. Nierengarten, J.-F. Nierengarten, *Chem. Eur. J.* **2023**, in press.
 - 6) T. M. N. Trinh, I. Nierengarten, M. Holler, J.-L. Gallani, J.-F. Nierengarten, *Chem. Eur. J.* **2015**, *21*, 8019-8022.
 - 7) J.-F. Nierengarten, *J. Porphyrins Phthalocyanines* **2023**, *27*, 1253-1262.
 - 8) a) M. E. Zandler, F. D'Souza, *C. R. Chimie* **2006**, *9*, 960-981; b) T. T. H. Tran, Y. Chang, T. K. A. Hoang, M. Kuo, Y. O. Su, *J. Phys. Chem. A* **2016**, *120*, 5504-5511.
 - 9) a) J. L. M. Abboub, C. Foces-Foces, R. Notorio, R. E. Trifonov, A. P. Volovodenco, V. A. Ostrovskii, I. Alkorta, J. Elguero, *Eur. J. Org. Chem.* **2001**, 3013-3024; b) M. Lokov, S. Tshepelevitsh, P. G. Heering, R. Vianello, I. Leito, *Eur. J. Org. Chem.* **2017**, 4475-4489.
 - 10) M. D. Tissandier, K. A. Cowen, W. Y. Feng, E. Gundlach, M. H. Cohen, A. D. Earhart, J. V. Coe, T. R. Tuttle, *J. Phys. Chem. A* **1998**, *102*, 7787-7794.
 - 11) A. Bagno, G. Lovato, G. Scorrano, *J. Chem. Soc., Perkin Trans. 2* **1993**, 1091-1098.
 - 12) a) X. Zhang, J. M. Herbert, *J. Phys. Chem. B* **2014**, *118*, 7806-7817; b) A. W. Lange J. M. Herbert, *Chem. Phys. Lett.* **2011**, *509*, 77-87; c) T. N. Truong, E. V. Stefanovich, *Chem. Phys. Lett.* **1995**, *240*, 253-260; d) V. Barone, M. Cossi, *J. Phys. Chem. A* **1998**, *102*, 1995-2001.
 - 13) Y. Mo, J. Gao, *J. Phys. Chem. A* **2001**, *105*, 6530-6536.
 - 14) R. G. Compton, C. E. Banks, *Understanding Voltammetry*, Imperial College Press, London, **2011**.
 - 15) M. Rémy, PhD thesis, University of Strasbourg, April 21, 2021.
 - 16) M. Z. Wiloch, E. Kuna, S. Kosiorek, V. Sashuk, M. Jönsson-Niedziolka, *ChemElectroChem* **2021**, *8*, 1507-1515.
 - 17) N. Pearce, E. S. Davies, N. R. Champness, *Molecules* **2020**, *25*, 1627.

Conclusion

As part of our ongoing research program on pillar[5]arene-based rotaxanes, the major goal of the present thesis was further evaluate the potential of the stopper exchange strategy for the construction of sophisticated supramolecular ensembles and new molecular machines. Starting from building block **1** previously developed in our group, we have reported detailed investigations on its mono-functionalization. Upon a first stopper exchange, the pillar[5]arene moiety of the mono-acylated product is preferentially located close to its reactive pentafluorophenyl ester stopper. As a result, the accessibility of the reactive carbonyl group by the nucleophilic reagents is more difficult thus allowing the efficient preparation of mono-amide rotaxanes from **1**. The synthetic utility of the resulting building blocks bearing only one activated stopper has been demonstrated with the efficient preparation of dissymmetrical rotaxanes, [2]rotaxanes with elongated axles, [3]rotaxanes and molecular shuttles. Beyond the synthetic aspects, we have also shown through in-depth physicochemical studies the structural and electronic effects involved in the intercomponent interactions between the pillar[5]arene subunit and its axle moiety in rotaxanes allowing to understand the conformational preferences of sophisticated supramolecular ensembles. All the knowledge acquired is fundamental for the molecular design of new pillar[5]arene-containing molecular machines in which the conformational changes can be strictly controlled. Future developments rely on our ability to further increase the complexity of the molecular machines by incorporating new functions to the rotaxane scaffold. This will be most likely achieved by combining the principles developed during this PhD thesis with the recent results obtained in our group on the use of pillar[5]arene-based rotaxanes as scaffolds for the development of nanomaterials with specific properties. Incorporating elements allowing to trigger controlled conformational changes to multifunctional nanomaterials will pave the way towards the construction of new drug delivery systems for biomedical applications or new systems for materials science applications in the field of molecular electronics.

Experimental section

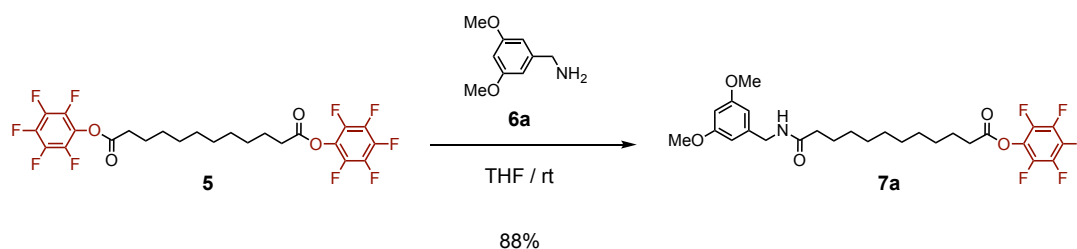
VI-1. General

Reagents were purchased as reagent grade and used without further purification. Compounds **1**,¹ **3**² and **5**¹ were prepared according to previously reported procedures. All reactions were performed in standard glassware under an inert Ar atmosphere. Evaporation and concentration were done at water aspirator pressure and drying in vacuo at 10⁻² Torr. Column chromatography: silica gel 60 (230-400 mesh, 0.040-0.063 mm) was purchased from E. Merck. Thin Layer Chromatography (TLC) was performed on aluminum sheets coated with silica gel 60 F₂₅₄ purchased from E. Merck. NMR spectra were recorded with a Bruker AC 400 or AC 500 spectrometer with solvent peaks as reference. In the assignments, the chemical shift (δ) (in ppm) is given first, followed, in brackets, by the multiplicity of the signal (s, singlet; d, doublet; t, triplet; q, quartet; quint, quintet; dd, doublet of doublets; m, multiplet), the value of the coupling constants in Hz if applicable and finally the number of protons implied. The ¹H signals were assigned by 2D experiments (COSY and ROESY). IR spectra (cm⁻¹) were recorded with a Perkin–Elmer Spectrum One spectrophotometer. Absorption spectral measurements were carried out in QS Hellma cuvettes with a PerkinElmer Lambda 365 spectrophotometer equipped with PCB 1500 water peltier system. MALDI-TOF mass spectra were recorded by the analytical service of the School of Chemistry (Strasbourg, France). Melting points were measured with a Gallenkamp apparatus. Elemental analyses and X-ray single crystal structure determinations were performed by the services of the *Fédération de Chimie Le Bel* (Strasbourg, France).

VI-2. Synthesis

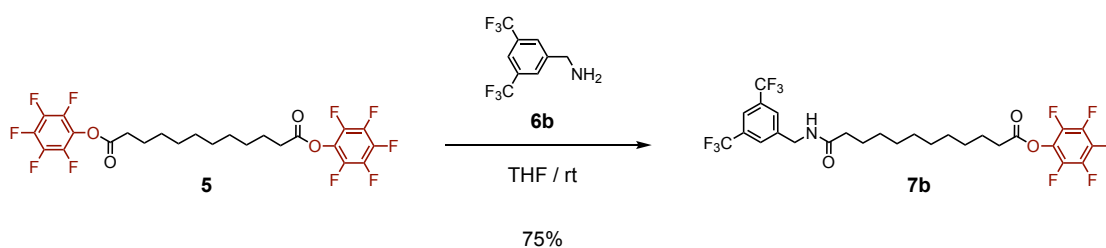
General procedure for the preparation of compounds 7a-b. A solution of the appropriate amine reagent (**6a-b**, 1.0 eq.) in anhydrous THF was added to a solution of **5** (3.0 eq.) in anhydrous THF at rt. The resulting mixture was stirred overnight, concentrated and purified as indicated.

Compound 7a.



Prepared from **6a** (0.329 g, 1.97 mmol) and **5** (3.323 g, 5.91 mmol) in anhydrous THF (53 mL). Column chromatography (SiO₂, CH₂Cl₂ containing 2% MeOH) followed by gel permeation chromatography (Biobeads SX-1, CH₂Cl₂) afforded **7a** (0.946 g, 88%). Colorless solid (m.p.: 87°C). IR (neat): 1791 (C=O), 1657 (C=O) cm⁻¹. ¹H NMR (500 MHz, CD₂Cl₂): δ = 6.40 (d, *J* = 2.3 Hz, 2H), 6.34 (t, *J* = 2.3 Hz, 1H), 6.17 (m, 1H), 4.31 (d, *J* = 5.9 Hz, 2H), 3.75 (s, 6H), 2.67 (t, *J* = 7.5 Hz, 2H), 2.19 (t, *J* = 7.5 Hz, 2H), 1.76 (quint, *J* = 7.5 Hz, 2H), 1.62 (m, 2H), 1.44-1.27 (m, 12H) ppm. ¹³C NMR (125 MHz, CD₂Cl₂): δ = 173.3, 170.0, 161.5, 142.6 (m), 141.8, 140.7 (m), 139.3 (m), 138.8 (m), 137.3 (m), 125.7 (m), 105.7, 99.3, 55.6, 43.7, 37.0, 33.6, 29.8 (two peaks), 29.7, 29.5, 29.2, 26.2, 25.1 ppm. ¹⁹F NMR (470 MHz, CDCl₃): δ = -152.8 (m), -158.2 (t, *J* = 21.7 Hz), -162.4 (m) ppm. MALDI-TOF-MS: *m/z* = 546.01 ([M+H]⁺, calcd for C₂₇H₃₃F₅NO₅: 546.23), 567.99 ([M+Na]⁺, calcd for C₂₇H₃₂F₅NO₅Na: 568.21). Anal. (%) calcd for C₂₇H₃₂F₅NO₅ (545.54): C, 59.44; H, 5.91; N, 2.57; found: C, 59.48; H, 5.96; N, 2.59.

Compound 7b.

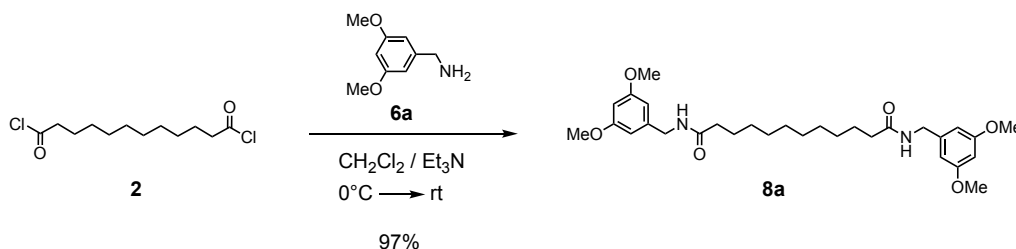


Prepared from **6b** (0.479 g, 1.97 mmol) and **5** (3.323 g, 5.91 mmol) in anhydrous THF (53 mL). Column chromatography (SiO₂, CH₂Cl₂ containing 2% MeOH) followed by gel permeation chromatography (Biobeads SX-1, CH₂Cl₂) afforded **7b** (0.918 g, 75%). Colorless solid (m.p.: 83°C). IR (neat): 3287 (NH), 1790 (C=O), 1648 (C=O) cm⁻¹. ¹H NMR (400 MHz, CDCl₃): δ = 7.78 (broad s, 1H), 7.72 (broad s, 2H), 5.89 (m, 1H), 4.57 (d, *J* = 6.1 Hz, 2H), 2.65 (t, *J* = 7.5 Hz, 2H), 2.27 (t, *J* = 7.5 Hz, 2H), 1.77 (quint, *J* = 7.5 Hz, 2H), 1.68 (quint, *J* = 7.5 Hz, 2H),

1.44-1.24 (m, 12H) ppm. ^{13}C NMR (125 MHz, CD_2Cl_2): $\delta = 173.6, 170.0, 142.4, 142.6$ (m), 140.7 (m), 139.4 (m), 138.8 (m), 137.3 (m), 132.0 (q, $^2J_{\text{C-F}} = 33$ Hz), 128.1, 128.0, 125.7 (m), 123.8 (q, $^1J_{\text{C-F}} = 273$ Hz), 121.6 (quint, $^3J_{\text{C-F}} = 3.9$ Hz), 42.8, 36.8, 33.7, 29.8, 29.7, 29.6, 29.5, 29.2, 26.1, 25.1 ppm. ^{19}F NMR (470 MHz, CD_2Cl_2): $\delta = -63.3, -153.6$ (m), -159.4 (t, $J = 21.6$ Hz), -163.5 (m) ppm. MALDI-TOF-MS: $m/z = 622.10$ ($[\text{M}+\text{H}]^+$, calcd for $\text{C}_{27}\text{H}_{27}\text{F}_{11}\text{NO}_3$: 622.18), 644.17 ($[\text{M}+\text{Na}]^+$, calcd for $\text{C}_{27}\text{H}_{26}\text{F}_{11}\text{NO}_3\text{Na}$: 644.16). Anal. (%) calcd for $\text{C}_{27}\text{H}_{26}\text{F}_{11}\text{NO}_3$ (621.48): C, 52.18; H, 4.22; N, 2.25; found: C, 52.39; H, 4.30; N, 2.28.

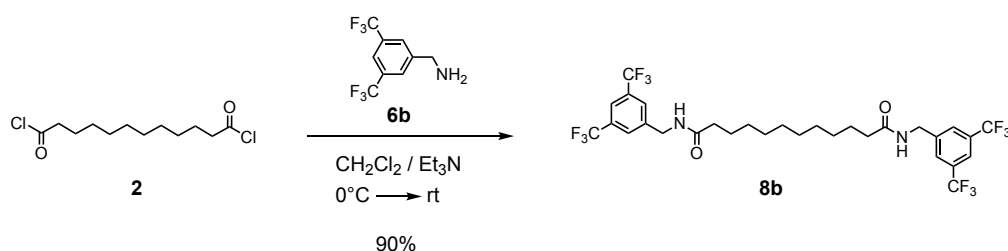
General procedure for the preparation of compounds 8a-b. A solution of the appropriate amine reagent (**6a-b**, 2.2 eq.) and Et_3N (2.2 eq.) in anhydrous CH_2Cl_2 was added to a solution of **2** (1.0 eq.) in anhydrous CH_2Cl_2 (1 mL/40 mg) at 0°C . The mixture was allowed to slowly warm to rt and stirring was continued at this temperature for 2 h. The resulting mixture was filtered through a short plug (SiO_2 , CH_2Cl_2 containing 2% MeOH), concentrated and purified as indicated.

Compound 8a.



Prepared from **6a** (0.279 g, 1.67 mmol), Et_3N (0.169 g, 1.67 mmol) and **2** (0.203 g, 0.76 mmol) in anhydrous CH_2Cl_2 (5 mL). Column chromatography (SiO_2 , CH_2Cl_2 containing 2% MeOH) gave **8a** (0.390 g, 97%). Colorless solid (m.p.: 151°C). IR (neat): 3289 (N-H), 1643 (C=O) cm^{-1} . ^1H NMR (CD_2Cl_2 , 400 MHz): $\delta = 6.40$ (d, $J = 2.3$ Hz, 4H), 6.34 (t, $J = 2.3$ Hz, 2H), 5.89 (broad s, 2H), 4.32 (d, $J = 5.8$ Hz, 4H), 3.75 (s, 12H), 2.18 (t, $J = 7.6$ Hz, 4H), 1.59 (m, 4H), 1.36-1.23 (m, 12H) ppm. ^{13}C NMR (125 MHz, DMSO-d_6): $\delta = 172.2, 160.5, 142.2, 105.0, 98.4, 55.1, 42.0, 35.4, 29.0, 28.9, 28.7, 25.4$ ppm. MALDI-TOF-MS: $m/z = 529.19$ ($[\text{M}+\text{H}]^+$, calcd for $\text{C}_{30}\text{H}_{45}\text{N}_2\text{O}_6$: 529.33), 551.17 ($[\text{M}+\text{Na}]^+$, calcd for $\text{C}_{30}\text{H}_{44}\text{N}_2\text{O}_6\text{Na}$: 551.31). Anal. (%) calcd for $\text{C}_{30}\text{H}_{44}\text{N}_2\text{O}_6$ (528.68): C, 68.15; H, 8.39; N, 5.30; found: C, 67.91; H, 8.35; N, 5.26.

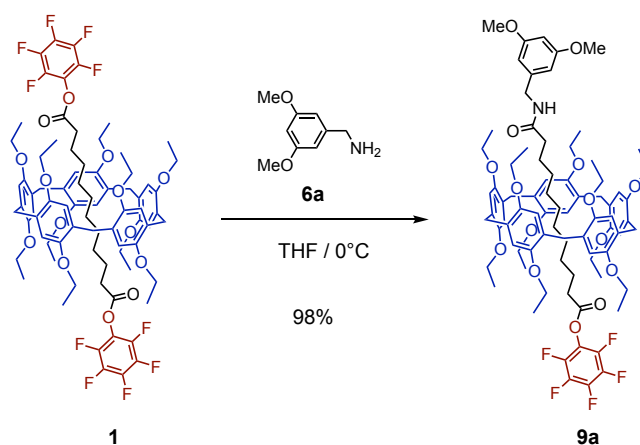
Compound 8b.



Prepared from **6b** (0.374 g, 1.54 mmol), Et₃N (0.156 g, 1.54 mmol) and **2** (0.187 g, 0.70 mmol) in anhydrous CH₂Cl₂ (5 mL). Column chromatography (SiO₂, CH₂Cl₂ containing 2% MeOH) gave **8b** (0.428 g, 90%). Colorless solid (m.p.: 146°C). IR (neat): 3292 (N-H), 1652 (C=O) cm⁻¹. ¹H NMR (400 MHz, CD₂Cl₂): δ = 7.79 (broad s, 2H), 7.74 (broad s, 4H), 6.11 (m, 2H), 4.51 (d, *J* = 6.2 Hz, 4H), 2.23 (t, *J* = 7.5 Hz, 4H), 1.62 (m, 4H), 1.35-1.23 (m, 12H) ppm. ¹³C NMR (125 MHz, (CD₃)₂CO): δ = 173.6, 144.7, 131.9 (q, ²*J*_{C-F} = 33 Hz), 128.8, 124.5 (q, ¹*J*_{C-F} = 272 Hz), 121.4 (quint, ³*J*_{C-F} = 4 Hz), 42.6, 36.5, 30.1, 30.0, 29.9, 26.4 ppm. ¹⁹F NMR (470 MHz, (CD₃)₂CO): δ = -63.3 ppm. MALDI-TOF-MS: *m/z* = 680.85 ([M]⁺, calcd for C₃₀H₃₂F₁₂N₂O₂: 680.23), 702.84 ([M+Na]⁺, calcd for C₃₀H₃₂F₁₂N₂O₂Na: 703.22). Anal. (%) calcd for C₃₀H₃₂F₁₂N₂O₂ (680.57): C, 52.94; H, 4.74; N, 4.12; found: C, 52.97; H, 4.79; N, 4.11.

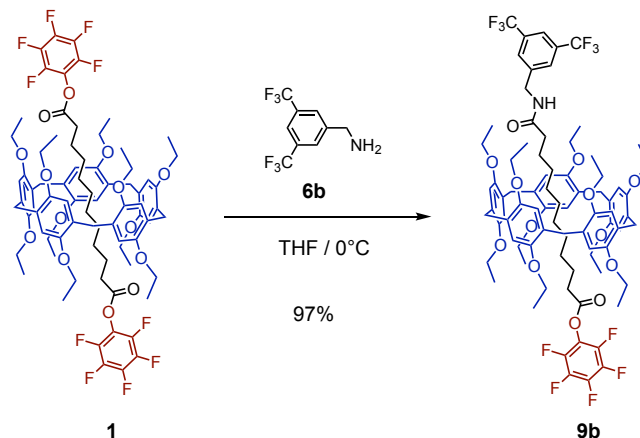
General procedure for the preparation of [2]rotaxanes 9a-e. A mixture of **1** (2.0 eq.) and the appropriate primary amine reagent (**6a-e**, 1.0 eq.) in anhydrous THF (1 mL/110 mg of **1**) was stirred at 0 °C for 3 h. The resulting mixture was filtered through a short plug (SiO₂, CH₂Cl₂), concentrated and purified as indicated.

Compound 9a.



Prepared from **1** (0.750 g, 0.52 mmol) and **6a** (0.043 g, 0.26 mmol) in anhydrous THF (7 mL). Column chromatography (SiO₂, petroleum ether/diethyl ether 9:1 → 5:5) afforded unreacted **1** (0.376 g) and the product which was further purified by gel permeation chromatography (Biobeads SX-1, CH₂Cl₂) to afford **9a** (0.366 g, 98%). Colorless solid (m.p.: 175°C). IR (neat): 1791 (C=O), 1657 (C=O) cm⁻¹. ¹H NMR (500 MHz, CDCl₃): δ = 6.96 (s, 5H), 6.92 (s, 5H), 6.50 (m, 2H), 6.43 (m, 1H), 5.82 (m, 1H), 4.44 (dAB, *J* = 15.6 Hz, *J* = 5.6 Hz, 2H), 4.06-3.96 (m, 10H), 3.89 (m, 10H), 3.84 (s, 6H), 3.79 (AB, *J* = 12.5 Hz, 10H), 2.13 (t, *J* = 7.9 Hz, 2H), 1.86 (m, 2H), 1.49 (t, *J* = 6.9 Hz, 15H), 1.45 (t, *J* = 6.9 Hz, 17H), 0.88 (m, 2H), 0.65 (m, 2H), 0.35 (m, 2H), -0.05 (m, 2H), -0.37 (m, 2H), -1.69 (m, 2H), -1.83 (m, 2H) ppm. ¹³C NMR (125 MHz, CDCl₃): δ = 172.7, 169.9, 161.2, 149.7, 149.6, 142.4 (m), 141.0, 140.4 (m), 139.0 (m), 138.4 (m), 137.0 (m), 128.3 (two peaks), 125.5 (m), 114.2, 113.9, 105.9, 99.1, 63.4, 55.4, 43.7, 37.1, 32.6, 30.8, 30.5, 30.1 (two peaks), 29.2, 27.3, 26.9, 26.4, 23.5, 15.6, 15.3 ppm. ¹⁹F NMR (470 MHz, CDCl₃): δ = -153.6 (m), -158.2 (t, *J* = 21.6 Hz), -162.5 (m) ppm. MALDI-TOF-MS: *m/z* = 1436.52 ([M+H]⁺, calcd for C₈₂H₁₀₃F₅NO₁₅: 1436.72). Anal. (%) calcd for C₈₂H₁₀₂F₅NO₁₅ (1436.68): C, 68.55; H, 7.16; N, 0.97; found: C, 68.44; H, 7.24; N, 0.96.

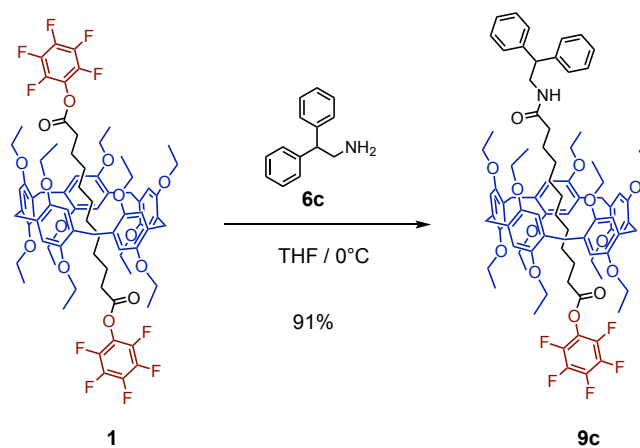
Compound 9b.



Prepared from **1** (1.337 g, 0.92 mmol) and **6b** (0.112 g, 0.46 mmol) in anhydrous THF (12 mL). Column chromatography (SiO₂, petroleum ether/diethyl ether 9:1 → 5:5) afforded unreacted **1** (0.661 g) and the product which was further purified by gel permeation chromatography (Biobeads SX-1, CH₂Cl₂) to afford **9b** (0.675 g, 97%). Colorless solid (m.p.: 168°C). IR (neat): 1791 (C=O), 1684 (C=O) cm⁻¹. ¹H NMR (500 MHz, CDCl₃): δ = 7.85 (broad s, 1H), 7.82 (broad s, 2H), 6.95 (s, 5H), 6.91 (s, 5H), 6.10 (t, *J* = 6.1 Hz, 1H), 4.61 (dAB, *J* = 15.5 Hz, *J* = 6.1 Hz, 2H), 4.05-3.95 (m, 10H), 3.93-3.86 (m, 10H), 3.78 (AB, *J* = 12.3 Hz, 10H), 2.08-1.97 (m, 2H),

1.91 (t, $J = 8.2$ Hz, 2H), 1.46 (t, $J = 6.9$ Hz, 15H), 1.45 (t, $J = 6.9$ Hz, 15H), 1.00 (m, 2H), 0.28 (m, 8H), -0.15 (m, 2H), -1.13 (m, 2H), -1.21 (m, 2H) ppm. ^{13}C NMR (125 MHz, CDCl_3): $\delta = 173.5, 169.9, 149.8, 149.6, 142.4$ (m), 141.9, 140.4 (m), 139.1 (m), 138.4 (m), 137.1 (m), 132.1 (q, $^2J_{\text{C-F}} = 33$ Hz), 128.6, 128.3, 127.8 (two peaks), 125.4 (m), 123.5 (q, $^1J_{\text{C-F}} = 273$ Hz), 121.4 (quint, $^3J_{\text{C-F}} = 3.9$ Hz), 114.6, 114.0, 63.7, 63.4, 42.7, 36.8, 32.8, 30.5, 30.3, 30.1, 29.5, 29.3, 28.0, 27.5, 26.0, 23.9, 15.5, 15.4 ppm. ^{19}F NMR (470 MHz, CDCl_3): $\delta = -62.8, -153.5$ (m), -158.1 (t, $J = 21.7$ Hz), -162.5 (m) ppm. MALDI-TOF-MS: $m/z = 1512.48$ ($[\text{M}+\text{H}]^+$, calcd for $\text{C}_{82}\text{H}_{97}\text{F}_{11}\text{NO}_{13}$: 1512.67). Anal. (%) calcd for $\text{C}_{82}\text{H}_{96}\text{F}_{11}\text{NO}_{13}$ (1512.62): C, 65.11; H, 6.39; N, 0.93; found: C, 65.03; H, 6.53; N, 0.89.

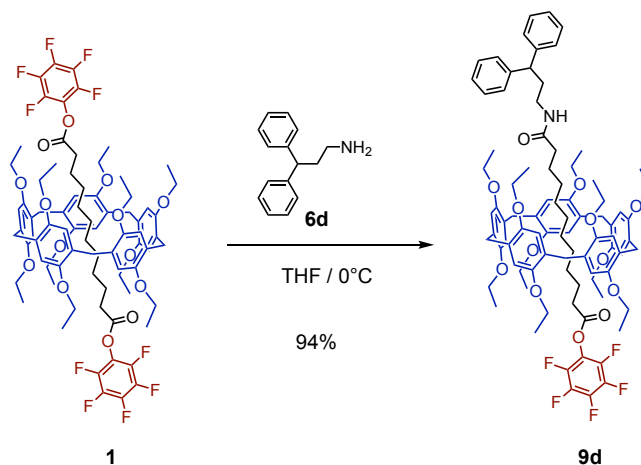
Compound 9c.



Prepared from **1** (0.320 g, 0.22 mmol) and **6c** (0.022 g, 0.11 mmol) in anhydrous THF (3 mL). Column chromatography (SiO_2 , cyclohexane/ CH_2Cl_2 6:4 \rightarrow 1:9) afforded unreacted **1** (0.158 g) and the product which was further purified by gel permeation chromatography (Biobeads SX-1, CH_2Cl_2) to afford **9c** (0.147 g, 91%). Colorless glassy product. IR (neat): 1791 (C=O), 1669 (C=O) cm^{-1} . ^1H NMR (400 MHz, CDCl_3): $\delta = 7.35\text{--}7.29$ (m, 4H), 7.27–7.21 (m, 6H), 6.90 (s, 5H), 6.84 (s, 5H), 5.34 (t, $J = 5.4$ Hz, 1H), 4.20 (t, $J = 8.0$ Hz, 1H), 4.00–3.79 (m, 22H), 3.73 (AB, $J = 12.6$ Hz, 10H), 2.04 (m, 2H), 1.71 (m, 2H), 1.50 (m, 2H), 1.42 (t, $J = 6.9$ Hz, 15H), 1.39 (t, $J = 6.9$ Hz, 15H), 1.08 (m, 2H), 0.83 (m, 2H), 0.35 (m, 2H), -0.31 (m, 2H), -0.56 (m, 2H), -2.07 (m, 2H), -2.25 (m, 2H) ppm. ^{13}C NMR (100 MHz, CDCl_3): $\delta = 172.8, 170.0, 149.7, 149.6, 142.6$ (m), 142.0, 140.2 (m), 139.3 (m), 138.0 (m), 136.8 (m), 128.9, 128.3, 128.2, 127.0, 125.6 (m), 114.1, 113.9, 63.4, 63.2, 50.8, 43.9, 37.1, 32.5, 31.2, 30.5, 30.4, 30.0, 29.2, 26.9, 26.7, 26.5, 23.4, 15.6, 15.4 ppm. ^{19}F NMR (376 MHz, CDCl_3): $\delta = -153.7$ (m), -158.3 (t, $J = 21.3$ Hz), -162.6 (m) ppm. MALDI-TOF-MS: $m/z = 1466.67$ ($[\text{M}+\text{H}]^+$, calcd for

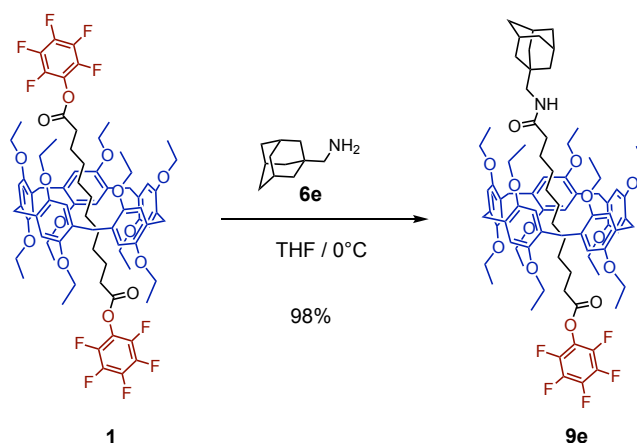
$C_{87}H_{105}F_5NO_{13}$: 1466.75). Anal. (%) calcd for $C_{87}H_{104}F_5NO_{13}$ (1466.75): C, 71.24; H, 7.15; N, 0.95; found: C, 71.16; H, 7.21; N, 0.91.

Compound 9d.



Prepared from **1** (0.320 g, 0.22 mmol) and **6d** (0.023 g, 0.11 mmol) in anhydrous THF (3 mL). Column chromatography (SiO_2 , cyclohexane/ CH_2Cl_2 6:4 \rightarrow 1:9) afforded unreacted **1** (0.159 g) and the product which was further purified by gel permeation chromatography (Biobeads SX-1, CH_2Cl_2) to afford **9d** (0.153 g, 94%). Colorless glassy product. IR (neat): 1791 (C=O), 1661 (C=O) cm^{-1} . 1H NMR (400 MHz, $CDCl_3$): δ = 7.36-7.29 (m, 8H), 7.26-7.21 (m, 2H), 6.96 (s, 5H), 6.92 (s, 5H), 5.43 (t, J = 5.7 Hz, 1H), 4.07-3.86 (m, 21H), 3.80 (AB, J = 12.6 Hz, 10H), 3.31 (m, 2H), 2.36 (m, 2H), 1.98 (m, 2H), 1.86 (m, 2H), 1.49 (t, J = 6.9 Hz, 15H), 1.46 (t, J = 6.9 Hz, 15H), 1.36 (m, 2H), 0.85 (m, 2H), 0.67 (m, 2H), 0.37 (m, 2H), -0.06 (m, 2H), -0.36 (m, 2H), -1.70 (m, 2H), -1.85 (m, 2H) ppm. ^{13}C NMR (100 MHz, $CDCl_3$): δ = 172.8, 169.9, 149.7, 149.6, 144.4, 142.6 (m), 140.3 (m), 139.3 (m), 138.1 (m), 136.8 (m), 128.7, 128.3 (two peaks), 127.8, 126.5, 125.5 (m), 114.2, 113.9, 63.3, 49.5, 38.7, 37.0, 35.6, 32.6, 30.9, 30.5, 30.1, 29.2, 27.3, 26.9, 26.3, 23.5, 15.6, 15.3 ppm. ^{19}F NMR (376 MHz, $CDCl_3$): δ = -153.6 (m), -158.2 (t, J = 22.2 Hz), -162.5 (m) ppm. MALDI-TOF-MS: m/z = 1480.62 ($[M+H]^+$, calcd for $C_{88}H_{107}F_5NO_{13}$: 1480.77). Anal. (%) calcd for $C_{88}H_{106}F_5NO_{13}$ (1480.78): C, 71.38; H, 7.21; N, 0.95; found: C, 71.48; H, 7.26; N, 0.91.

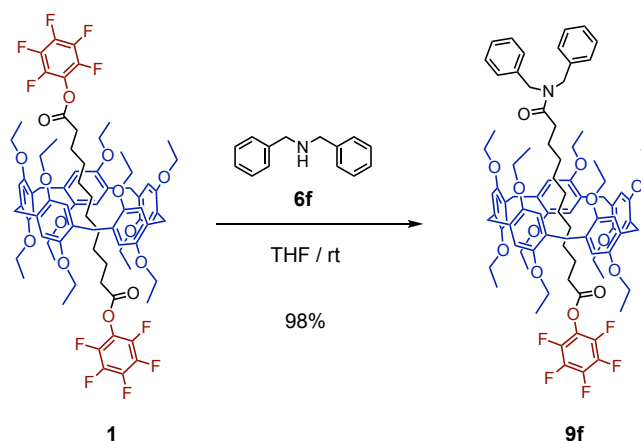
Compound 9e.



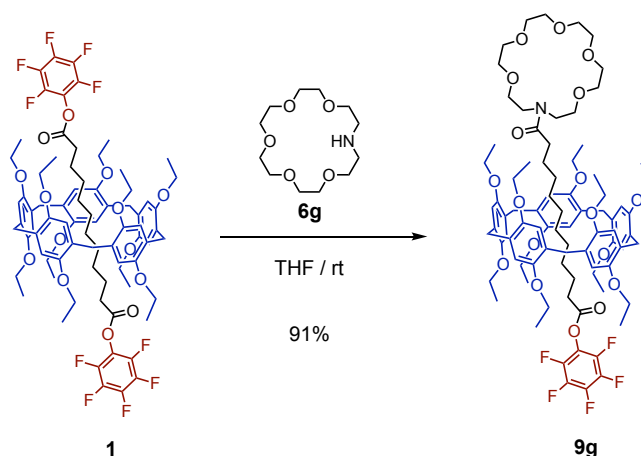
Prepared from **1** (0.320 g, 0.22 mmol) and **6e** (0.018 g, 0.11 mmol) in anhydrous THF (3 mL). Column chromatography (SiO₂, petroleum ether/diethyl ether 9:1 → 5:5) afforded unreacted **1** (0.157 g) and the product which was further purified by gel permeation chromatography (Biobeads SX-1, CH₂Cl₂) to afford **9e** (0.155 g, 98%). Colorless glassy product. IR (neat): 1791 (C=O), 1657 (C=O) cm⁻¹. ¹H NMR (400 MHz, CDCl₃): δ = 7.00 (m, 5H), 6.95 (m, 5H), 5.52 (broad s, 1H), 4.11-4.01 (m, 10H), 3.97-3.90 (m, 10H), 3.83 (s, 10H), 3.06 (d, *J* = 5.6 Hz, 2H), 2.26 (t, *J* = 7.2 Hz, 2H), 2.08 (broad s, 3H), 1.86-1.65 (m, 10H), 1.59-1.46 (m, 36H), 1.24 (broad s, 2H), 0.97 (broad s, 2H), 0.49 (broad s, 2H), -0.22 (m, 2H), -0.41 (m, 2H), -1.93 (m, 2H), -2.13 (m, 2H) ppm. ¹³C NMR (100 MHz, CDCl₃): δ = 172.9, 169.9, 149.6, 149.5, 142.6 (m), 140.2 (m), 139.2 (m), 137.9 (m), 136.7 (m), 128.2, 125.5 (m), 114.0, 113.8, 63.3, 63.1, 50.9, 40.3, 37.2, 37.0, 33.7, 32.4, 31.2, 30.5, 30.4, 30.0, 29.1, 28.3, 26.9, 26.7, 26.6, 23.3, 15.5, 15.2 ppm. ¹⁹F NMR (376 MHz, CDCl₃): δ = -153.6 (m), -158.3 (t, *J* = 21.4 Hz), -162.6 (m) ppm. MALDI-TOF-MS: *m/z* = 1434.68 ([M+H]⁺, calcd for C₈₄H₁₀₉F₅NO₁₃: 1434.78). Anal. (%) calcd for C₈₄H₁₀₈F₅NO₁₃ (1434.75): C, 70.32; H, 7.59; N, 0.98; found: C, 70.33; H, 7.65; N, 0.96.

General procedures for the preparation of [2]rotaxanes 9f-g. A mixture of **1** (2.0 eq.) and the appropriate secondary amine reagent (**6f-g**, 1.0 eq.) in anhydrous THF (1 mL/110 mg of **1**) was stirred at rt for 6 days (**9f**) or 4 days (**9g**). The resulting mixture was filtered through a short plug (SiO₂, CH₂Cl₂), concentrated and purified as indicated.

Compound 9f.



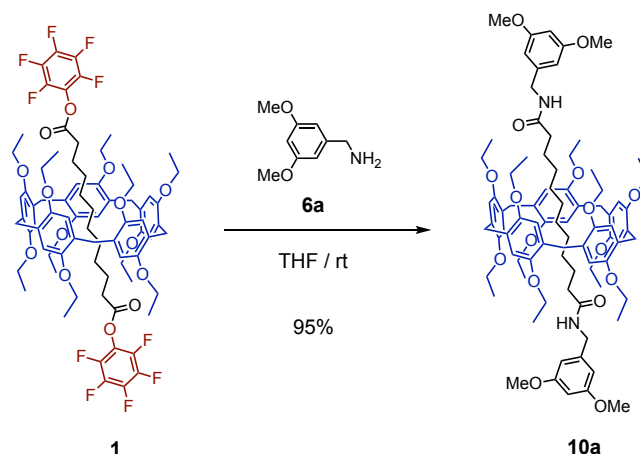
Prepared from **1** (0.407 g, 0.28 mmol) and **6f** (0.028 g, 0.14 mmol) in anhydrous THF (4 mL). Column chromatography (SiO₂, petroleum ether/diethyl ether 9:1 → 5:5) afforded unreacted **1** (0.197 g) and the product which was further purified by gel permeation chromatography (Biobeads SX-1, CH₂Cl₂) to afford **9f** (0.201 g, 98%). Colorless glassy product. IR (neat): 1791 (C=O), 1653 (C=O) cm⁻¹. ¹H NMR (400 MHz, CDCl₃): δ = 7.50-7.34 (m, 8H), 7.28 (broad s, 2H), 7.01 (s, 5H), 6.95 (s, 5H), 4.80 (broad s, 2H), 4.65 (broad s, 2H), 4.12-3.90 (m, 20H), 3.84 (AB, *J* = 12.5 Hz, 10H), 2.56 (broad s, 2H), 1.92-1.73 (m, 4H), 1.55-1.45 (m, 30H), 1.35 (broad s, 2H), 1.08 (broad s, 2H), 0.52 (broad s, 2H), -0.27 (m, 2H), -0.44 (m, 2H), -2.04 (m, 2H), -2.25 (m, 2H) ppm. ¹³C NMR (100 MHz, CDCl₃): δ = 170.0, 149.6 (two peaks), 142.6 (m), 140.3 (m), 139.2 (m), 137.9 (m), 137.8, 136.9, 136.7 (m), 129.1, 128.7, 128.4, 128.2, 127.8, 127.5, 126.3, 125.5 (m), 114.0, 113.8, 63.3, 63.1, 50.0, 48.2, 34.0, 32.4, 31.5, 30.7, 30.5, 30.0, 29.2, 26.7, 26.4, 26.3, 23.3, 15.6, 15.3 ppm. ¹⁹F NMR (376 MHz, CDCl₃): δ = -153.6 (m), -158.3 (t, *J* = 21.7 Hz), -162.6 (m) ppm. MALDI-TOF-MS: *m/z* = 1466.85 ([M+H]⁺, calcd for C₈₇H₁₀₅F₅NO₁₃: 1466.75). Anal. (%) calcd for C₈₇H₁₀₄F₅NO₁₃ (1466.75): C, 71.24; H, 7.15; N, 0.95; found: C, 71.20; H, 7.17; N, 0.93.

Compound **9g**.

Prepared from **1** (0.203 g, 0.14 mmol) and **6g** (0.018 g, 0.07 mmol) in anhydrous THF (2 mL). Column chromatography (SiO₂, CHCl₃/cyclohexane 7:3 → CHCl₃) afforded unreacted **1** (0.100 g) and the product which was further purified by gel permeation chromatography (Biobeads SX-1, CH₂Cl₂) to afford **9g** (0.098 g, 91%). Colorless glassy product. IR (neat): 1791 (C=O), 1636 (C=O) cm⁻¹. ¹H NMR (400 MHz, CDCl₃): δ = 6.94 (s, 5H), 6.90 (s, 5H), 4.05-3.82 (m, 22H), 3.77 (s, 14H), 3.72 (broad s, 18H), 2.42 (broad s, 2H), 1.69 (m, 4H), 1.50 (m, 15H), 1.43 (t, *J* = 6.8 Hz, 15H), 1.29 (m, 2H), 1.04 (broad s, 2H), 0.50 (broad s, 2H), -0.37 (m, 2H), -0.48 (m, 2H), -2.11 (m, 2H), -2.35 (m, 2H) ppm. ¹³C NMR (100 MHz, CDCl₃) δ = 173.2, 169.9, 149.5, 142.5 (m), 140.2 (m), 139.2 (m), 138.0 (m), 136.7 (m), 128.2, 128.1, 125.5 (m), 113.9, 113.8, 71.0, 70.9, 70.6, 70.4, 69.8 (broad), 63.3, 63.1, 49.5 (broad), 46.9, 33.6, 32.4, 31.6, 30.8, 30.5, 30.1, 29.1, 26.7, 26.3, 26.2, 23.1, 15.6, 15.2 ppm. ¹⁹F NMR (376 MHz, CDCl₃): δ = -153.7 (m), -158.3 (t, *J* = 21.5 Hz), -162.6 (m) ppm. MALDI-TOF-MS: *m/z* = 1532.66 ([M+H]⁺, calcd for C₈₅H₁₁₅F₅NO₁₈: 1532.80). Anal. (%) calcd for C₈₅H₁₁₄F₅NO₁₈ (1532.81): C, 66.60; H, 7.50; N, 0.92; found: C, 66.62; H, 7.58; N, 0.86.

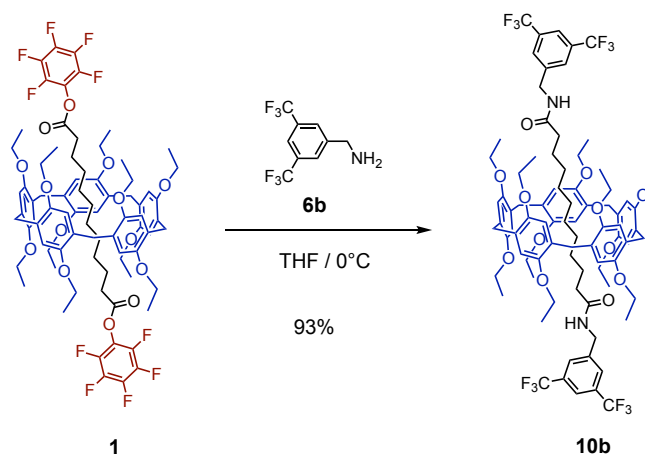
General procedures for the preparation of [2]rotaxanes 10a-b. A solution of **1** (1.0 eq.) and the appropriate amine reagent (**6a-b**, 2.2 eq.) in anhydrous THF was stirred overnight at rt. The resulting mixture was filtered through a short plug (SiO₂, CH₂Cl₂ containing 2% MeOH), concentrated and purified as indicated.

Compound 10a.



Prepared from **1** (0.407 g, 0.28 mmol) and **6a** (0.104 g, 0.62 mmol) in anhydrous THF (2 mL). Column chromatography (SiO₂, CH₂Cl₂ containing 0.3% MeOH) followed by gel permeation chromatography (Biobeads SX-1, CH₂Cl₂) gave **10a** (0.380 g, 95%). Colorless glassy product. IR (neat): 1671 (C=O) cm⁻¹. ¹H NMR (400 MHz, CDCl₃): δ = 6.90 (s, 10H), 6.51 (broad s, 4H), 6.40 (s, 2H), 6.05 (broad s, 2H), 4.42 (broad s, 4H), 4.02-3.84 (m, 20H), 3.82 (s, 12H), 3.75 (s, 10H), 1.62 (t, *J* = 8 Hz, 4H), 1.44 (t, *J* = 6.9 Hz, 30H), 0.58 (broad s, 4H), -0.05 (broad s, 4H), -0.46 (broad s, 8H) ppm. ¹³C NMR (125 MHz, CDCl₃): δ = 173.2, 161.1, 149.7, 141.4, 128.4, 114.7, 105.9, 98.8, 63.8, 55.4, 43.5, 36.9, 30.2, 29.2, 29.1, 28.8, 25.6, 15.5 ppm. MALDI-TOF-MS: *m/z* = 1419.87 ([M+H]⁺, calcd for C₈₅H₁₁₅N₂O₁₆: 1419.82). Anal. (%) calcd for C₈₅H₁₁₄N₂O₁₆ (1419.82): C, 71.90; H, 8.09; N, 1.97; found: C, 71.66; H, 8.20; N, 1.93.

Compound 10b.

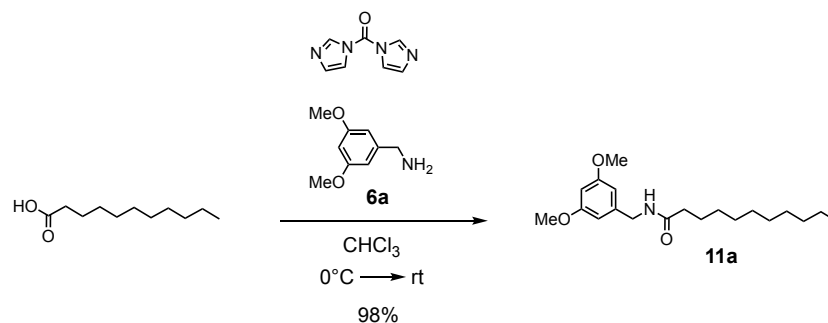


Prepared from **1** (0.407 g, 0.28 mmol) and **6b** (0.150 g, 0.62 mmol) in anhydrous THF (2 mL). Column chromatography (SiO₂, CH₂Cl₂ containing 0.2% MeOH) followed by gel permeation

chromatography (Biobeads SX-1, CH₂Cl₂) gave compound **10b** (0.409 g, 93%). Colorless glassy product. Analytical data identical to the one previously reported in the literature for **10b**.³

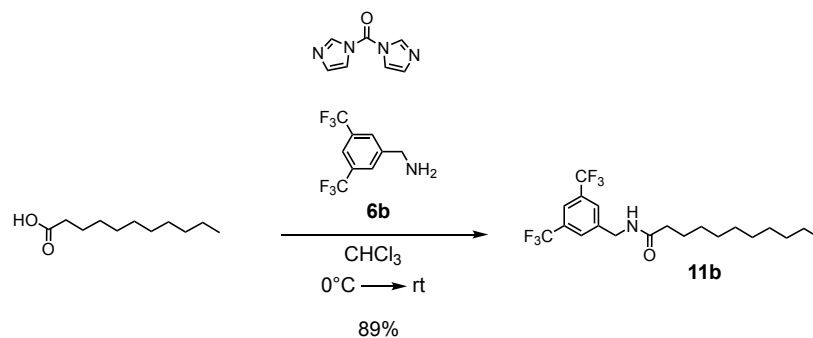
Preparation of model compounds 11a-c

Compound 11a.



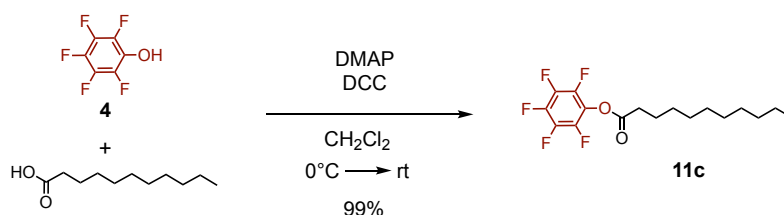
A solution of undecanoic acid (0.300 g, 1.61 mmol) and CDI (0.287 g, 1.77 mmol) in anhydrous CHCl₃ (4 mL) was stirred at 0°C. After 1 h, **6a** (0.323 g, 1.93 mmol) was added. The resulting mixture was stirred overnight at rt, filtered through a short plug (SiO₂, CHCl₃) and concentrated. Column chromatography (SiO₂, CHCl₃) gave compound **11a** (0.531 g, 98%). Colorless solid (m.p.: 86°C). IR (neat): 3290 (N-H), 1645 (C=O) cm⁻¹. ¹H NMR (400 MHz, CDCl₃): δ = 6.42 (d, *J* = 2.2 Hz, 2H), 6.37 (t, *J* = 2.2 Hz, 1H), 5.67 (broad s, 1H), 4.38 (d, *J* = 5.7 Hz, 2H), 3.78 (s, 6H), 2.21 (t, *J* = 7.6 Hz, 2H), 1.65 (quint, *J* = 7.6, 2H), 1.35-1.21 (m, 14H), 0.88 (t, *J* = 6.8 Hz, 3H) ppm. ¹³C NMR (125 MHz, CDCl₃): δ = 173.3, 161.0, 141.0, 105.5, 99.2, 55.2, 43.5, 36.7, 31.9, 29.6, 29.5, 29.4 (two peaks), 29.3, 25.8, 22.7, 14.1 ppm. MALDI-TOF-MS: *m/z* = 336.37 ([M+H]⁺, calcd for C₂₀H₃₄NO₃: 336.25), 358.37 ([M+Na]⁺, calcd for C₂₀H₃₃NO₃Na: 358.26). Anal. (%) calcd for C₂₀H₃₃NO₃ (335.48): C, 71.60, H, 9.92, N, 4.18; found: C, 71.64, H, 9.94, N, 4.08.

Compound 11b.



A solution of undecanoic acid (0.300 g, 1.61 mmol) and CDI (0.287 g, 1.77 mmol) in anhydrous CHCl_3 (4 mL) was stirred at 0°C . After 1 h, **6b** (0.469 g, 1.93 mmol) was added. The resulting mixture was stirred overnight at rt, filtered through a short plug (SiO_2 , CHCl_3) and concentrated. Column chromatography (SiO_2 , CHCl_3) gave compound **11b** (0.590 g, 89%). Colorless solid (m.p.: 73°C). IR (neat): 3286 (N-H), 1648 (C=O) cm^{-1} . ^1H NMR (500 MHz, CDCl_3): δ = 7.76 (s, 1H), 7.71 (s, 2H), 6.23 (m, 1H), 4.53 (d, J = 6.1 Hz, 2H), 2.24 (t, J = 7.6 Hz, 2H), 1.64 (quint, J = 7.6 Hz, 2H), 1.34-1.20 (m, 14H), 0.87 (t, J = 7.0 Hz, 3H) ppm. ^{13}C NMR (125 MHz, CDCl_3): δ = 173.7, 141.5, 132.0 (q, $^2J_{\text{C-F}}$ = 33 Hz), 127.7 (two peaks), 123.4 (q, $^1J_{\text{C-F}}$ = 273 Hz), 121.5 (quint, $^3J_{\text{C-F}}$ = 3.9 Hz), 42.7, 36.7, 32.0, 29.7, 29.6, 29.5, 29.4, 25.8, 22.8, 14.2 ppm. ^{19}F NMR (470 MHz, CDCl_3): δ = -62.9 ppm. MALDI-TOF-MS: m/z = 412.38 ($[\text{M}+\text{H}]^+$, calcd for $\text{C}_{20}\text{H}_{28}\text{F}_6\text{NO}$: 412.20), 434.37 ($[\text{M}+\text{Na}]^+$, calcd for $\text{C}_{20}\text{H}_{27}\text{F}_6\text{NONa}$: 434.19). Anal. (%) calcd for $\text{C}_{20}\text{H}_{27}\text{F}_6\text{NO}$ (411.43): C, 58.39, H, 6.62, N, 3.40; found: C, 58.49, H, 6.64, N, 3.23.

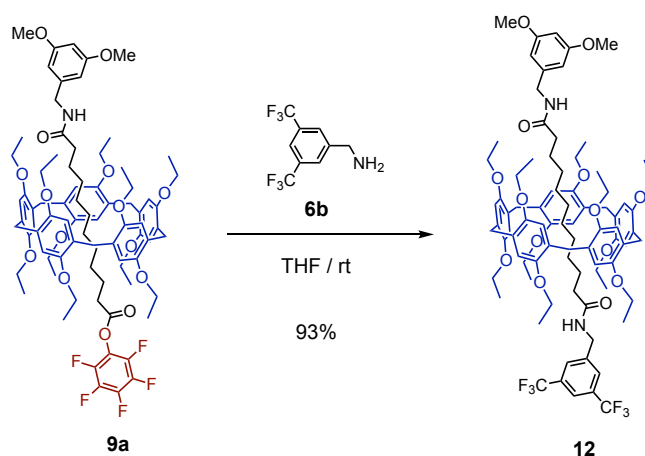
Compound 11c.



DCC (0.365 g, 1.77 mmol) was added to a solution of undecanoic acid (0.300 g, 1.61 mmol), **4** (0.355 g, 1.93 mmol) and DMAP (0.010 g, 0.08 mmol) in anhydrous CH_2Cl_2 (6 mL) at 0°C . After 2 h, the precipitate was filtered and the solvent concentrated. Column chromatography (SiO_2 , CHCl_3) gave compound **11c** (0.560 g, 99%). Colorless oil. IR (neat): 1792 (C=O) cm^{-1} . ^1H NMR (500 MHz, CDCl_3): δ = 2.66 (t, J = 7.5 Hz, 2H), 1.78 (quint, J = 7.5 Hz, 2H), 1.42 (m, 2H), 1.36-1.22 (m, 12H), 0.87 (t, J = 7.0 Hz, 3H) ppm. ^{13}C NMR (125 MHz, CDCl_3): δ = 169.7, 142.3 (m), 140.5 (m), 139.1 (m), 138.6 (m), 137.0 (m), 125.3 (m), 33.5, 32.1, 29.7, 29.6, 29.5, 29.3, 29.0, 24.9, 22.8, 14.2 ppm. ^{19}F NMR (470 MHz, CDCl_3): δ = -153.0 (m), -158.4 (m), -162.6 (m) ppm. Anal. (%) calcd for $\text{C}_{17}\text{H}_{21}\text{F}_5\text{O}_2$ (352.34): C, 57.95, H, 6.01; found: C, 57.72, H, 5.99.

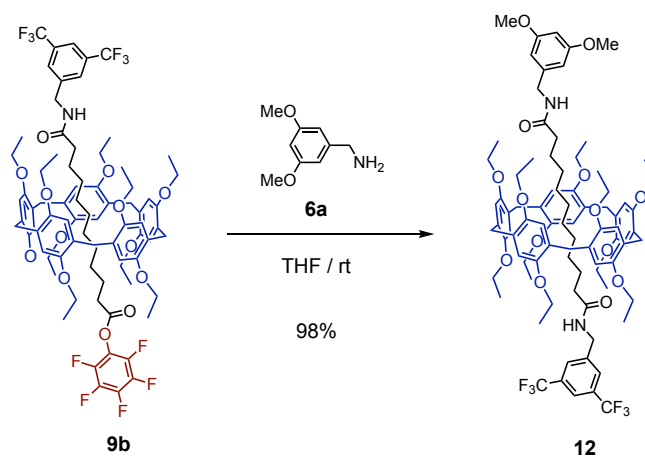
Preparation of compound 12

From 9a.

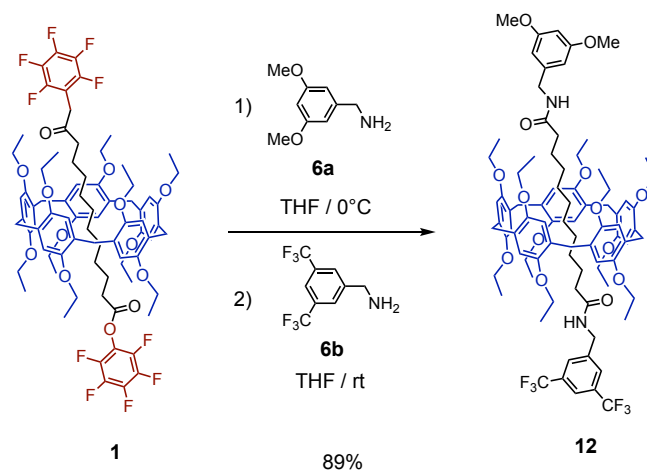


A mixture of **9a** (0.117 g, 0.08 mmol) and **6b** (0.024 g, 0.10 mmol) in anhydrous THF (1 mL) was stirred at rt overnight. The resulting mixture was filtered through a short plug (SiO₂, CHCl₃) and concentrated. Gel permeation chromatography (Biobeads SX-1, CHCl₃) afforded **12** (0.106 g, 93%).

From 9b.

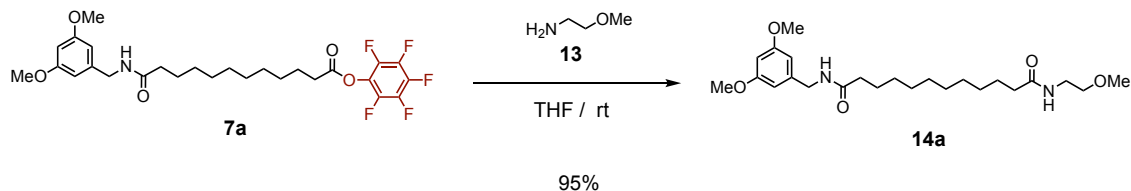


A mixture of **9b** (0.439 g, 0.29 mmol) and **6a** (0.059 g, 0.35 mmol) in anhydrous THF (3 mL) was stirred at rt overnight. The resulting mixture was filtered through a short plug (SiO₂, CH₂Cl₂ containing 2% MeOH) and concentrated. Column chromatography (SiO₂, CH₂Cl₂ containing 2% MeOH) followed by gel permeation chromatography (Biobeads SX-1, CH₂Cl₂) afforded **12** (0.419 g, 98%).

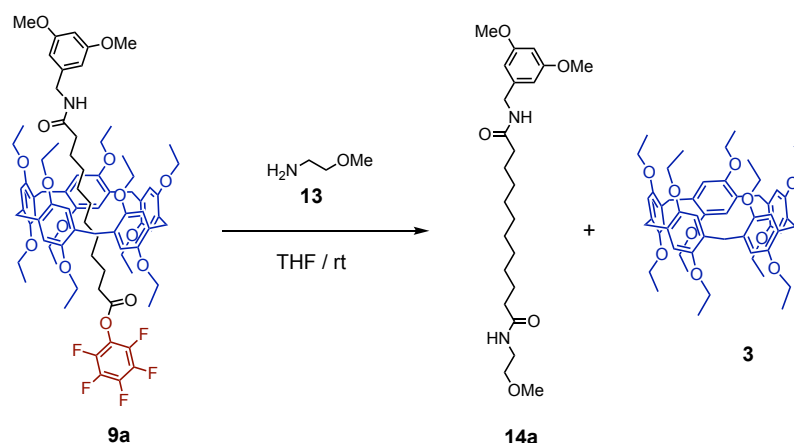
From **1** (one-pot strategy).

A solution of **1** (0.306 g, 0.21 mmol) and **6a** (0.035 g, 0.21 mmol) in anhydrous THF (3 mL) was stirred at 0°C under Ar. After 3h, **6b** (0.051 g, 0.21 mmol) was added. The resulting mixture was stirred at rt for 1 h and concentrated. Column chromatography (SiO_2 , Petroleum ether/diethyl ether: 1/1) followed by gel permeation chromatography (Biobeads SX-1, CHCl_3) afforded **10** (0.280 g, 89%).

12. Colorless solid (m.p.: 163°C). IR (neat): 1672 ($\text{C}=\text{O}$) cm^{-1} . ^1H NMR (500 MHz, CD_2Cl_2): $\delta = 7.87$ (broad s, 2H), 7.85 (broad s, 1H), 6.88 (s, 5H), 6.87 (s, 5H), 6.47 (d, $J = 2.3$ Hz, 2H), 6.38 (t, $J = 2.3$ Hz, 1H), 6.28 (t, $J = 6.1$ Hz, 1H), 5.93 (t, $J = 6$ Hz, 1H), 4.55 (dAB, $J = 15.4$, $J = 6.1$ Hz, 2H), 4.36 (d, $J = 4.8$ Hz, 2H), 3.99 - 3.91 (m, 10H), 3.89 - 3.82 (m, 10H), 3.80 (s, 6H), 3.72 (AB, $J = 12.4$ Hz, 10H), 1.80 (t, $J = 8.1$ Hz, 2H), 1.44 (t, $J = 7.0$ Hz, 15H), 1.39 (t, $J = 7.0$ Hz, 15H), 1.23 (m, 2H), 0.93 (m, 2H), 0.27 (m, 2H), 0.15 (m, 4H), -0.13 (m, 2H), -0.84 (m, 2H), -1.17 (m, 2H) ppm. ^{13}C NMR (100 MHz, CDCl_3): $\delta = 174.1$, 172.9 , 161.2 , 149.9 , 149.6 , 142.7 , 141.2 , 131.8 (q, $^2J_{\text{C-F}} = 33$ Hz), 128.8 , 128.4 , 127.9 (two peaks), 123.4 (q, $^1J_{\text{C-F}} = 273$ Hz), 121.2 (quint, $^3J_{\text{C-F}} = 3.8$ Hz), 115.1 , 114.5 , 105.9 , 98.9 , 64.2 , 63.6 , 55.3 , 43.6 , 42.6 , 36.9 , 36.5 , 30.4 (two peaks), 30.0 , 29.5 , 29.2 , 28.6 , 28.0 , 25.9 , 25.1 , 15.5 , 15.4 ppm. ^{19}F NMR (470 MHz, CDCl_3): $\delta = -62.8$ ppm. MALDI-TOF-MS: $m/z = 1495.63$ ($[\text{M}+\text{H}]^+$, calcd for $\text{C}_{85}\text{H}_{109}\text{F}_6\text{N}_2\text{O}_{14}$: 1495.78). Anal. (%) calcd for $\text{C}_{85}\text{H}_{108}\text{F}_6\text{N}_2\text{O}_{14}$ (1495.77): C, 68.25; H, 7.28; N, 1.87; found: C, 68.05; H, 7.34; N, 1.88.

Preparation of compound **14a**From **7a**.

A solution of **7a** (0.251 g, 0.46 mmol) and **13** (0.041 g, 0.55 mmol) in anhydrous THF (6 mL) was stirred at rt. After 3 h, the reaction mixture was concentrated. Column chromatography (SiO₂, CH₂Cl₂ containing 3% MeOH) gave compound **14a** (0.191 g, 95%).

From **9a**.

A solution of **9a** (0.172 g, 0.12 mmol) and **13** (0.010 g, 0.13 mmol) in anhydrous THF (1.5 mL) was stirred at rt. After 3 h, the reaction mixture was concentrated. Column chromatography (SiO₂, cyclohexane/CH₂Cl₂: 1/1 to CH₂Cl₂ containing 3% MeOH) gave compound **3** (0.098 g, 92%) and compound **14a** (0.049 g, 93%).

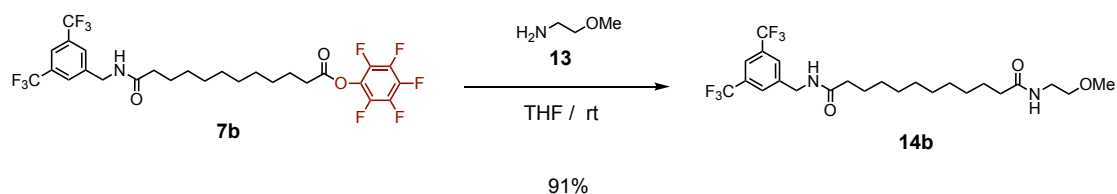
8. Analytical data identical to the one previously reported in the literature.²

14a. Colorless solid (m.p.: 119°C). IR (neat): 3301 (N-H), 1638 (C=O) cm⁻¹. ¹H NMR (500 MHz, CD₂Cl₂): δ = 6.41 (d, *J* = 2.3 Hz, 2H), 6.34 (t, *J* = 2.3 Hz, 1H), 5.95 (broad s, 1H), 5.85 (broad s, 1H), 4.32 (d, *J* = 5.9 Hz, 2H), 3.76 (s, 6H), 3.42-3.39 (m, 2H), 3.38-3.35 (m, 2H), 3.32 (s, 3H), 2.18 (t, *J* = 7.6 Hz, 2H), 2.12 (t, *J* = 7.6 Hz, 2H), 1.65-1.54 (m, 4H), 1.33-1.27 (m, 12H)

ppm. ^{13}C NMR (125 MHz, CD_2Cl_2): $\delta = 173.2, 173.1, 161.5, 141.8, 105.7, 99.4, 71.7, 58.9, 55.7, 43.7, 39.4, 37.0$ (two peaks), $29.8, 29.7$ (two peaks), $29.6, 26.2, 26.1$ ppm. MALDI-TOF-MS: $m/z = 437.18$ ($[\text{M}+\text{H}]^+$, calcd for $\text{C}_{24}\text{H}_{41}\text{N}_2\text{O}_5$: 437.30). Anal. (%) calcd for $\text{C}_{24}\text{H}_{40}\text{N}_2\text{O}_5$ (436.59): C, 66.03; H, 9.24; N, 6.42; found: C, 65.92; H, 9.28; N, 6.38.

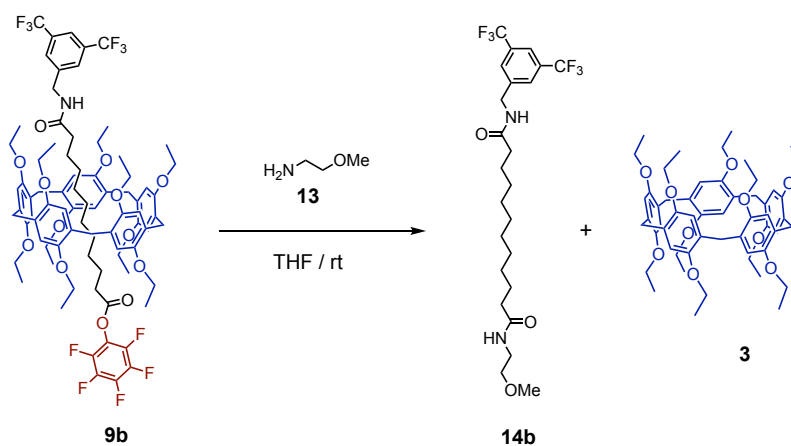
Preparation of compound **14b**

From **7b**.



A solution of **7b** (0.186 g, 0.30 mmol) and **13** (0.027 g, 0.36 mmol) in anhydrous THF (6 mL) was stirred at rt. After 3 h, the reaction mixture was concentrated. Column chromatography (SiO_2 , CH_2Cl_2 containing 3% MeOH) gave compound **14b** (0.140 g, 91%).

From **9b**.

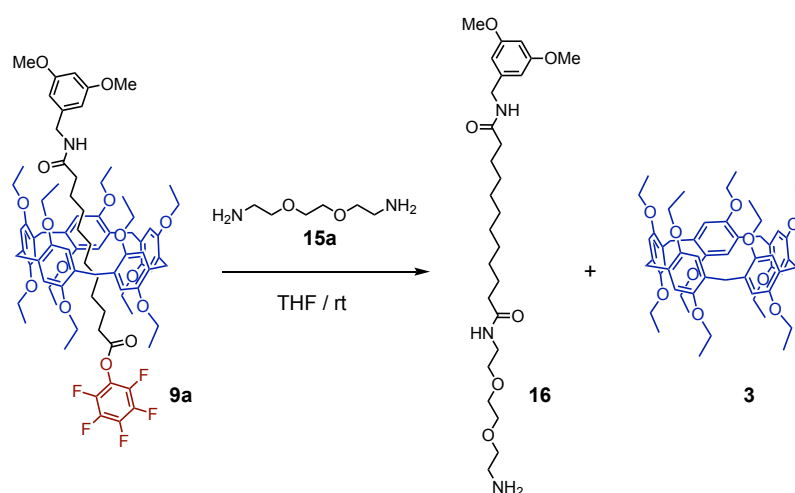


A solution of **9b** (0.106 g, 0.07 mmol) and **13** (0.006 g, 0.08 mmol) in anhydrous THF (1 mL) was stirred at rt. After 3 h, the reaction mixture was concentrated. Purification by column chromatography (SiO_2 , cyclohexane/ CH_2Cl_2 : 1/1 to CH_2Cl_2 containing 3% MeOH) afford **3** (0.060 g, 97%) and **14b** (0.033 g, 92%).

14b. Colorless solid (m.p.: 103°C). IR (neat): 3300 (NH), 1638 (C=O) cm^{-1} . ^1H NMR (500 MHz, CDCl_3): δ = 7.76 (broad s, 1H), 7.72 (broad s, 2H), 6.47-6.19 (broad m, 1H), 5.84 (broad s, 1H), 4.55 (m, 2H), 3.42 (m, 4H), 3.34 (m, 3H), 2.25 (m, 2H), 2.14 (m, 2H), 1.70-1.55 (m, 4H), 1.26 (broad s, 12H) ppm. ^{13}C NMR (125 MHz, CDCl_3): δ = 173.4, 173.1, 141.4, 131.7 (q, $^2J_{\text{C-F}} = 33$ Hz), 127.5, 123.1 (q, $^1J_{\text{C-F}} = 273$ Hz), 121.2, 71.1, 58.6, 42.4, 39.0, 36.6, 36.4, 29.3 (two peaks), 29.2, 25.8, 25.7 ppm. ^{19}F NMR (470 MHz, CDCl_3): δ = -62.9 ppm. MALDI-TOF-MS: m/z = 513.10 ($[\text{M}+\text{H}]^+$, calcd for $\text{C}_{24}\text{H}_{35}\text{F}_6\text{N}_2\text{O}_3$: 513.25), 535.06 ($[\text{M}+\text{Na}]^+$, calcd for $\text{C}_{24}\text{H}_{34}\text{F}_6\text{N}_2\text{O}_3\text{Na}$: 535.23). Anal. (%) calcd for $\text{C}_{24}\text{H}_{34}\text{F}_6\text{N}_2\text{O}_3$ (512.53): C, 56.24; H, 6.69; N, 5.47; found: C, 56.30; H, 6.74; N, 5.50.

Preparation of compounds 16 and 17.

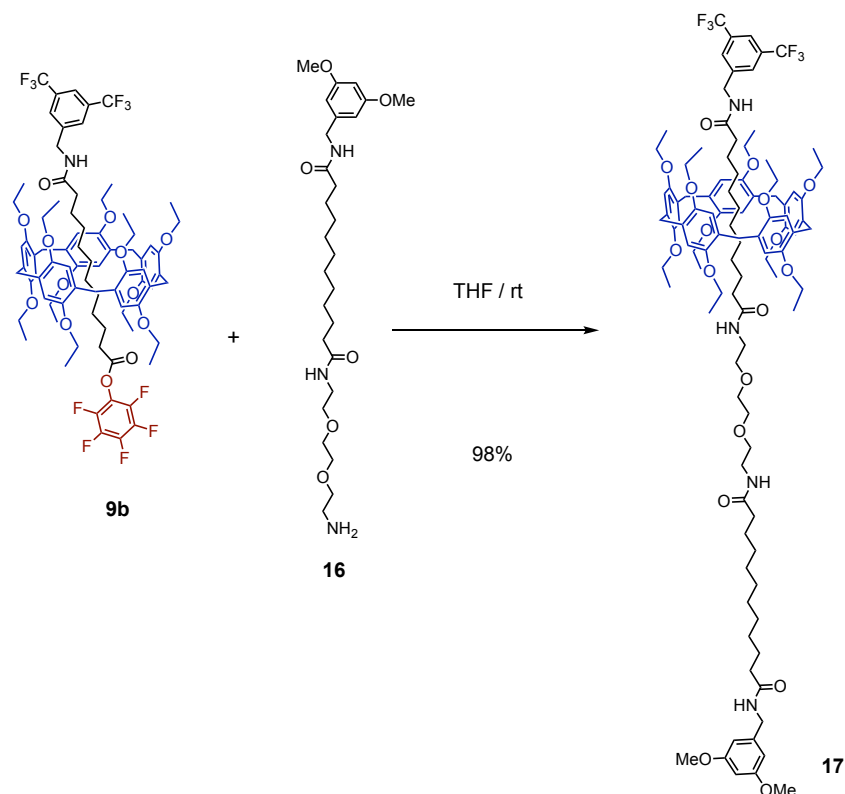
Compound 16.



A solution of **9a** (0.345 g, 0.24 mmol) and **15a** (0.178 g, 1.20 mmol) in anhydrous THF (3 mL) was stirred at rt for 1 h. The reaction mixture was filtered through a short plug (Al_2O_3 , CHCl_3 containing 5% MeOH) and concentrated. Column chromatography (Al_2O_3 , CHCl_3 to CHCl_3 containing 5% MeOH) followed by gel permeation chromatography (Biobeads SX-1, CHCl_3) gave **3** (0.212 g, 99%) and **16** (0.084 g, 69%). **16.** Pale yellow oil. IR (neat): 3287 (N-H), 1644 (C=O) cm^{-1} . ^1H NMR (400 MHz, CDCl_3): δ = 6.40 (broad s, 2H), 6.34 (broad s, 1H), 6.26 (broad s, 1H), 5.92 (broad s, 1H), 4.35 (d, $J = 5.7$ Hz, 2H), 3.76 (broad s, 6H), 3.62-3.58 (m, 4H), 3.56-3.48 (m, 4H), 3.42 (m, 2H), 2.86 (t, $J = 5$ Hz, 2H), 2.19 (t, $J = 7.7$ Hz, 2H), 2.15 (t, J

= 7.5 Hz, 2H), 1.61 (m, 4H), 1.25 (m, 12H) ppm. MALDI-TOF-MS: $m/z = 510.20$ ($[M+H]^+$, calcd for $C_{27}H_{48}N_3O_6$: 510.35).

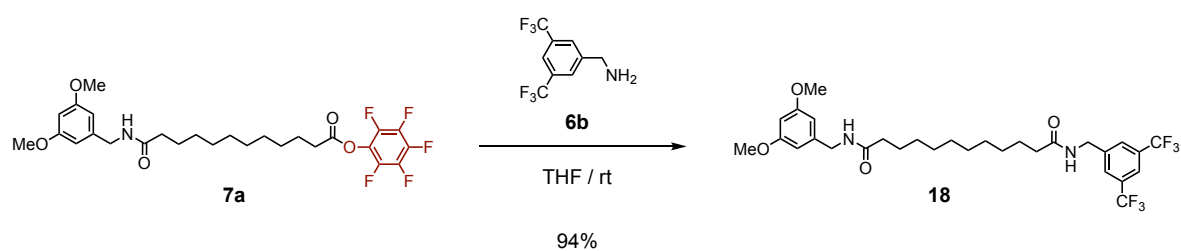
Compound 17.



A solution of **9b** (0.076 g, 0.05 mmol) and **16** (0.031 g, 0.06 mmol) in anhydrous THF (2 mL) was stirred at rt for 5 days. The resulting mixture was filtered through a short plug (SiO_2 , CH_2Cl_2 containing 4% MeOH) and concentrated. Column chromatography (SiO_2 , $CHCl_3$) followed by gel permeation chromatography (Biobeads SX-1, $CHCl_3$) afforded **17** (0.090 g, 98%). Colorless glassy product. IR (neat): 3300 (N-H), 1647 (C=O) cm^{-1} . 1H NMR (500 MHz, $CDCl_3$): $\delta = 7.78$ (s, 3H), 6.88 (s, 5H), 6.87 (s, 5H), 6.58 (t, $J = 6.1$ Hz, 1H), 6.43 (m, 2H), 6.35 (t, $J = 2.3$ Hz, 1H), 6.10 (m, 3H), 4.51 (dAB, $J = 15.5$, $J = 6.1$ Hz, 2H), 4.35 (dAB, $J = 19$ Hz, $J = 5.8$ Hz, 2H), 3.99-3.91 (m, 10H), 3.89-3.81 (m, 10H), 3.77 (s, 6H), 3.73 (AB, $J = 12.9$ Hz, 10H), 3.62 (s, 4H), 3.55 (t, $J = 5.4$ Hz, 4H), 3.45 (m, 4H), 1.97 (m, 2H), 1.91 (m, 4H), 1.63 (broad s, 2H), 1.44 (t, $J = 6.9$ Hz, 15H), 1.41 (t, $J = 6.9$ Hz, 15H), 1.25 (m, 2H), 1.14 (broad s, 4H), 0.80-0.38 (m, 22H), 0.03-(-0.20) (m, 4H) ppm. ^{13}C NMR (125 MHz, $CDCl_3$): $\delta = 173.9$, 173.4, 173.3, 173.2, 161.0, 149.8, 149.6, 142.3, 141.2, 131.7 (q, $^2J_{C-F} = 33$ Hz), 128.6, 128.4, 127.7 (two peaks), 123.3 (q, $^1J_{C-F} = 273$ Hz), 121.1 (quint, $^3J_{C-F} = 3.9$ Hz), 114.8, 114.5, 105.7,

99.0, 70.3 (2 peaks), 70.1, 64.0, 63.6, 55.3, 43.5, 42.5, 39.2, 39.1(broad), 36.7, 36.4, 29.9 (two peaks), 29.7, 29.4, 29.2, 29.1 (two peaks), 29.0, 28.8, 28.5, 25.7 (two peaks), 25.6, 25.3, 15.4 (two peaks) ppm. ^{19}F NMR (470 MHz, CDCl_3): $\delta = -62.7$ ppm. MALDI-TOF-MS: $m/z = 1838.05$ ($[\text{M}+\text{H}]^+$, calcd for: $\text{C}_{103}\text{H}_{143}\text{F}_6\text{N}_4\text{O}_{18}$: 1838.03). Anal. (%) calcd for $\text{C}_{103}\text{H}_{142}\text{F}_6\text{N}_4\text{O}_{18}$ (1838.24): C, 67.30; H, 7.79; N, 3.05; found: C, 67.13; H, 7.80; N, 2.88.

Preparation of compound 18

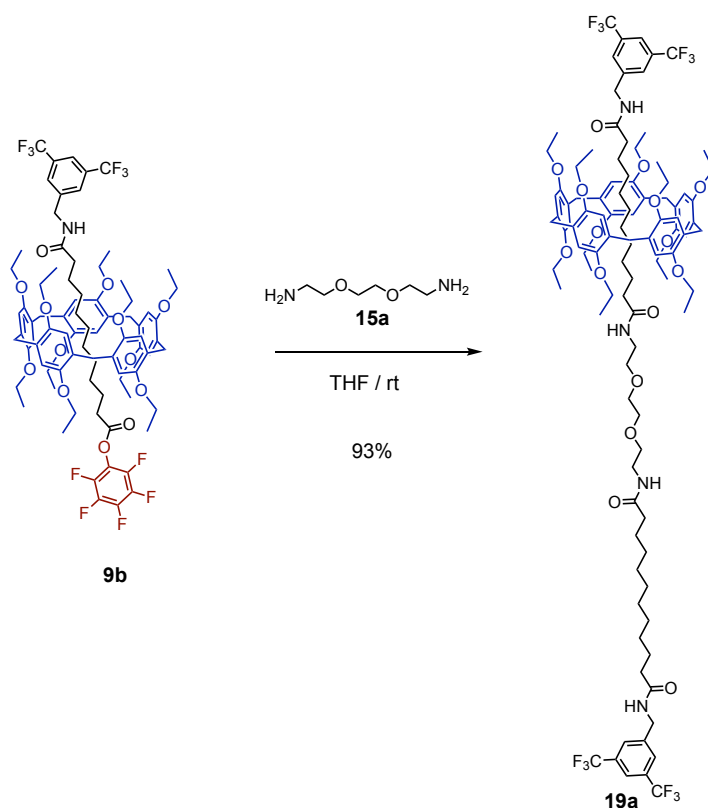


A mixture of **7a** (0.250 g, 0.46 mmol) and **6b** (0.134 g, 0.55 mmol) in anhydrous THF (4 mL) was stirred overnight at rt. The resulting mixture was filtered through a short plug (SiO_2 , CH_2Cl_2 /ethyl acetate: 7/3) and concentrated. Column chromatography (SiO_2 , CH_2Cl_2 /ethyl acetate: 7/3) gave compound **18** (0.262 g, 94%). Colorless solid (m.p.: 121°C). IR (neat): 3279 (N-H), 1644 (C=O) cm^{-1} . ^1H NMR (500 MHz, CD_2Cl_2): $\delta = 7.79$ (s, 1H), 7.75 (s, 2H), 6.39 (d, $J = 2.2$ Hz, 2H), 6.34 (t, $J = 2.2$ Hz, 1H), 6.26 (m, 1H), 5.87 (m, 1H), 4.50 (d, $J = 6.1$ Hz, 2H), 4.31 (d, $J = 5.9$ Hz, 2H), 3.75 (s, 6H), 2.23 (t, $J = 7.6$ Hz, 2H), 2.18 (t, $J = 7.6$ Hz, 2H), 1.65-1.58 (m, 4H), 1.35-1.23 (m, 12H) ppm. ^{13}C NMR (125 MHz, CD_2Cl_2): $\delta = 173.6$, 173.1, 161.5, 142.5, 141.7, 131.9 (q, $^2J_{\text{C-F}} = 33$ Hz), 128.1, 123.8 (q, $^1J_{\text{C-F}} = 273$ Hz), 121.5 (quint, $^3J_{\text{C-F}} = 3.9$ Hz), 105.7, 99.4, 55.7, 43.7, 42.8, 37.0, 36.8, 29.5, 26.1, 26.0 ppm. ^{19}F NMR (470 MHz, CD_2Cl_2): $\delta = -63.2$ ppm. MALDI-TOF-MS: $m/z = 605.51$ ($[\text{M}+\text{H}]^+$, calcd for $\text{C}_{30}\text{H}_{39}\text{F}_6\text{N}_2\text{O}_4$: 605.28). Anal. (%) calcd for $\text{C}_{30}\text{H}_{38}\text{F}_6\text{N}_2\text{O}_4$ (604.63): C, 59.59, H, 6.34, N, 4.63; found: C, 59.80, H, 6.44, N, 4.68.

General procedure for the preparation of [2]rotaxanes 19a-d et [3]rotaxanes 20e in solution.

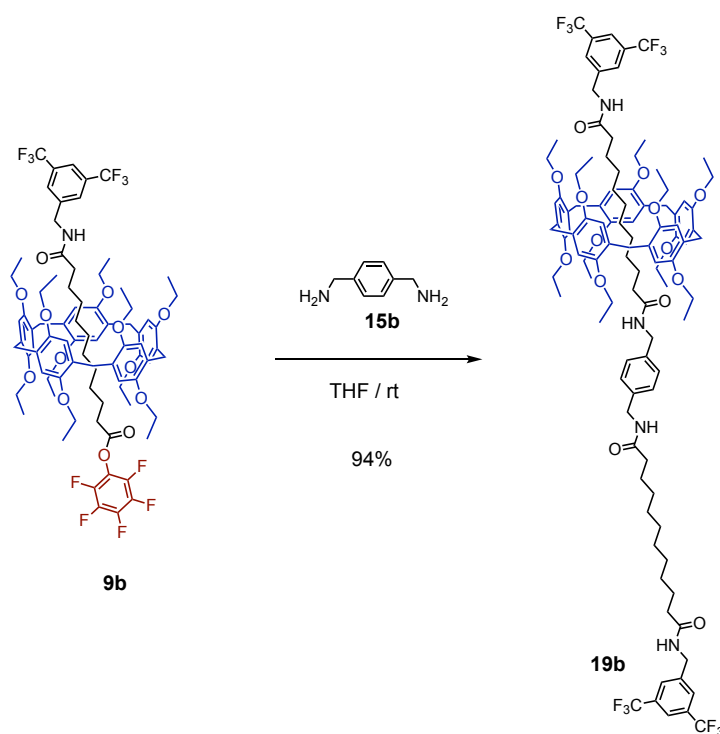
A mixture of **9b** (2.0 eq.) and the appropriate diamine reagent (**15a-e**, 1.0 eq.) in anhydrous THF (1 mL/110 mg of **9b**) was stirred at rt for 6 days (**19a-d**) or 2 days (**20e**). The resulting mixture was filtered through a short plug (SiO_2 , CH_2Cl_2 containing 5% MeOH), concentrated and purified by gel permeation chromatography (Biobeads SX-1, CHCl_3).

Compound 19a.



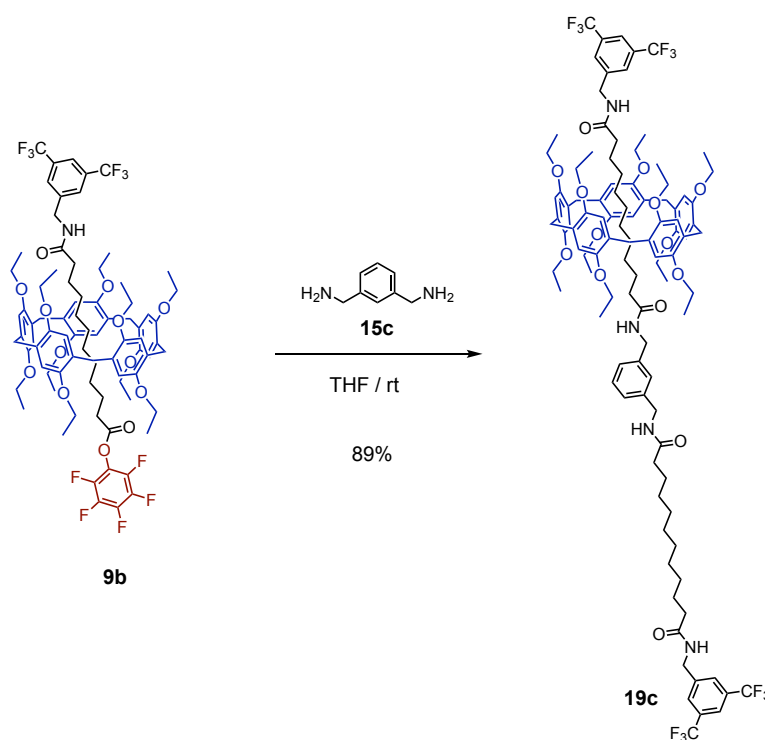
Prepared from **9b** (0.182 g, 0.12 mmol) and **15a** (0.009 g, 0.06 mmol) in anhydrous THF (1.5 mL) and purified to give **19a** as colorless glassy product (0.107 g, 93%). R (neat): 3300 (N-H), 1650 (C=O) cm^{-1} . ^1H NMR (500 MHz, CDCl_3): δ = 7.79 (broad s, 6H), 6.88 (s, 10H), 6.39 (m, 2H), 6.02 (m, 2H), 4.54 (m, 4H), 4.00-3.92 (m, 10H), 3.90-3.82 (m, 10H), 3.73 (s, 10H), 3.63 (broad s, 4H), 3.56 (m, 4H), 3.47 (m, 4H), 2.03 (m, 4H), 1.69 (broad s, 4H), 1.42 (t, J = 6.9 Hz, 30H), 1.36 (m, 6H), 0.96-(-0.24) (m, 26H) ppm. ^{13}C NMR (125 MHz, CDCl_3): δ = 173.9, 173.4, 149.8, 142.2, 131.9 (q, $^2J_{\text{C-F}}$ = 33 Hz), 128.6, 127.8 (two peaks), 123.4 (q, $^1J_{\text{C-F}}$ = 273 Hz), 121.3 (quint, $^3J_{\text{C-F}}$ = 3.9 Hz), 114.8, 70.4, 70.1, 63.9, 42.6, 39.2, 36.9, 36.6, 29.9, 29.8, 29.7, 29.5, 29.3, 28.9, 28.6, 25.8, 25.4, 15.5 ppm. ^{19}F NMR (470 MHz, CDCl_3): δ = -62.8 ppm. MALDI-TOF-MS: m/z = 1913.97 ($[\text{M}+\text{H}]^+$, calcd for: $\text{C}_{103}\text{H}_{137}\text{F}_{12}\text{N}_4\text{O}_{16}$: 1913.98). Anal. (%) calcd for $\text{C}_{103}\text{H}_{136}\text{F}_{12}\text{N}_4\text{O}_{16}$ (1914.18): C, 64.63; H, 7.16; N, 2.93; found: C, 64.68; H, 7.22; N, 2.73.

Compound 19b.



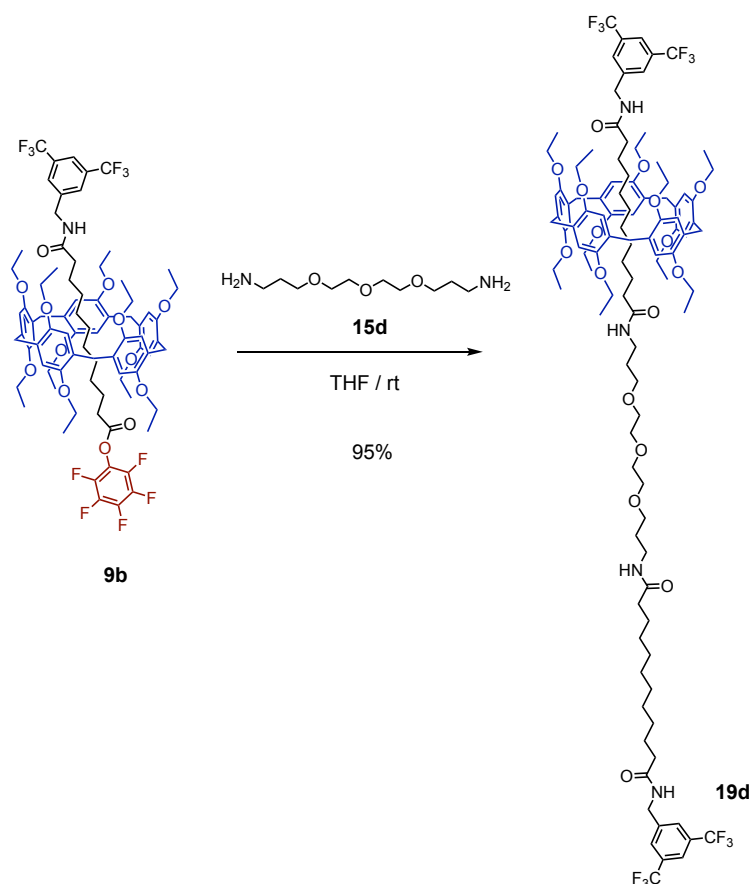
Prepared from **9b** (0.182 g, 0.12 mmol) and **15b** (0.008 g, 0.06 mmol) in anhydrous THF (1.5 mL) and purified to give **19b** as a colorless glassy product (0.107 g, 94%). IR (neat): 3301 (N-H) cm^{-1} , 1649 (C=O) cm^{-1} . ^1H NMR (500 MHz, CDCl_3): δ = 7.79 (s, 2H), 7.78 (s, 4H), 7.27 (broad s, 4H), 6.88 (s, 10H), 6.29 (broad s, 2H), 5.94 (broad s, 2H), 4.55 (m, 4H), 4.44 (broad s, 4H), 3.94 (m, 10H), 3.85 (m, 10H), 3.73 (s, 10H), 2.04 (broad s, 4H), 1.73 (broad s, 2H), 1.41 (t, J = 6.9 Hz, 32H), 1.63-1.22 (broad m, 6H), 0.79 (broad s, 12H), 0.68-(-0.33) (broad m, 14H) ppm. ^{13}C NMR (125 MHz, CDCl_3): δ = 173.9, 173.3, 149.9, 142.1, 138.0, 132.0 (q, $^2J_{\text{C-F}}$ = 33 Hz), 128.7, 128.2, 127.9 (two peaks), 123.4 (q, $^1J_{\text{C-F}}$ = 271 Hz), 121.4 (quint, $^3J_{\text{C-F}}$ = 3.7 Hz), 114.9, 64.0, 43.4, 42.7, 36.9, 36.6, 29.9, 29.8, 29.6, 29.4, 29.3, 29.0, 28.7, 25.9, 25.5, 15.6 ppm. ^{19}F NMR (376 MHz, CDCl_3): δ = -62.8 ppm. MALDI-TOF-MS: m/z = 1901.98 ($[\text{M}+\text{H}]^+$), calcd for: $\text{C}_{105}\text{H}_{133}\text{F}_{12}\text{N}_4\text{O}_{14}$: 1901.96). Anal. (%) calcd for $\text{C}_{105}\text{H}_{132}\text{F}_{12}\text{N}_4\text{O}_{14}$ (1902.17): C, 66.30, H, 7.00, N, 2.95; found: C, 66.22, H, 6.99, N, 2.97.

Compound 19c.



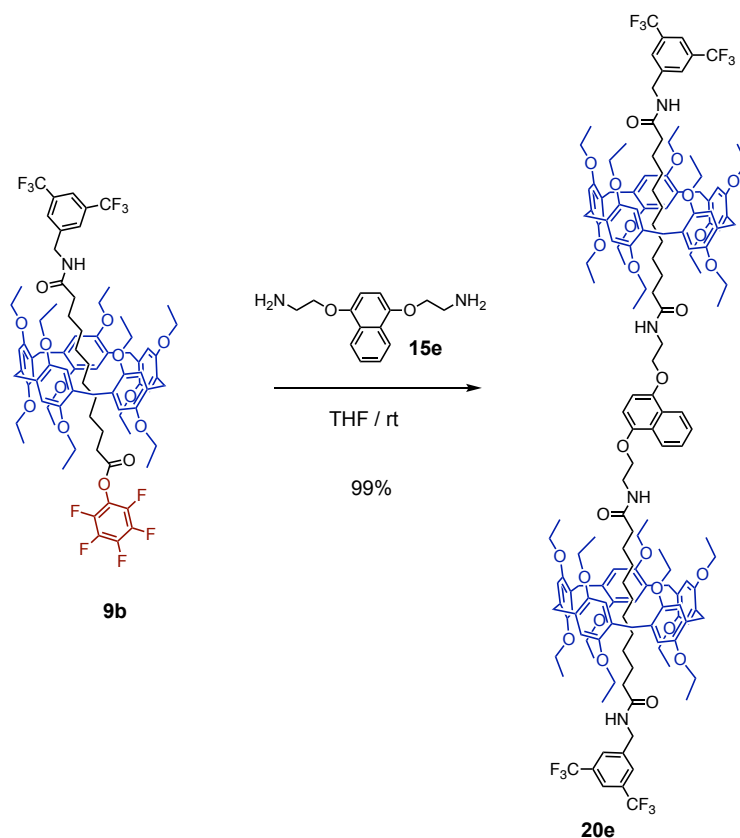
Prepared from **9b** (0.182 g, 0.12 mmol) and **15c** (0.008 g, 0.06 mmol) in anhydrous THF (1.5 mL) and purified to give **19c** as a colorless glassy product (0.102 g, 89%). IR (neat): 3301 (N-H) cm^{-1} , 1651 (C=O) cm^{-1} . ^1H NMR (500 MHz, CDCl_3): δ = 7.90-7.65 (broad m, 6H), 7.33 (m, 1H), 7.22 (broad s, 3H), 6.88 (s, 10H), 6.39-6.11 (broad m, 2H), 5.94 (broad s, 2H), 4.65-4.49 (broad m, 4H), 4.45 (broad s, 4H), 3.94 (m, 10H), 3.85 (m, 10H), 3.73 (s, 10H), 2.23 (broad s, 4H), 1.91 (broad s, 2H), 1.66 (broad s, 4H), 1.40 (broad s, 30H), 1.34-1.00 (broad m, 16H), 0.52-0.20 (m, 6H), 0.04-(-0.37) (broad m, 4H), -0.97 (broad s, 2H), -1.35 (broad s, 2H) ppm. ^{13}C NMR (125 MHz, CDCl_3): δ = 173.3, 149.9, 132.0 (q, $^2J_{\text{C-F}} = 33$ Hz), 129.3, 128.7 (broad), 127.9 (broad), 126.9, 123.4 (q, $^1J_{\text{C-F}} = 271$ Hz), 121.4 (broad), 115.3 (broad), 114.6 (broad), 64.3, 63.7, 43.6, 42.7, 37.0, 36.6, 29.3, 15.6 ppm. ^{19}F NMR (376 MHz, CDCl_3): δ = -62.8 ppm. MALDI-TOF-MS: m/z = 1901.95 ($[\text{M}+\text{H}]^+$, calcd for: $\text{C}_{105}\text{H}_{133}\text{F}_{12}\text{N}_4\text{O}_{14}$: 1901.96). Anal. (%) calcd for $\text{C}_{105}\text{H}_{132}\text{F}_{12}\text{N}_4\text{O}_{14}$ (1902.17): C, 66.30, H, 7.00, N, 2.95; found: C, 66.01, H, 7.00, N, 2.99.

Compound 19d.



Prepared from **9b** (0.182 g, 0.12 mmol) and **15d** (0.013 g, 0.06 mmol) in anhydrous THF (1.5 mL) and purified to give **19d** as a colorless glassy product (0.113 g, 95%). IR (neat): 3289 (N-H), 1646 (C=O) cm^{-1} . ^1H NMR (500 MHz, CDCl_3): δ = 7.79 (s, 6H), 6.88 (s, 10H), 6.37 (m, 2H), 6.17 (broad s, 2H), 4.54 (dAB, J = 15.5, J = 6.1 Hz, 4H), 3.98-3.92 (m, 10H), 3.88-3.82 (m, 10H), 3.73 (s, 10H), 3.65 (m, 4H), 3.60 (m, 4H), 3.52 (t, J = 5.7 Hz, 4H), 3.32 (m, 4H), 2.04 (m, 4H), 1.74 (m, 4H), 1.67 (broad s, 4H), 1.42 (t, J = 7.0 Hz, 36H), 0.95-(-0.32) (m, 26H) ppm. ^{13}C NMR (125 MHz, CDCl_3): δ = 174.0, 173.3 (two peaks), 149.8, 142.3, 131.9 (q, $^2J_{\text{C-F}}$ = 33 Hz), 128.7, 127.9 (two peaks), 123.4 (q, $^1J_{\text{C-F}}$ = 271 Hz), 121.3 (m), 114.9, 70.6, 70.3, 70.0, 64.0, 42.6, 37.9 (two peaks), 36.9, 36.6, 29.9, 29.6, 29.4, 29.3, 28.8, 28.5, 26.0, 25.4, 15.5 ppm. ^{19}F NMR (376 MHz, CDCl_3): δ = -62.8 ppm. MALDI-TOF-MS: m/z = 1985.98 ($[\text{M}+\text{H}]^+$, calcd for: $\text{C}_{107}\text{H}_{145}\text{F}_{12}\text{N}_4\text{O}_{17}$: 1986.04). Anal. (%) calcd for $\text{C}_{107}\text{H}_{144}\text{F}_{12}\text{N}_4\text{O}_{17}$ (1986.29): C, 64.70; H, 7.31; N, 2.82; found: C, 64.69; H, 7.37; N, 2.82.

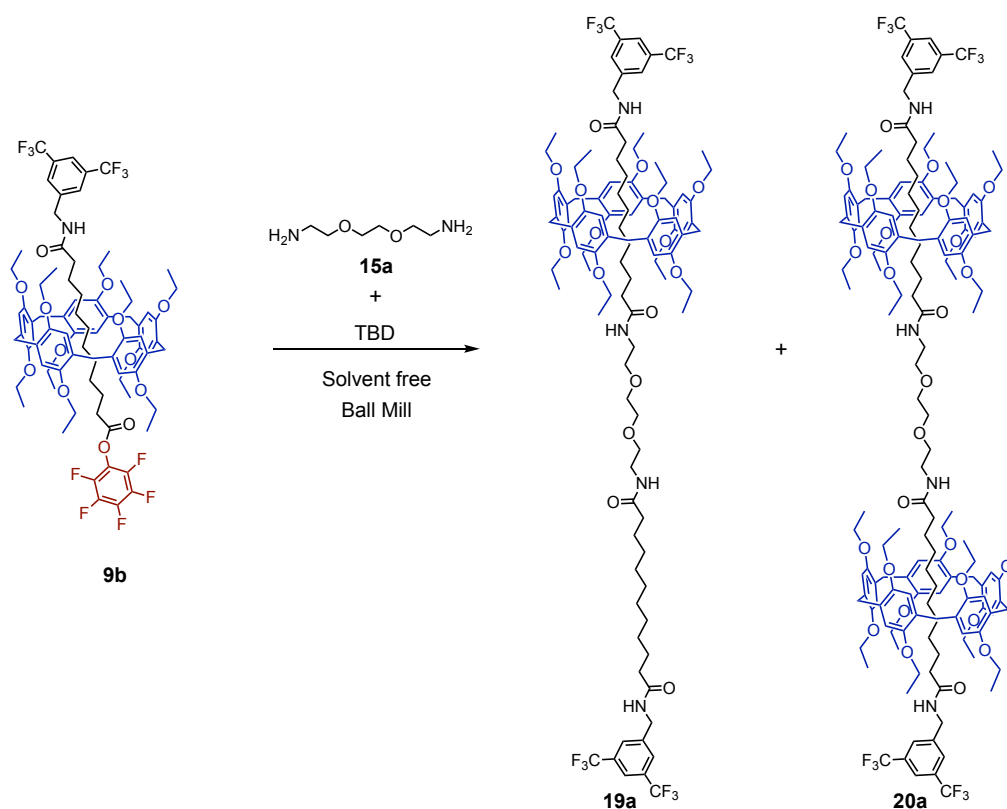
Compound 20e.



Prepared from **9b** (0.393 g, 0.26 mmol) and **15e** (0.032 g, 0.13 mmol) in anhydrous THF (3.5 mL) and purified to give **20e** as a pink solid product (0.374 g, 99%). (m.p.: 110°C). IR (neat): 3387 (N-H), 1668 (C=O) cm^{-1} . ^1H NMR (500 MHz, CDCl_3): δ = 8.38 (m, 2H), 7.85 (s, 4H), 7.84 (s, 2H), 7.59 (m, 2H), 6.91 (s, 10H), 6.90 (s, 10H), 6.77 (s, 2H), 6.27 (s, 2H), 6.19 (s, 2H), 4.58 (dAB, J = 15.6, J = 4.2 Hz, 4H), 4.23 (s, 4H), 4.02-3.82 (m, 44H), 3.76 (AB, J = 13.3 Hz, 20H), 1.70 (m, 4H), 1.42 (m, 64H), 0.72 (m, 4H), 0.25-0.08 (m, 12H), -0.09 (m, 8H), -0.56 (m, 4H), -0.80 (m, 4H) ppm. ^{13}C NMR (125 MHz, CDCl_3): δ = 174.0, 173.7, 149.9, 149.6, 148.7, 142.4, 131.9 (q, $^2J_{\text{C-F}}$ = 33 Hz), 128.8, 128.6, 127.9 (two peaks), 126.4, 126.2, 123.4 (q, $^1J_{\text{C-F}}$ = 271 Hz), 121.9, 121.3 (m), 115.1, 114.7, 104.5, 67.7, 64.1, 63.8, 42.7, 39.3, 36.9, 36.7, 30.5, 30.4, 29.6 (two peaks), 29.3, 29.1 (two peaks), 28.5, 28.4, 25.6, 25.4, 15.6, 15.5 ppm. ^{19}F NMR (470 MHz, CDCl_3): δ = -62.7 ppm. MALDI-TOF-MS: m/z = 2902.42 ($[\text{M}+\text{H}]^+$, calcd for: $\text{C}_{166}\text{H}_{209}\text{F}_{12}\text{N}_4\text{O}_{26}$: 2902.50). Anal. (%) calcd for $\text{C}_{166}\text{H}_{208}\text{F}_{12}\text{N}_4\text{O}_{26}$ (2903.43): C, 68.67, H, 7.22, N, 1.93; found: 68.26, H, 7.21, N, 1.99.

General procedure for the preparation of [2]rotaxanes 19a-c et [3]rotaxanes 20a-c in the solid state. Compound **9b** (2.2 eq.), the appropriate diamine reagent (**15a-c**, 1.0 eq.) and TBD (2.0 eq.) were placed in a stainless-steel vial containing four stainless-steel balls. The resulting mixture was mixed in a Retsch MM400 mill at 30 Hz for 2h. The crude was filtered through a short plug (SiO₂, CHCl₃ containing 5% MeOH), concentrated and purified by gel permeation chromatography (Biobeads SX-1, CHCl₃).

Compound 19a et 20a.

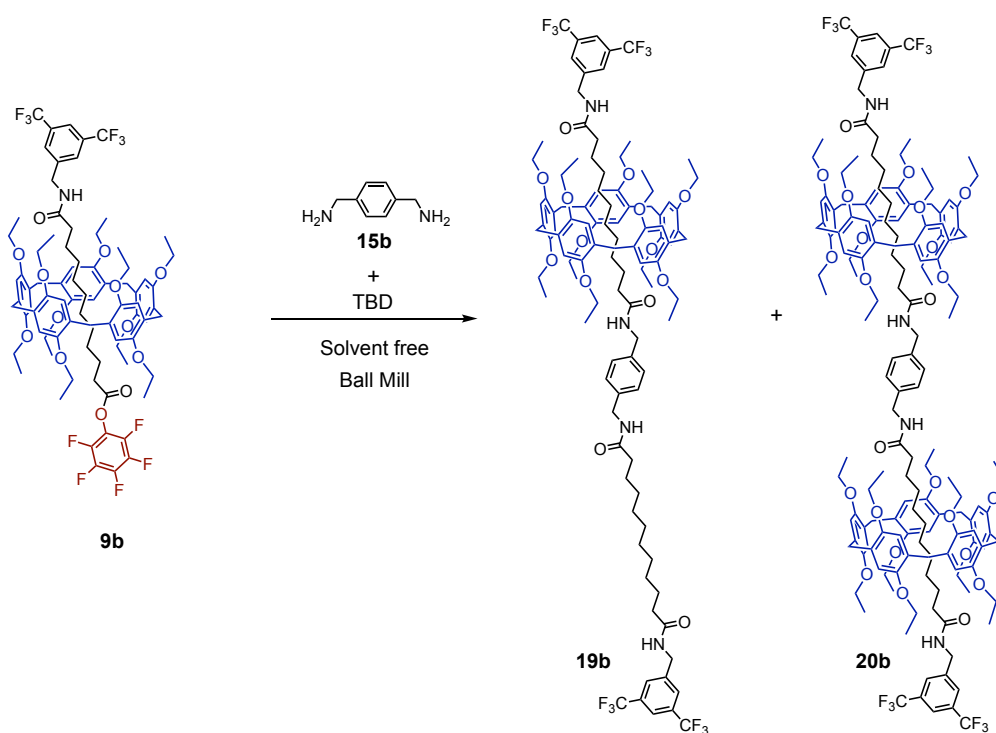


Prepared from **9b** (0.400 g, 0.26 mmol), **15a** (0.018 g, 0.12 mmol) and TBD (0.033 g, 0.24 mmol) and purified to give **19a** (0.165 g, 72%) and **20a** (0.081 g, 24%).

20a. Colorless glassy product. IR (neat): 1672 (C=O) cm⁻¹. ¹H NMR (500 MHz, CDCl₃): δ = 7.86 (s, 4H), 7.83 (s, 2H), 6.89 (s, 20H), 6.33 (t, *J* = 6.1 Hz, 2H), 5.93 (t, *J* = 5.4 Hz, 2H), 4.56 (dAB, *J* = 15.5, *J* = 6.1 Hz, 4H), 4.01-3.83 (m, 40H), 3.75 (AB, *J* = 12.5 Hz, 20H), 3.66 (s, 4H), 3.60 (t, *J* = 5.4 Hz, 4H), 3.50 (q, *J* = 5.4 Hz, 4H), 1.93 (t, *J* = 8.0 Hz, 4H), 1.48 (t, *J* = 6.9 Hz, 30H), 1.38 (t, *J* = 6.9 Hz, 30H), 1.18-1.10 (m, 8H), 0.57-0.37 (m, 12H), -0.07 (m, 4H), (-0.23)-(-0.42) (m, 4H), (-1.00)-(-1.12) (m, 4H), (-1.42)-(-1.53) (m, 4H) ppm. ¹³C NMR (125 MHz, CDCl₃): δ = 174.3, 173.2, 150.0, 149.7, 142.7, 131.9 (q, ²*J*_{C-F} = 33 Hz), 128.9, 128.5, 128.0, 123.5 (q, ¹*J*_{C-F} = 273 Hz), 121.3 (m), 115.3, 114.4, 70.4, 70.3, 64.4, 63.5, 42.6, 39.3, 36.9, 36.6,

30.5 (two peaks), 30.4, 29.8, 29.3, 28.5, 27.9, 26.0, 25.1, 15.6, 15.5 ppm. ^{19}F NMR (470 MHz, CDCl_3): $\delta = -62.8$ ppm. MALDI-TOF-MS: $m/z = 2804.09$ ($[\text{M}+\text{H}]^+$, calcd for: $\text{C}_{158}\text{H}_{207}\text{F}_{12}\text{N}_4\text{O}_{26}$: 2804.48). Anal. (%) calcd for $\text{C}_{158}\text{H}_{206}\text{F}_{12}\text{N}_4\text{O}_{26}$ (2805.32): C, 67.65, H, 7.40, N, 2.00; found: 67.44, H, 7.40, N, 1.97.

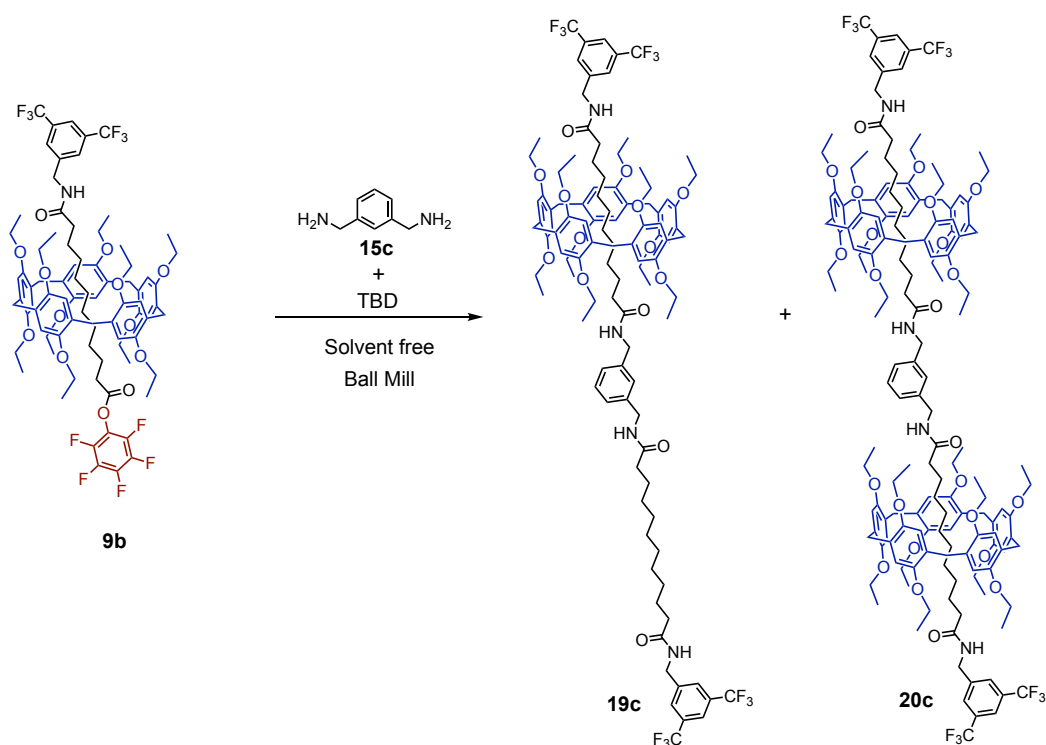
Compound 19b et 20b.



Prepared from **9b** (0.166 g, 0.11 mmol) and **15b** (0.007g, 0.05 mmol) and TBD (0.014 g, 0.10 mmol) and purified to give **19b** (0.047 g, 50%) and **20b** (0.066 g, 47%).

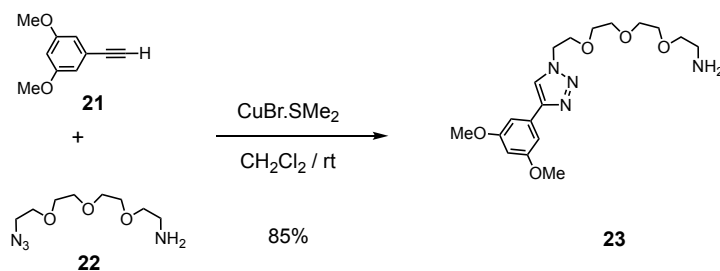
20b: Colorless glassy product. IR (neat): 1672 (C=O) cm^{-1} . ^1H NMR (500 MHz, CDCl_3): $\delta = 7.86$ (s, 4H), 7.84 (s, 2H), 7.34 (s, 4H), 6.90 (s, 20H), 6.32 (s, 2H), 5.94 (s, 2H), 4.64-4.45 (m, 8H), 4.03-3.82 (m, 40H), 3.76 (AB, $J = 13.8$ Hz, 20H), 1.89 (m, 4H), 1.46 (t, $J = 6.9$ Hz, 30H), 1.43 (t, $J = 6.9$ Hz, 30H), 1.26 (m, 4H), 1.03 (broad s, 4H), 0.35-0.17 (m, 12H), 0.02-(-0.20) (m, 8H), -0.86 (broad s, 4H), -1.19 (broad s, 4H) ppm. ^{13}C NMR (125 MHz, CDCl_3): $\delta = 174.1$, 173.1, 149.9, 149.7, 142.6, 138.2, 131.9 (q, $^2J_{\text{C-F}} = 33$ Hz), 128.8, 128.5, 128.1, 127.9 (two peaks), 123.4 (q, $^1J_{\text{C-F}} = 273$ Hz), 121.3 (quint, $^3J_{\text{C-F}} = 3.8$ Hz), 115.2, 114.5, 64.2, 63.6, 43.3, 42.6, 37.0, 36.6, 30.5, 30.4, 30.0, 29.5, 29.3, 28.7, 28.1, 26.0, 25.2, 15.6, 15.5 ppm. ^{19}F NMR (470 MHz, CDCl_3): $\delta = -62.7$ ppm. MALDI-TOF-MS: $m/z = 2791.99$ ($[\text{M}]^+$, calcd for: $\text{C}_{160}\text{H}_{202}\text{F}_{12}\text{N}_4\text{O}_{24}$: 2791.45). Anal. (%) calcd for $\text{C}_{160}\text{H}_{202}\text{F}_{12}\text{N}_4\text{O}_{24}$ (2793.32): C, 68.80, H, 7.29, N, 2.00; found: C, 68.89, H, 7.35, N, 1.97.

Compound 19c et 20c.

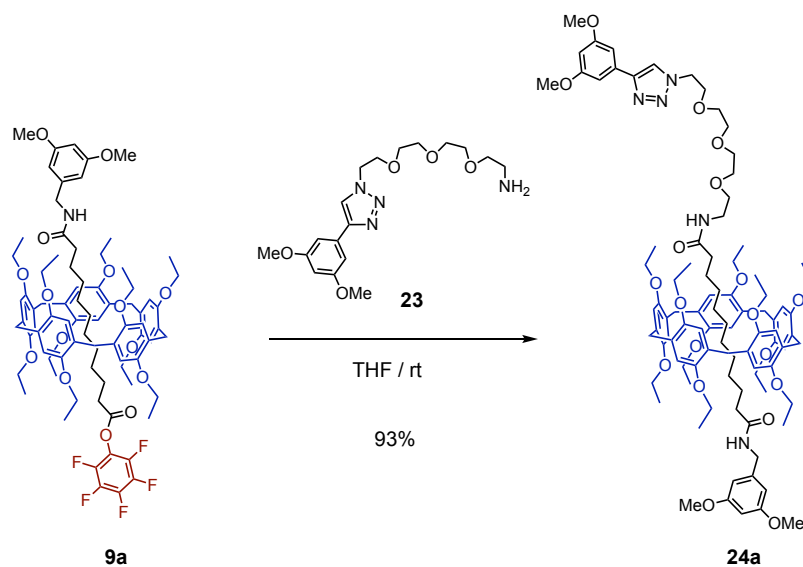


Prepared from **9b** (0.166 g, 0.11 mmol), **15c** (0.007 mg, 0.05 mmol) and TBD (0.014 g, 0.10 mmol) and purified to give **20c** (0.028 g, 29%) and **20c** (0.095 g, 68%).

Data for 20c. Colorless glassy product. IR (neat): 3302 (N-H) cm^{-1} , 1650 (C=O) cm^{-1} . ^1H NMR (500 MHz, CDCl_3): δ = 7.87 (s, 4H), 7.84 (s, 2H), 7.39 (t, J = 7.7 Hz, 1H), 7.30-7.28 (m, 3H), 6.91 (s, 10H), 6.90 (s, 10H), 6.33 (t, J = 6.2 Hz, 2H), 5.96 (t, J = 5.9 Hz, 2H), 4.64-4.47 (m, 8H), 4.01-3.84 (m, 40H), 3.76 (AB, J = 12.6 Hz, 20H), 1.94 (t, J = 8.0 Hz, 4H), 1.47 (t, J = 6.9 Hz, 30H), 1.40 (t, J = 6.9 Hz, 30H), 1.22 (t, J = 8.0 Hz, 4H), 1.14-1.07 (m, 4H), 0.41-0.27 (m, 12H), -0.04 (m, 4H), (-0.09)-(-0.26) (m, 4H), (-0.86)-(-0.98) (m, 4H), (-1.23)-(-1.35) (m, 4H) ppm. ^{13}C NMR (125 MHz, CDCl_3): δ = 174.2, 173.1, 145.0, 149.7, 142.7, 139.4, 131.9 (q, $^2J_{\text{C-F}}$ = 33 Hz), 129.2, 128.8, 128.5, 128.0, 127.9, 127.5, 126.7, 123.4 (q, $^1J_{\text{C-F}}$ = 273 Hz), 121.3 (quint, $^3J_{\text{C-F}}$ = 3.8 Hz), 115.2, 114.6, 64.3, 63.6, 43.5, 42.6, 37.0, 36.6, 30.5, 30.4, 30.1, 29.6, 29.3, 28.6, 28.0, 26.0, 25.2, 15.6, 15.5 ppm. ^{19}F NMR (470 MHz, CDCl_3): δ = -62.8 ppm. MALDI-TOF-MS: m/z = 2792.17 ($[\text{M}+\text{H}]^+$, calcd for: $\text{C}_{160}\text{H}_{203}\text{F}_{12}\text{N}_4\text{O}_{24}$: 2792.45). Anal. (%) calcd for $\text{C}_{160}\text{H}_{202}\text{F}_{12}\text{N}_4\text{O}_{24}$ (2793.32): C, 68.80, H, 7.29, N, 2.00; found: C, 68.85, H, 7.39, N, 1.96.

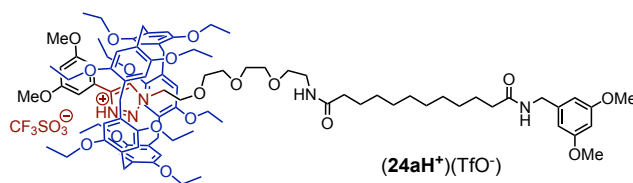
Preparation of compound **23**

$\text{CuBr}\cdot\text{SMe}_2$ (0.082 g, 0.40 mmol) was added to a solution of **21** (0.389 g, 2.40 mmol) and **22** (0.437 g, 2.00 mmol) and in anhydrous CH_2Cl_2 (8 mL) was stirred for 3h at rt. The reaction mixture was filtered through a short plug (Al_2O_3 , CH_2Cl_2) and concentrated. Column chromatography (Al_2O_3 , CH_2Cl_2 containing 3% MeOH) gave **23** (0.647 g, 85 %). Yellow oil product. IR (neat): 1595 (C=C) cm^{-1} . ^1H NMR (400 MHz, CDCl_3): δ = 7.97 (s, 1H), 6.99 (d, J = 2.3 Hz, 2H), 6.42 (t, J = 2.3 Hz, 1H), 4.56 (t, J = 5.0 Hz, 2H), 3.89 (t, J = 5.0 Hz, 2H), 3.82 (s, 6H), 3.62-3.54 (m, 8H), 3.44 (t, J = 5.0 Hz, 2H), 2.81 (t, J = 5.0 Hz, 2H), 1.96 (broad s, 2H) ppm. ^{13}C NMR (125 MHz, CD_2Cl_2): δ = 161.6, 147.5, 133.2, 121.7, 121.6, 103.8, 100.3 (two peaks), 73.8, 72.2, 70.9 (two peaks), 70.8, 70.7, 70.5, 69.8, 55.7, 51.6, 50.7, 42.2 ppm. MALDI-TOF-MS: m/z = 381.21 ($[\text{M}+\text{H}]^+$, calcd for $\text{C}_{18}\text{H}_{29}\text{N}_4\text{O}_5$: 381.21).

Preparation of compound **24a**

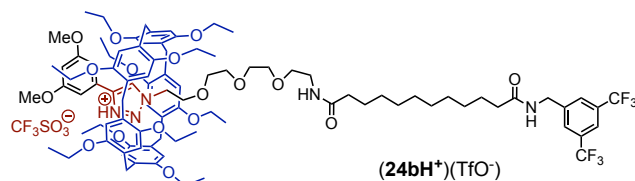
containing 1% MeOH) and gel permeation chromatography (Biobeads SX-1, CH₂Cl₂) gave **24b** (0.190 g, 79%). Colorless glassy product. IR (neat): 1652 (C=O) cm⁻¹. ¹H NMR (400 MHz, CDCl₃): δ = 7.85 (m, 3H), 7.82 (broad s, 1H), 7.03 (d, J = 2.3 Hz, 2H), 6.88 (s, 5H), 6.87 (s, 5H), 6.45 (t, J = 2.3 Hz, 1H), 6.34 (t, J = 6.2 Hz, 1H), 6.01 (t, J = 5.2 Hz, 1H), 4.56 (dAB, J = 15.4, J = 6.2 Hz, 2H), 4.31 (m, 2H), 3.98-3.81 (m, 26H), 3.74 (AB, J = 12.4 Hz, 10H), 3.64 (m, 2H), 3.60-3.51 (m, 10H), 3.45 (m, 2H), 1.99 (t, J = 8.0 Hz, 2H), 1.44 (t, J = 6.9 Hz, 15H), 1.38 (t, J = 6.9 Hz, 15H), 1.31-1.25 (m, 2H), 1.14 (t, J = 8.0 Hz, 2H), 0.77-0.59 (m, 4H), 0.53-0.45 (m, 2H), -0.03 (quint, J = 8.0 Hz, 2H), (-0.20)-(-0.40) (m, 2H), (-0.95)-(-1.09) (m, 2H), (-1.38)-(-1.50) (m, 2H) ppm. ¹³C NMR (125 MHz, CDCl₃): δ = 174.3, 173.1, 161.3, 150.0, 149.6, 147.4, 142.7, 132.8, 131.9 (q, ² J_{C-F} = 33 Hz), 128.9, 128.4, 127.9 (two peaks), 123.4 (q, ¹ J_{C-F} = 273 Hz), 121.2, 121.2 (m), 115.3, 114.4, 103.9, 100.2, 70.6 (two peaks), 70.5, 70.3, 70.2, 69.2, 64.3, 63.5, 55.6, 50.1, 42.6, 39.2, 36.9, 36.6, 30.4 (two peaks), 29.9, 29.3, 28.4, 27.8, 26.0, 25.0, 15.5, 15.4 ppm. ¹⁹F NMR (470 MHz, CDCl₃): δ = -62.7 ppm. MALDI-TOF-MS: m/z = 1708.76 ([M+H]⁺, calcd for C₉₄H₁₂₄F₆N₅O₁₇: 1708.89). Anal. (%) calcd for C₉₄H₁₂₃F₆N₅O₁₇ (1709.00): C, 66.06, H, 7.25, N, 4.10; found: C, 65.75, H, 7.31, N, 4.07.

Preparation of compound 24aH⁺



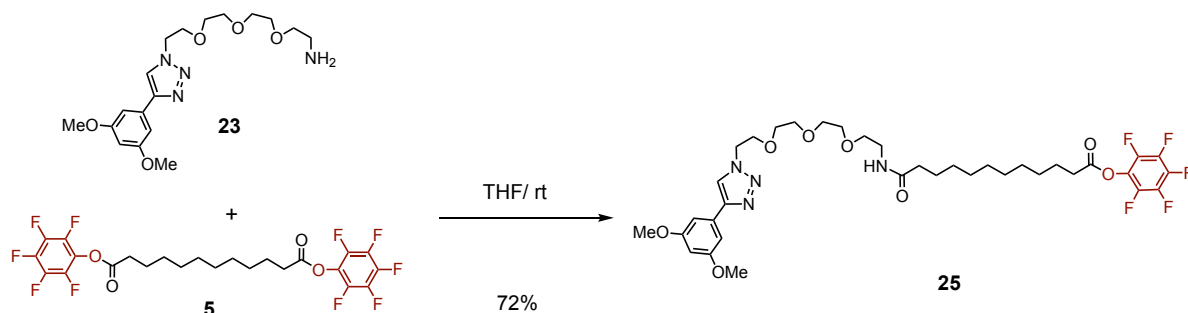
A solution of **24a** (0.109 g, 0.067 mmol, 1 eq.) in CHCl₃ was added to a solution of TfOH (0.011 g, 0.073 mmol, 1.1 eq.) in CHCl₃. Evaporation of solvent resulted in **24aH⁺**. Glassy product (0.119 g, quantitative). ¹H NMR (400 MHz, C₂D₂Cl₄, 100°C): δ = 7.01 (s, 6H), 6.84 (s, 5H), 6.73 (broad s, 1H), 6.64 (s, 1H), 6.55-6.48 (m, 5H), 6.44 (broad s, 1H), 4.70 (broad s, 1H), 4.41 (m, 2H), 4.16-4.08 (m, 5H), 4.03 (m, 11H), 3.83-3.74 (m, 26H), 3.71-3.65 (m, 8H), 3.56 (m, 4H), 3.39 (m, 2H), 3.18 (m, 2H), 2.30 (t, J = 7.5 Hz, 2H), 2.24 (t, J = 7.5 Hz, 2H), 1.55 (t, J = 6.8, 15H), 1.37 (t, J = 6.8, 15H), 1.21 (m, 14H) ppm. ¹⁹F NMR (376 MHz, CDCl₃): δ = -78.3 ppm.

Preparation of compound **24bH⁺**



A solution of **24b** (0.098 g, 0.057 mmol, 1 eq.) in CHCl₃ was added to a solution of TfOH (9.5 mg, 0.063 mmol, 1.1 eq.) in CHCl₃. Evaporation of solvent resulted in **24bH⁺**. Glassy product (0.105 g, 99%). ¹H NMR (400 MHz, C₂D₂Cl₄, 100°C): δ = 8.00 (broad s, 1H), 7.82 (s, 3H), 7.02 (s, 5H), 6.22 (broad s, 1H), 6.83 (s, 5H), 6.73 (broad s, 1H), 6.64 (broad s, 1H), 6.41 (broad s, 2H), 4.70 (broad s, 1H), 4.60 (m, 2H), 4.17-4.09 (m, 5H), 4.06-3.98 (m, 10H), 3.81-3.77 (m, 20H), 3.73-3.69 (m, 8H), 3.66-3.60 (m, 5H), 3.46 (m, 2H), 3.32 (m, 2H), 2.45 (t, *J* = 7.5 Hz, 2H), 2.29 (t, *J* = 7.5 Hz, 2H), 1.67 (m, 2H), 1.55 (t, *J* = 7.0 Hz, 16H), 1.36 (t, *J* = 7.0 Hz, 18H), 1.29-1.19 (m, 10H) ppm. ¹⁹F NMR (376 MHz, CDCl₃): δ = -62.8, -78.4 ppm.

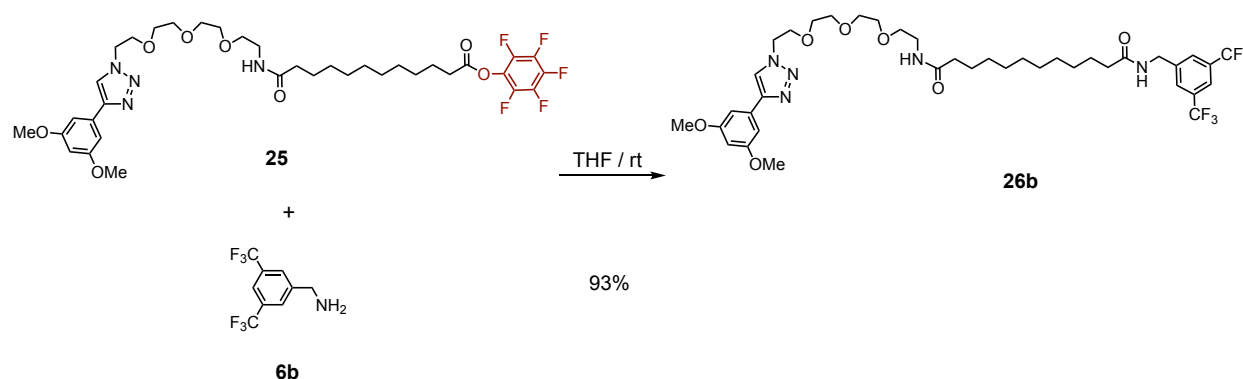
Preparation of compounds **25**



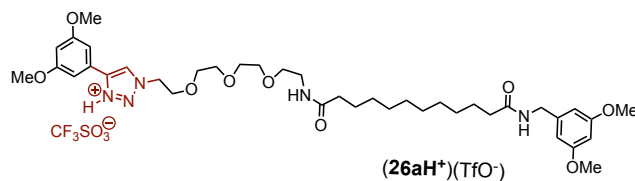
A solution of **5** (4.724 g, 8.40 mmol) and **23** (0.800 g, 2.10 mmol) in anhydrous THF (51 mL) was stirred overnight at rt. The mixture was filtered through a short plug (SiO₂, CH₂Cl₂ containing 3% MeOH) and evaporated. Purification by column chromatography (SiO₂, CH₂Cl₂ containing 2% MeOH) gave **25** (1.144 g, 72%). Colorless glassy product. IR (neat): 1788 (C=O), 1653 (C=O) cm⁻¹. ¹H NMR (500 MHz, CD₂Cl₂): δ = 8.02 (s, 1H), 7.00 (d, *J* = 2.3 Hz, 2H), 6.42 (t, *J* = 2.3 Hz, 1H), 6.19 (broad s, 1H), 4.56 (t, *J* = 5.1 Hz, 2H), 3.89 (t, *J* = 5.1 Hz, 2H), 3.82 (s, 6H), 3.61-3.51 (m, 8H), 3.46 (t, *J* = 5.3 Hz, 2H), 3.34 (q, *J* = 5.3 Hz, 2H), 2.65 (t, *J* = 7.5 Hz, 2H), 2.11 (t, *J* = 7.5 Hz, 2H), 1.74 (quint, *J* = 7.5 Hz, 2H), 1.56 (quint, *J* = 7.5 Hz, 2H), 1.43-1.23 (m, 12H) ppm. ¹³C NMR (125 MHz, CD₂Cl₂): δ = 173.2, 169.9, 161.6, 147.5,

= 742.81 ($[M+H]^+$, calcd for $C_{39}H_{60}N_5O_9$: 742.44). Anal. (%) calcd for $C_{39}H_{59}N_5O_9$ (741.92): C, 63.14, H, 8.02, N, 9.44; found: C, 62.92, H, 8.05, N, 9.25.

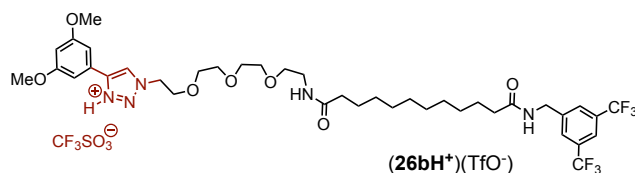
Compound 26b.



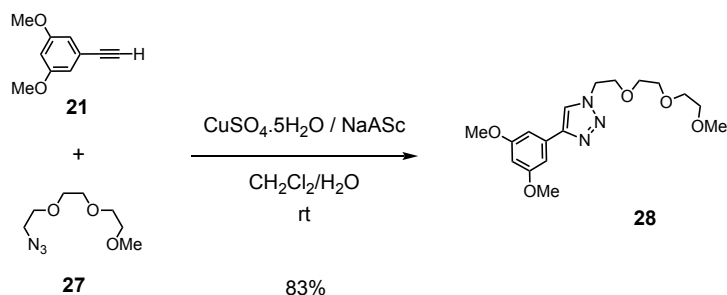
Prepared from **25** (0.304 g, 0.40 mmol) and **6b** (0.117 g, 0.48 mmol) in anhydrous THF (6 mL). Column chromatography (SiO_2 , CH_2Cl_2 containing 1.5% MeOH) and gel permeation chromatography (Biobeads SX-1, CH_2Cl_2) gave **26b** (0.304 g, 93%). Colorless glassy product. IR (neat): 3290 (N-H), 1649 (C=O) cm^{-1} . ^1H NMR (500 MHz, CD_2Cl_2): δ = 8.01 (s, 1H), 7.77 (s, 1H), 7.75 (s, 2H), 7.09 (t, J = 6.1 Hz, 1H), 6.98 (d, J = 2.3 Hz, 2H), 6.43 (t, J = 2.3 Hz, 1H), 6.18 (t, J = 5.1 Hz, 1H), 4.56 (t, J = 5.1 Hz, 2H), 4.50 (d, J = 6.1 Hz, 2H), 3.89 (t, J = 5.1 Hz, 2H), 3.82 (s, 6H), 3.62-3.51 (m, 8H), 3.45 (t, J = 5.3 Hz, 2H), 3.33 (q, J = 5.3 Hz, 2H), 2.22 (t, J = 7.6 Hz, 2H), 2.09 (t, J = 7.6 Hz, 2H), 1.63-1.51 (m, 4H), 1.31-1.21 (m, 12H) ppm. ^{13}C NMR (125 MHz, CD_2Cl_2): δ = 173.9, 173.4, 161.7, 147.6, 142.7, 133.1, 131.8 (q, $^2J_{\text{C-F}}$ = 33 Hz), 128.0 (two peaks), 123.8 (q, $^1J_{\text{C-F}}$ = 273 Hz), 121.7, 121.3 (quint, $^3J_{\text{C-F}}$ = 3.8 Hz), 104.0, 100.3, 71.0, 70.8, 70.7, 70.6, 70.1, 69.8, 55.8, 50.8, 42.7, 39.5, 36.8, 36.7, 29.7, 29.6 (three peaks), 29.5, 26.0 ppm. ^{19}F NMR (470 MHz, CD_2Cl_2): δ = -63.1 ppm. MALDI-TOF-MS: m/z = 818.83 ($[M+H]^+$, calcd for $C_{39}H_{54}F_6N_5O_7$: 818.39). Anal. (%) calcd for $C_{39}H_{53}F_6N_5O_7$ (817.86): C, 57.27, H, 6.53, N, 8.56; found: C, 57.45, H, 6.68, N, 8.35.

Preparation of compounds 26aH⁺

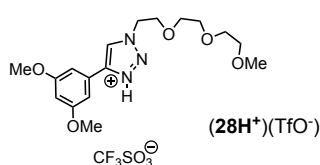
A solution of **26a** (0.099 g, 0.133 mmol, 1 eq.) in CHCl₃ was added to a solution of TfOH (0.022 g, 0.146 mmol, 1.1 eq.) in CHCl₃. Evaporation of solvent resulted in **26aH⁺**. Pale yellow viscous oil (0.119 g, quantitative). ¹H NMR (500 MHz, CDCl₃): δ = 8.45 (s, 1H), 7.12 (broad s, 1H), 7.01 (d, *J* = 2.3 Hz, 2H), 6.94 (broad s, 1H), 6.51 (t, *J* = 2.3 Hz, 1H), 6.42 (d, *J* = 2.3 Hz, 2H), 6.35 (t, *J* = 2.3 Hz, 1H), 4.70 (t, *J* = 5.1 Hz, 2H), 4.38 (d, *J* = 5.9 Hz, 2H), 3.98 (t, *J* = 5.1 Hz, 2H), 3.83 (s, 6H), 3.76 (s, 6H), 3.66-3.64 (m, 2H), 3.61-3.58 (m, 2H), 3.56 (s, 4H), 3.54-3.52 (m, 2H), 3.45-3.42 (m, 2H), 2.30 (t, *J* = 7.6 Hz, 2H), 2.25 (t, *J* = 7.6 Hz, 2H), 1.66-1.56 (m, 4H), 1.30-1.20 (m, 12H) ppm. ¹⁹F NMR (376 MHz, CDCl₃): δ = -78.4 ppm.

Preparation of compounds 26bH⁺

A solution of **26b** (0.069 g, 0.084 mmol, 1 eq.) in CHCl₃ was added to a solution of TfOH (0.014 g, 0.093 mmol, 1.1 eq.) in CHCl₃. Evaporation of solvent resulted in **26bH⁺**. Yellish viscous oil (0.082 g, quantitative). ¹H NMR (400 MHz, CDCl₃): δ = 8.3 (broad s, 1H), 7.76 (broad s, 1H), 7.74 (broad s, 2H), 7.01 (d, *J* = 2.3 Hz, 2H), 6.62 (broad s, 1H), 6.53 (broad s, 1H), 6.50 (t, *J* = 2.3 Hz, 1H), 4.68 (t, *J* = 4.7 Hz, 2H), 4.56 (t, *J* = 6.1 Hz, 2H), 3.97 (t, *J* = 4.7 Hz, 2H), 3.84 (s, 6H), 3.66-3.64 (m, 2H), 3.61-3.58 (m, 2H), 3.56 (s, 4H), 3.53-3.51 (m, 2H), 3.44-3.41 (m, 2H), 2.28 (t, *J* = 7.3 Hz, 2H), 2.20 (t, *J* = 7.3 Hz, 2H), 1.68-1.55 (m, 4H), 1.31-1.21 (m, 12H) ppm. ¹⁹F NMR (376 MHz, CDCl₃): δ = -62.8, -78.4 ppm.

Preparation of compounds 28

A mixture of **21** (0.170 g, 1.05 mmol), **27** (0.165 g, 0.87 mmol), sodium ascorbate (0.052 g, 0.26 mmol) and $\text{CuSO}_4 \cdot 5\text{H}_2\text{O}$ (0.021 g, 0.09 mmol) in $\text{CH}_2\text{Cl}_2/\text{H}_2\text{O}$ (4:2 mL) was stirred at rt for 4 days. After the resulting mixture was washed with H_2O (3 x 100 mL) and extracted with CH_2Cl_2 , dried over MgSO_4 , filtered and concentrated. Purification by column chromatography (SiO_2 , $\text{CH}_2\text{Cl}_2/\text{Et}_2\text{O}$: 7/3) gave **28** (0.253 g, 83 %). Yellow oil. IR (neat): 1596 (C=C) cm^{-1} . ^1H NMR (500 MHz, CD_2Cl_2): δ = 8.00 (s, 1H), 7.00 (d, J = 2.3 Hz, 2H), 6.43 (t, J = 2.3 Hz, 1H), 4.57 (t, J = 5.1 Hz, 2H), 3.89 (t, J = 5.1 Hz, 2H), 3.83 (s, 6H), 3.63-3.53 (m, 6H), 3.46 (m, 2H), 3.29 (s, 3H) ppm. ^{13}C NMR (125 MHz, CD_2Cl_2): δ = 161.6, 147.6, 133.3, 121.6, 103.9, 100.4, 72.3, 71.0, 70.8, 70.7, 69.8, 58.9, 55.8, 50.8 ppm. MALDI-TOF-MS: m/z = 352.18 ($[\text{M}+\text{H}]^+$, calcd for $\text{C}_{17}\text{H}_{26}\text{N}_3\text{O}_5$: 352.18). Anal. (%) calcd for $\text{C}_{17}\text{H}_{25}\text{N}_3\text{O}_5$ (351.40): C, 58.11, H, 7.17, N, 11.96; found: C, 58.27, H, 7.12, N, 12.00.

Preparation of compound 28H⁺

A solution of **28** (0.107 g, 0.306 mmol, 1 eq.) in CHCl_3 was added to a solution of TfOH (0.046 g, 1.05 mmol, 1 eq.) in CHCl_3 . Evaporation of solvent resulted in **28H⁺**. Yellow viscous oil (0.152 g, 99.5%). ^1H NMR (500 MHz, CDCl_3): δ = 8.72 (s, 1H), 6.97 (d, J = 2.3 Hz, 2H), 6.55 (t, J = 2.3 Hz, 1H), 4.77 (t, J = 5.1 Hz, 2H), 4.00 (t, J = 5.1 Hz, 2H), 3.85 (s, 6H), 3.69 (m, 2H), 3.63 (m, 4H), 3.52 (m, 2H), 3.28 (s, 3H) ppm. ^{19}F NMR (470 MHz, CDCl_3): δ = -78.4 ppm.

VI-3. Binding studies

The binding studies have been carried out by Iwona Nierengarten.

All ^1H NMR titration experiments were performed on a Bruker AC 400 at 25(1) $^\circ\text{C}$, in CDCl_3 purchased from Sigma Aldrich Chemical Company. The appropriate amount of a stock solution of model compound **11a** (0.70 M), **11b** (0.57 M), **11c** (0.65 M) and **28** (0.67 M) in CDCl_3 , was added to a solution of pillar[5]arene **3** in CDCl_3 , or a stock solution of pillar[5]arene **3** was added to a solution of model compound **28H⁺** in CDCl_3 . The association constants (K_a) for the 1:1 complexes were determined based on the complexation-induced changes in chemical shifts of the signals arising from host **3** or from appropriate model compound as mentioned above. The calculations were done using the nonlinear least-square regression analysis program HypNMR.⁴

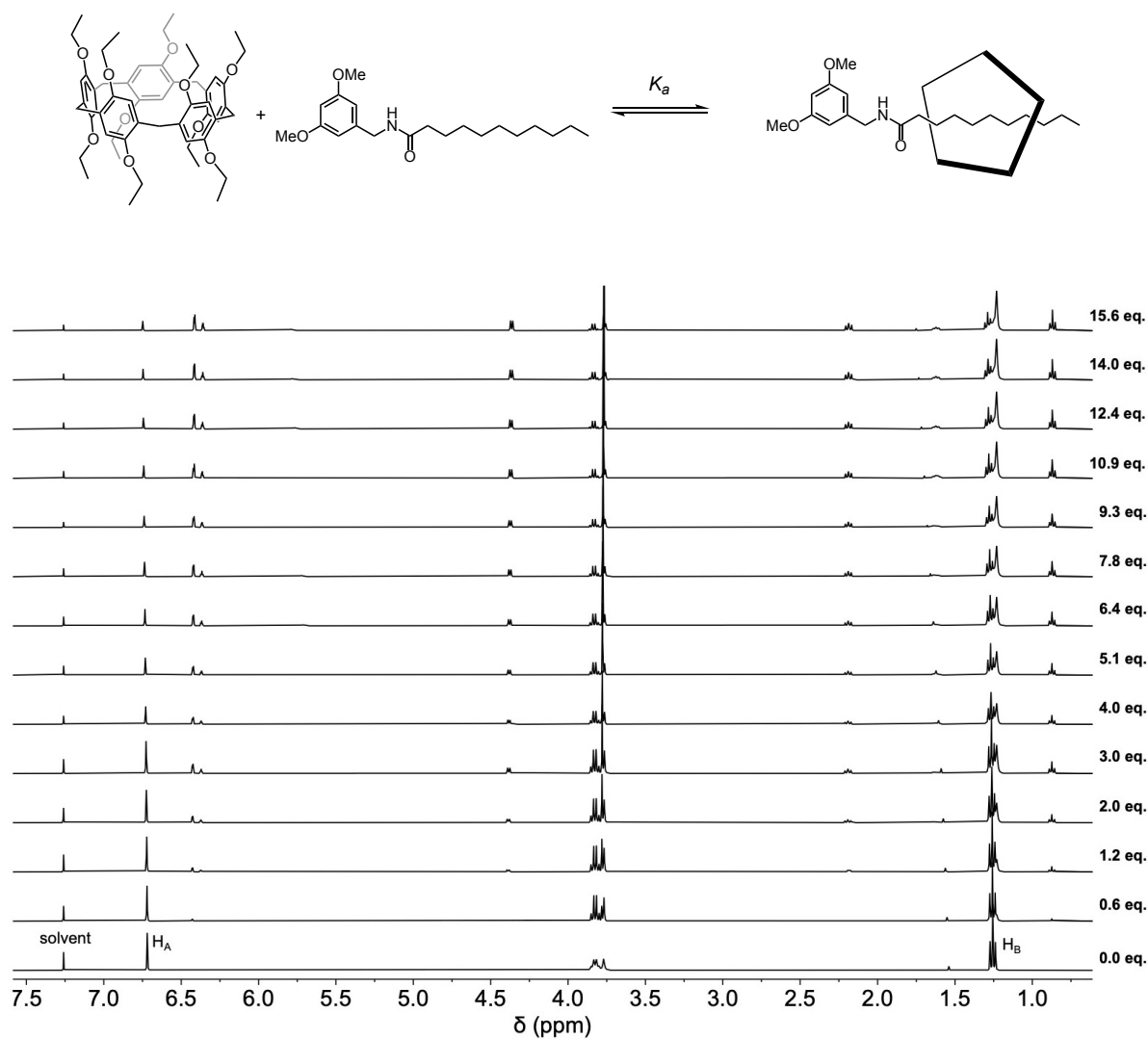


Figure 1a. ^1H NMR spectra (400 MHz, CDCl_3 , 298 K) recorded upon successive additions of model compound **11a** to a solution of pillar[5]arene **3** (9.0 mM).

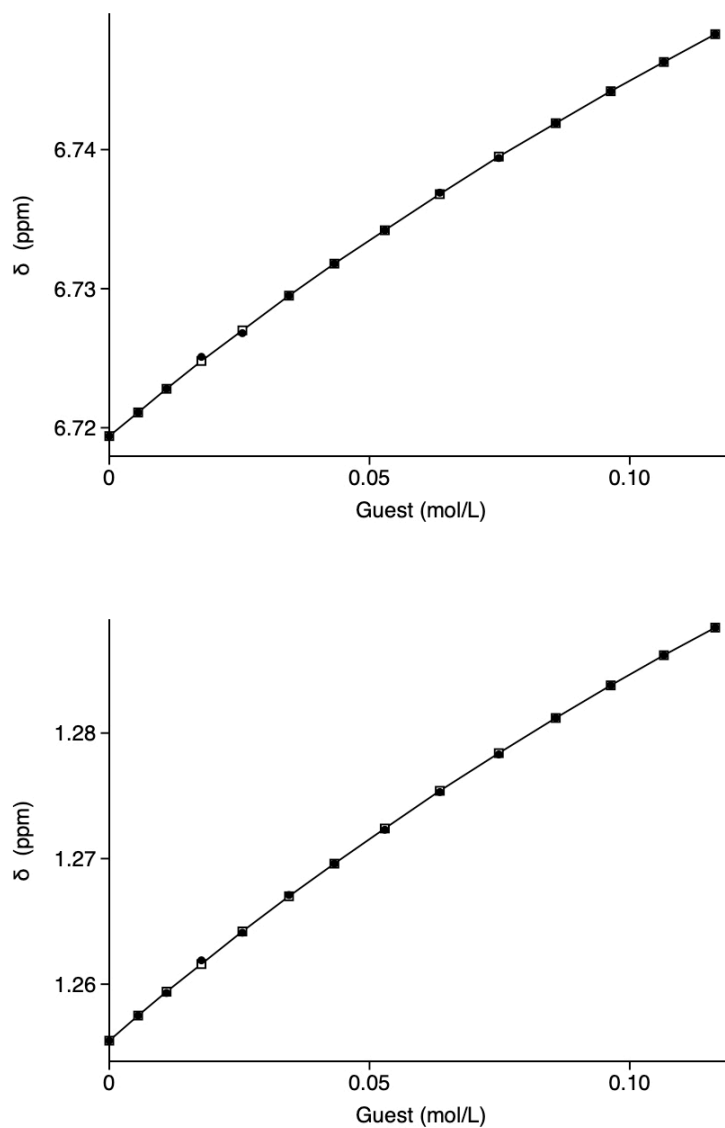


Figure 1b. Chemical shifts of H_A and H_B (**3**, calculated: □, experimental: ●) as a function of guest (**11a**) concentration. The association constant was calculated by considering simultaneously the changes in chemical shifts of H_A and H_B.

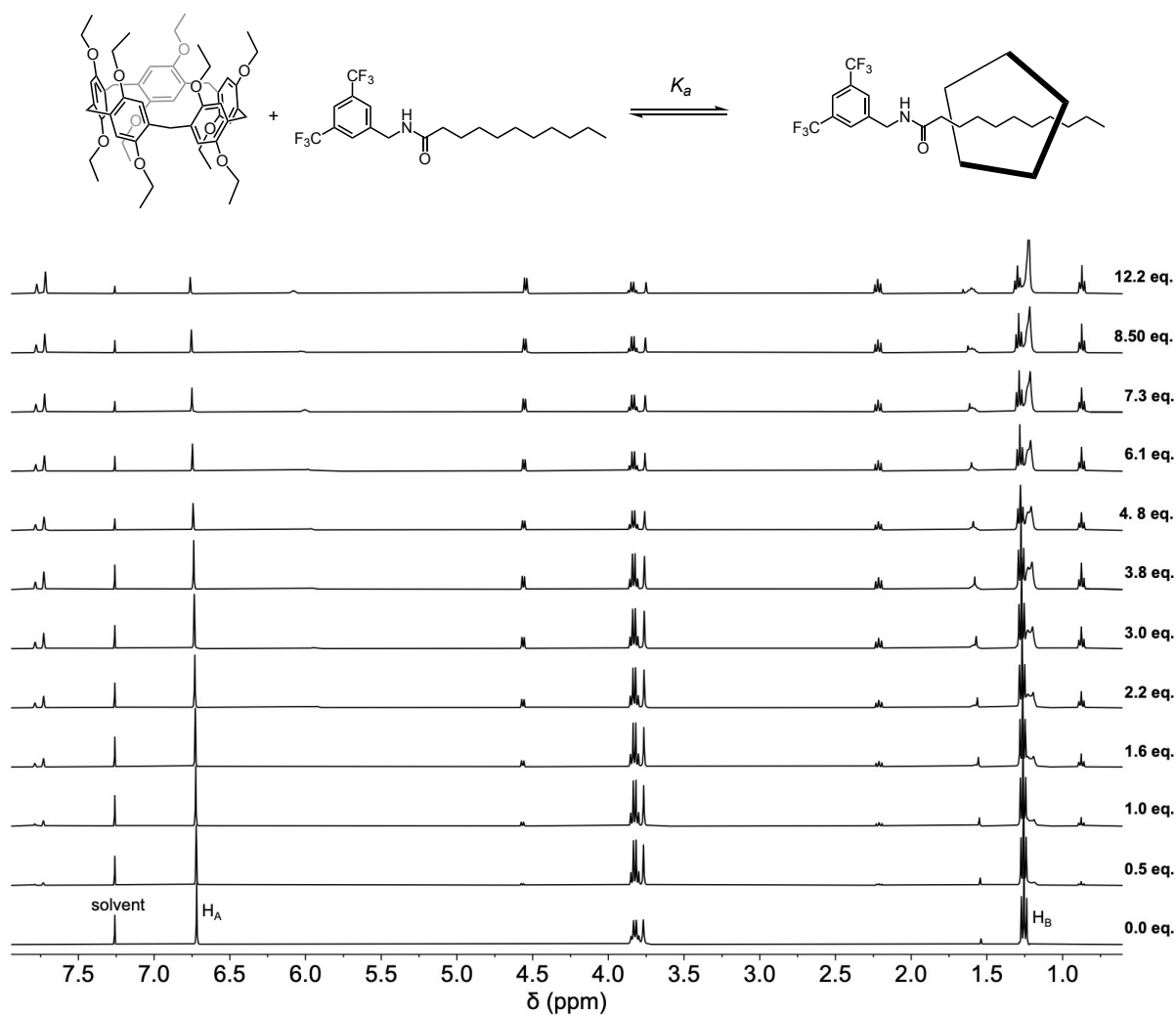


Figure 2a. ^1H NMR spectra (400 MHz, CDCl_3 , 298 K) recorded upon successive additions of model compound **11b** to a solution of pillar[5]arene **3** (9.2 mM).

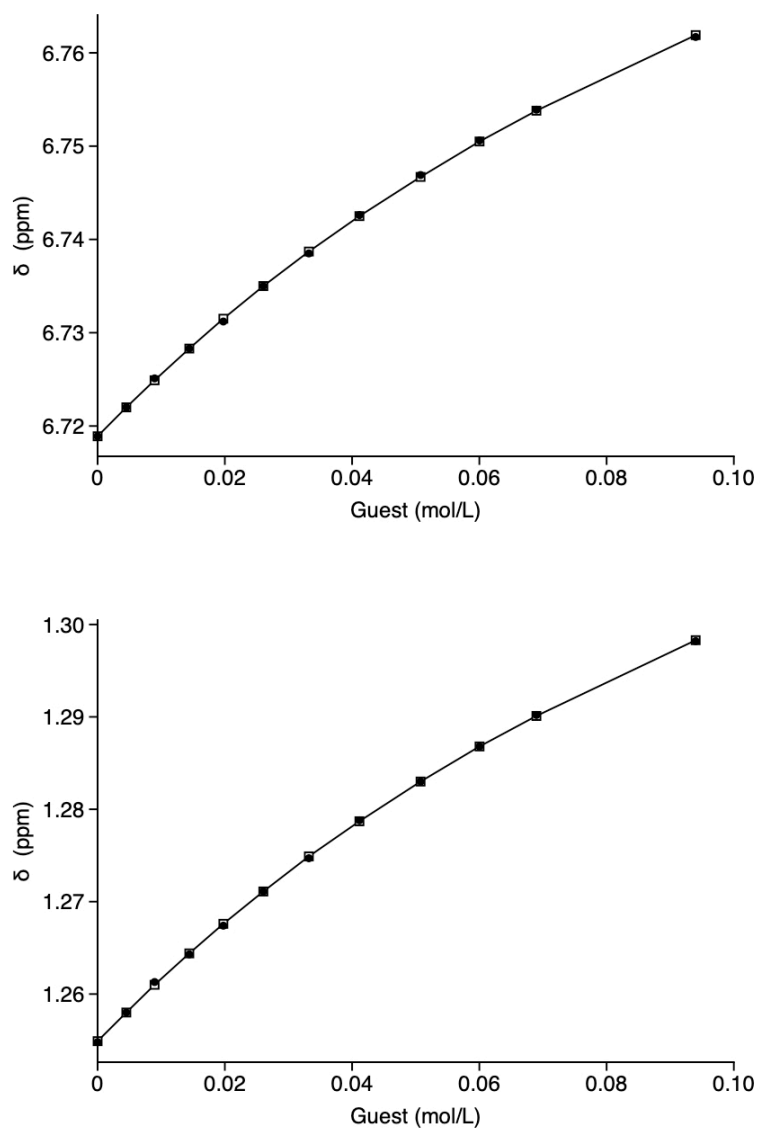


Figure 2b. Chemical shifts of H_A and H_B (**3**, calculated: \square , experimental: \bullet) as a function of guest (**11b**) concentration. The association constant was calculated by considering simultaneously the changes in chemical shifts of H_A and H_B .

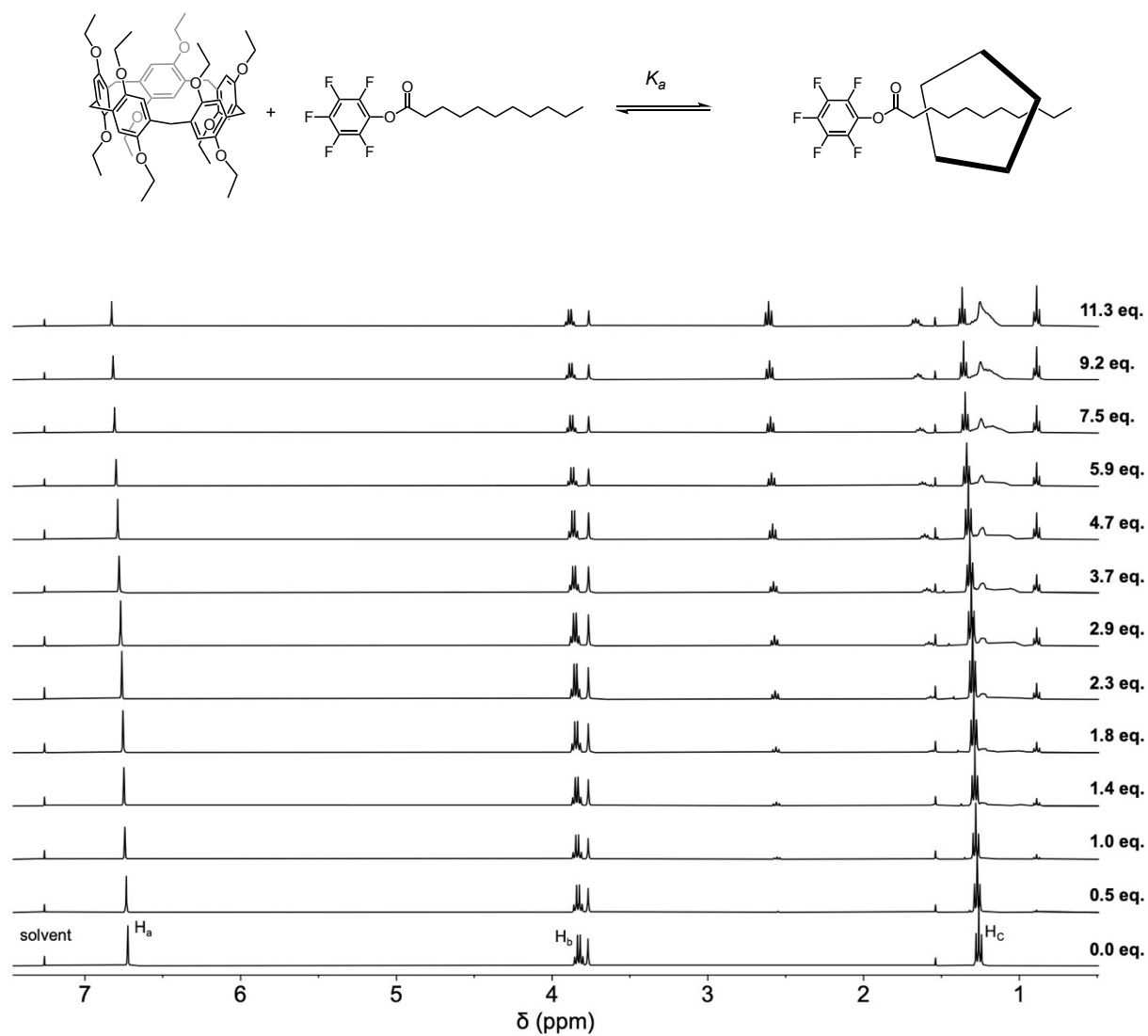


Figure 3a. ^1H NMR spectra (400 MHz, CDCl_3 , 298 K) recorded upon successive additions of model compound **11c** to a solution of pillar[5]arene **3** (10.3 mM).

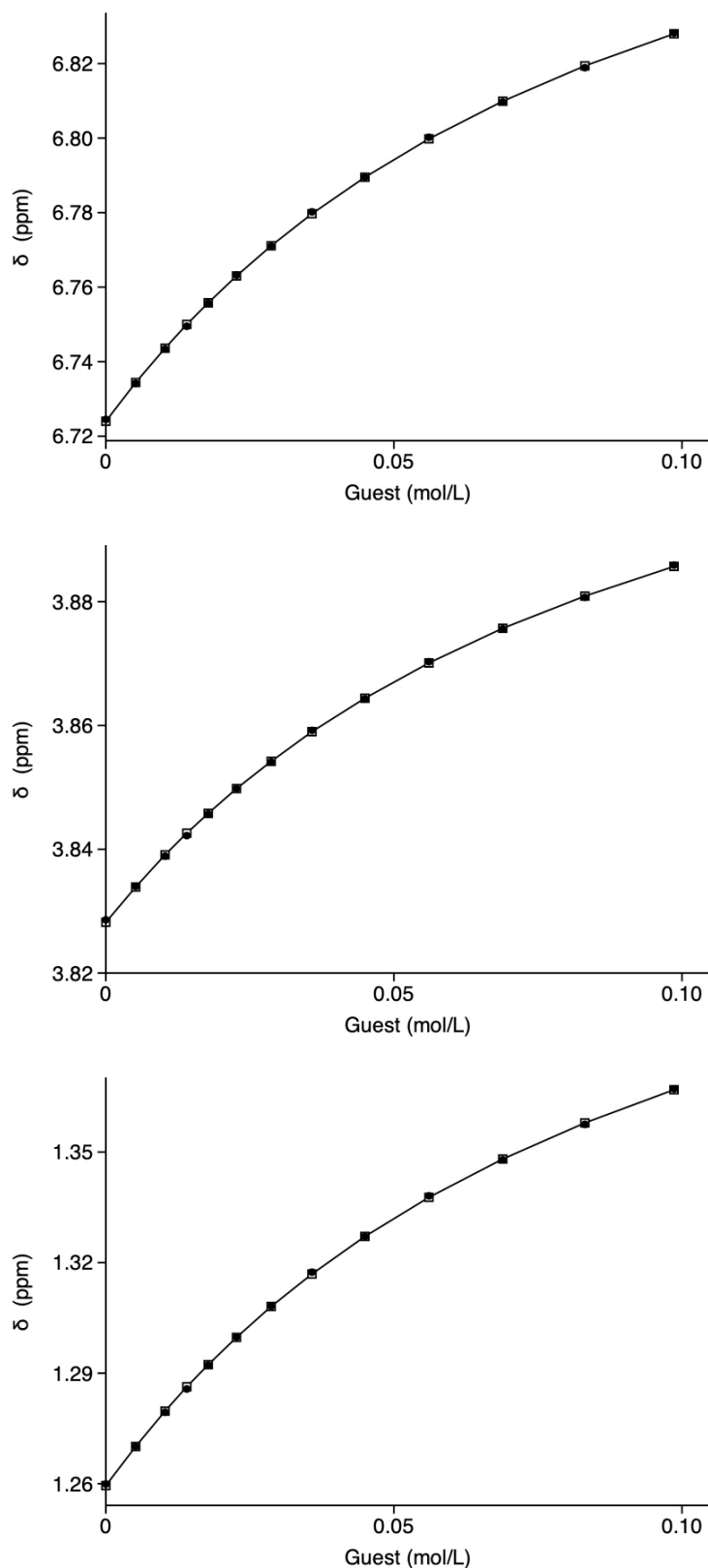


Figure 3b. Chemical shifts of H_A , H_B and H_C (**3**, calculated: \square , experimental: \bullet) as a function of guest (**11c**) concentration. The association constant was calculated by considering simultaneously the changes in chemical shifts of H_A , H_B and H_C .

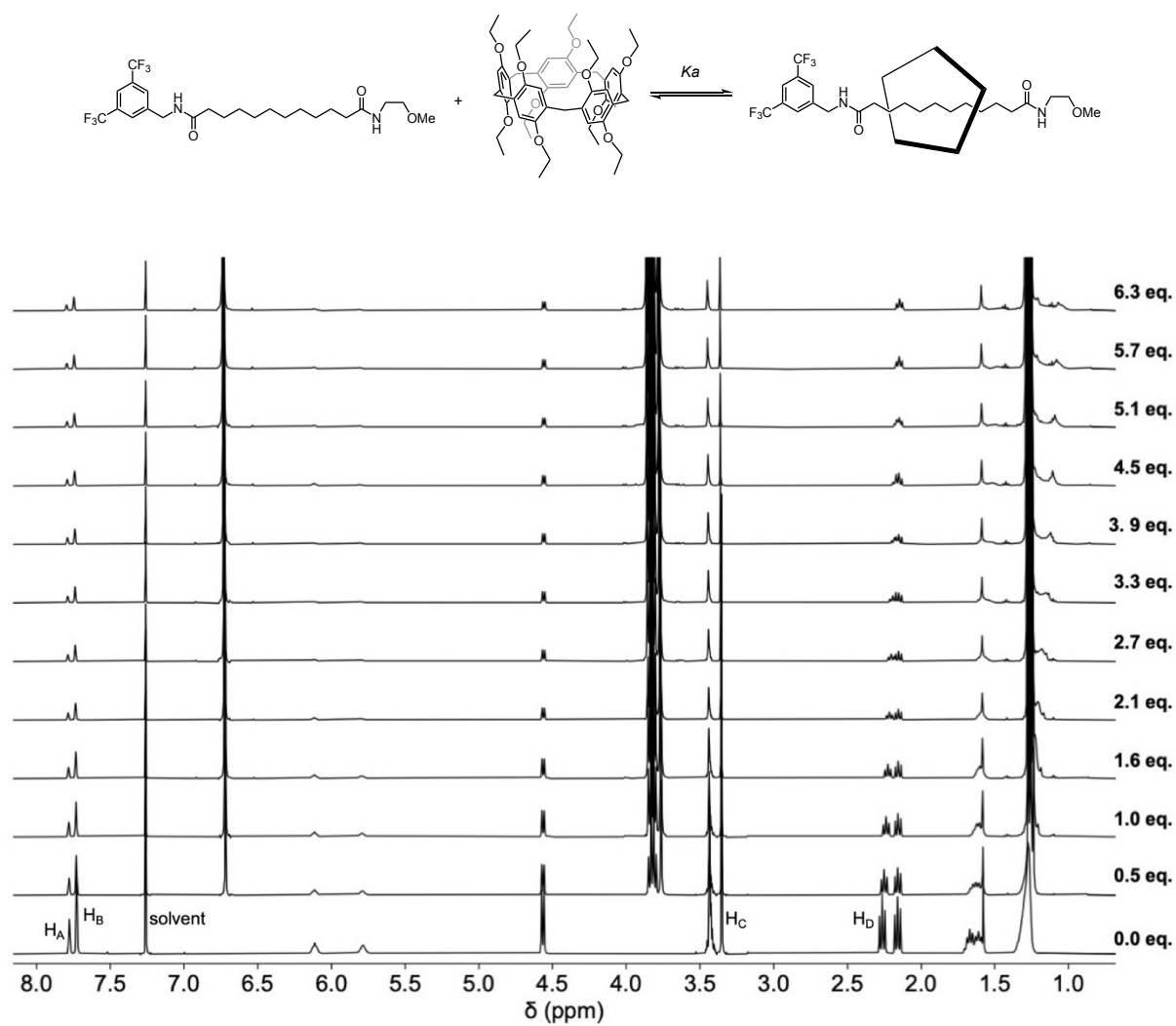


Figure 4a. ^1H NMR spectra (400 MHz, CDCl_3 , 298 K) recorded upon successive additions of pillar[5]arene **3** to a solution of model compound **14b** (10.1 mM).

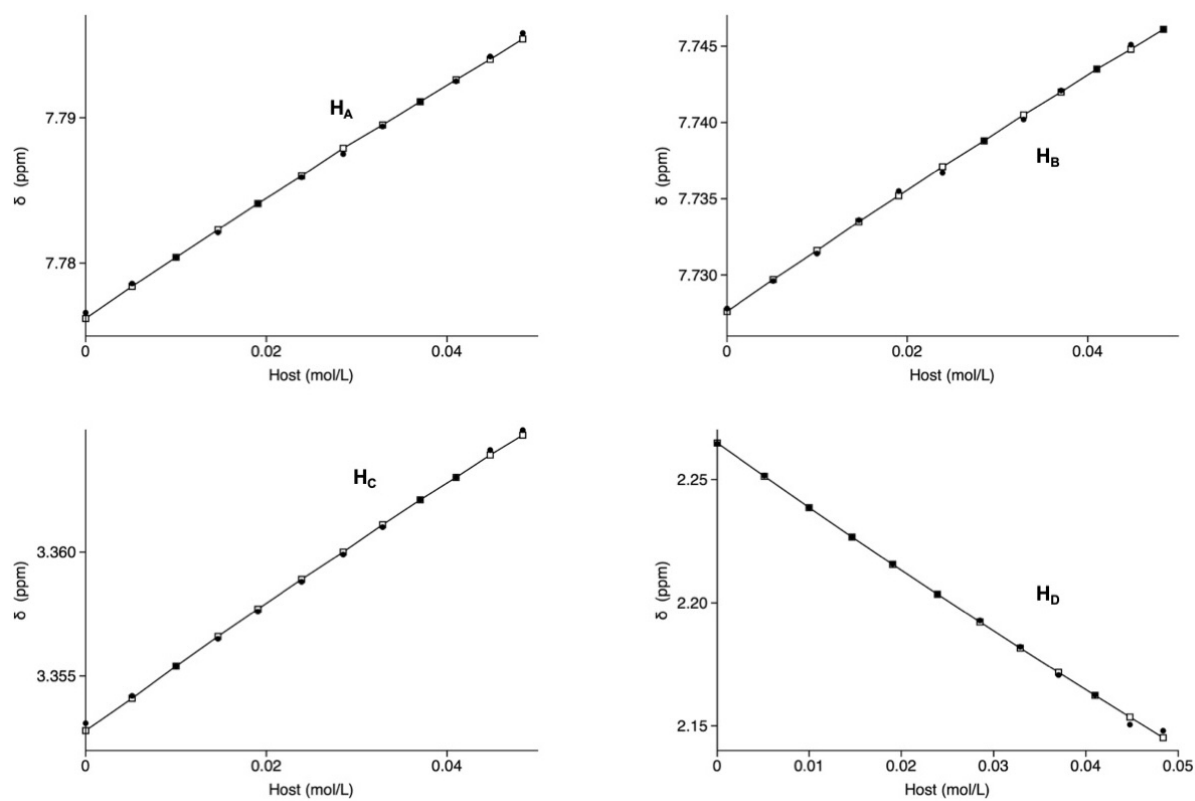


Figure 4b. Chemical shifts of H_A , H_B , H_C and H_D (**14b**, calculated: \square , experimental: \bullet) as a function of host (**3**) concentration. The association constant was calculated by considering simultaneously the changes in chemical shifts of H_A , H_B , H_C and H_D .

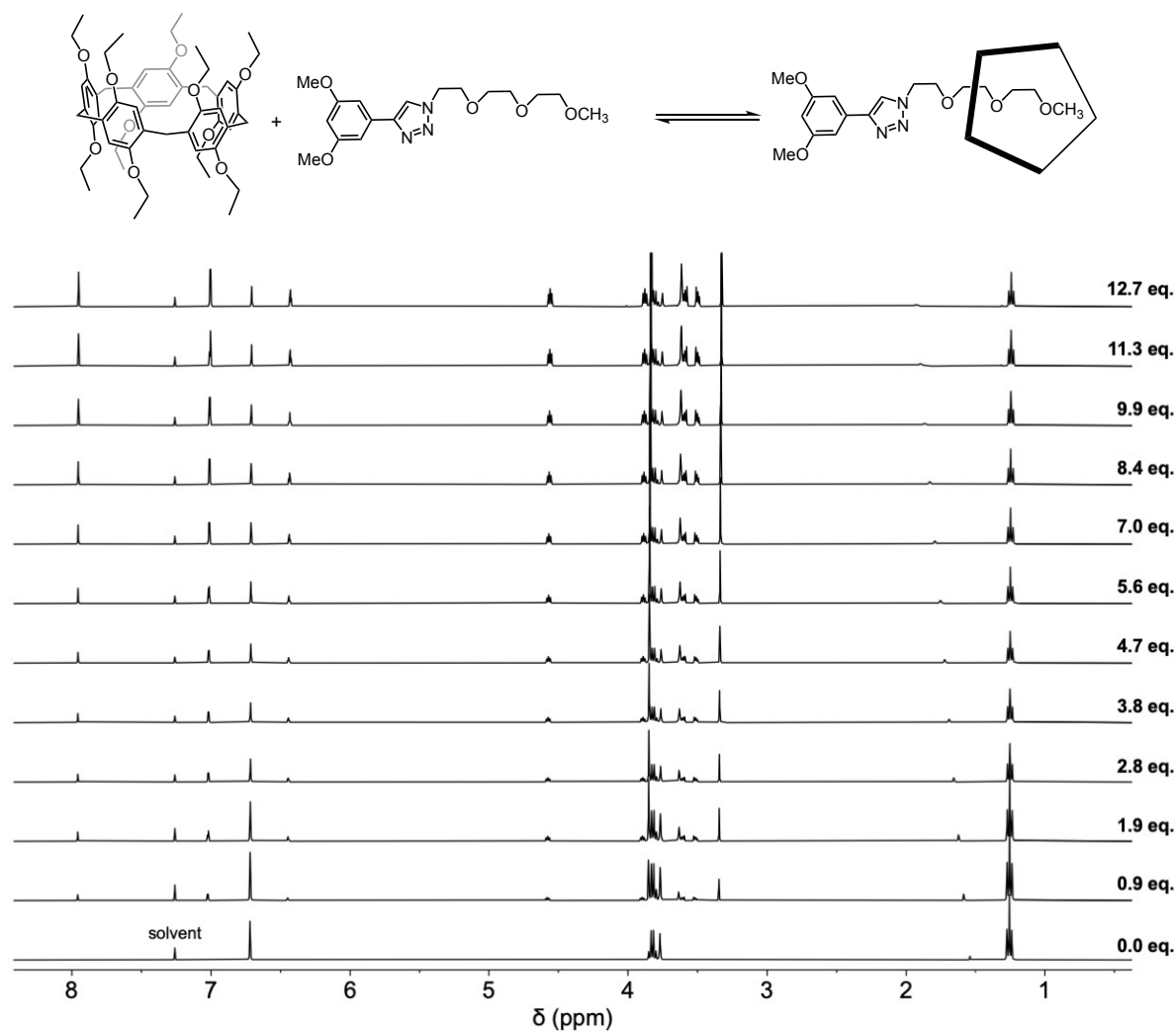


Figure 5. ¹H NMR spectra (400 MHz, CDCl₃, 298 K) recorded upon successive additions of model compound **28** to a solution of pillar[5]arene **3** (12.1 mM). No chemical shift changes could be detected thus showing that no complexation took place under these conditions.

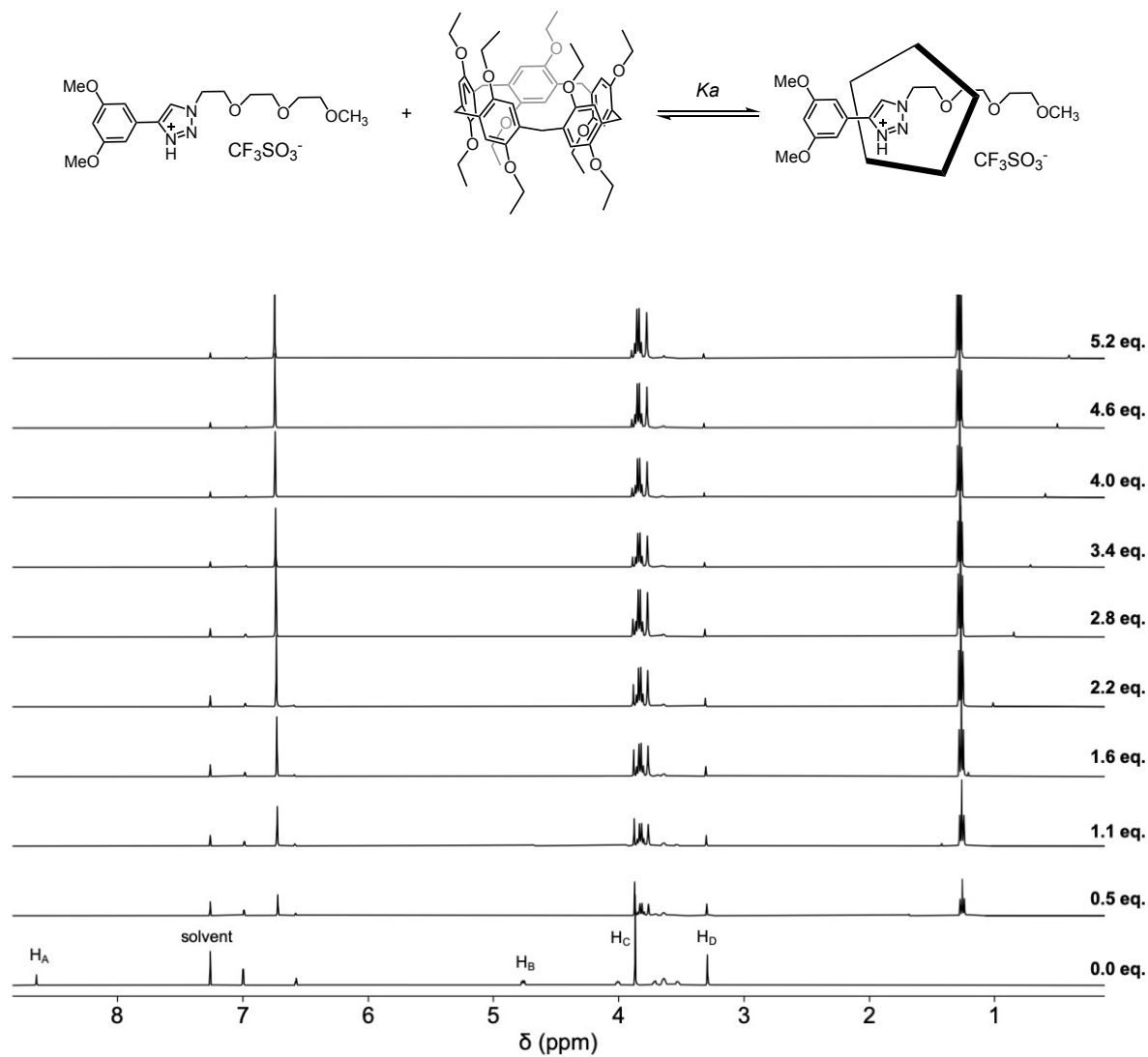


Figure 6a. ^1H NMR spectra (400 MHz, CDCl_3 , 298 K) recorded upon successive additions of pillar[5]arene **3** to a solution of model compound **28H⁺** (9.6 mM).

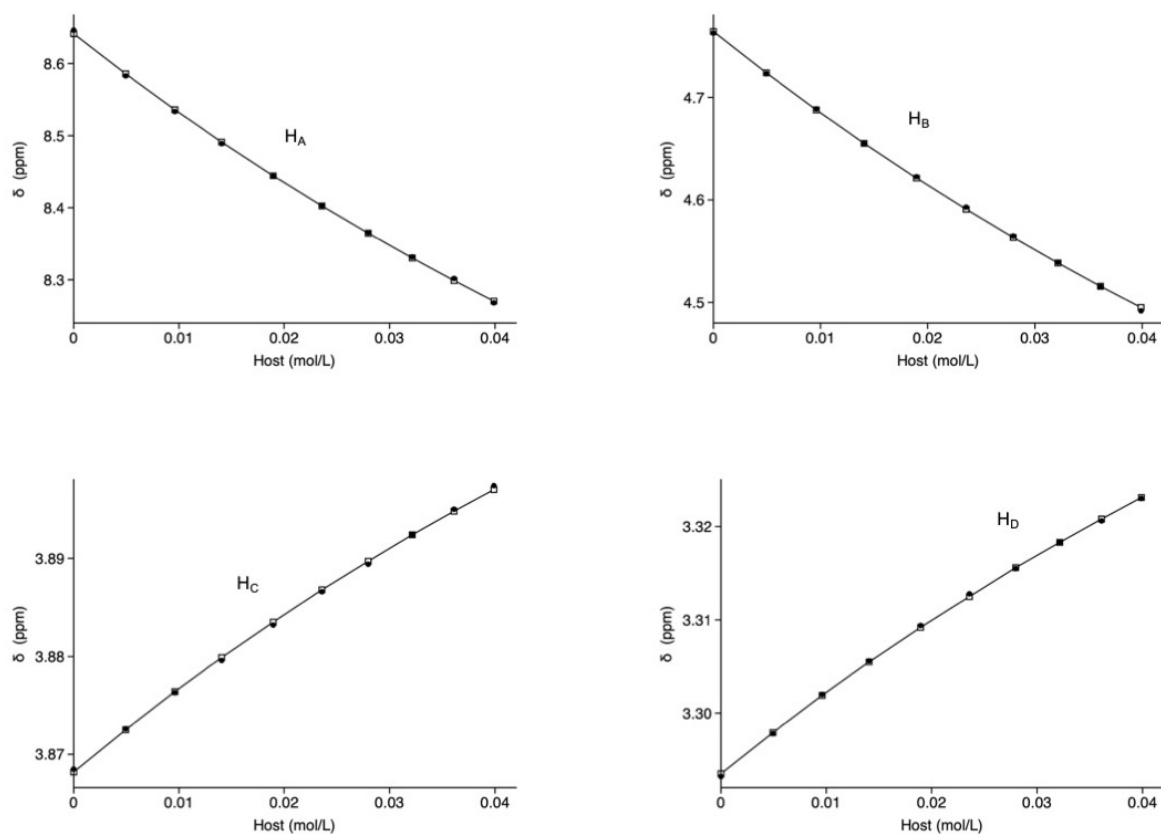


Figure 6b. Chemical shifts of H_A , H_B , H_C and H_D ($28H^+$, calculated: □, experimental: ●) as a function of pillar[5]arene (**3**) concentration. The association constant was calculated by considering simultaneously the changes in chemical shifts of H_A , H_B , H_C and H_D .

VI-4. Electrochemistry

The electrochemistry investigations have been carried out by Béatrice Delavaux-Nicot (LCC, Toulouse, France).

The electrochemical properties of compounds **3**, **10a-b**, **12**, **24a-b**, **(24a-bH⁺)(TfO⁻)**, **28** and **(28H⁺)(TfO⁻)** were determined by cyclic voltammetry (CV) and Osteryoung Square Wave Voltammetry (OSWV). The cyclic voltammetric measurements were carried out with a potentiostat Autolab PGSTAT100. Experiments were performed at room temperature in a homemade airtight three-electrode cell connected to a vacuum/argon line. The reference electrode consisted of a saturated calomel electrode (SCE) separated from the solution by a bridge compartment. The counter electrode was a platinum wire of ca. 1 cm² apparent surface. The working electrode was a Pt microdisk (0.5 mm diameter). The supporting electrolyte [nBu₄N][BF₄] (Fluka, 99% electrochemical grade) was used as received and simply degassed under argon. Dichloromethane was freshly distilled over CaH₂ prior to use. The solutions used during the electrochemical studies were typically 2 × 10⁻⁴ or 3 × 10⁻³ M in compound and 0.1 M in supporting electrolyte. Before each measurement, the solutions were degassed by bubbling Ar and the working electrode was polished with a polishing machine (Presi P230). Under these experimental conditions, Fc⁺/Fc is observed at + 0.55 ± 0.01 V vs. SCE. OSWVs were obtained using an amplitude of 20 mV, a frequency of 20 Hz, and a step potential of 5 mV..

VI-5. DFT calculations

The DFT calculations have been carried out by Jean-François Nierengarten.

All DFT calculations were performed with Spartan 20 on a Mac Pro with 8 cores 3 GHz Intel Xeon E5 processors. For the pK_A calculations of the ligands, geometry optimization as well as subsequent frequency analysis at 298.15 K were performed at the B3LYP/6-311+G(2df,2p) level using the CPCM model with the dielectric constant of water (78.30). As revealed by the frequency analysis, imaginary frequencies were absent in all ground states.

For the host-guest complexes, geometry optimization of all compounds was first performed in the gas phase with the B3LYP or the ωB97X-D functional using the 6-31G* basis set. The structures were further optimized at the same level using the CPCM model in THF (dielectric constant of 7.43). In all cases, the frequencies were computed at the same level to confirm that each optimized structure is an energy minimum and to evaluate its zero-point vibration energy (ZPVE) and thermal corrections at 298.15 K. The UV/vis spectra were also calculated in the

gas phase at the TD- ω B97X-D/6-31G* level of theory. Single point energy calculations were performed at the ω B97X-D/6-31G* level to evaluate the distortion and interaction energies.

The Boltzmann distribution were calculated from:

$$N_i / N = \exp(-E_i/kT) / \sum_j \exp(-E_j/kT)$$

where N_i is the number of molecules in conformation i , N is the total number of molecules in the system, E_i is the energy of state i , T is the equilibrium temperature of the system, and k is the Boltzmann constant.

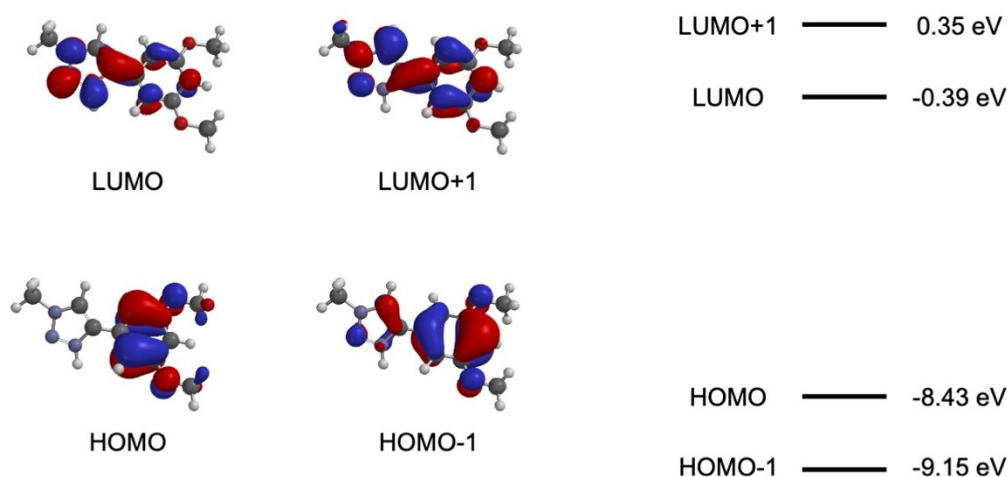


Figure 7. FMOs of B3H^+ calculated at the ω B97X-D/6-31G* level using the CPCM model with the dielectric constant of THF.

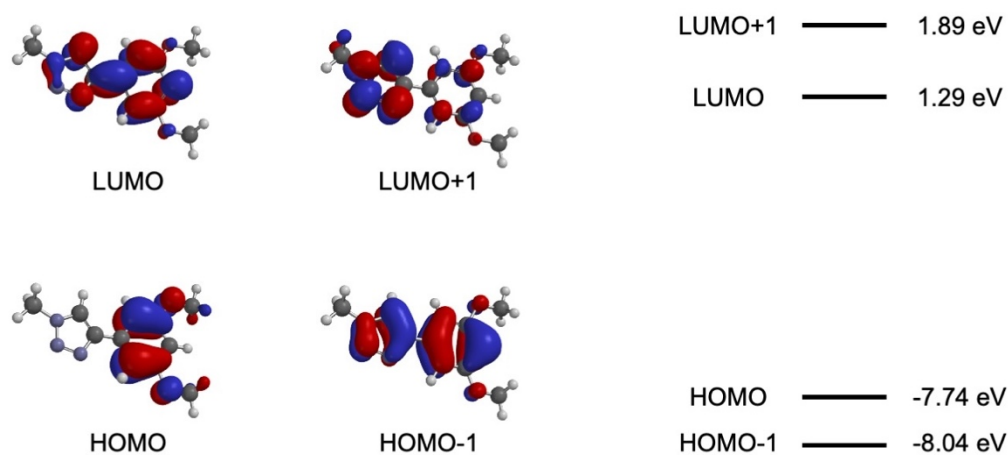


Figure 8. FMOs of B3 calculated at the ω B97X-D/6-31G* level using the CPCM model with the dielectric constant of THF.

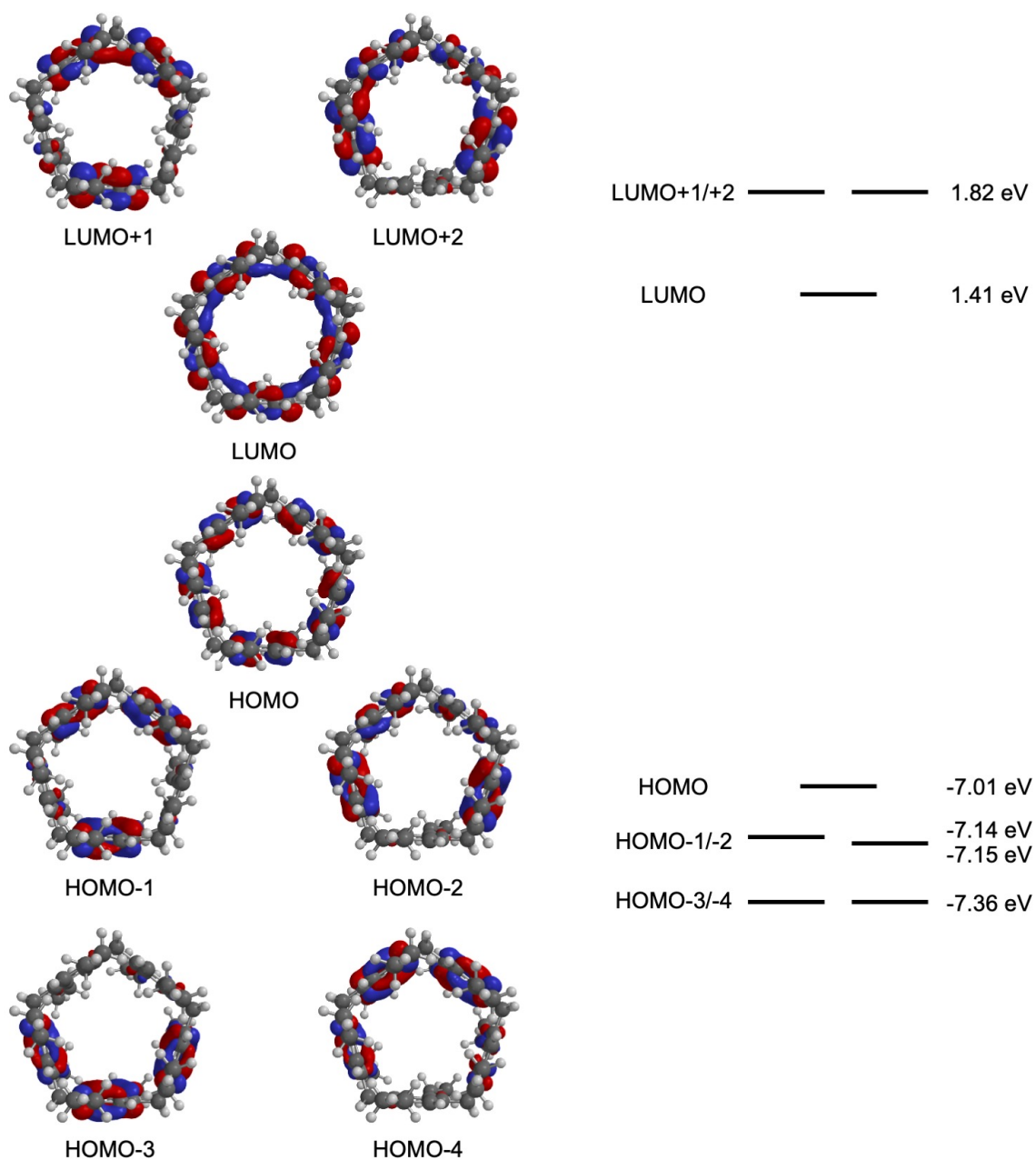


Figure 9. FMOs of **P** calculated at the ω B97X-D/6-31G* level using the CPCM model with the dielectric constant of THF.

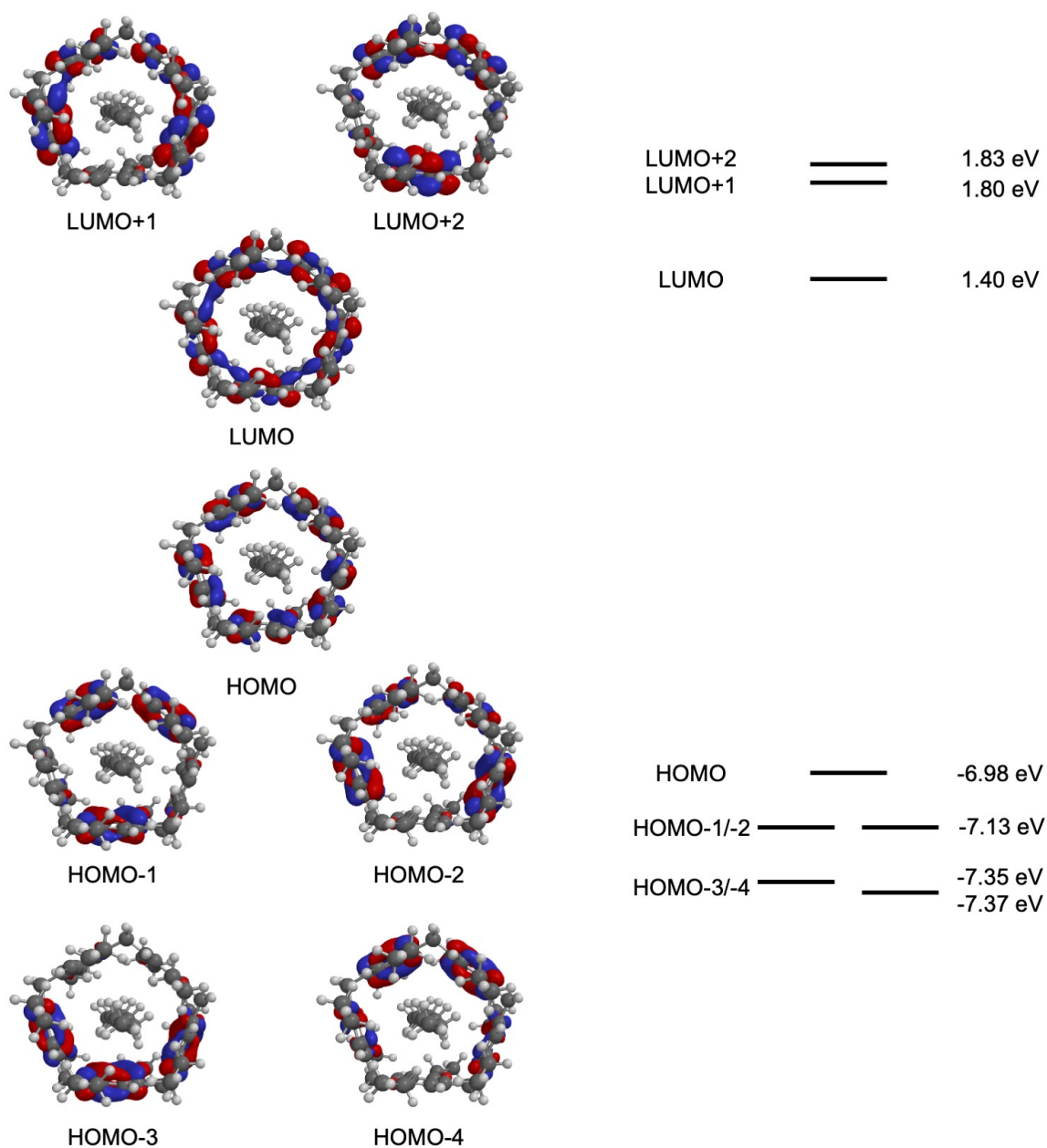


Figure 10. FMOs of (P.Oct) calculated at the ω B97X-D/6-31G* level using the CPCM model with the dielectric constant of THF.

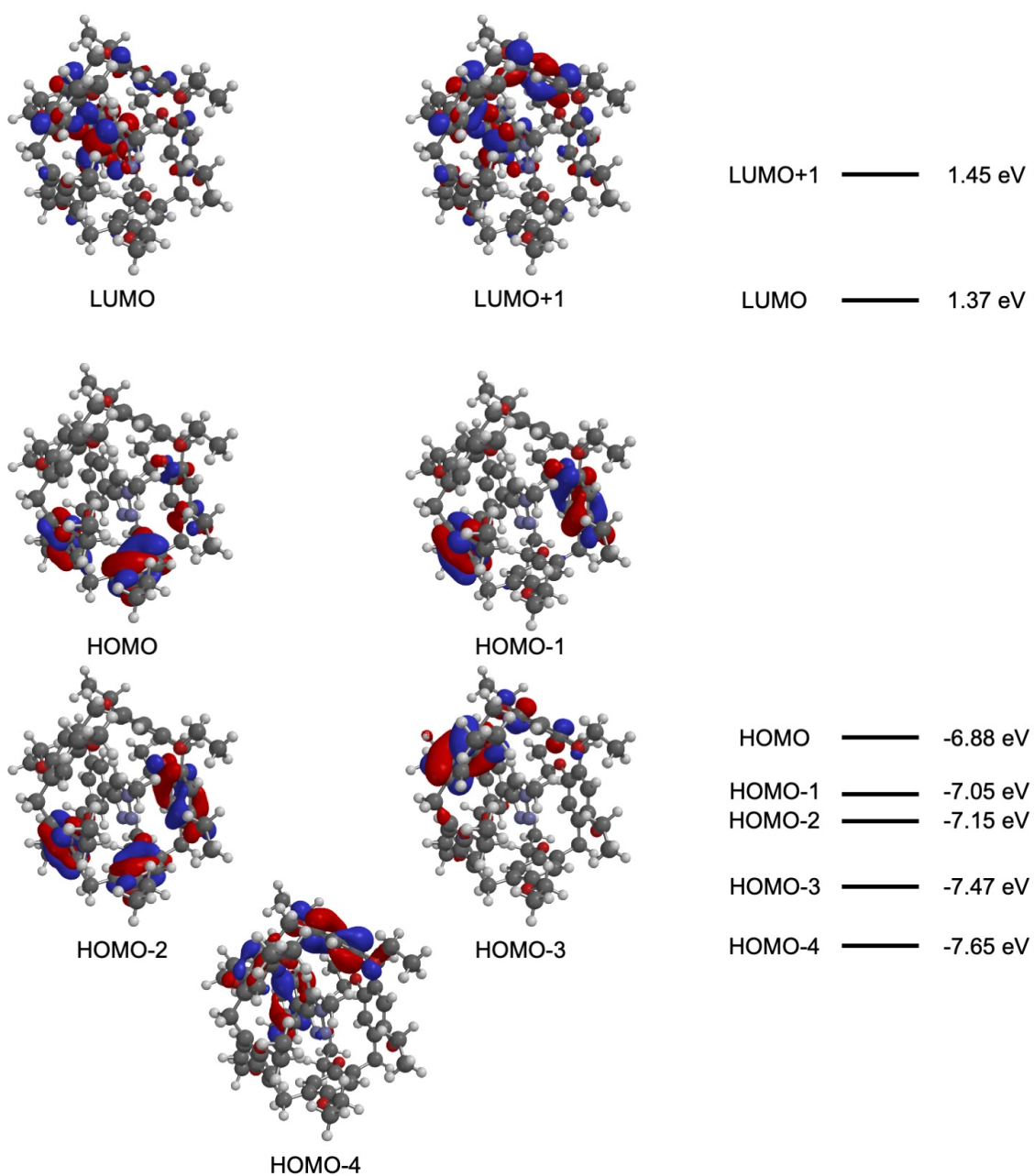


Figure 11. FMOs of (**P.B3**) calculated at the ω B97X-D/6-31G* level using the CPCM model with the dielectric constant of THF.

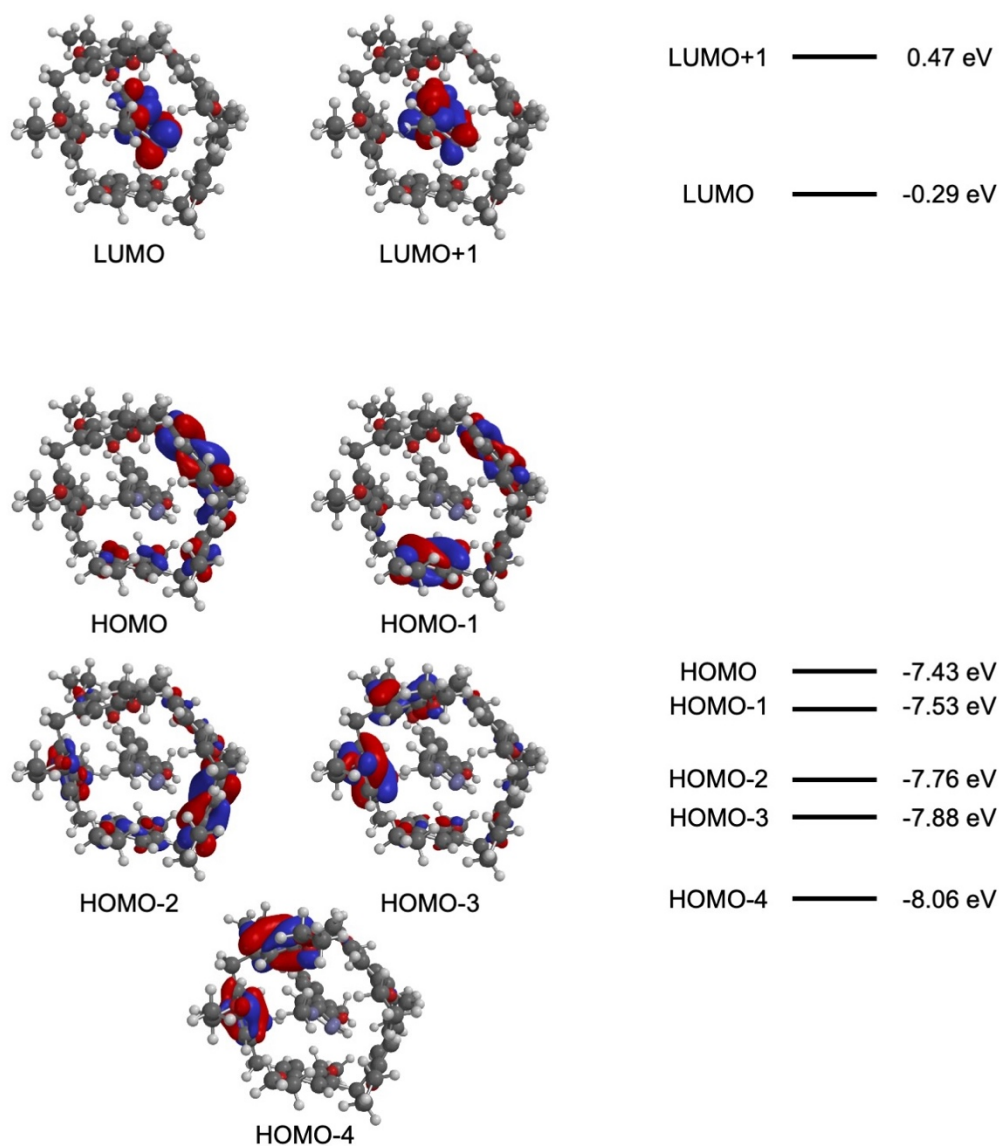


Figure 12. FMOs of (P.B3H⁺) calculated at the ω B97X-D/6-31G* level using the CPCM model with the dielectric constant of THF.

VI-6. X-ray crystal structures

X-ray crystal structure of compound 9a. Crystals suitable for X-ray crystal-structure analysis were obtained by slow diffusion of acetonitrile into a CH₂Cl₂ solution of compound **9a**. Data were collected at 120(2) K on a Bruker PHOTON-III CPAD diffractometer (Mo-K α radiation, $\lambda = 0.71073$ Å). The structure was solved by direct methods (SHELXL-97) and refined against F² using the SHELXL-2014 software. The non-hydrogen atoms were refined anisotropically, using weighted full-matrix least-squares on F². The H-atoms were included in calculated positions and treated as riding atoms using SHELXL default parameters. Crystallographic data: formula: (C₅₅H₇₀O₁₀).(C₂₇H₃₂F₅NO₅) (M = 1436.64 g.mol⁻¹); colourless crystal, 0.30 × 0.25 × 0.22 mm; crystal system: monoclinic, space group *P*2₁/*c*; *a* = 16.9133(6) Å; *b* = 20.0270(8) Å; *c* = 23.2987(10) Å; $\beta = 92.719(2)^\circ$; *V* = 7882.9(5) Å³; *Z* = 4; F(000) = 3064; a total of 230190 reflections collected; $2.36^\circ < \theta < 27.87^\circ$, 18873 independent reflections with 15066 having *I* > 2 σ (*I*); 944 parameters; Final results: R₁(F²) = 0.0568; wR₂(F²) = 0.152, Goof = 1.045. Full data collection parameters and structural data are available as CIF file (Cambridge Crystallographic Data Center deposition number CCDC 2302604).

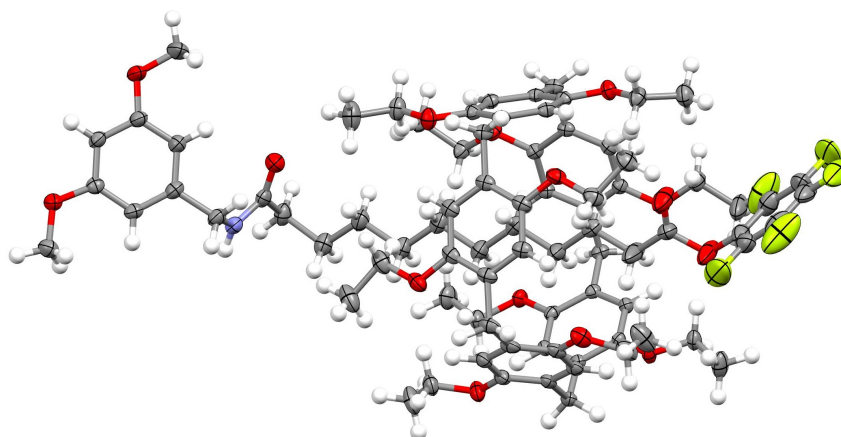


Figure 13. ORTEP plot of the structure of **9a** (H: white, F: light green, O: red, N: blue, C: grey; thermal ellipsoids are shown at 50% probability level).

X-ray crystal structure of compound 9b. Crystals suitable for X-ray crystal-structure analysis were obtained by slow diffusion of *n*-hexane/MeOH into a CH₂Cl₂ solution of compound **9b**. Data were collected at 120(2) K on a Bruker PHOTON-III CPAD diffractometer (Mo-K α radiation, $\lambda = 0.71073$ Å). The structure was solved by direct methods (SHELXL-97) and

refined against F^2 using the SHELXL-2014 software. The non-hydrogen atoms were refined anisotropically, using weighted full-matrix least-squares on F^2 . The H-atoms were included in calculated positions and treated as riding atoms using SHELXL default parameters. Crystallographic data: formula: $(C_{55}H_{70}O_{10}) \cdot (C_{27}H_{26}F_{11}NO_3)$ ($M = 1512.59 \text{ g} \cdot \text{mol}^{-1}$); colourless crystal, $0.22 \times 0.20 \times 0.15 \text{ mm}$; crystal system: monoclinic, space group $P2_1/n$; $a = 18.5569(76) \text{ \AA}$; $b = 17.4913(7) \text{ \AA}$; $c = 24.1219(9) \text{ \AA}$; $\beta = 90.4130(10)^\circ$; $V = 7829.4(5) \text{ \AA}^3$; $Z = 4$; $F(000) = 3192$; a total of 163566 reflections collected; $2.051^\circ < \theta < 27.936^\circ$, 18731 independent reflections with 12133 having $I > 2\sigma(I)$; 975 parameters; Final results: $R_1(F^2) = 0.0756$; $wR_2(F^2) = 0.2205$, $Goof = 1.037$. Full data collection parameters and structural data are available as CIF file (Cambridge Crystallographic Data Center deposition number CCDC 2302607).

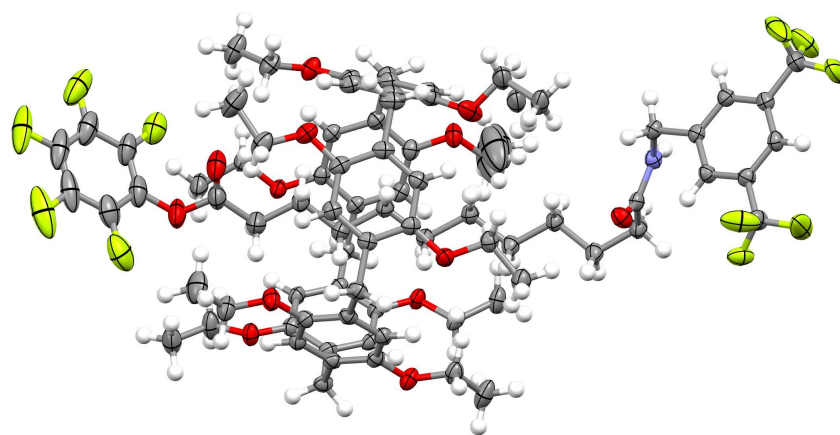


Figure 14. ORTEP plot of the structure of **9b** (H: white, F: light green, O: red, N: blue, C: grey; thermal ellipsoids are shown at 50% probability level).

X-ray crystal structure of compound 12. Crystals suitable for X-ray crystal-structure analysis were obtained by slow diffusion of *n*-hexane/MeOH into a CH_2Cl_2 solution of compound **12**. Data were collected at 120(2) K on a Bruker PHOTON-III CPAD diffractometer (Mo- $K\alpha$ radiation, $\lambda = 0.71073 \text{ \AA}$). The structure was solved by direct methods (SHELXL-97) and refined against F^2 using the SHELXL-2018 software. The non-hydrogen atoms were refined anisotropically, using weighted full-matrix least-squares on F^2 . The H-atoms were included in calculated positions and treated as riding atoms using SHELXL default parameters. Crystallographic data: formula: $(C_{55}H_{70}O_{10}) \cdot (C_{30}H_{38}F_6N_2O_4)(CH_4O)$ ($M = 1527.77 \text{ g} \cdot \text{mol}^{-1}$); pink crystal, $0.20 \times 0.15 \times 0.102 \text{ mm}$; crystal system: triclinic, space group $P-1$; $a = 14.4490(13) \text{ \AA}$; $b = 15.0041(14) \text{ \AA}$; $c = 21.825(2) \text{ \AA}$; $\alpha = 73.431(3)^\circ$; $\beta = 85.599(3)^\circ$; $\gamma = 64.039(3)^\circ$; $V =$

4071.1(7) Å³; Z = 2; F(000) = 1632; a total of 94369 reflections collected; 2.57° < θ < 27.10°, 19448 independent reflections with 10448 having I > 2σ(I); 1011 parameters; Final results: R₁(F²) = 0.0836; wR₂(F²) = 0.2614, Goof = 1.013. Full data collection parameters and structural data are available as CIF file (Cambridge Crystallographic Data Center deposition number CCDC 2302603).

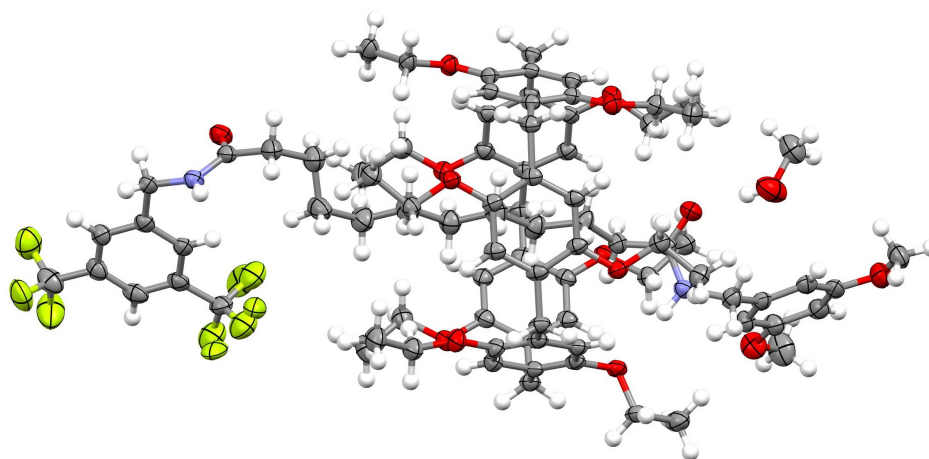


Figure 15. ORTEP plot of the structure of **12.MeOH** (H: white, F: light green, O: red, N: blue, C: grey; thermal ellipsoids are shown at 50% probability level).

VI-6. References

- 1) M. Rémy, I. Nierengarten, B. Park, M. Holler, U. Hahn, J.-F. Nierengarten, *Chem. Eur. J.* **2021**, *27*, 8492-8499.
- 2) T. Ogoshi, K. Kitajima, T. Aoki, S. Fujinami, T.-a. Yamagishi, Y. Nakamoto, *J. Org. Chem.* **2010**, *75*, 3268-3273; (b) M. Holler, N. Allenbach, J. Sonet, J.-F. Nierengarten, *Chem. Commun.* **2012**, *48*, 2576-2578.
- 3) I. Nierengarten, E. Meichsner, M. Holler, P. M. Pieper, R. Deschenaux, B. Delavaux-Nicot, J.-F. Nierengarten, *Chem. Eur. J.* **2018**, *24*, 169-177.
- 4) (a) C. Frassinetti, S. Ghelli, P. Gans, A. Sabatini, M. S. Moruzzi, A. Vacca, *Anal. Biochem.* **1995**, *231*, 374-382. (b) C. Frassinetti, L. Alderighi, P. Gans, A. Sabatini, A. Vacca, S. Ghelli, *Anal. Bioanal. Chem.* **2003**, *376*, 1041-1052.

Préparation de rotaxanes incorporant une sous-unité pillar[5]arène

Résumé

Les rotaxanes constituent un domaine de recherche particulièrement actif en chimie. Dans cette thèse, nous décrivons le potentiel de la stratégie de synthèse développée dans notre groupe pour la synthèse de rotaxanes par des réactions d'échange de bouchons. Nous avons ainsi montré qu'un [2]rotaxane possédant deux bouchons activés peut être mono-fonctionnalisé avec des rendements quasi-quantitatifs. Les dérivés de [2]rotaxanes mono-fonctionnalisés peuvent alors être utilisés pour conduire soit à des [2]rotaxanes, soit à des [3]rotaxanes, suivant la nature de la diamine utilisée. Ces méthodes de synthèse ont alors été utilisées pour la préparation de machines moléculaires. Nous avons montré que la position de macrocycle peut être contrôlée par un stimulus acide-base.

Mots-clés: chimie supramoléculaire, pillar[5]arène, rotaxane, échange de bouchon, machine moléculaire, molécules mécaniquement imbriquées (MIMs).

Abstract

Rotaxanes are a particularly active field of research in chemistry. In this thesis we describe the potential of the synthesis strategy developed in our group for the synthesis of new rotaxanes by the stopper exchange method. We have shown that a [2]rotaxane with two activated stoppers can be mono-functionalized in almost quantitative yields. To further explore the potential of mono-functionalized [2]rotaxane derivatives, we then used to give either [2]rotaxanes or [3]rotaxanes, depending on the nature of the diamine used. These synthetic methods were then used to prepare molecular machines. We have shown that the position of the macrocycle can be controlled by an acid-base stimulus.

Keywords: supramolecular chemistry, pillar[5]arene, rotaxane, stoppers exchange, molecular machines, mechanically interlocked molecules (MIMs).